A LAGRANGIAN AND EULERIAN DIFFUSION STUDY IN THE COASTAL SURFACE LAYERS

DOE/EV 10250-1

A LAGRANGIAN AND EULERIAN DIFFUSION STUDY IN THE COASTAL SURFACE LAYERS

FINAL REPORT

For the period

1 July, 1979 - 30 September, 1982

Akira Okubo
Harry H. Carter
Robert E. Wilson
Brian G. Sanderson
Eric N. Partch

Marine Sciences Research Center
State University of New York
Stony Brook, New York 11794

Prepared for the

U.S. Department of Energy
Assistant Secretary for Environment
Office of Health and Environmental Research
Washington, D.C. 20545

Special Report 46
Reference 83-1

Approved for Distribution

J.R. Schubel, Director

DISCLAIMER

ABSTRACT

Our study addressed a fundamental problem in turbulent diffusion, namely the comparability of various existing Lagrangian and Eulerian techniques for quantitating dispersion. The techniques range from purely Lagrangian methods, i.e., drogues and dye tracers, to an Eulerian method, i.e., moored current meters. For this purpose, two field experiments were carried out in the coastal waters off the south shore of Long Island. The experiments, one in July, 1980 (summer) and one in March, 1981 (winter), consisted of simultaneous measurements of dye and drogue dispersion within a current meter array. This report provides details of the field studies, experimental results, and an analysis and discussion of the results. Both dye patch and plume experiments were carried out. The time rate of change of variance relative to the centroid for the dye patches and the time rate of change of variance, both relative and absolute, for the dye plumes are presented. For each drogue experiment, results are provided in terms of the time rate of change of the drogue cluster centroid, of the cluster variance and covariance and variance relative to the cluster principal axis, of the cluster rotation and elongation, of diffusivities, of velocity gradients and velocity gradient parameters, i.e., divergence, shear, vorticity, etc., and of the cluster areas both measured and predicted. Rotational invariants (rotary auto spectra and cross spectra) of the current meter records are presented as are mean values of the alongshore and

on/offshore components of the current and horizontal and vertical velocity gradients.

Analysis of these results showed that the time history of variance of drogues and dye patches compared favorably if one accounts for the additional dispersive effect of vertical shear and vertical mixing on the dye patches. After about 5 hours, the ratio of the dye patch variance to the drogue cluster variance was constant and about 5 times the variance of the drogue cluster; at this time both were observed to be following a t^2 relation.

For short times, i.e., $t < 10^6 - 10^7$ s, drogue cluster areas could be predicted reasonably well from the integrated divergence from the current meter array when scale differences were taken into account. However, for larger times, an effect due to turbulence at scales smaller than the drogue separations must also be taken into account.

Comparative studies of velocity gradients using an array of current meters and a cluster of drogues revealed, aside from the scale dependence of these quantities, that i) the velocity gradient field was predominantly divergent, with convergences apparently localized in time and space, ii) the velocity gradients observed in summer were generally one order of magnitude larger than those in winter, and iii) the overall behavior of velocity gradients shown in the stability diagrams was very similar for both the Eulerian and the Lagrangian measurements.

Taylor's formula was applied to estimate relative diffusion from a continuous source. In this context Hay-Pasquill's hypothesis was used to relate the Lagrangian autocorrelation to its Eulerian counterpart computed from filtered current meter records. Band pass filtering produced a relatively good agreement between the observed variance of dye plume and the calculated variance, however, low frequency fluctuations in the filtered record caused unsatisfactory wavy behaviors of the variance with respect to diffusion time. By properly removing the oscillatory component from the autocorrelation calculation, the agreement between data and theory is shown to be much improved. These low frequency velocity fluctuations contribute little to the lateral diffusion of dye plume relative to its centerline.

ACKNOWLEDGEMENTS

Many MSRC staff members made substantial contributions to the LEDS study. The dye data owes much to Mr. Andrew Hamilton who supervised acquisition of the dye data on cassette onboard the R/V ONRUST and its subsequent transfer to the UNIVAC for analysis. Mr. George Carroll wrote many programs for both the current meter and dye data analysis and assisted all of the authors materially with special computation problems as they arose. Mr. G. Michael Schmidt assisted in editing the dye data tapes for the summer dye study. Ms. Eileen Goldsmith kept our project financial records, ordered our equipment and supplies, and last but not least typed our rather long manuscript. Mr. Clifford Jones and C.E. Firstenberg assisted in the drogue studies and in deploying and retrieving the current meters.

TABLE OF CONTENTS

TABLE OF CONTENTS - *continued*

LIST OF FIGURES

LIST OF FIGURES - *continued*

LIST OF FIGURES - *continued*

LIST OF FIGURES - *continued*

LIST OF FIGURES - *continued*

LIST OF FIGURES - *continued*

LIST OF TABLES

LIST OF SYMBOLS

a	see equation (1); also $a \equiv 1/t_E$,
a_i	Lagrangian coordinate; also a constant,
a_0, a_1	intercept and slope of a regression line,
A	area,
A_J	area calculated from deformations,
A_{JK}	area calculated from deformations and diffusivity,
A_m	a characteristic area over which divergence is measured,
A_o	initial drogue cluster area,
A_{obs}	observed drogue cluster area and equal to $4\pi\sigma_X\sigma_Y$,
$A_{x,y,z}$	eddy diffusivity in x,y,z-directions,
b_i	Lagrangian coordinate; also a constant,
B_i	Lagrangian "shear effect" parameters (Okubo *et al.*, 1976b),
C	dye concentration,
C'	$(C/q_d)10^9$,
$C_{u_i v_j}$	real part of regular one-sided cross spectrum,
D	depth over which dye is uniformly mixed,
D.L.	detectable limit of dye,
FFT	fast Fourier transform,
$G_{u_i u_i}$	regular one-sided auto spectrum,
H	depth of bottom or pycnocline,
h	shearing deformation rate,
i	ith drogue,
k	kth time,
K_a	apparent eddy diffusivity,

K_{ij} Lagrangian eddy diffusivities,

K_{xy} cross eddy diffusivity; see equation (21),

$K_{x,y,z,}$ eddy diffusivity in x,y,z-direction,

ℓb pound,

L large; also length scale

m meters; also a positive number in equations (1) and (59),

M mass of dye released,

M_4 quarter-diurnal tidal period,

n an arbitrary direction; also nano (10^{-9}),

ppb parts per billion,

P a diffusion velocity; $P \equiv \sigma_{rc}/t\sqrt{6}$,

q_d pumping rate of dry dye in g g^{-1},

$Q_{u_i v_j}$ imaginary part of regular one-sided cross spectrum;

rms root-mean-square ($\sqrt{\overline{(\ )^2}}$)

r_e equivalent circular radius of the irregular area within a given isoline of dye concentration, i.e., $\sqrt{\text{area}/\pi}$,

R_E Eulerian autocorrelation coefficient,

R_L, R_{t_s} Lagrangian autocorrelation coefficients,

r^2 coefficient of determination,

S salinity; also location of dye source; also concentration of tracer (equation (30),

$S_{w_i w_j}$ inner auto cross spectrum between w_i and w_j,

t temperature; also time of diffusion,

t_a or $\bar{t}_a$ age of dye at particular location and equal to $t_{obs} - t_{rel}$,

t_c critical time,

t_E Eulerian correlation time scale,

t_{obs} average local time of observation of plume profile,

t_p time since dye discharge was initiated,

t_{rel} local time a parcel of dye is released from dye source,

t_s sampling time or time required to inventory the patch or to complete N runs at a particular section of a plume,

t_v estimate of time required for dye to be uniformly mixed to a depth of H,

T temperature; also true direction,

T_L, T_E Lagrangian and Eulerian integral time scales,

u,U velocity in the x-direction,

u" turbulent velocity,

$\bar{u}$ average velocity over the drogue cluster in the x-direction.

v velocity in the y-direction,

v'_{t_s} see equation (51),

v",v' turbulent velocity,

$\bar{v}$ average velocity over the drogue cluster in the y-direction,

V_o mean velocity in the x-direction (equation (30)),

w_j horizontal velocity vector where $w_j(t) = u_j(t) + i\ v_j(t)$ for $j = 1,2$ and $i = \sqrt{-1}$,

x down-plume or alongshore (parabathic) direction; also east direction,

X	major principal axis direction; also major axis of dye plume,
y	lateral (diabathic) or cross-plume direction; also north direction,
Y	minor principal axis direction; also minor axis of dye patch,
$\overline{y^2}$	lateral variance,
z	vertical direction,
α	stretching deformation rate,
β	the ratio of Eulerian to Lagrangian time scales,
γ	horizontal divergence,
γ^2	coherency,
Γ	concentration of dye solution as released or pumped; also the gamma function,
Δ	a difference,
ε	rate of energy dissipation,
η	relative vorticity,
θ	direction of major principal axis of dye patch relative to 069°T,
μ	micro (10^{-6}),
ρ	ratio of minor principal axis to major principal axis; $\rho \equiv \sigma_Y/\sigma_X$,
σ_{rc}	standard deviation of a radially symmetric dye patch; $\sigma_{rc}^2 \equiv 2\sigma_x\sigma_y$,
σ_t	density of sea water at salinity S, temperature t, and atmospheric pressure,

$\sigma_{x,y,z}$	standard deviation in the x,y,z-directions,
$\sigma_{X,Y}$	standard deviation in the direction of the major and minor principal axis,
σ^2	variance,
$\sigma^2_{a,b}$	initial variance of drogue displacements in the x and y-directions,
$\sigma_o{}^2$	initial radially symmetric horizontal variance,
τ	a small time difference,
ϕ	phase angle,
ω	a diffusion velocity; $\omega \equiv \sigma_{rc}/t$,
$\Omega_{x,y,z}$	horizontal and vertical shears.

INTRODUCTION

The disposal of anthropogenic wastes, e.g., radioactivity, sewage, toxic chemicals, heat, etc. in coastal waters, estuaries, rivers, lakes and oceans gives rise to many questions of a scientific nature. Of fundamental importance for dispersion are the physical processes of transport and mixing, i.e., advection and diffusion. Knowledge of the processes by which contaminated water is mixed and dispersed in the receiving waters is essential for even a first order evaluation of contaminant concentration levels. Thus a study of these dispersion processes should provide information required by those charged with managing our aquatic resources.

Because of the complex nature of the process of turbulent diffusion in the sea, no single theory can adequately interpret or predict the entire pattern of contamination. Our present understanding of oceanic diffusion still comes largely from experimental studies in the field.

Various methods and techniques have been developed and used in experimental studies of turbulent diffusion in the environment. They range from a purely Lagrangian method, i.e., the use of identifiable particles, to an Eulerian method, i.e., the use of moored current meters.

Since dispersion is a Lagrangian process, dye tracer studies are the most appropriate for the determination of contamination levels, although Lagrangian measurements are usually more difficult than

Eulerian to conduct in the field. For example, fixed-point velocity measurements are much easier to obtain in coastal waters than fluorescent dye measurements especially if information is required at depth. Therefore, if it could be shown that an Eulerian data set, i.e., data from a current meter array, could be substituted for the more difficult Lagrangian experiments, a considerable reduction in field work could be achieved. Only a very few field studies have attempted to make a comparison of results obtained by both Lagrangian and Eulerian methods in the sea (Ahn (1974)). A more serious comparison is urgently needed.

Our objective, therefore, is three-fold. First of all we will compare certain Lagrangian statistics, i.e., variance of particle displacement from the centroid, derived from direct measurements of dye and drogues. Secondly, we will compare, by means of the current meter and drogue measurements, velocity gradient parameters and drogue areas versus integrated divergence from current meters, and finally variances derived from both Eulerian measurements (current meters) and Lagrangian measurements (dye plume observations). We will also analyze any differences.

HISTORICAL BACKGROUND

Lagrangian Methods

Tracers for diffusion studies can be classified into two categories, "soluble" or "particulate", according to their state in water. A soluble tracer such as dye is ideal for simulating the dispersion of (neutrally buoyant) waste solutes in the sea. On the other hand, a particulate tracer, when its size is properly chosen, is also useful in simulating the dispersion of particulate waste materials in the sea. Both tracers have advantages and disadvantages. The characteristics of dye and drogue tracers are summarized in Table 1; those of current meters (an Eulerian method) are also included for comparison.

Dye Studies

Of the various types of soluble tracers, fluorescent dyes have proved the most useful; in particular rhodamine B (or WT) is considered most accessible, stable, and convenient for use in the sea (Carpenter (1960)). A comprehensive review of dye studies in the sea was presented by Carter and Okubo (1978).

Since Pritchard and Carpenter (1960) developed the field technique for direct continuous observation of tracer concentrations by fluorescent assay, numerous experimental studies have been carried out on natural water bodies, i.e., lakes, rivers, estuaries, etc. (Joseph, Sendner and Weidmann (1964); Pritchard, Okubo and Carter (1966); Carter and Okubo (1965); Foxworthy, Tibby and Barson

TABLE 1

Characteristics of Lagrangian and Eulerian Experimental Methods

	Advantages	Disadvantages
Dye Study		
	1. Three-dimensional response	1. Can't follow individual particles (dye molecules); quasi-Lagrangian
	2. Ideally simulates the dispersion of a dynamically passive contaminant	2. Lengthy experiments are labor intensive
	3. Low levels of detection are easily attainable (1 part in 10^{11})	3. Relatively expensive to tag large volumes of water
		4. Depending on the dye, it may be subject to photochemical decay and adsorption on suspended sediments
Dye Photography		
	1. Instantaneous patterns of dispersion can be obtained	1. Difficult to relate photos to the concentration field without ground truth
	2. Provides completely synoptic picture; i.e., no distortion due to sampling	2. Studied only for an initial period of diffusion
		3. Experiments are almost impossible at night
Drogue Study		
	1. Individual drogues can be followed (purely Lagrangian)	1. Two-dimensional response
	2. Drogues are retrievable and reusable	2. Size effect ("filtering out")
	3. Provides vorticity, divergence, deformation rates and eddy diffusivities as function of time	3. Experiments must be confined to times < 1 day in confined waters
Current Meter Measurements		
	1. Long continuous records can be obtained and internally stored for subsequent retrieval	1. Essentially Eulerian information: difficult to relate to Lagrangian dispersion
	2. Provides information on flow field at distinct spatial positions	2. Two-dimensional response
	3. Provides vorticity, divergence, deformation rates	3. Current meters are expensive and subject to loss

(1966); Ichiye (1967); Csanady (1963, 1964, 1970); Murthy and Csanady (1971); Murthy (1972); Huang (1971); Bendiner and Ewart (1972); Ewart and Bendiner (1981); Kullenberg (1969, 1971, 1972); Schuert (1970); Schott and Quadfasel (1979)).

In simplest terms, the dye technique consists of releasing, either instantaneously or continuously, a known quantity of the tracer and measuring its subsequent distribution as a function of space and time. The concentration distribution is used to calculate the variances in the horizontal and vertical directions, on the basis of which an effective diffusivity may be computed. Diffusion diagrams, which show the relationship between the variance and diffusion time, and that of the diffusivity and the scale of diffusion provide basic information on turbulent diffusion in the sea (Okubo (1971, 1974)). Often the time behavior of the peak concentration in a dye patch gives another useful evaluation of oceanic diffusion (Carter and Okubo (1965); Ling (1981)).

The early stages of dispersion of dye are difficult to measure by sampling because the patch of dye has a small areal extent and disturbance of the patch by the sampling vessel can distort the real pattern of diffusion. At this stage, therefore, aerial photography is useful for obtaining information regarding the movement and dispersion of a dye patch or plume (Linfield (1965); Katz, Gerard and Costin (1965); Ichiye and Plutchak (1966); Ichiye and Carnes (1980 /1981); Kenny (1967)). Aerial photography may also be used

in the later stages of diffusion (up to one day after release of dye (Carter and Okubo (1965)).

Aerial photographs also provide information on detailed concentration fluctuations in patches and plumes of dye. In order to assess the suitability of a water mass as a medium for living organisms, information concerning the mean concentration field alone is not sufficient. The variance of the concentration field, the magnitude and duration of concentration peaks, and the frequency of occurrence of concentration levels are all important parameters for assessing the possible effects of contaminants on living organisms. A complete knowledge of the probability distribution of concentrations is required to predict these statistical characteristics (El-Shaarawi and Murthy (1976); Venkatram (1979)).

Although aerial photography is useful, some difficulty is encountered in determining uniquely the concentration distribution from photographs (Ichiye and Plutchak (1966)). An obvious question is what the visible dye boundary in the photography represents. We may imagine that the boundary represents a certain threshold concentration of dye, presumably integrated vertically. If so, a dye patch observed from the air appears to grow in the beginning, reach a maximum size, and then gradually decrease in size as diffusion progresses. On the other hand, the variance of dye concentration should keep increasing with time. Hence the convenience of using a visible boundary as a measure of dispersion is short lived. Recently airborne fluorescence systems (LIDAR) were developed (Franz *et al.*, 1982) to survey dye patches, although the method is still limited to an

initial stage of dispersion.

To resolve this problem, we included aerial photography in this project so as to make a simple comparison of dye photographs with underway concentration measurements for dye plumes. Thus the sampling vessel entered a dye plume at a distance from the source along a track perpendicular to the plume centerline and measured the lateral and vertical distributions of dye. At the same time an aircraft equipped with a camera passed over the sampling vessel and photographs were taken.

Drogue Studies

Among particulate tracers for simulating subsurface dispersion, drogues are both inexpensive and convenient. They have been used extensively to study dispersion as well as mean currents (Stevenson, Garvine and Wyatt (1974); Stommel (1949); Chew and Berberian (1970, 1971, 1972); Denner, Green and Synder (1968); Csanady (1963); Okubo and Farlow (1967); Ahn (1974); Ichiye, Inoue and Carnes (1981); Yanagi, Murashita and Higuchi (1982); Sanderson (1982)).

A drogue has obvious drawbacks, partly because of its finite size and partly because its response is limited primarily to horizontal motions of the water. On the other hand, drogues can be tracked individually and dispersion can be studied purely in a Lagrangian framework. In addition, by simultaneously following a cluster of drogues, we may be able to estimate not only the mean flow and dispersion but also a field of Lagrangian deformations and velocity gradients such as vorticity, shear, divergence, etc.

The potential of drogues for obtaining these latter fields of deformations and velocity gradients seems to have been mostly overlooked. Attempts have been made to determine the horizontal divergence and shear by means of drogues (Chew and Berberian (1971, 1972); Reed (1971)) but only recently have Molinari and Kirwan (1975), Okubo and Ebbesmeyer (1976) and Yanagi *et al.* (1982) developed methods for determining mean velocity-gradient parameters and turbulent velocity characteristics from drogues. In addition, Okubo, Ebbesmeyer and Helseth (1976) have presented methods for determining Lagrangian deformations and turbulent statistics and have shown that such determinations allow generalized Lagrangian diffusion equations such as in Okubo (1966) and Okubo, Ebbesmeyer and Sanderson (1983) to be directly evaluated.

There is a serious problem, however, due to the effect of the finite size of the drogue on the diffusion of a particulate tracer. That is, due to a "filtering effect", the particle responds only to motions whose characteristic scales are larger than the particle. Ogura (1952) developed a kinematic model of the response to evaluate the filtering effect and showed that the dispersion effect of particles on the particle size depends on the ratio of the particle size to the size of the "energy-containing eddies" in the turbulent field. For a ratio of 1:10, Ogura showed that the relative diffusivity was about 90%. Cederwall's experimental results in a laboratory flume supported Ogura's theory (Cederwall (1971)). All of this suggests that the drogue size should be smaller by at least one order

of magnitude than the characteristic size of energy-containing eddies. In the coastal waters south of Long Island, the size of energy containing eddies is estimated to be of the order of 1000 m. Therefore the use of drogues whose effective area is about 2 m^2 minimizes the size-effect problem.

Another limitation to the use of drogues for studying turbulent diffusion is that they provide no information on vertical mixing. The effect of vertical diffusion, in particular when combined with vertical shear in the mean flow, on the mixing of a solute in the sea plays an important role in the dispersion of solute (Bowden (1965); Csanady (1966)). This so-called "shear effect" is due to the combined effect of shear and diffusion acting in the same direction. Apparently a dye tracer is subject to this effect in both the vertical and horizontal directions while drogues are subject to the shear effect only in a horizontal plane. Nevertheless, some experimental evidence (Okubo and Farlow (1967)) shows that values of diffusivity obtained from drogue studies are comparable to those found in dye studies, although the two studies were not made simultaneously at the same locality. In our project (LEDS), we attempted to carry out these two types of diffusion experiments at the same time and locality in order to resolve the problem.

Eulerian Methods

Current Meter Studies

Although the diffusion process is Lagrangian by its nature, we can study diffusion by means of an Eulerian device if proper

care is taken. A current meter serves as such a device. It should, however, be remembered that the problem of relating Eulerian statistics to Lagrangian statistics of turbulence has not been basically solved (Corrsin (1962); Lumley (1962)). Thus only with a seemingly reasonable approximation can the eddy diffusivity of Lagrangian particles be expressed in terms of the more accessible Eulerian statistics (Palmer and Izatt (1970); Ahn (1974); Callaway (1974); Schott and Quadfasel (1979)).

Taylor's formula (Taylor (1921)) for expressing the variance of Lagrangian particle displacements in terms of the Lagrangian velocity autocorrelation or simply "Lagrangian correlation" is used as the basis of this study. The eddy diffusivity can then be calculated from the rate of change of the variance with time. The main problem is that direct determination of the Lagrangian correlation is usually extremely difficult in the field. Alternatively, the Lagrangian correlation may be computed indirectly by double differentiation of measured values of the variance with respect to time, although great difficulty and errors are involved in the procedure. In this context, Shlien and Corrsin's method (Shlien and Corrsin (1974)) is appealing.

On the other hand, current meter records easily provide the Eulerian velocity correlation. The problem is then reduced to finding the relationship between the Eulerian and Lagrangian correlations. There is little theoretical basis for assuming that the shapes of the Eulerian and Lagrangian correlations are similar

(Shlien and Corrsin (1974); Davis (1982)). Nevertheless, Hay and Pasquill (1959) suggested that under an assumption of similarity of the Eulerian and Lagrangian correlations, the ratio of the Eulerian and Lagrangian time scales can be used as a parameter to replace the Lagrangian statistics of the variance by the Eulerian counterpart. The ratio is customarily called the β-factor. In short, use of the β-factor enables us to evaluate diffusion characteristics from a current-meter record.

Callaway (1974) and Ahn (1974) used the Hay-Pasquill hypothesis to compute the horizontal dispersion of pollutants in coastal waters. Calloway took $\beta = 1$ and Ahn took $\beta = 1.25$ as tentative values for oceanic flow with high Reynolds numbers. Although Callaway's computations for eddy diffusivity appear to be reasonable and encouraging, he considered it urgent to conduct the rather difficult Lagrangian-Eulerian field experiments to compare the results. Should the Hay-Pasquill hypothesis be shown to be valid as a reasonable approximation, our prediction of oceanic dispersion of contaminants would become much easier by utilizing current-meter records. In LEDS we have attempted to make careful comparisons of diffusion characteristics obtained from Lagrangian methods and those obtained from Eulerian methods.

THE EXPERIMENTAL PROGRAM

Three field studies were carried out in the coastal waters off the south shore of Long Island. See Figure 1. The first, during March, 1980, was a preliminary study to obtain information on the velocity gradients, the Lagrangian and Eulerian length scales of the energy-containing eddies, and to test our drogue design. Details of that study are contained in Carter *et al.* (1980). Table 2 gives the chronology of the various components of the other two studies; a summer study (July, 1980) during stratified conditions and a winter study (March, 1981) during unstratified conditions. Figures 2 through 6 show typical vertical profiles of temperature (T), salinity (S), and σ_t for these two studies.

As shown in Table 2 our experimental program consisted of simultaneous measurements of the spread of dye either as patches or as continuous plumes, a large number of drogue trajectories either simultaneously or sequentially released, and current meter speeds and directions from an array of current meters. For the diffusion characterisics calculated by these three different sets of measurements to be comparable, the following criteria must be satisfied by the current meter array:

(a) The calculation of velocity gradients from current meters requires simultaneous records from at least 3 meters arranged in a triangle. The array should provide several such triads of varying size.

(b) The minimum meter separation or spacing of the meters of the smallest triad may be limited by the speed resolution of the current meter to be used. For example, the ENDECO Model 174 current meter used in our study cannot resolve speeds less than 1 cms^{-1} assuming perfect calibration. If the smallest velocity gradient, $\frac{\partial u}{\partial n}$, we wish to resolve is of order 5×10^{-5} s^{-1}, then the meters should not be closer than 200 m. However, the minimum separation can be as large as the length scale of the energy-containing eddies and still insure that the meter records will be coherent for all larger scales ($\sim$1000 m).

(c) The maximum meter separation or the dimensions of the largest triad are determined by the expected drogue separations and/or dye patch dimensions at the end of the observation period.

(d) The array should be large enough so that the dye (patches and/or plumes) and drogues will remain within its boundaries for at least a substantial part of the period of observation since the velocity gradients have horizontal structure.

Criteria (c) and (d) may be incompatible in a region with a large mean flow due to a lack of current meters. In our case, the period of observation was ½ day. Assuming a mean flow of 10 cms^{-1} in the alongshore direction, a maximum alongshore separation of 4320 m was indicated. It was necessary to shorten the maximum alongshore separation to 1750 m, however, because of a limited

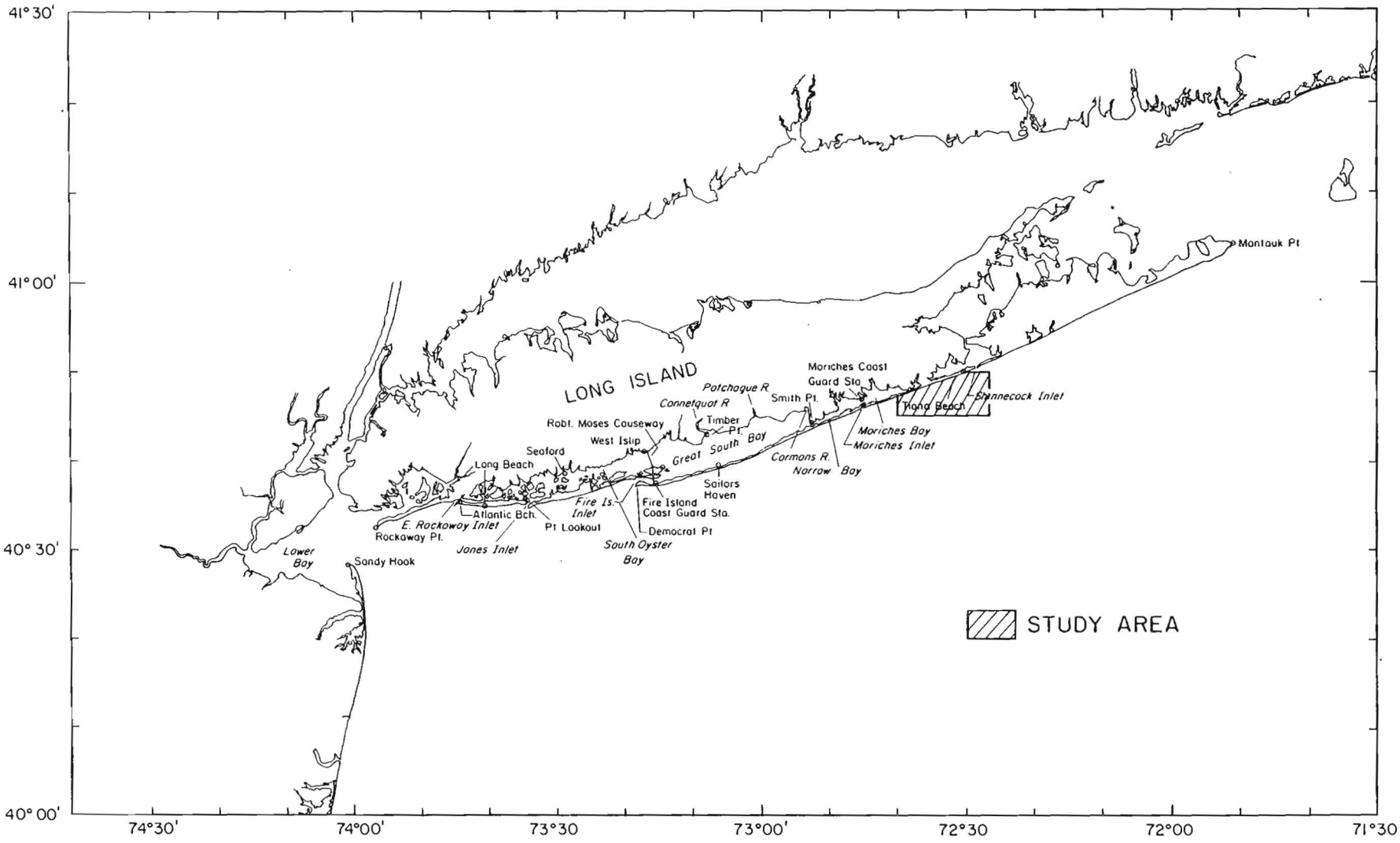

Figure 1. Chart showing the location of the study area in the coastal waters of Long Island.

Table 2

LEDS Chronology

	Sequence of Events												
	July 1980 Date							February/March 1981 Date					
Activity	14	22	23#	24	25	26	28	27	9	10	11	12*	23
Current Meters in:	X							X					
Current Meters out:							X						X
Continuous Dye:		X		X	X	X							
Instantaneous Dye:										X	X	X	
Drogue Measurements:		X		X	X	X			X	X	X		
Aerial Photography:		X		X	X	X							

No sampling due to adverse weather conditions.

* No drogue tracking due to adverse weather conditions.

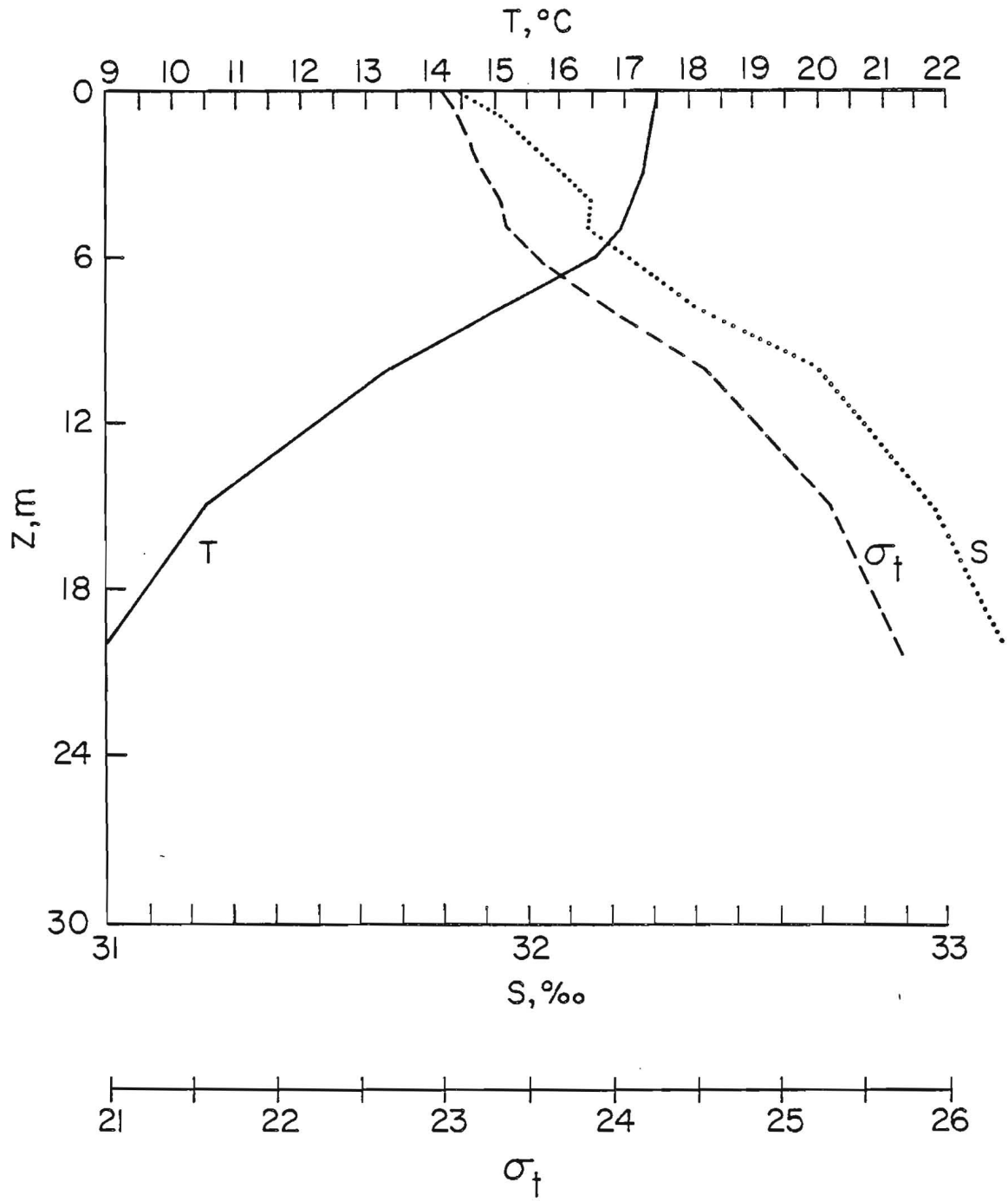

Figure 2. Vertical distribution of temperature (T), salinity (S), and density (σ_t) at dye raft at 0920 on 24 July, 1980.

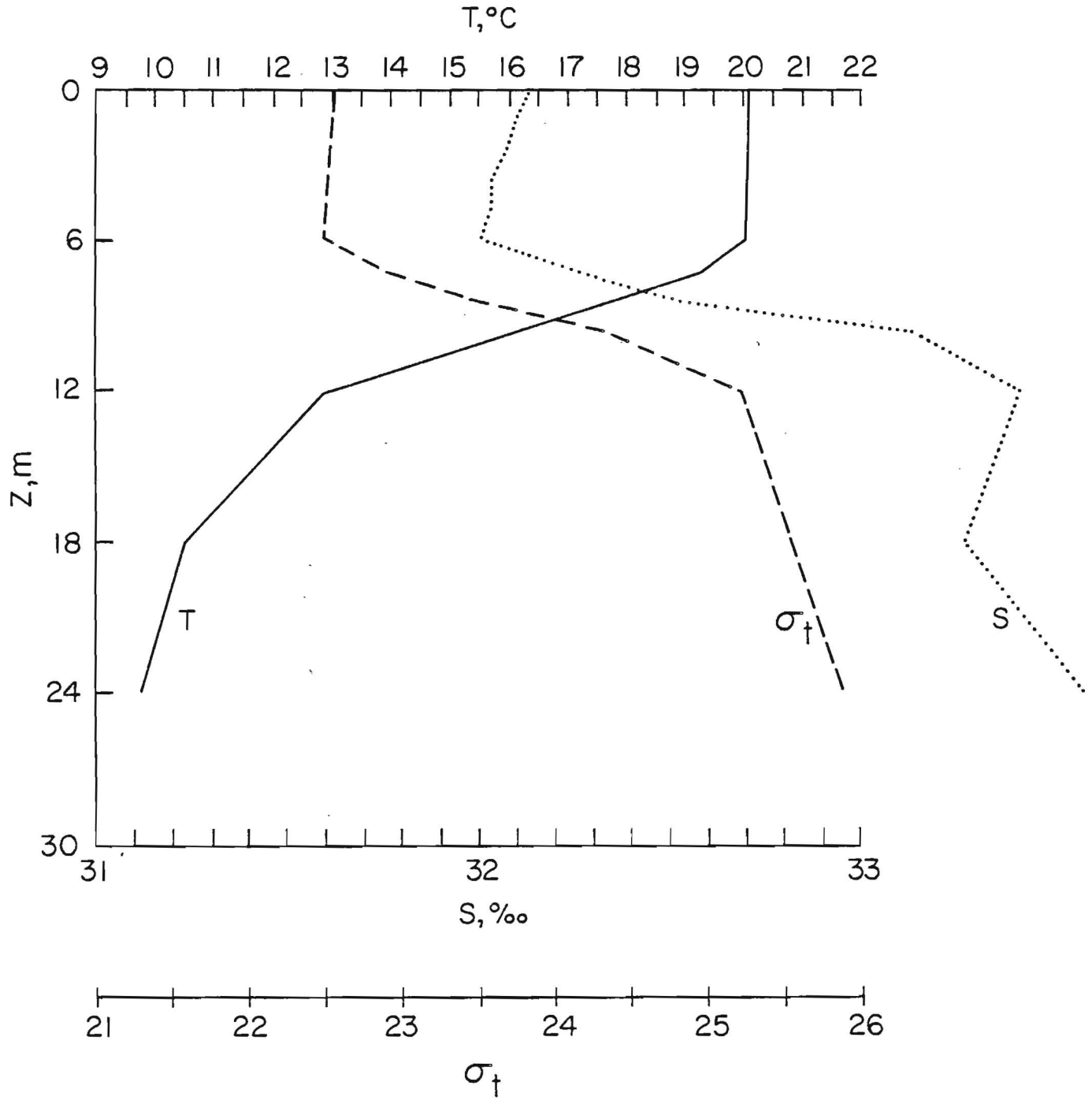

Figure 3. Vertical distribution of temperature (T), salinity (S), and density (σ_t) at mooring "C" at 0745 on 25 July, 1980.

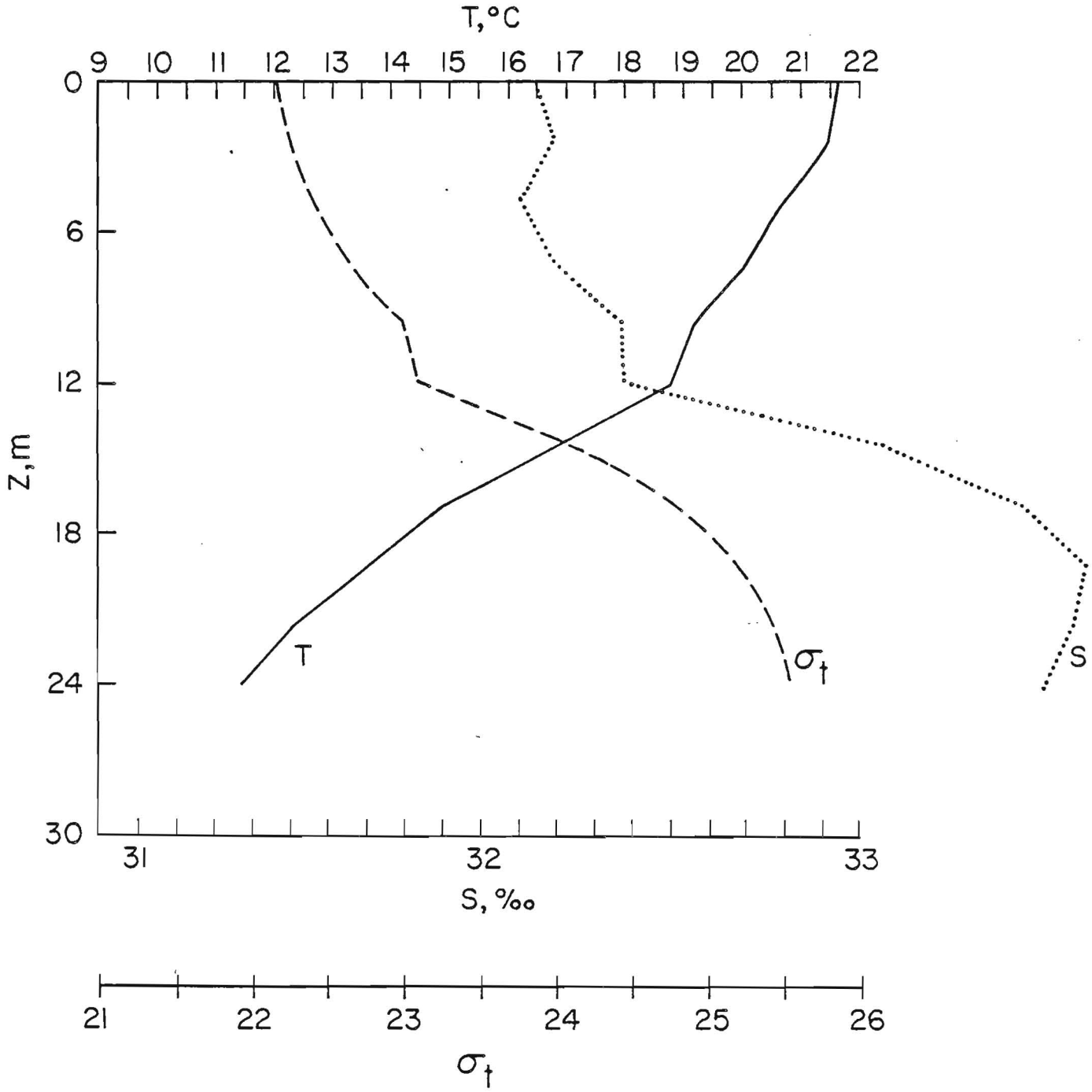

Figure 4. Vertical distribution of temperature (T), salinity (S), and density (σ_t) at mooring "B" at 1555 on 26 July, 1980.

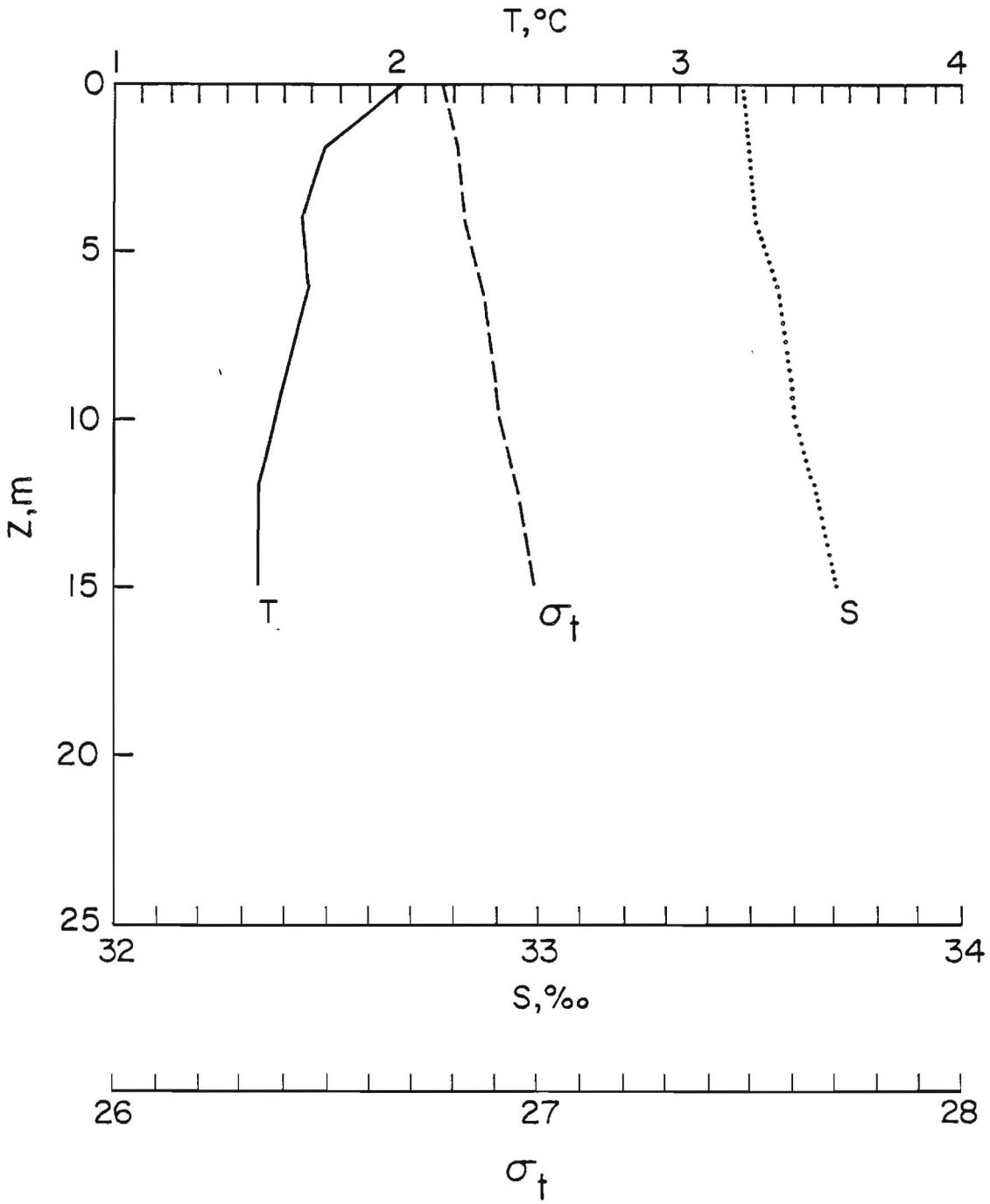

Figure 5. Vertical distribution of temperature (T), salinity (S), and density (σ_t) at mooring "C" at 1425 on 9 March, 1981.

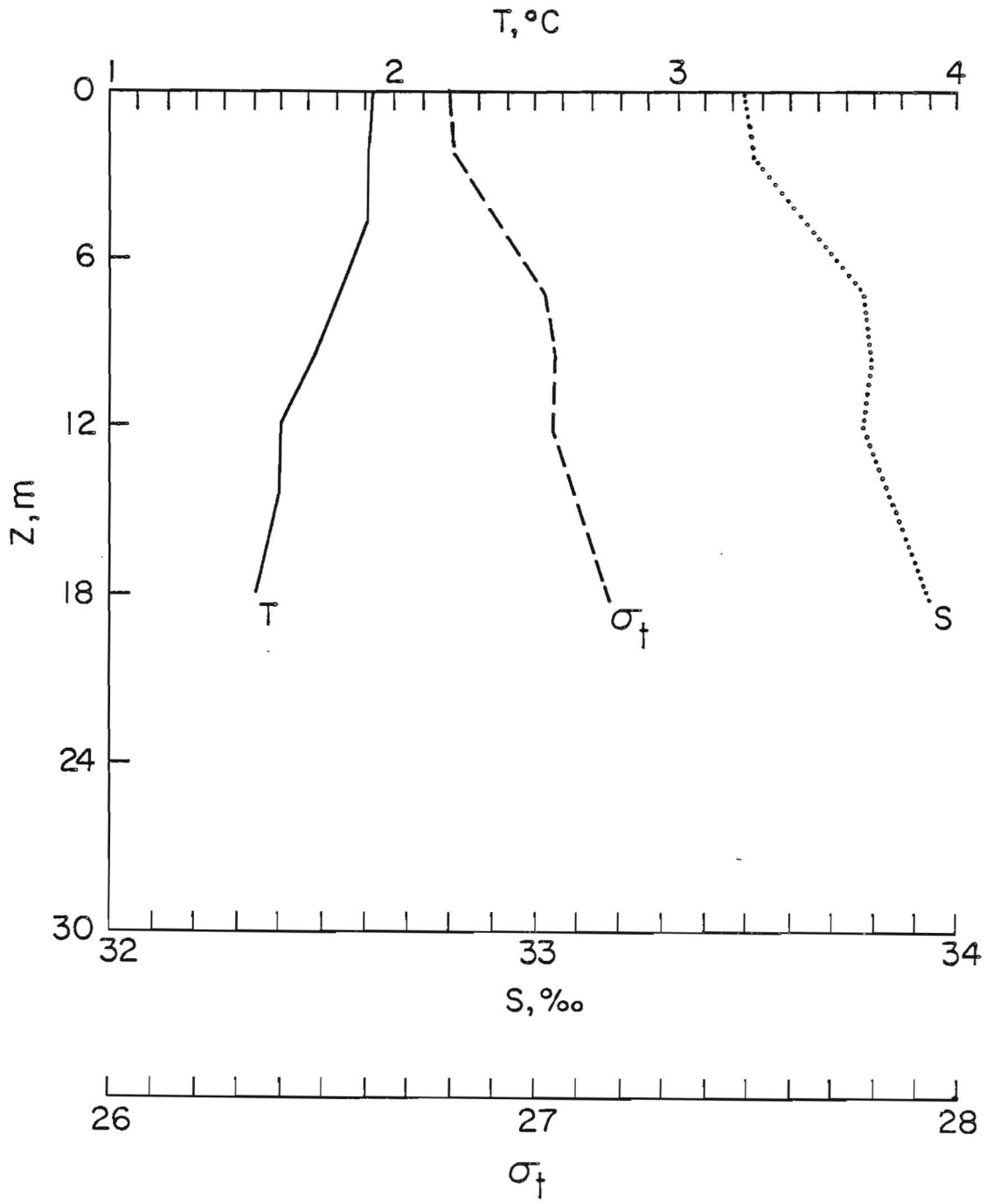

Figure 6. Vertical distribution of temperature (T), salinity (S), and density (σ_t) at mooring "C" at 0845 on 10 March, 1981.

number of current meters (14). This also required that the drogues be picked up and returned to the array when they drifted outside its boundaries and the dye to be released at an upstream location so as to account for the anticipated drift of the patch.

How well our current meter arrays satisfied these criteria will be discussed in subsequent sections.

The Current Meter Studies

Except for two sampling points (see Table 3a) where Braincon Model 1381 meters were employed, Endeco Model 174 and Model 105 current meters were used to measure speed and direction of the currents. Both instruments can be trimmed to maintain a horizontal attitude and ballasted to be neutrally buoyant; both employ ducted impellers to minimize wave contamination. In addition, they are attached to the mooring by means of nylon tethers, 5 feet or more in length, which serve to decouple the instruments from mooring motions. The Model 105's record geared down (5750 to 1) rotor revolutions on 16 mm film in the form of an exposed bar whose length is proportional to the average speed for the exposure interval (30 minutes). Orientation of the instrument relative to magnetic north is similarly recorded on film also in the form of an exposed bar whose length is a measure of the direction variability during the 30 minute exposure interval and whose maximum intensity represents the average direction over the exposure interval. Speed and direction resolutions of 2.6 cm s^{-1} and ± 1°, respectively, are claimed by

the manufacturer. The Model 174's as configured for our studies recorded speed, direction, temperature, and conductivity on magnetic tape at 2 minute intervals. Speed and direction resolutions are 1 cm s^{-1} and 1.4°, respectively. Speed sensitivity of both instruments is approximately 1 rpm/1 cm s^{-1}; accuracy, or course, depends on calibration and in the case of the 105's, film reading errors.

The Braincon Model 1381 current meter records speed and direction on 16 mm film in a manner similar to the Endeco Model 105. It's suspension is part of the mooring, however, and it utilizes a Savonius rotor to sense speed. The rotor was stuck on B198 and data from B197 was not used for this study but was archived.

During both studies taut wire moorings were employed with approximately 49 pounds of buoyancy/meter. The moorings were anchored with railroad wheels. Figures 7 and 8 show the locations of the current meter moorings for the July 80 study and the March 81 study, respectively. Tables 3a and 3b list the meter locations by depth and station.

During July 1980 there was 100% data recovery from all meters except B198; on B198 the masking tape retainer on the rotor was apparently not removed on deployment. We were not so lucky during the March 1981 deployment. Within a few hours after deployment, the mooring at "F" was struck by a large vessel or towed barge. The mooring wire was severed near the surface meter separating the two Viny buoys that provided the buoyancy from the rest of the mooring causing the two meters to sink to the bottom. Meter 174109

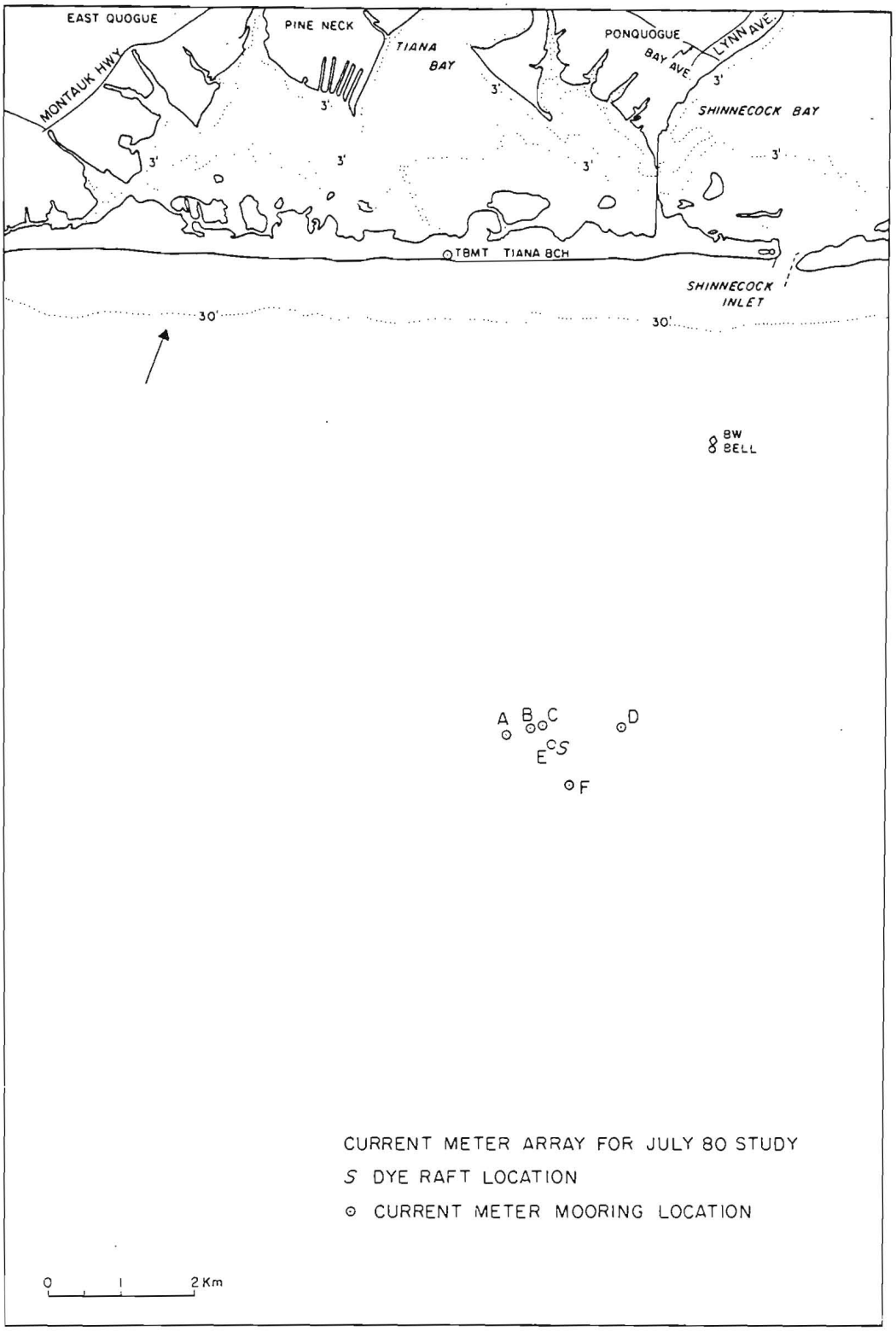

Figure 7. Chart showing current meter mooring locations during July 80 study.

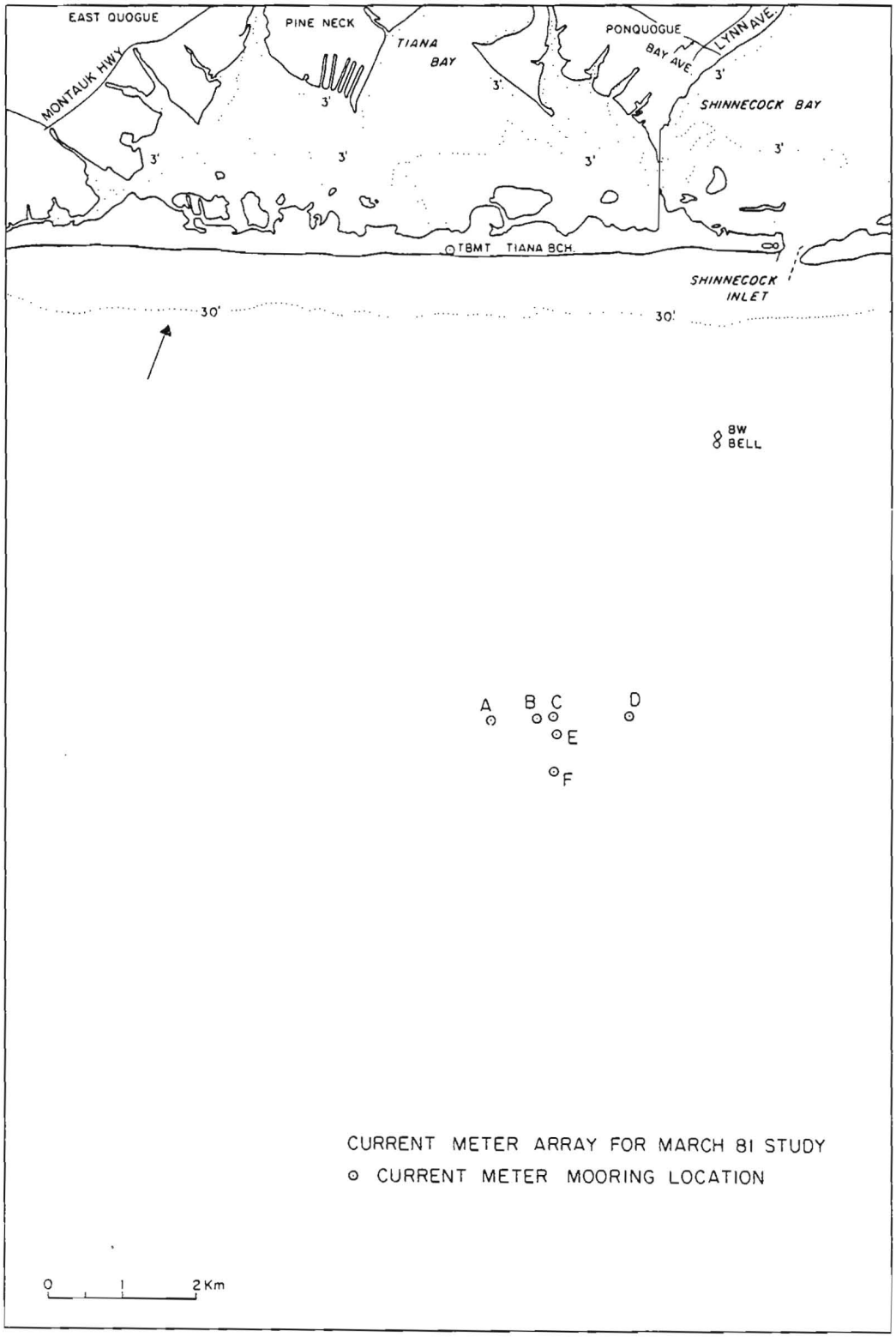

Figure 8. Chart showing current meter mooring location during March 81 study.

Table 3a

Current Meter Locations by Station and by Depth for the July 1980 Study

	Station					
Depth, m[#]	A	B	C	D	E	F
4.6	105314	174181	174107	105417	174183	105582
12.2	-	174109	174122	-	174112	-
18.3	-	-	B197	-	-	-
24.4	-	-	B198	-	-	-

Table 3b

Current Meter Locations by Station and by Depth for the March 1981 Study

	Station					
Depth, m[#]	A	B	C	D	E	F
4.6	174032	174107	174183	174181	174122	174109
12.2	105314	105437	174110	105587	105575	105421
18.3	-	-	105571	-	-	-
24.4	-	-	105312	-	-	-

[#] nominal; relative to MLW

was damaged beyond repair; 105421 was undamaged but provided only a record of 5 hours in length. In addition, 174110 was apparently torn from its mooring at Station "C" by a fishing boat recovering a gill net. Portions of the net were still on the mooring when it was recovered on 23 March, 1981. The meter was not recovered.

The Dye Studies

In the study of turbulent diffusion in natural systems, water soluble and dynamically passive fluorescent dyes have long been the standard method for quantifying the dispersive processes (Carter and Okubo (1978)). The technique consists of releasing a known quantity of dye solution either instantaneously (patch diffusion) or over time (plume diffusion) and measuring its subsequent distribution as a function of space and time. Thus, the required quantities to be measured are the concentration of the fluorescent dye and the position of the sampling vessel as a function of time.

For our experiments, position information was obtained with a Motorola Mini-Ranger III electronic positioning system. It is a range-range system, i.e., it measures the ranges from the sampling vessel to several (4 or less) reference stations. In our case, 2 reference stations were used, one mounted on the Shinnecock Inlet Light tower and the other on the Tiana Beach meteorological tower (TMBT) operated by Brookhaven National Laboratory. See Figure 7. Typically this system exhibits a range repeatability of ± 5 m. When calibrated its probable error is ±3.5 m.

Table 4a shows the concentration and amount of Rhodamine WT solution used, discharge start and end times, solution pumping rate, and discharge location for the July, 1980 study. Table 4b provides comparable information for the March, 1981 study. As noted earlier in Table 2, the dye solution was released continuously during the July 80 study at a depth of 0.5 m and as 3 separate instantaneous surface releases during March, 1981.

Table 4a

Details of the July, 1980 Dye Study

Date	Start of Discharge	End of Discharge	Solution Concentration	Solution Pumping Rate, g/s	Location of Discharge
7/21/80	1249	1359	20%	0.524	Identified as S on Figure 7
7/21/80	1811	-	-	-	
7/22/80	-	0740	20%	0.965	
7/22/80	0740	1735	20%	0.571	
7/22/80	1932	-	-	-	
7/23/80	-	0900	20%	0.362	
7/24/80	0735	-	-	-	
7/26/80	-	1630	20%	0.362	

NOTE: Rhodamine WT Lot 91 solution was discharged until 1735 on 22 July. Difficulty was encountered pumping this solution as it tended to coagulate and foul the metering pump. Pumping was halted at 1359 on 21 July and the solution filtered through a plankton net (100 μm mesh). After filtering, it pumped satisfactorily until 1735 on 22 July at which time the amount of Lot 91 on hand had been expended. Lot 96 was used thereafter with no further pump difficulties.

Table 4b

Details of the March 1981 Dye Study

Date	Time of Release	Solution Concentration	Mass of Dry Dye Released, g	Type of Release	Location of Release
3/10/81	0739	13.03%	7101.5	Surface	Near Mooring "B"
3/11/81	0739	13.03%	2434.9	Surface	Near Mooring "D"
3/12/81	0746	13.10%	2403.2	Surface	Near Mooring "C"

NOTE: All solutions were originally 20% RhWT (Lot 98) whose density was adjusted to 1.024 prior to deployment (our estimate of the density of the surface waters in the release area) by the addition of methanol.

During July, 1980 the concentrations of the dye tracer were determined by continuous underway sampling from the R/V ONRUST[1] at 3 depths with Turner Design Model 10 fluorometers. After filtering the fluorescence to remove the noise, the fluorometer outputs (fluorescence and scale) were fed to a specially constructed data logger with 4 channels for temperature and 4 channels for fluorescence/scale. It digitized these analog inputs (up to 4 channels of fluorescence, scale and temperature) and recorded them with ranges to the two Mini-Ranger reference stations every 2 seconds on magnetic tape and a printer (Anadex Model DP650). The thermistors for the temperature channels were located in poly-flo tubing just downstream from each fluorometer. All fluorometers were optically filtered on the input side so as to maximize the excitation energy appropriate for rhodamine (546 nm) and the emission energy on the output side (580 nm) while at the same time minimizing scattering of excitation light into the output side (minimal filter overlap between 546 and 580 nm).

[1]The R/V ONRUST is a 55' steel hull vessel of 50 tons.

The continuous underway samples were drawn by pumping through three one-half inch polyethylene hoses (poly-flo). The hoses were cut to the same length (approximately 25 m), married together to minimize drag, and then loosely coupled to the hydro wire with snap hooks. The hoses terminated at a heavy lead depressor (~66 kg). Hose separations varied between 1 and 4 m.

The set-up for the March 1981 study was identical except for the substitution of a Turner Associates Model 111 for one of the TD Model 10 fluorometers.

The fluorometers, data logger, etc. were calibrated as a system using a stainless steel tank as a reservoir and circulating sea water continuously through the flow cells of the fluorometers with an immersion pump. The tank was filled with 7 liters of sea water from the operating area and circulated through the fluorometers continuously. The fluorescence (in arbitrary units) and temperatures were then recorded on tape and printer as small additions of diluted rhodamine WT 20% solution ($\sim$ 1 to 211,117 for July and 1 to 222,136 for March) were made. For the July experiment our fluorometers were calibrated in terms of C/q_d where C is the dye concentration in gg^{-1} and q_d is the pumping rate of dry dye in $g\ s^{-1}$. In March we calibrated in terms of C/Γ where Γ is the concentration of the rhodamine solution released in gg^{-1}. As purchased, Γ is ~0.20; as released it was 0.1303 after addition of the methanol. By calibrating

in terms of these ratios, precise knowledge of Γ is not necessary. See Carter (1974).

The output of our fluorometers when filtered with a filter with a 4s time constant are stable and reliable to ±0.3% of full scale. (Pritchard *et al.* (1982)). For our instruments, this translates into ±0.3 dial units on the most sensitive scale (31.6×100 scale) or ±0.004 ppb during July and ±0.009 during March. Background variations of the coastal waters were found to be on the same order.

Aerial Photography

As noted previously, the fluorescent spectrum of Rhodamine WT has a maximum at 580 nm. The Wratten No. 21 sharp cut filter cuts off all light below 540 nm and its percent transmittance at wavelengths $\geq$ 580 nm is $\geq$ 85.4%. The use of this filter with any good panchromatic film yields excellent photographic results. The prints will show a white dye cloud on a black sea.

Funds were available for aerial dye photography for only one field study. Accordingly, the July, 1980 study period was selected since it included a continuous dye discharge thereby ensuring that at least a portion of the dye plume would always be discernable in the photographs. The Aerographics Corporation of Bohemia, NY was selected to carry out the photography. For this purpose, they provided a Wild RC8 aerial mapping camera mounted in a Cessna 180 aircraft. This camera has a focal length of 152 mm ($\sim$ 6") and vides a 9"×9" negative. It is in a fixed mount but it can be leveled

in flight within limits by means of a bubble to maintain a level altitude. On 22, 24, 25 and 26 July, 1980 (See Table 2) three flights were made in the AM and three in the PM with 2 runs per flight and 5-8 exposures per run. The runs were flown at different altitudes, i.e., negative scales; 1000' and 2000' (negative scales of 1" = 166.67' and 1" = 333.33', respectively) were used for the most part. In addition, an occasional run was made at altitudes of 1500' and 5000'.

Kodak Double-X Aerographic film No. 2405 (Spec. 981) was used throughout at an exposure time of 1/425 seconds and a lens aperture of f5.6. The film was developed in D76 and 9" × 9" prints provided on Ilsord paper. The resolution of this film is ~25μm (Kodak Publication No. M-75).

The Drogue Studies

Drogue Design

Twenty drifters were constructed. They consisted of polystyrene floats mounted on shafts made of galvanized iron pipe (electrical conduit). One end of the shaft was tethered to a cross vane drogue and the other end supported a freely swivelling aluminum flag. A diagram of the complete drifter and design details are given in Figure 9.

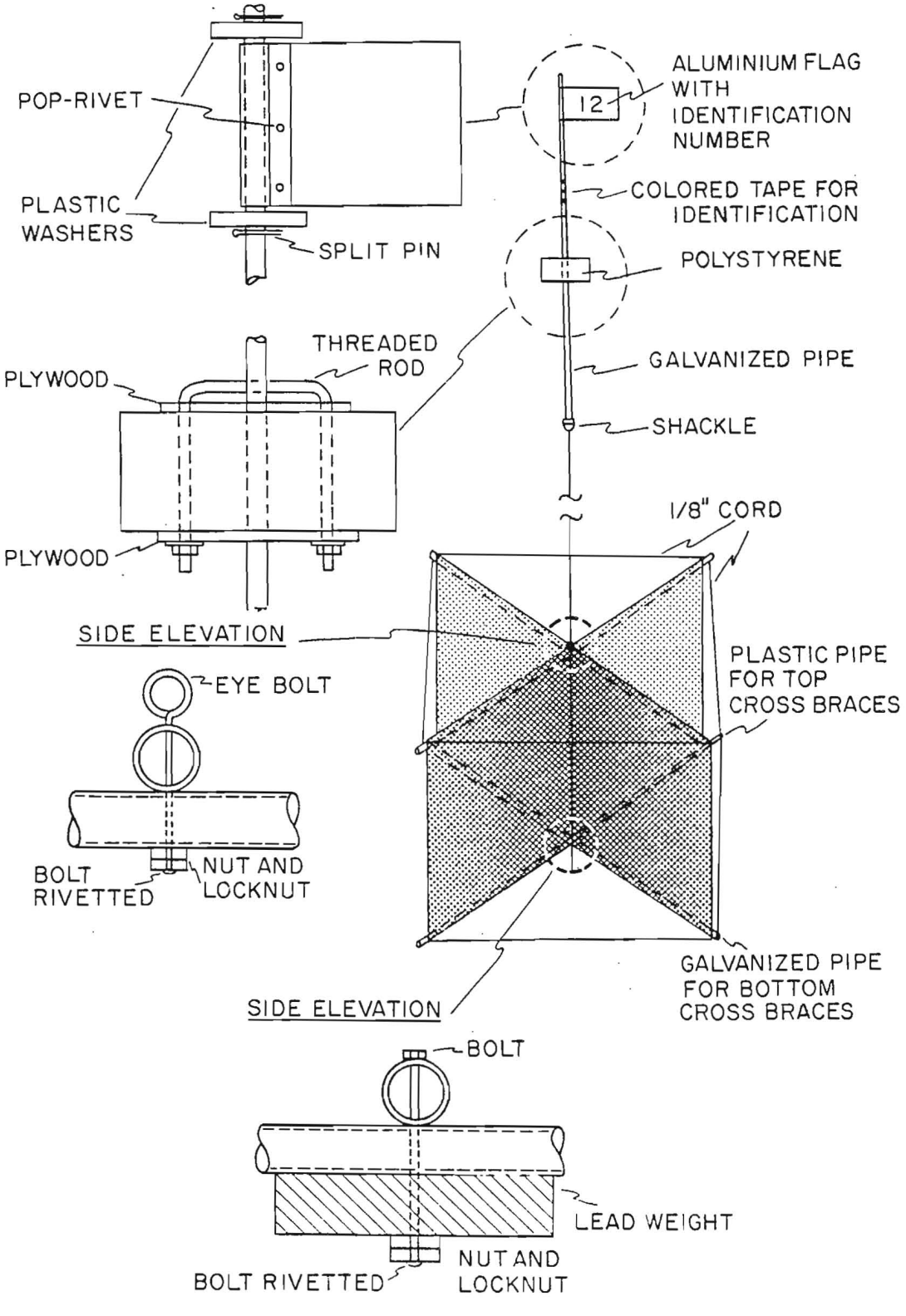

Figure 9. Details of drogue design.

The drifters generally performed adequately and none were lost or failed in any of the experiments. Drogues occasionally suffered small rips, mainly in the course of being retrieved or transported.

Methodology of Drogue Experiments

Drifters were deployed and tracked from two ∿ 20 foot power boats which were manned by two people; one to steer and the other to measure drifter positions and deploy and retrieve drifters. Stacking one drogue on top of the other allowed each boat to handle up to 10 drogues.

On arrival at the experimental site, which was generally upstream of the current meter array, all drogues were deployed as simultaneously as possible. Drifters were deployed at least 10 m from their nearest neighbor in order to minimize interaction between drogues. It usually took about ½ hour to deploy all the drifters. Both boats would then monitor the positions of all the drogues using a Motorola Mini-Ranger III system. Each boat chose its own route to circulate around the drogues. In general the position of each drifter was determined at intervals ranging from 5 to 15 minutes. Standard procedure consisted of positioning the boat so that the buoy brushed past the side of the boat that the Mini-Ranger antenna was fixed to. See Figure 10. Ranges to the shore stations were automatically printed out on strip paper (Anadex DP650 printer) along with the time at which the range was measured. The operator only had to add the drogues identifying number onto the printout. Several ranges were taken as the buoy was approached and a final range when the buoy and antenna were

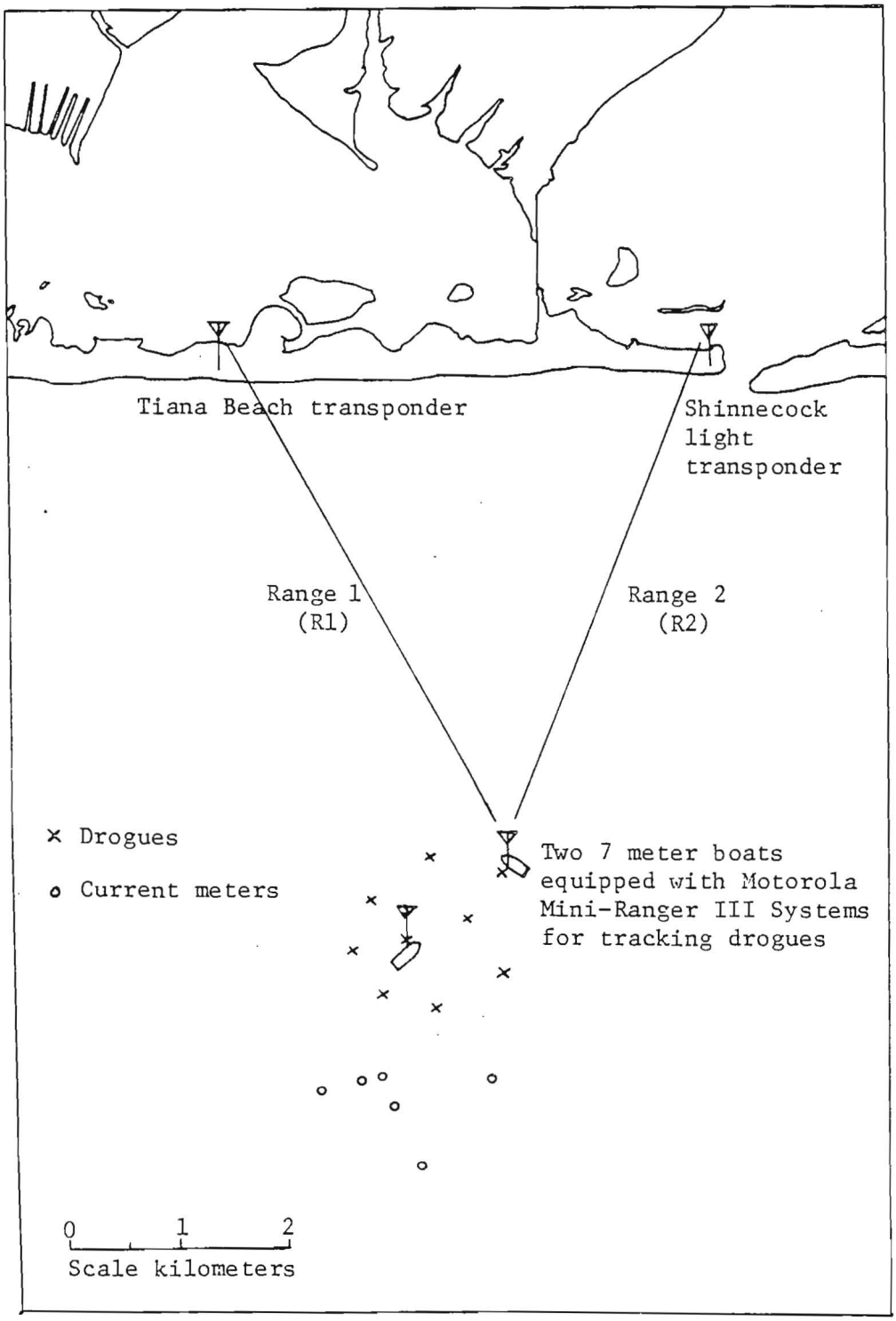

Figure 10. Schematic of drogue tracking.

Flags had identification numbers painted on them and were constructed of aluminum rather than cloth so that the flag would always be visible. Two large plastic washers ensured that the flag rotated freely with a minimum of wind drag. Bands of colored tape were used to encode the drifter number onto the shaft in case the flags were lost. The shaft and float top were both painted fluorescent orange.

Floatation consisted of several 1" thick slabs of polystyrene sandwiched between two pieces of plywood. The float was bolted to the shaft using a length of threaded steel rod. The drogue was attached to the shaft/float assembly with ¼" polypropylene rope clipped to a shackle bolted to the bottom of the shaft and an eye bolt on the top of the drogue.

The drogue was a cross vane type made of lightweight rip stop material. Its shape was formed using cross braces at the top and bottom that were held in a cross position by means of 4-pieces of 1/8 inch polypropylene rope tied around the ends of the braces. Plastic pipe was used for the top braces and the braces were bolted together, where they crossed, using an eye bolt. As noted above the eye bolt served as the fastening point for the drogue tether. Bottom cross braces were constructed of galvanized iron pipe and were bolted to a 5 lb lead weight where they crossed. The bottom braces were also tied in a rigid position using 1/8 inch polypropylene rope. Originally it had been planned to make the drogues collapsible and use clip on shock cord to hold their shape, however, this proved unworkable.

coincident (within the limits of maneuverability). By taking several approach ranges it was easy to identify gliches when the ranges were later typed into a computer. About 5-10% of the ranges were found to have spurious values. Often the approach ranges could be used to extrapolate a position when the fix was bad. Using a range averaging option resulted in a machine accuracy of ± 1 m according to the manufacturers. Of course the accuracy with which the boat could be positioned also contributed to errors which increased as the weather worsened. Relative motion between drogues due to systematic position measuring errors (such as the antenna always being on the boat side of the drifter) was minimized by always approaching a drogue from the same direction when fixing its position.

Drogue Experimental Program

The field work was performed about 3 miles off the south shore of Long Island in the vicinity of Shinnecock Inlet (Figures 1 and 10). The area was chosen in part for its linear shoreline and simple bottom topography. As shown in Table 2 experiments were carried out in July 1980 and March 1981, representative of summer and winter conditions respectively.

Throughout the summer experiment there was a relatively strong alongshore flow towards the west of about 15 cm s^{-1}. The summer thermocline was generally at 6-12 meters. The mean drift during the winter experiment was comparatively weak and the water column was well mixed. The sinking of a dye patch on 11 March, 1981 indicated that there were local regions of convergence.

Table 5 lists the essential details and purposes of all LEDS drifter experiments listed in the order in which they were performed. Additional information, comments, etc., are provided below.

Summer Experiments. Experiment #1 (21 July, 1980): This experiment was a shakedown experiment. Ten drifters were deployed with drogues at a depth of 15 feet. Each boat tracked five of the drifters. The method of tracking coupled with poor weather (5 foot swells) resulted in uneven coverage of the cluster. Regardless, useful data were obtained. A large initial elongation resulted from the drogues being poorly deployed in two almost distinct subclusters.

Experiment #2 (22 July, 1980): The crew of one of the small boats was needed to install new batteries for the Mini-Ranger shore stations. As a result, only 5 drifters were tracked by one boat from 1107 to 1433. Five additional drifters were deployed by 1433 and all ten drifters were tracked until 1547 when the experiment was called off because of bad weather. Winds were initially $\sim$ 10 knots from 240-270° and increased to 20 knots from 240-270° by 1500 hours. This data has not been processed yet because of the small number of drifters used for most of the experiment.

Experiment #3 (24 July, 1980): No experiments were carried out on 23 July due to rough weather. By 24 July, however, the seas were calm. Upon arriving at the current meter array, both boats measured the positions of the moorings. Each boat then deployed 7

Table 5. Details of LEDS Drifter Experiments

Experiment Designation Number	Date/Time of # First Position in Seconds after Midnight	Duration in ## Seconds after Midnight	Number of Drogues	Depth of Drogues feet	Comments
1	21 July 1980 43091	7,560	10	15	Single cluster
2	22 July 1980 40020*	12360/4440*	5/10	15	Single cluster initially 5 drogues with 5 more added after 12360 sec Not entered into computer
3	24 July 1980 30585	35,280	14	10	Single cluster
4S(small)	25 July 1980	6,120	8	10	Small cluster (4S) surrounded
4L(large)	34599	5,400	8	10	by larger cluster (4L)
5S(small)	25 July 1980	6,120	8	10	Small cluster (5S) surrounded
5L(large)	47539	6,120	8	10	by larger cluster (5L)
6S(small)	25 July 1980	2,880	8	10	Small cluster (6S) surrounded
6L(large)	60616	2,520	8	10	by larger cluster (6L)
7	26 July 1980 30960	12,540*	16	10	Consecutive releases from a current meter mooring
8S(shallow)	26 July 1980	4,320	7	10	Single cluster with drogues
8D(deep)	49420	4,680	9	15	at two depths
9	26 July 1980 55617	4,500	1	10	"Rapid" positioning on one drogue
10	9 March 1981 31685	18,600	20	15	Single cluster
11	10 March 1981 29227	21,600	20	15	Single cluster
12	11 March 1981 31840	10,200	20	15	Single cluster

Interpolated start time of experiment

Duration based on interpolated end time of experiment

* Based on times of deployment and retrieval.

drifters with drogues set at 10 feet. A 10 foot depth was selected so as to keep the drogues above the depth of the thermocline as measured by the R/V ONRUST. In doing so some comparability with current meter measurements was lost but comparability was gained with the dye experiments.

Initially each boat tracked the seven drogues that it released. After several hours, the method of tracking was changed so that each boat tracked all drifters. This method of tracking was used in all subsequent experiments.

The drifter cluster was tracked for $\sim$ 10 hours in which time it was swept far from the current meter array by the comparatively strong mean westerly drift. Rather than reposition the drogues within the array it was deemed desirable to obtain a long record for comparison with the dye plume and with the longer time scale information of the current meters.

Experiments #4S, 4L, 5S, 5L, 6S and 6L (25 July, 1980): Since the current meter array measured currents at several scales it was desirable to simultaneously measure the dispersion of drogues at different scales. In particular, it is important to measure the relationship between small and large scale velocity gradients, since for small time scales the divergence term dominates the diffusivity in describing the dispersion of drifters (Okubo *et al.* (1983) (in preparation)). It should be noted that generally the dye is released, or discharged at a "point" and so dye patch (or plume) scales corresponded generally to the scales of the small drifter clusters.

On the other hand, the size of the largest triad in the current meter array was as large or larger than the larger drifter clusters.

All drogues were set at a depth of 10 feet. First, a small scale cluster of 8 drifters were released and tracked by one boat at the upstream end of the current meter array. Then, the other boat released a much larger array of 8 drifters about the small array. Each boat then tracked the drifters that it released until the cluster has passed through the current meter array, at which point the experiment was repeated. The experiment was repeated three times hence the 6 different experiment numbers in Table 5. The larger scale cluster generally had linear dimensions $\sim$ 10 times as great as the smaller scale cluster.

Experiments #7, 8S, 8D and 9 (26 July, 1980): The first experiment (#7) to be carried out on this day consisted of consecutive releases of 16 drogues at a point 4-5 meters downstream from current meter mooring "D". Drifters had drogues set at 10 feet. The first drifter was released at 0836. Drifters were released from the same point at 10 minute intervals with the exception of two occasions when the timing of the release went awry. First one boat released its drifters and then the other. As each boat released its drifters the other tracked full time. When all drifters had been released both boats tracked all drifters for over an hour. This experiment had three objectives: (1) to relate the envelope of the drogue trajectories to the standard deviation in the lateral direction (σ_y) of the dye plume, (2) to estimate a cross-correlation function,

and (3) to provide a series of drifter velocities at a current meter site for comparison with the current meter record. This last objective is an important one, expecially since most drifter measurements for the LEDS summer experiments were at depths of 10 feet whereas the current meters were at a depth of 15 feet.

After the sequential release experiment, a two-depth experiment was performed. Nine drifters with drogues set at 15 feet and 7 drifters with drogues set at 10 feet were deployed in a single cluster at the eastern end of the current meter array. All drifters were deployed by 1315 and both boats tracked all drifters as they drifted through the current meter array. The deep cluster is referred to as experiment #8S. This experiment enabled us to measure the variability in both velocity gradients and diffusivities with depth and provided an estimate of the vertical shear. This latter quantity is important for comparing the dye and drifter results.

For the final experiment (#9), one drogue was tracked by one boat for a little more than an hour. Positions were obtained at better than 1 minute intervals. This experiment was performed in order to examine how much aliasing the normally less frequent position measurements caused.

Winter Experiments. Experiments #10, 11, and 12 (9, 10, 11 March, 1980): For these experiments the drogues were set at 15 feet since this was the depth of the uppermost current meters and also because there was no stratification that would confine the dye to

a shallow layer. Each winter experiment consisted of a single cluster of 20 drifters. The drifters were tracked by two small boats as during the summer experiments. The objective was to get as long a time series as possible for comparison with current meter records and dye patch measurements. The winter experiments were all essentially similar and so are not discussed individually.

Data Reduction. As noted above, raw drogue positions were obtained using two small powerboats equipped with Mini-Rangers. The boats would come alongside each drifter in turn and fix its position. The position was obtained from the two ranges to two reference stations, one at the Tiana Beach Meteorological Tower (TBMT) and the second at the Shinnecock Inlet Light Tower (Figures 1 and 10).

For the summer experiments the data were reduced to simultaneous positions of all drogues at 360 second intervals using linear interpolation of the time series of each drogues positions.

The raw data of the winter experiments, however, was found to have some systematic errors. In the course of the winter experiments three different Mini-Rangers were used; for experiments 10 and 11 Mini-Rangers 1 and 2 were used and for experiment 12 Mini-Rangers 1 and 3 were used.

Mini-Ranger 3 (a rental unit) was not calibrated correctly and its ranges differed from those measured by Mini-Ranger 1 by several

hundred meters. Fortunately, in the course of drogue tracking, there were 14 occasions when Mini-Rangers 1 and 3 measured the ranges to the same drogue at almost the same time (to within ± 20 seconds). A linear regression of ranges measured by Mini-Ranger 3 as a function of ranges measured by Mini-Ranger 1 (at almost the same time) enabled functions to be defined to correct the ranges of Mini-Ranger 3.

A further error that was more difficult to correct was also found. Mini-Ranger 2 drifted relative to Mini-Ranger 1 by about 20 meters in the course of the experiments. Mini-Ranger 3 was also found to drift but only by about 4 meters. The drift of one Mini-Ranger relative to another was found as a function of time in the following way. Simultaneous ranges for all the drogues were calculated using a cubic spline interpolation of ranges measured with Mini-Ranger 1 and then with ranges measured with Mini-Ranger 2 or 3. Since there were 20 drogues it was possible to calculate the mean and standard deviation of the difference between the range as measured by each Mini-Ranger as a function of time. These values are plotted in Figure 11 for experiments 10, 11, and 12. The mean differences were then used to correct ranges measured by Mini-Rangers 2 and 3.

After all processing the winter data consisted of simultaneous observations of positions on 20 drogues at intervals of 600 seconds.

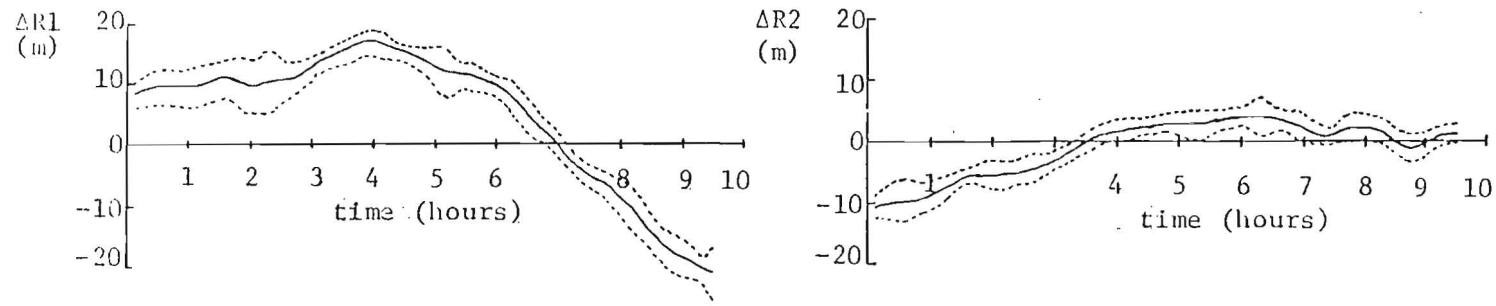

LEDS Experiment 10 (9 March 1981)

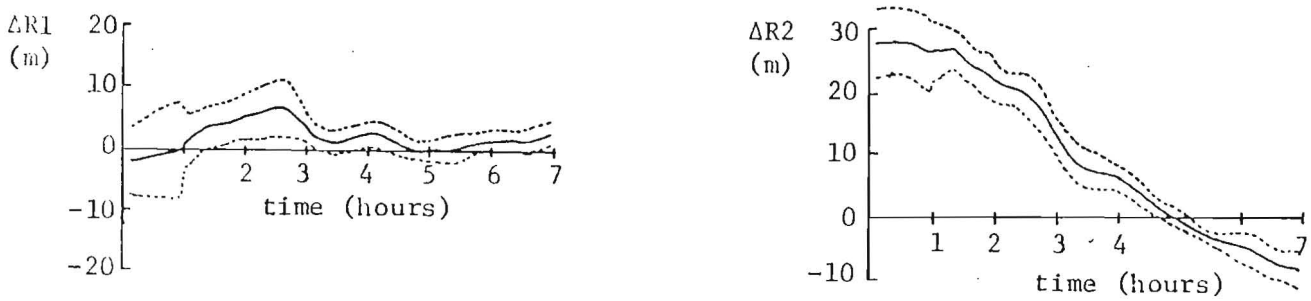

LEDS Experiment 11 (10 March 1981)

LEDS Experiment 12 (11 March 1981)

Figure 11. Root mean square differences between the range measured by one Mini-Ranger and that measured by the other as a function of time. R1 is range to TBMT; R2 is range to Shinnecock Light.

RESULTS

The Current Meter Studies

Eulerian data from both the July 1980 and March 1981 deployments were processed initially with the objective of examining some of the basic characteristics of the temporal and spatial structure of the velocity field. Special attention was paid to those characteristics which should be relevant to dispersion processes. These include the spectra of the velocity fluctuations, the principal axis orientation for velocity fluctuations of different periods, the coherency of the velocity fluctuations measured by instruments of different horizontal positions and the vertical shear measured by instruments at different depths on the same mooring. In general, records from both individual instruments and from pairs of instruments were analyzed in terms of rotational invariants (Mooers (1973)). One distinct advantage of this type of analysis is that the spectral quantities which are defined are independent of coordinate system; another is that the interpretation of cross spectra computed for pairs of horizontal velocity series is greatly simplified.

The basic methods used in the calculation of rotational invariants depend on the fact that a velocity vector can be decomposed, for each frequency, into a counterclockwise rotating (positive frequencies) vector and a clockwise rotating (negative frequencies). For these rotating vectors it is convenient to compute the auto spectrum for both positive and negative frequencies and the normalized difference,

that is, the spectral density for positive frequencies minus the spectral density for negative frequencies divided by the sum. This quantity is called the rotary coefficient; it will be zero for pure rectilinear oscillations, and plus or minus one for circular counter-clockwise or clockwise oscillations, respectively. Elliptical oscillations are represented by values between zero and one. The two auto spectra and the rotary coefficient are, therefore, useful for describing the distribution of variance and the rotational characteristics of the velocity vector as a function of frequency.

For elliptical and rectilinear oscillations the stability of the orientation of the axes of the oscillation can be defined in terms of the magnitude of the coherency between the clockwise and counterclockwise rotating vectors; similarily, the orientation of the principal axes can be defined in terms of the phase of the coherency (Mooers (1973)).

It should be mentioned that for several reasons related to data quality the ENDECO 105 records were not processed to the same extent as the ENDECO 174 records. One obvious problem with the ENDECO 105 records is the 1 hour Nyquist period; another very serious problem is associated with "wrap around", a film reading and speed calibration problem which can introduce artificial variance into the records with periods of a few hours.

July 1980 Deployment

Rotational invariants were computed for each of the current velocity records from the July 1980 deployment; only the invariants

computed for the ENDECO 174's are presented. A common 11.4 day record segment beginning on 14 July was extracted from each current vector file. The actual files were somewhat longer but the extracted files contained 8192 points which was convenient for FFT processing.

Mean values for the components of the current vectors resolved along 345°T and 45°T are presented in Table 6. Mean vectors at both 4.6 m and 12.2 m indicate some cross-isobath onshore flow. The mean direction of isobaths in the area is approximately along 69°T.

Figures 12 through 17 show for each of the instruments on moorings B, C and E the positive and negative auto spectra, the rotary coefficient, the magnitude of the coherency between positively and negatively rotating vectors and the phase of the coherency. The phase represents the orientation of the principal axis of the elliptical oscillation relative to the positive x axis. Note that all figures have a common logarithmic frequency axis, and that the frequencies are normalized by the Nyquist frequency which is .25 minutes^{-1}. The ordinate for both the negative auto spectrum (Figure A) and the positive auto spectrum (Figure B) is plotted on a logarithmic scale as relative spectral density in units of cm^2s^{-2} per unit frequency. The ordinate for the rotary coefficient (Figure C) is plotted on a linear scale and it is nondimensional. The coherency (Figure D) is, of course, nondimensional, and as mentioned above it provides an estimate of the stability of the principal axes defined in Figure E. The principal axes can be considered stable when the coherency is above the 95% significance level which is defined by the dashed line.

Table 6

Components of mean currents (cm s^{-1}) for an 11.4 day record beginning on 14 July, 1980. x component is positive along 045°T; y component is positive along 345°T.

	STATIONS		
Depth (m)	B	C	E
	Meter #174181	Meter #174107	Meter #174183
4.6	$\begin{pmatrix} -16.7 & -x \\ 5.8 & -y \end{pmatrix}$	$\begin{pmatrix} -12.9 & -x \\ 8.1 & -y \end{pmatrix}$	$\begin{pmatrix} -15.2 & -x \\ 6.6 & -y \end{pmatrix}$
	Meter #174109	Meter #174122	Meter #174112
12.2	$\begin{pmatrix} -13.5 & -x \\ 5.8 & -y \end{pmatrix}$	$\begin{pmatrix} -11.9 & -x \\ 6.2 & -y \end{pmatrix}$	$\begin{pmatrix} -11.8 & -x \\ 7.4 & -y \end{pmatrix}$

Table 7

Components of mean currents (cm s^{-1}) for an 11.4 day record beginning on 27 February, 1981. x component is positive along 045°T; y component is positive along 345°T.

	STATIONS			
Depth (m)	B	C	D	E
	Meter #174107	Meter #174183	Meter #174181	Meter #174122
4.6	$\begin{pmatrix} -4.6 & -x \\ 0.9 & -y \end{pmatrix}$	$\begin{pmatrix} -4.4 & -x \\ 1.6 & -y \end{pmatrix}$	$\begin{pmatrix} -3.9 & -x \\ 1.4 & -y \end{pmatrix}$	$\begin{pmatrix} -4.2 & -x \\ 0.7 & -y \end{pmatrix}$

Table 8

Components of mean current shear (s^{-1}) for an 11.4 day record beginning on 14 July, 1980. x component is positive along along 045°T; y component is positive along 345°T.

	STATIONS		
Depth (m)	B	C	E
4.6	$\begin{pmatrix} -6.9\times10^{-3} & -x \\ 3.9\times10^{-5} & -y \end{pmatrix}$	$\begin{pmatrix} -2.1\times10^{-3} & -x \\ 4.0\times10^{-3} & -y \end{pmatrix}$	$\begin{pmatrix} -7.5\times10^{-3} & -x \\ -1.8\times10^{-3} & -y \end{pmatrix}$

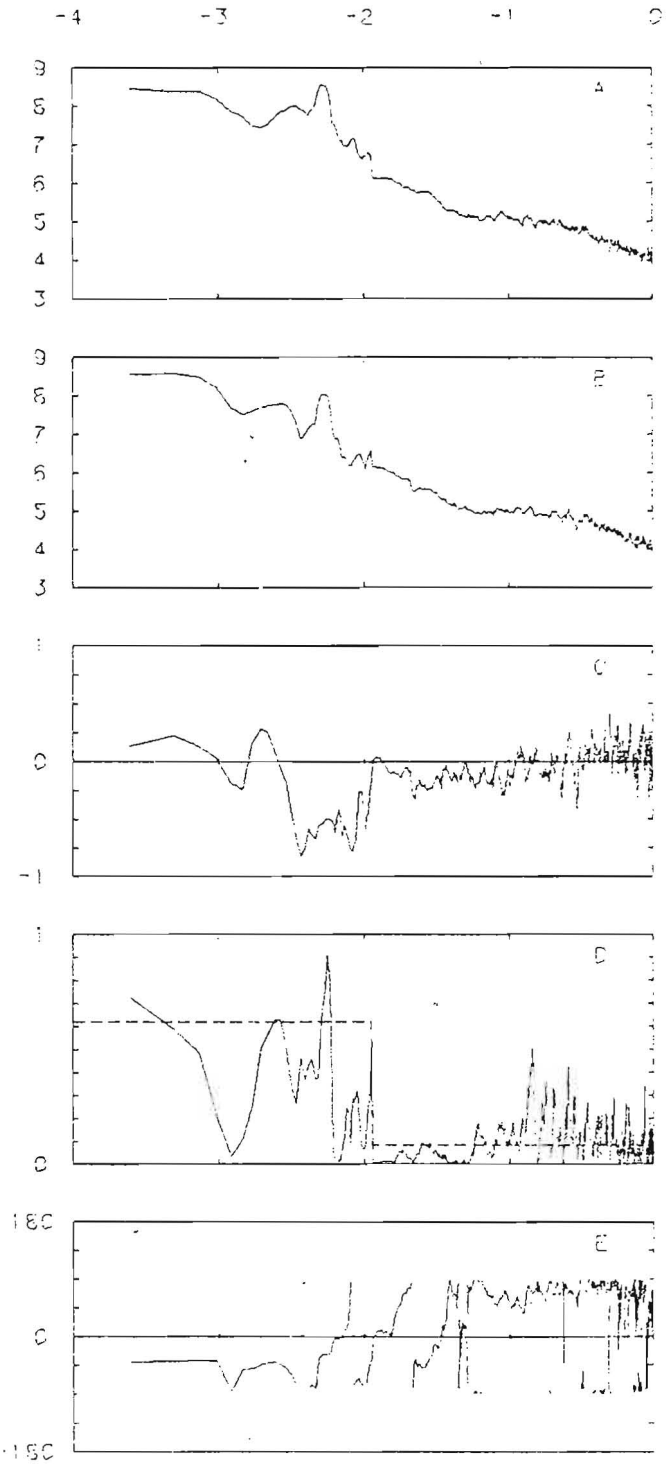

Figure 12.

Rotational invariants for an 11.4 day record beginning on 14 July, 1980 from Meter #174181 deployed at 4.6 m: auto spectrum for negative frequencies (Figure A); auto spectrum for positive frequencies (Figure B); rotary coefficient (Figure C); ellipse stability (Figure D); ellipse orientation (degrees) (Figure E). Degrees of freedom are 8.2 and 12.6 for periods less than and greater than 6 hours, respectively.

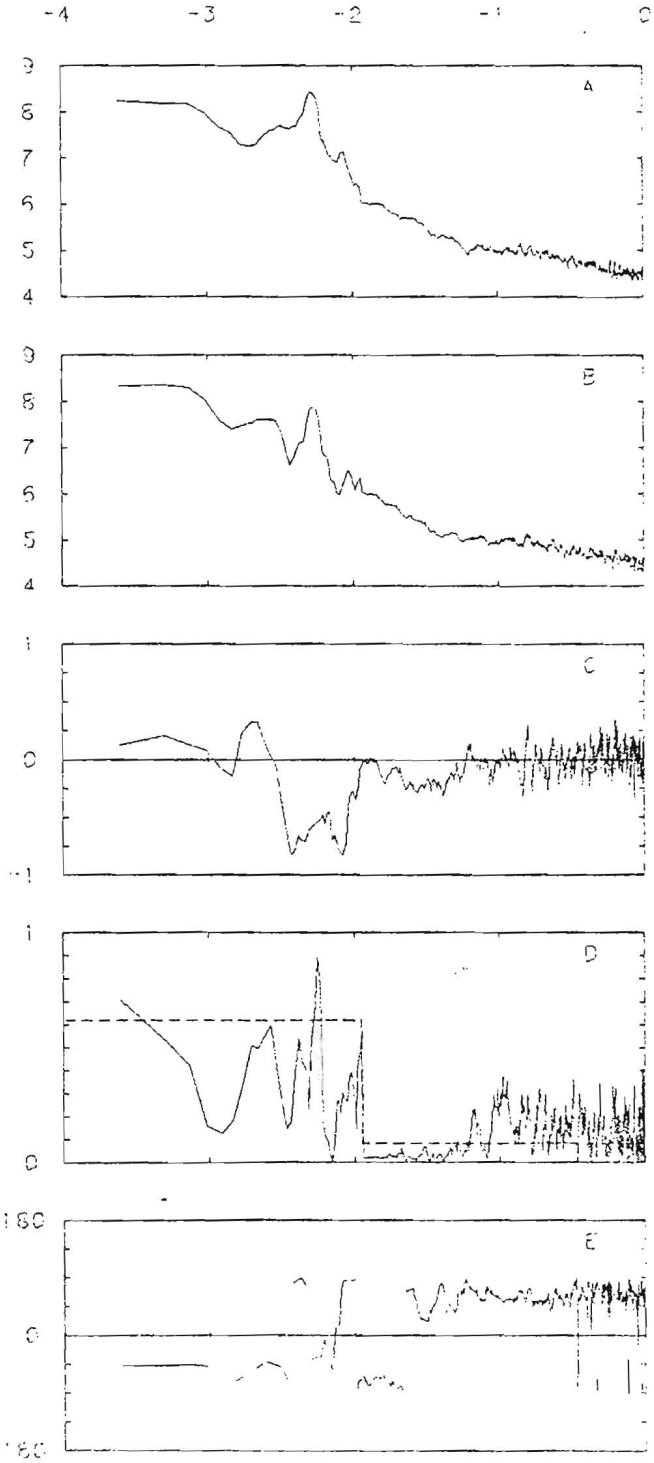

Figure 13.

Rotational invariants for an 11.4 day record beginning on 14 July, 1980 from Meter #174107 deployed at 4.6 m: auto spectrum for negative frequencies (Figure A); auto spectrum for positive frequencies (Figure B); rotary coefficient (Figure C); ellipse stability (Figure D); ellipse orientation (degrees) (Figure E). Degrees of freedom are 8.2 and 12.6 for periods less than and greater than 6 hours, respectively.

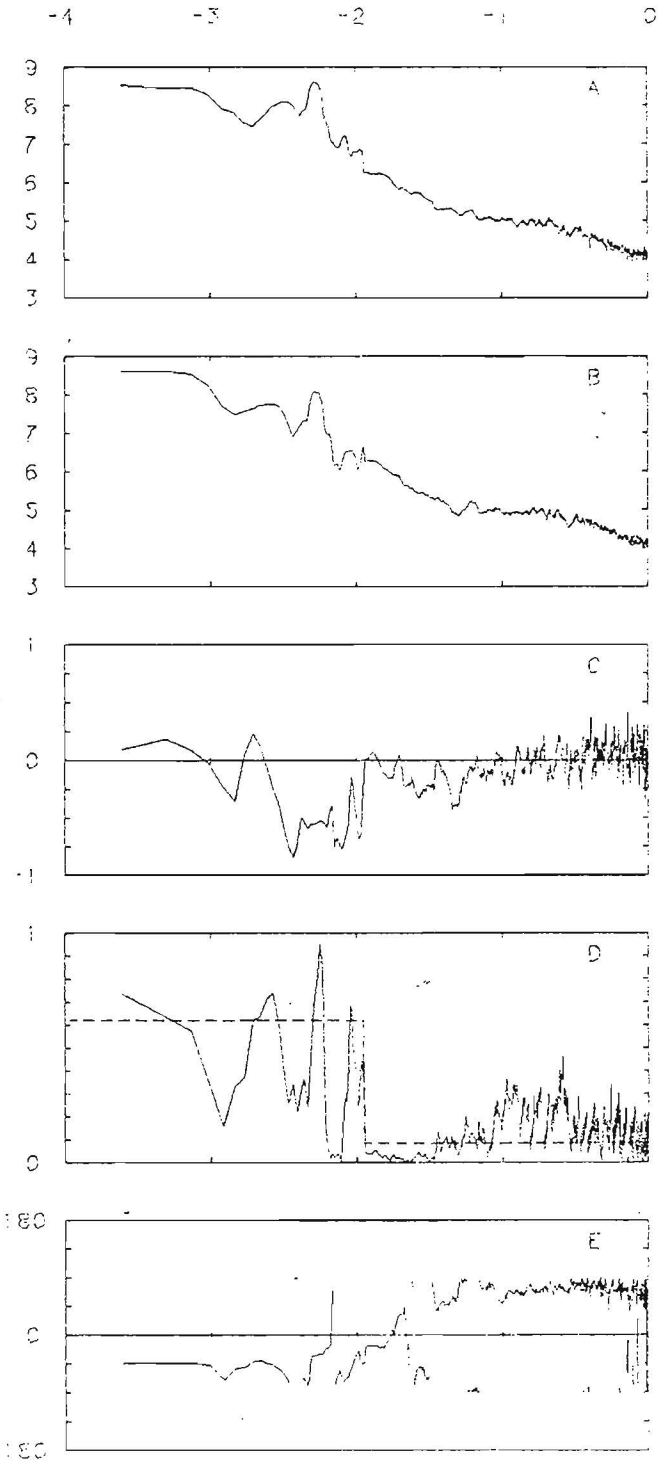

Figure 14.

Rotational invariants for an 11.4 day record beginning on 14 July, 1980 from Meter #174183 deployed at 4.6 m: auto spectrum for negative frequencies (Figure A); auto spectrum for positive frequencies (Figure B); rotary coefficient (Figure C); ellipse stability (Figure D); ellipse orientation (degrees) (Figure E). Degrees of freedom are 8.2 and 12.6 for periods less than and greater than 6 hours, respectively.

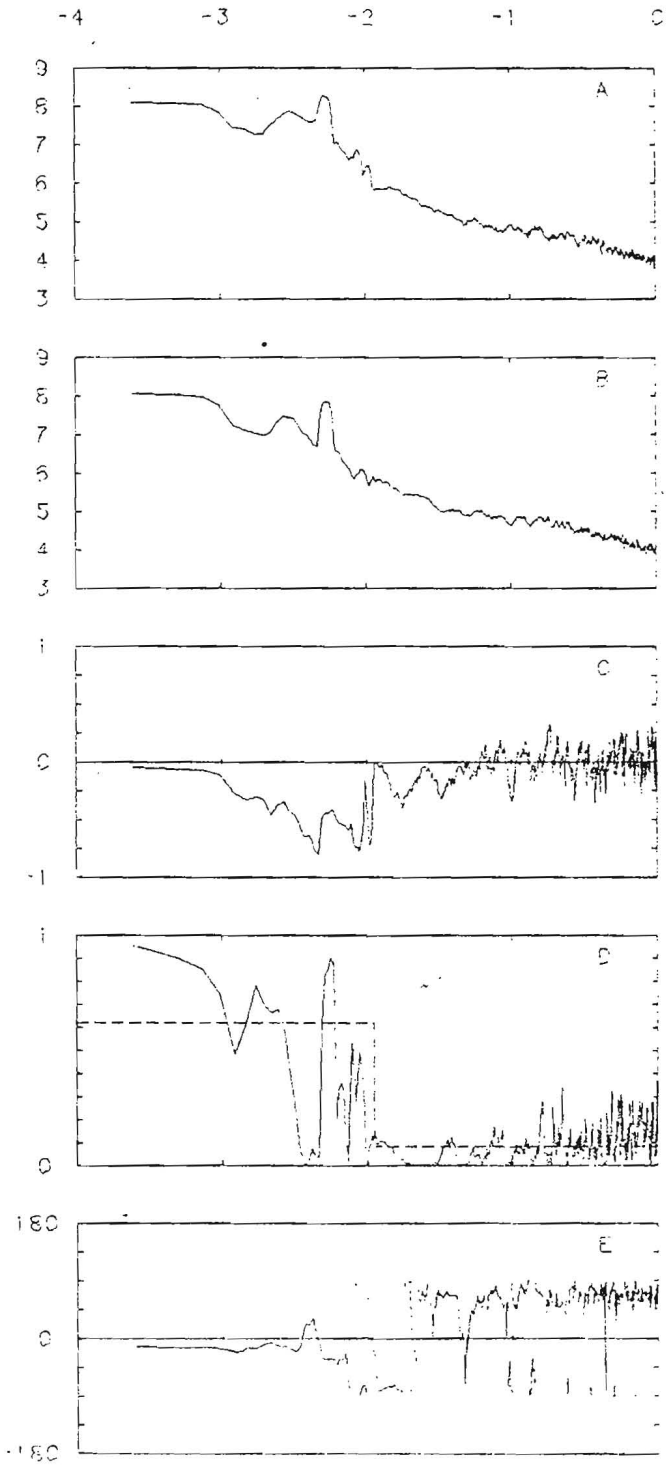

Figure 15.

Rotational invariants for an 11.4 day record beginning on 14 July, 1980 from Meter #174109 deployed at 12.2 m: auto spectrum for negative frequencies (Figure A); auto spectrum for positive frequencies (Figure B); rotary coefficient (Figure C); ellipse stability (Figure D); ellipse orientation (degrees) (Figure E). Degrees of freedom are 8.2 and 12.6 for periods less than and greater than 6 hours, respectively.

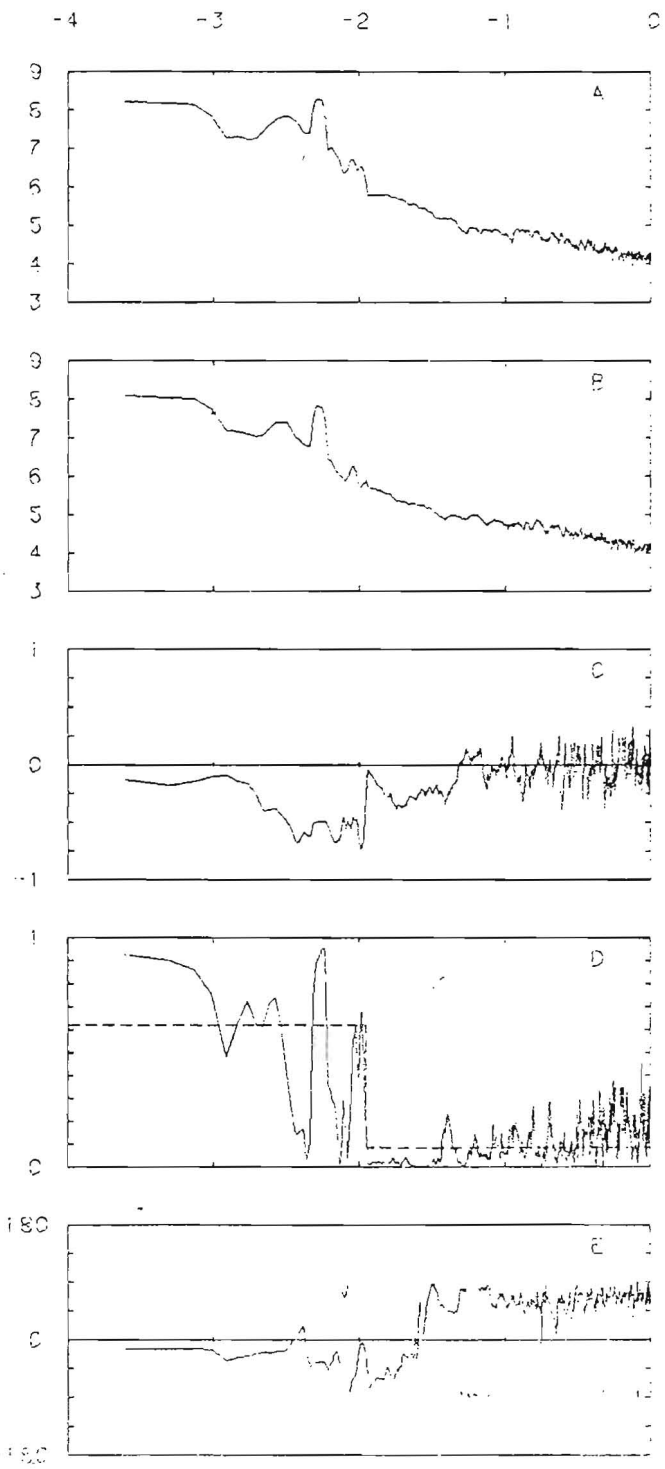

Figure 16.

Rotational invariants for an 11.4 day record beginning on 14 July, 1980 from Meter #174122 deployed at 12.2 m: auto spectrum for negative frequencies (Figure A); auto spectrum for positive frequencies (Figure B); rotary coefficient (Figure C); ellipse stability (Figure D); ellipse orientation (degrees) (Figure E). Degrees of freedom are 8.2 and 12.6 for periods less than and greater than 6 hours, respectively.

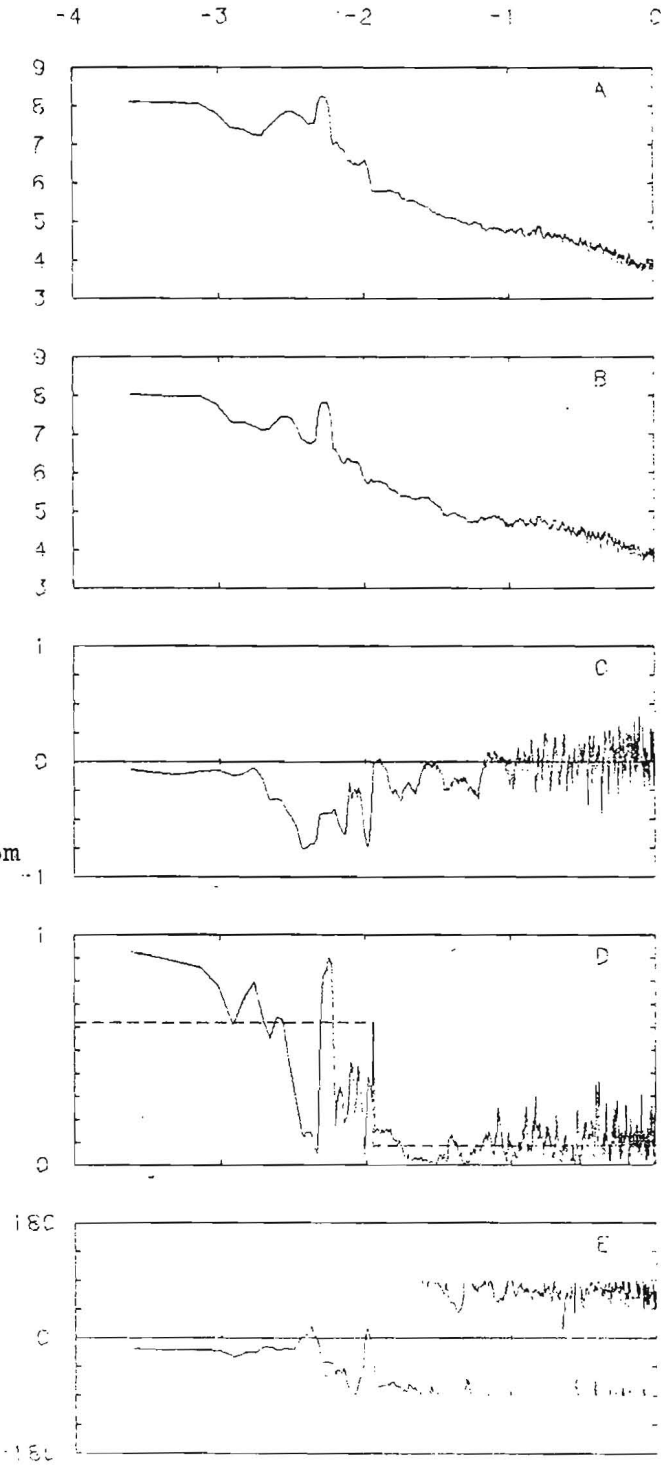

Figure 17.

Rotational invariants for an 11.4 day record beginning on 14 July, 1980 from Meter #174112 deployed at 12.2 m: auto spectrum for negative frequencies (Figure A); auto spectrum for positive frequencies (Figure B); rotary coefficient (Figure C); ellipse stability (Figure D); ellipse orientation (degrees) (Figure E). Degrees of freedom are 8.2 and 12.6 for periods less than and greater than 6 hours, respectively.

Note that the 95% significance level is not constant because a spectral window was used for smoothing the spectral estimates at periods longer or shorter than six hours. At periods longer than six hours the degrees of freedom are approximately 8.2, while at periods shorter than six hours the degrees of freedom are approximately 22.6. The principal axis orientation (Figure E) is a rotation measured in degrees *(positive when counterclockwise)* relative to 045°T. Current records were resolved along 045°T and 315°T because these axes were well off the local isobath orientation.

The spectral and rotational characteristics for the velocity vectors at the upper meters are all quite similar (Figures 12 through 14). For those oscillations at subtidal frequencies which have a stable axis the phase associated with the coherency varies between approximately -40° and -48°. The principal axis orientations, therefore, vary from 85°T to 93°T. Remembering that the heading of the isobaths is approximately 069°T, this implies that the principal axes of the subtidal current fluctuations are oriented at 16° to 24° relative to the isobaths. There is, therefore, appreciable cross isobath flow at low frequency; the mean current vectors for the upper meters in Table 6 are oriented approximately 0° to 10° relative to the isobaths. However, because of low frequency variability in the current the uncertainty in the mean estimates is very high.

The principal axes for low frequency oscillations at 12.2 m depth (Figures 15 through 17) show a counterclockwise veering from those at 4.6 m depth. The phase estimates at low frequency in Figures 15 through 17 vary from approximately -14° to -17° which means that the principal axes orientations vary from 059°T to 062°T. This again implies cross isobath flow at low frequency, but the component of flow normal to the isobaths would have a sign opposite to that at 4.6 m.

Figures 12 through 14 show that at those supertidal frequencies where the coherency (Figure D) is above the significance level the phase for the coherency is approximately +60°. This means that the principal axes for these shorter period oscillations is oriented at 345°T which is approximately normal to the isobaths. The principal axes for super tidal oscillations at 12.2 m depth are also oriented approximately normal to the isobaths (Figures 15 through 17).

The ellipse stability diagrams for all six instruments show that semidiurnal oscillations have a very stable principal axis; its orientation varies from approximately 075°T to 080°T. The rotary coefficient for these oscillations is approximately -0.4.

Figures 12 through 14 also show that diurnal oscillations have marginally stable principal axes whose orientation is very similar to that of the very low frequency oscillations discussed earlier. These records are not long enough, however, to resolve the characteristics of diurnal and even inertial oscillations properly. The

characteristics of these oscillations will be discussed in connection with the March 1981 deployment which produced a number of records which were roughly twice as long as the July records.

Before proceeding to a discussion of the March 1981 deployment some of the characteristics of the coherency between different pairs of instruments will be discussed. This provides some limited information on the spatial structure of the velocity field, but as will be shown it is critical to the interpretation of velocity gradients computed for groups of current meters.

Figures 18 through 23 show the coherency and phase between pairs of current meters at 4.6 m depth for both corotating vectors (called the inner coherency) and counterrotating vectors (the outer coherency). Coherencies and phase are plotted on two frequency scales, one of which has been expanded to provide increased resolution at low frequency. General features which are common to all of the coherency plots are an inner coherency which is much higher than the outer coherency, very small phase lag for the inner coherency at low frequency, and a frequency dependent phase lag for both inner and outer coherency at shorter periods. These phase characteristics would suggest that the very low frequency velocity fluctuations are associated with long wave phenomena and that the shorter period fluctuations could be eddies convected through the array by the lower frequency motions.

An estimate for the magnitude of the component of the convection velocity for the shorter period fluctuations along the line between

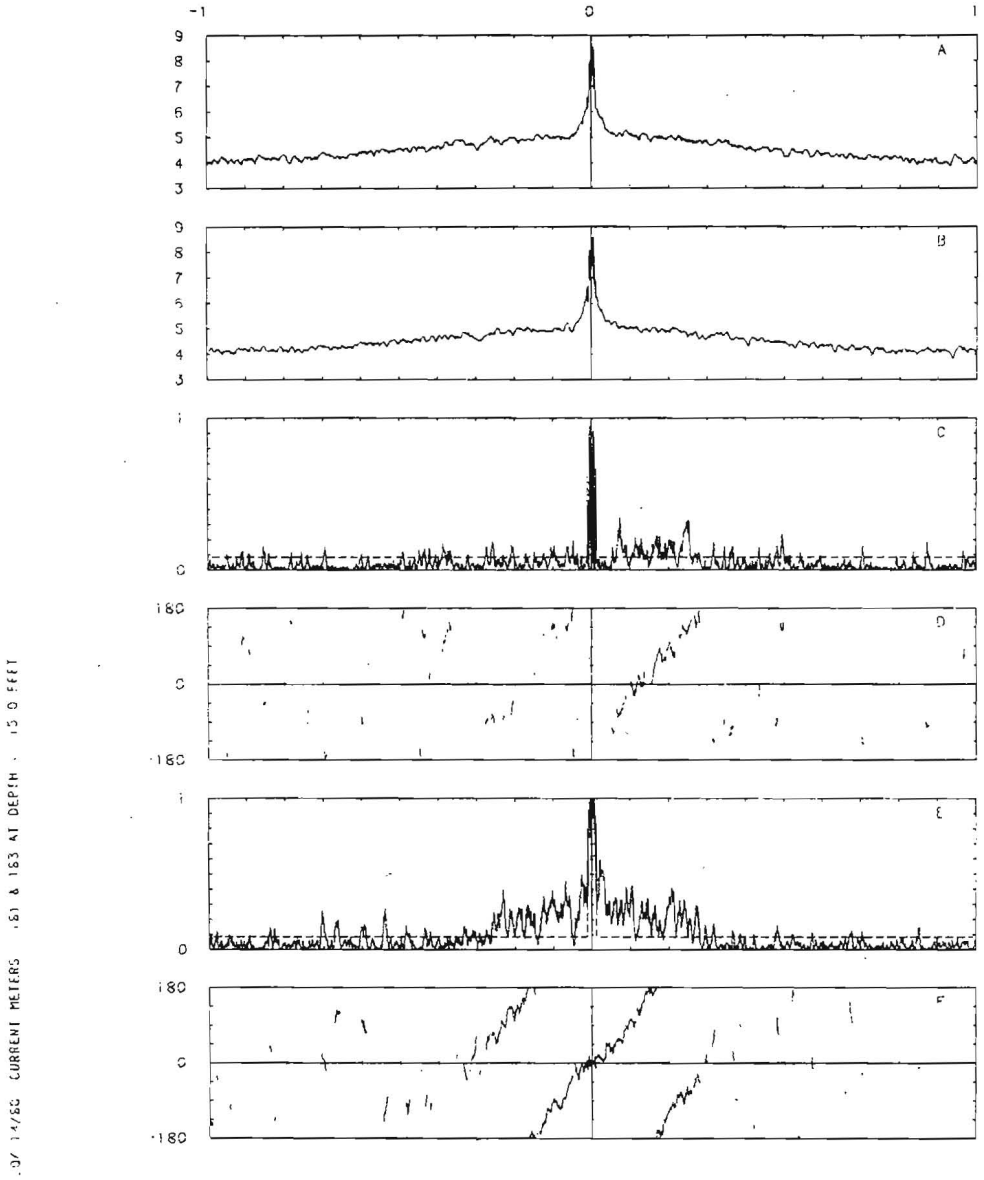

Figure 18. Rotational invariants for 11.4 day records beginning on 14 July, 1980 for meters deployed at 4.6 m: auto spectra for Meters #174181 and #174183 (Figures A and B), outer coherency squared and phase (Figures C and D), inner coherency squared and phase (Figures E and F). Degrees of freemom are 8.2 and 82.6 for periods less than and greater than 6 hours. Frequency scale is linear; values are normalized by the Nyquist frequency which is $4.17 \times 10^{-3} s^{-1}$.

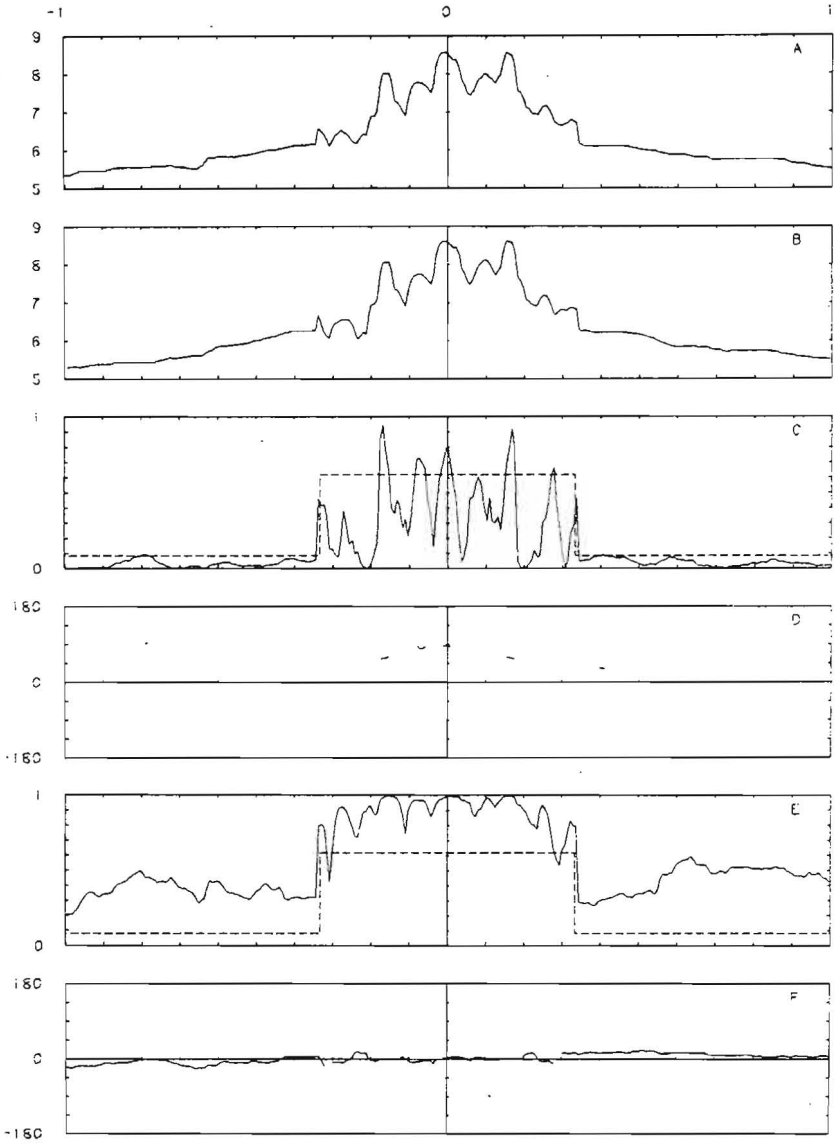

Figure 19. Rotational invariants for 11.4 day records beginning on 14 July, 1980 for meters deployed at 4.6 m: auto spectra for Meters #174181 and #174183 (Figures A and B), outer coherency squared and phase (Figures C and D), inner coherency squared and phase (Figures E and F). Degrees of freedom are 8.2 and 82.6 for periods less than and greater than 6 hours. Frequency scale is linear; values are normalized by the Nyquist frequency which is $1.39 \times 10^{-4} s^{-1}$.

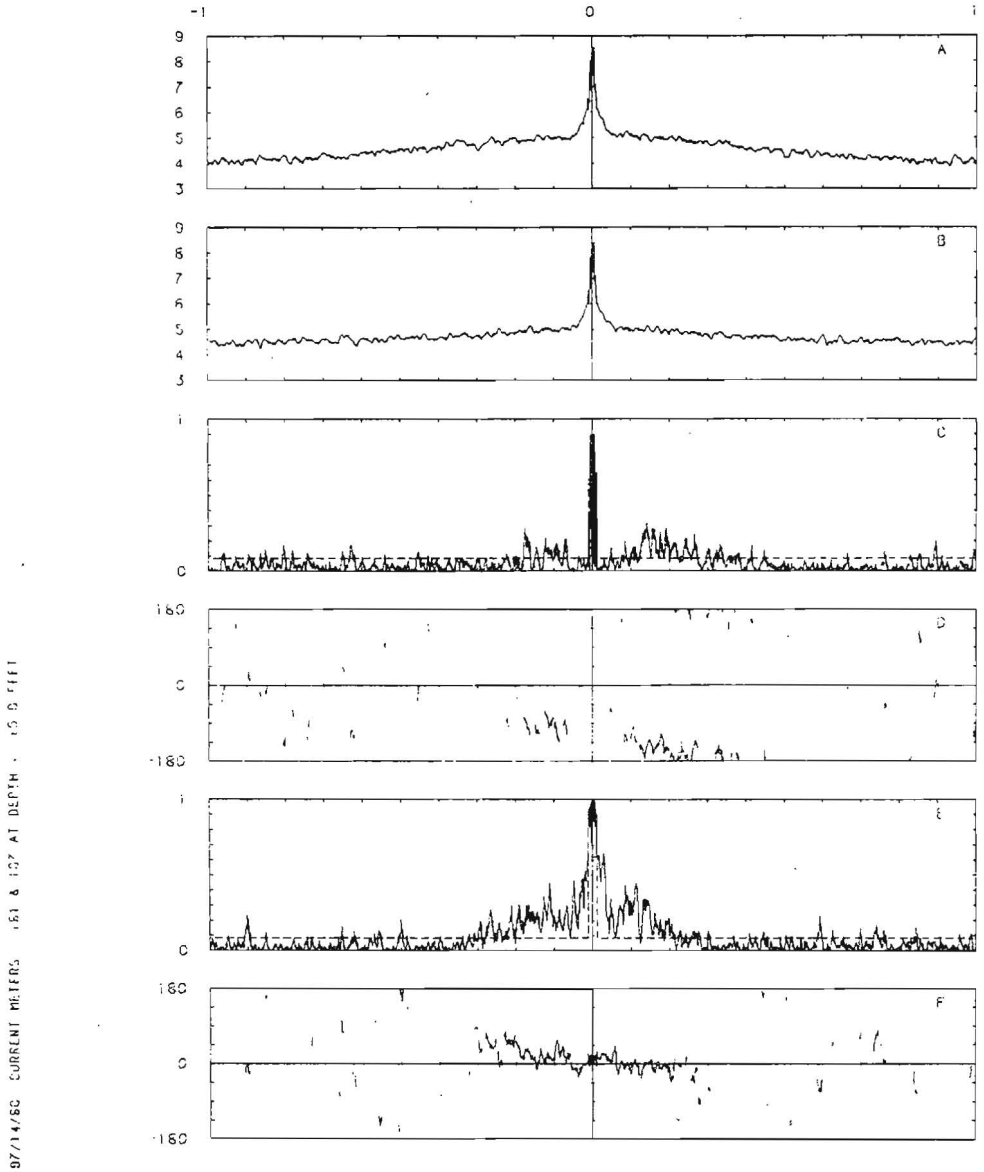

Figure 20. Rotational invariants for 11.4 day records beginning on 14 July, 1980 for meters deployed at 4.6 m: auto spectra for Meters #174181 and #174107 (Figures A and B), outer coherency squared and phase (Figures C and D), inner coherency squared and phase (Figures E and F). Degrees of freedom are 8.2 and 22.6 for periods less than and greater than 6 hours. Frequency scale is linear; values are normalized by the Nyquist frequency which is $4.17 \times 10^{-3} s^{-1}$.

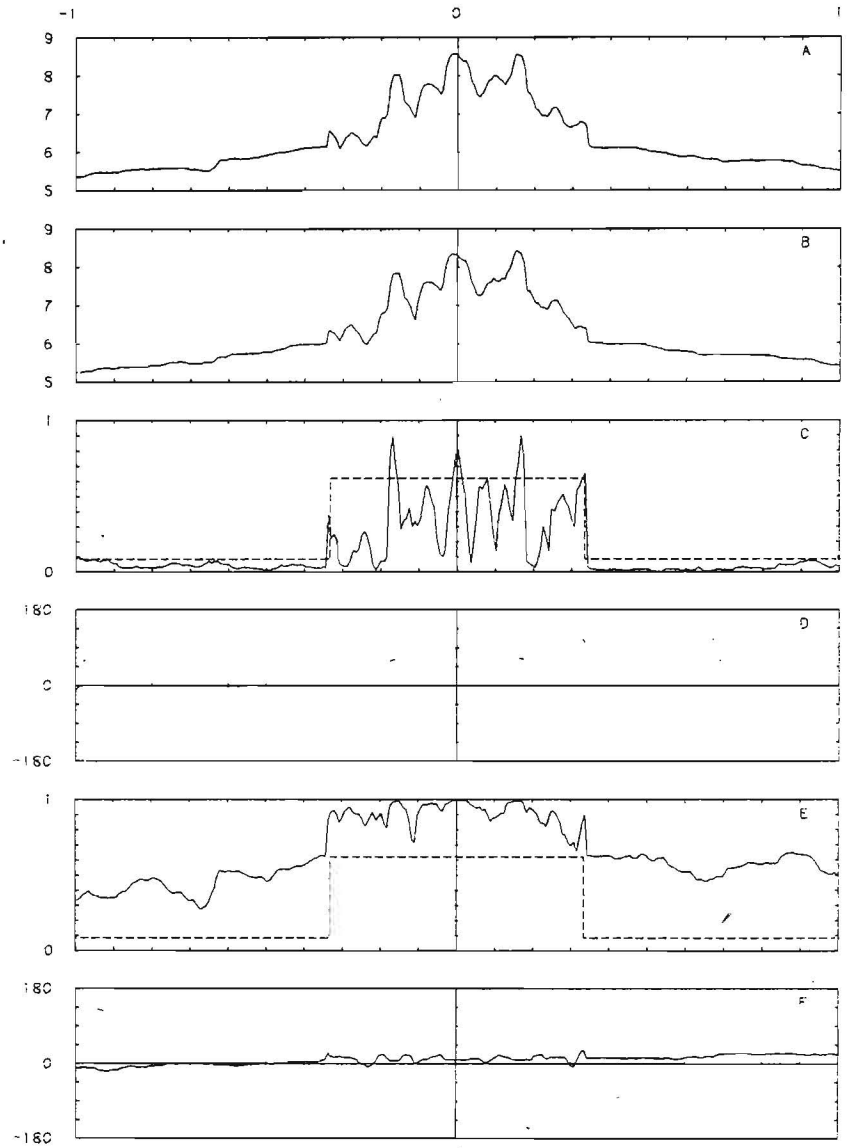

Figure 21. Rotational invariants for 11.4 day records beginning on 14 July, 1980 for meters deployed at 4.6 m: auto spectra for Meters #174181 and #174107 (Figures A and B0, outer coherency squared and phase (Figures C and D), inner coherency squared and phase (Figures E and F). Degrees of freedom are 8.2 and 22.6 for periods less than and greater than 6 hours. Frequency scale is linear; values are normalized by the Nyquist frequency which is $1.39 \times 10^{-4} s^{-1}$.

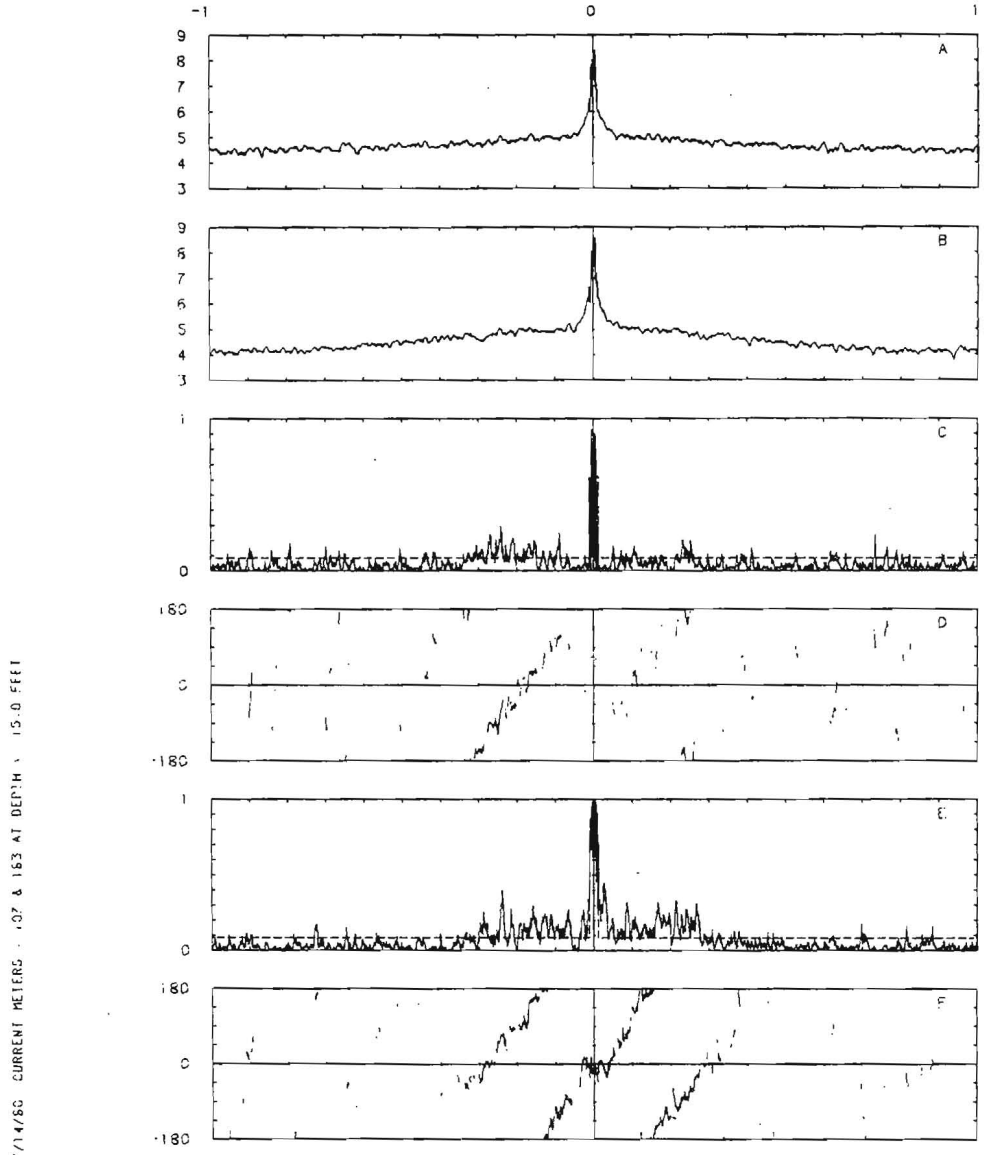

Figure 22. Rotational invariants for 11.4 day records beginning on 14 July, 1980 for meters deployed at 4.6 m: auto spectra for Meters #174107 and #174183 (Figures A and B), outer coherency squared and phase (Figures C and D), inner coherency squared and phase (Figures E and F). Degrees of freedom are 8.2 and 22.6 for periods less than and greater than 6 hours. Frequency scale is linear; values are normalized by the Nyquist frequency which is $4.17 \times 10^{-3} s^{-1}$.

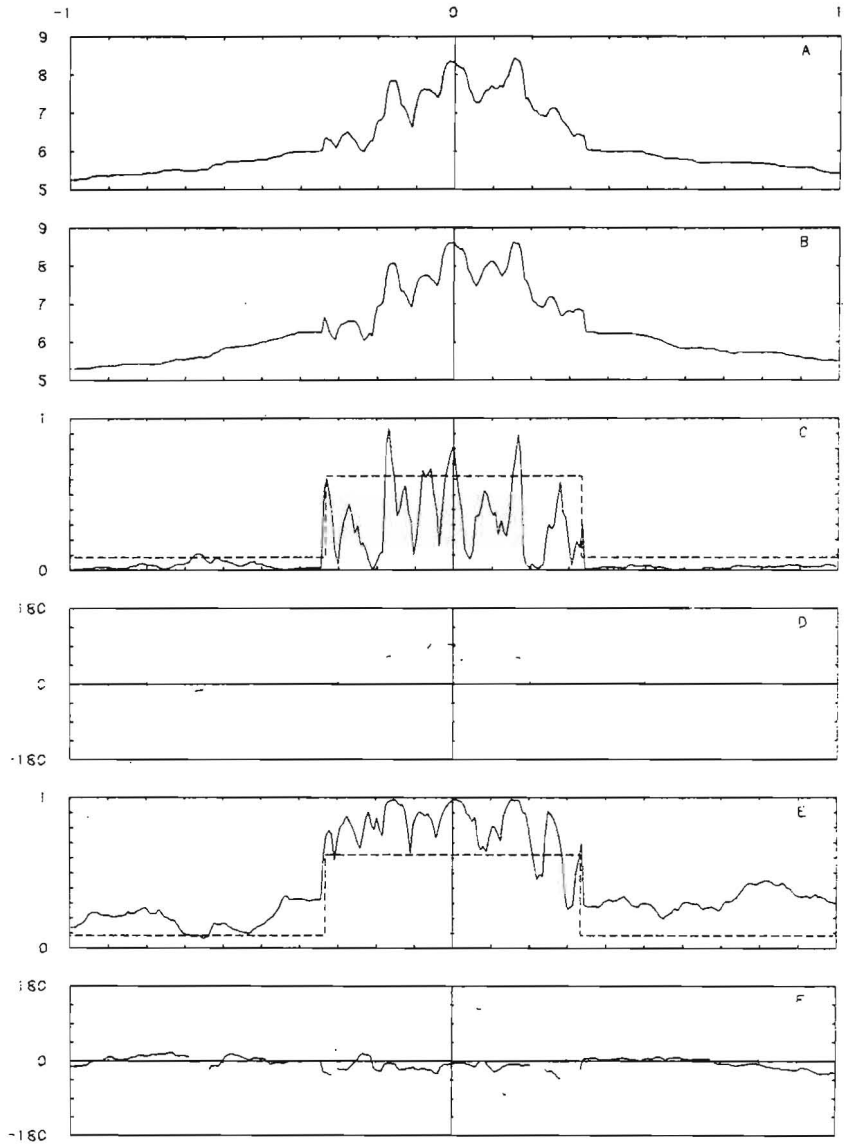

07/14/80 CURRENT METERS : 107 & 183 AT DEPTH = 15.0 FEET

Figure 23. Rotational invariants for 11.4 day records beginning on 14 July, 1980 for meters deployed at 4.6 m: auto spectra for Meters #174107 and #174183 (Figures A and B), outer coherency squared and phase (Figures C and D), inner coherency squared and phase (Figures E and F). Degrees of freedom are 8.2 and 22.6 for periods less than and greater than 6 hours. Frequency scale is linear; values are normalized by the Nyquist frequency which is $1.39 \times 10^{-4} s^{-1}$.

two instruments can be obtained from the rate of change of phase angle with frequency. Figures 18 through 23 suggest that velocity fluctuations with periods between approximately 6 hours and 13 minutes are produced by convected disturbances. The magnitude of the convection velocity is approximately 48 cm s^{-1} (approximately equal to the rms tidal current velocity) and its direction is similar to that of the principal axes of the tidal and lower frequency oscillations discussed earlier.

The inner coherencies tend to fall below the 95% significance level rather abruptly at a period of approximately 13 minutes. Using the convection velocity determined earlier a wavelength of approximately 375 m can be estimated for the velocity fluctuations with a period of 13 minutes; this is of the order of the array dimensions.

The coherency and phase relationships between pairs of instruments at 12.2 m (Figures 24 through 29) are quite similar to those for corresponding pairs of instruments at 4.6 m in Figures 18 through 23. The fluctuations are highly coherent and in phase (phase lag for the inner coherency is nearly zero) at very low frequencies, and they remain coherent with phase lag increasing with frequency up to a period of approximately 13 minutes, suggesting that both the long period wave like disturbances and the shorter period convected disturbances are not strong functions of depth.

In general, it should be noted that spectral and cross spectral estimates were calculated for 11.4 day records. Spectral characteristics for shorter records could vary significantly. The

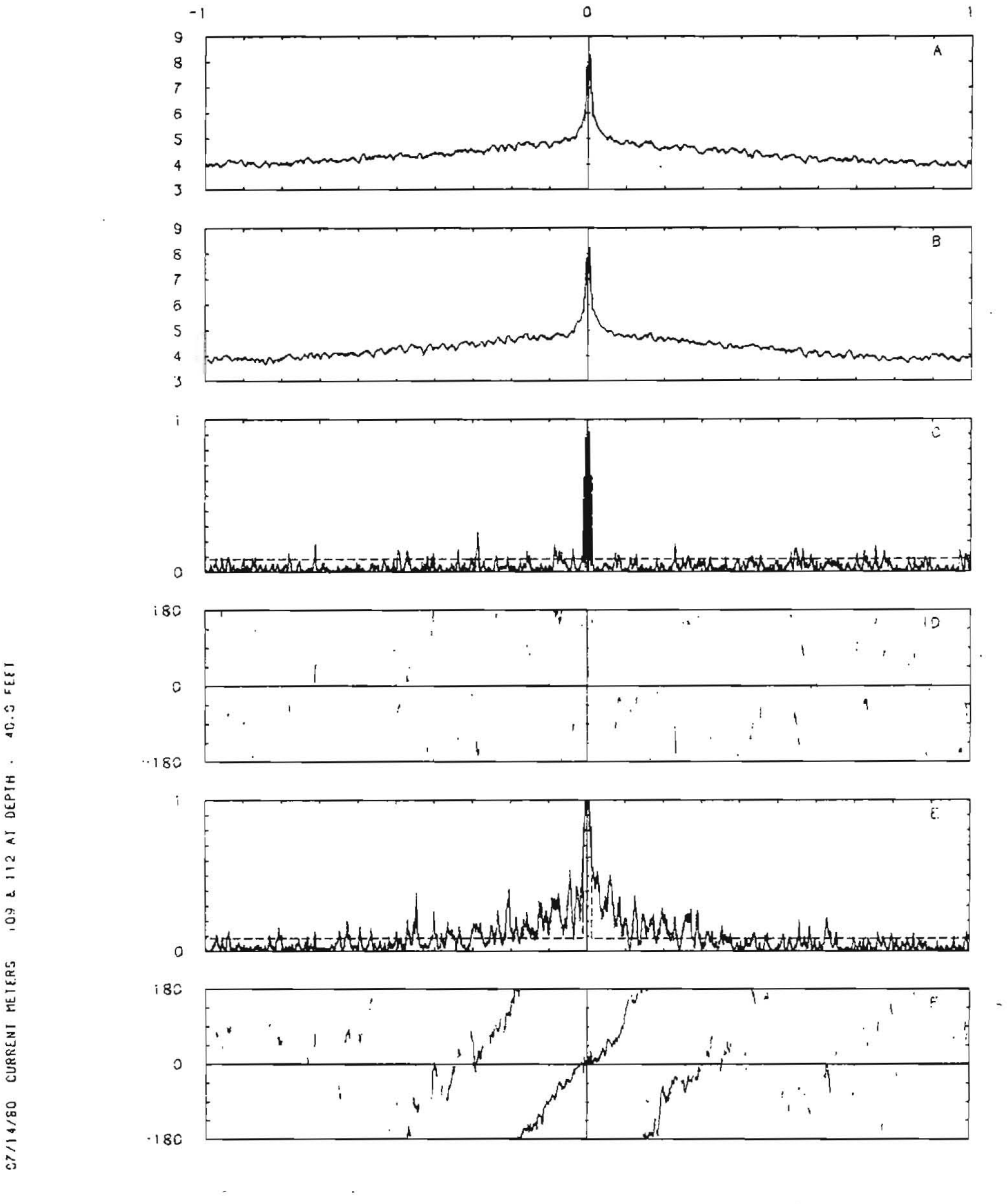

Figure 24. Rotational invariants for 11.4 day records beginning on 14 July, 1980 for meters deployed at 12.2 m; auto spectra for Meters #174109 and #174112 (Figures A and B), outer coherency squared and phase (Figures C and D), inner coherency squared and phase (Figures E and F). Degrees of freedom are 8.2 and 22.6 for periods less than and greater than 6 hours. Frequency scale is linear; values are normalized by the Nyquist frequency which is $4.17 \times 10^{-3} s^{-1}$.

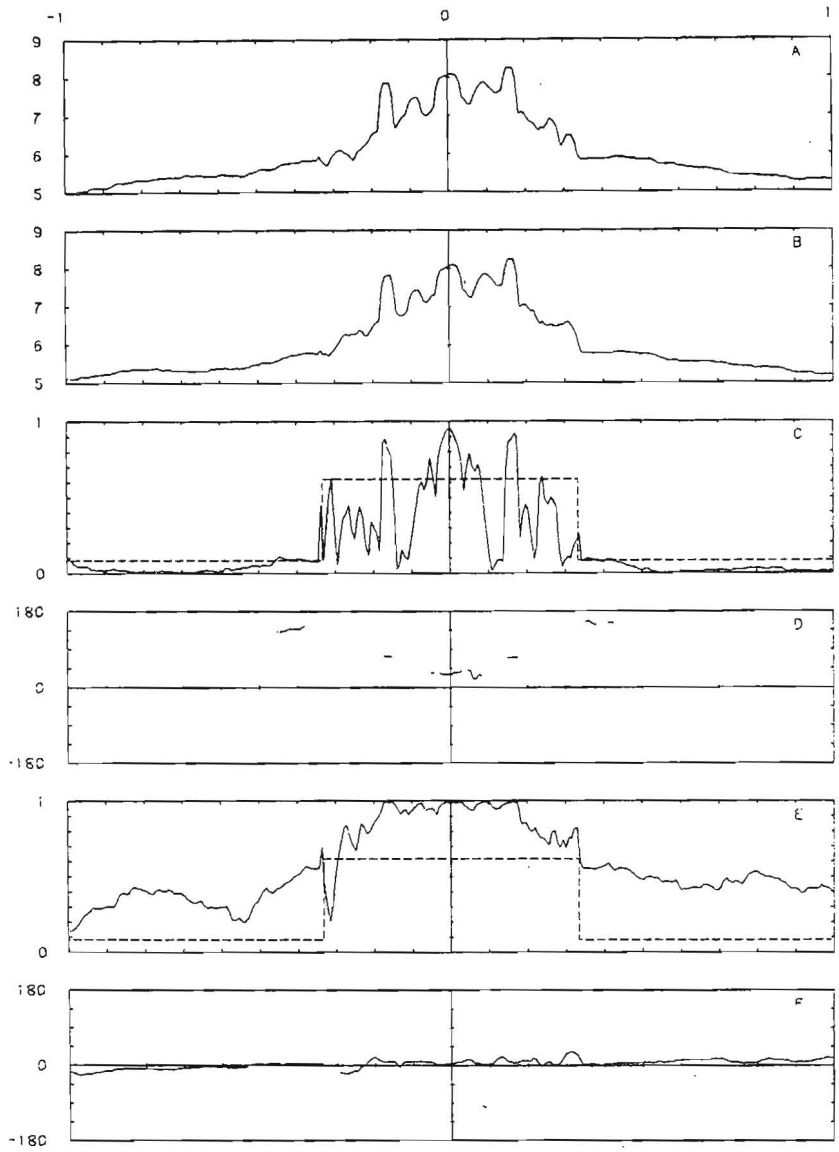

Figure 25. Rotational invariants for 11.4 day records beginning on 14 July, 1980 for meters deployed at 12.2 m: auto spectra for Meters #174109 and #174112 (Figures A and B), outer coherency squared and phase (Figures C and D), inner coherency squared and phase (Figures E and F). Degrees of freedom are 8.2 and 22.6 for periods less than and greater than 6 hours. Frequency scale is linear; values are normalized by the Nyquist frequency which is $1.39 \times 10^{-4} s^{-1}$.

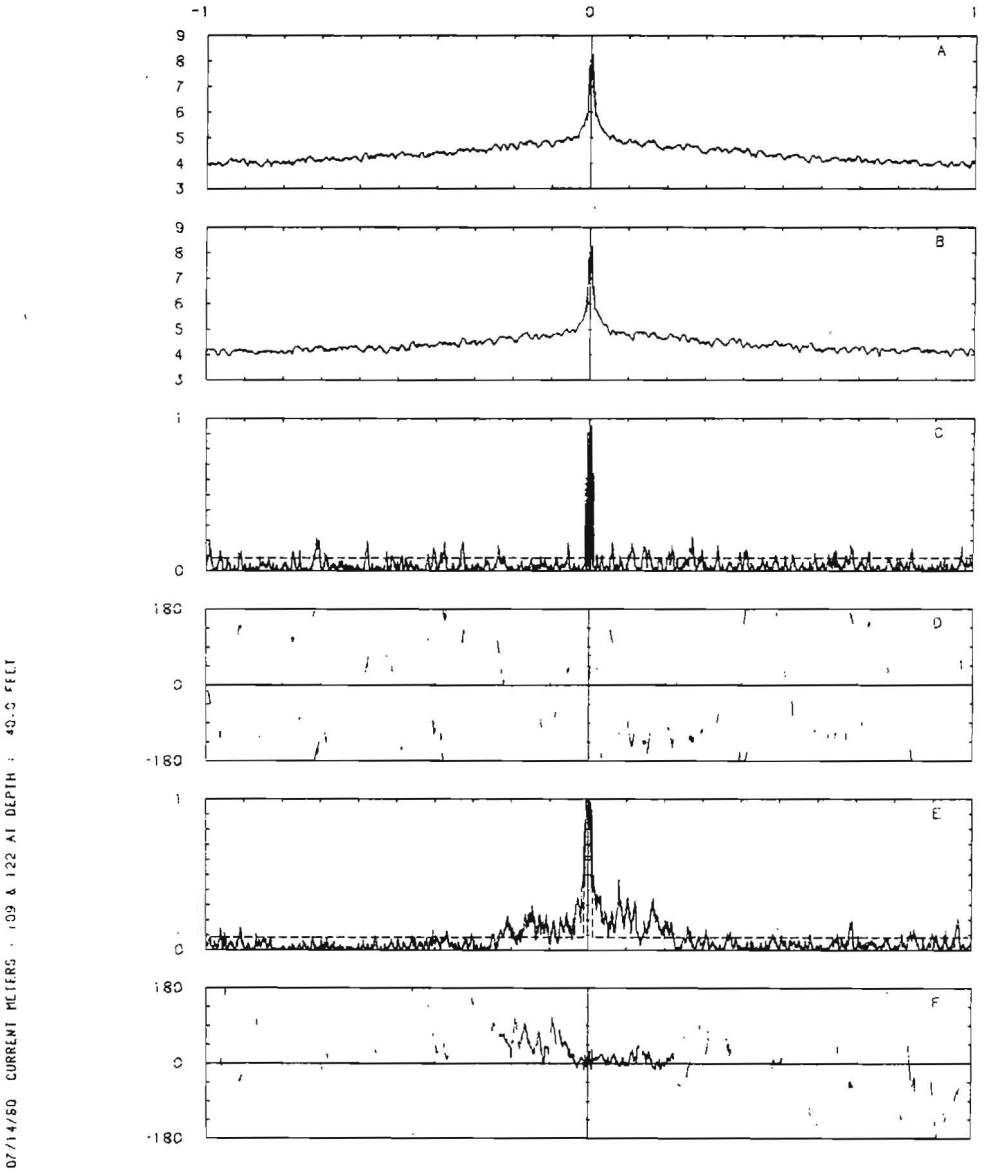

Figure 26. Rotational invariants for 11.4 day records beginning on 14 July, 1980 for meters deployed at 12.2 m: auto spectra for Meters #174109 and #174122 (Figures A and B), outer coherency squared and phase (Figures C and D), inner coherency squared and phase (Figures E and F). Degrees of freedom are 8.2 and 22.6 for periods less than and greater than 6 hours. Frequency scale is linear; values are normalized by the Nyquist frequency which is $4.17 \times 10^{-3} s^{-1}$.

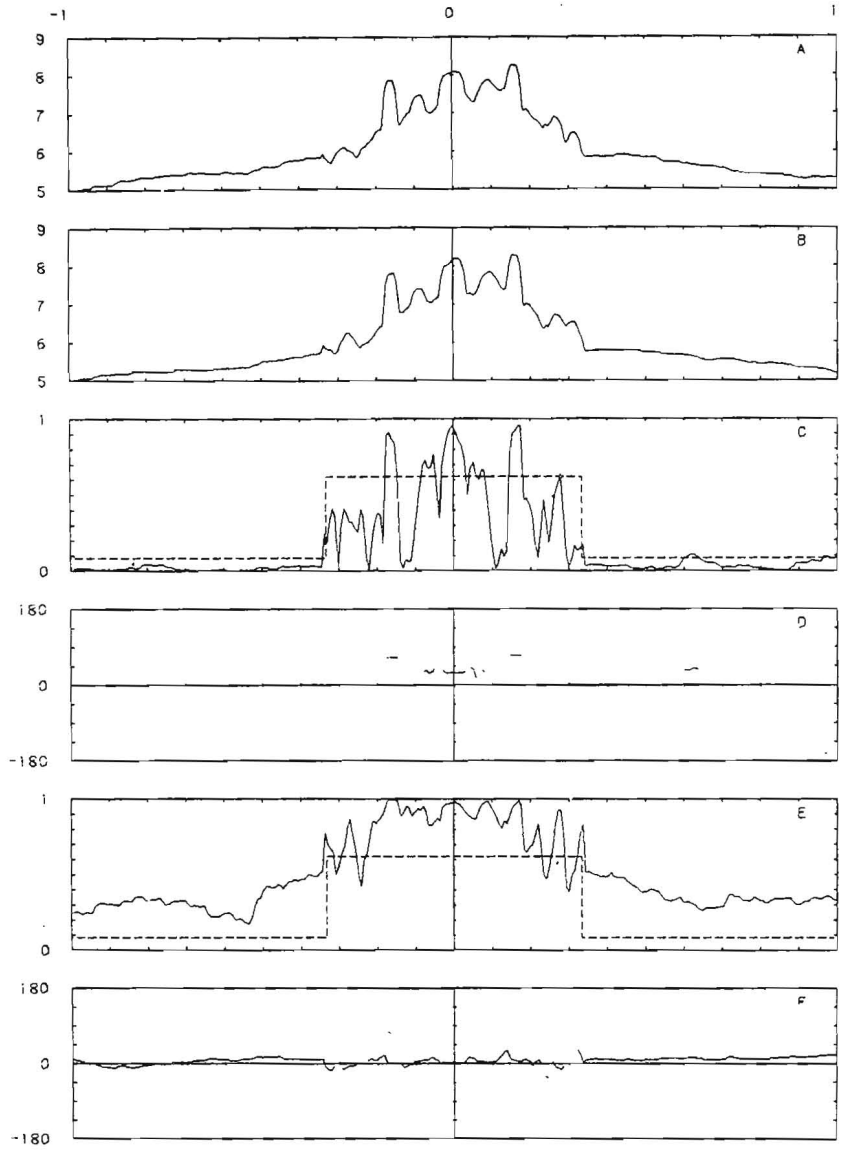

Figure 27. Rotational invariants for 11.4 day records beginning on 14 July, 1980 for meters deployed at 12.2 m: auto spectra for Meters #174109 and #174122 (Figures A and B), outer coherency squared and phase (Figures C and D), inner coherency squared and phase (Figures E and F). Degrees of freedom are 8.2 and 22.6 for periods less than and greater than 6 hours. Frequency scale is linear; values are normalized by the Nyquist frequency which is $1.39 \times 10^{-4} s^{-1}$.

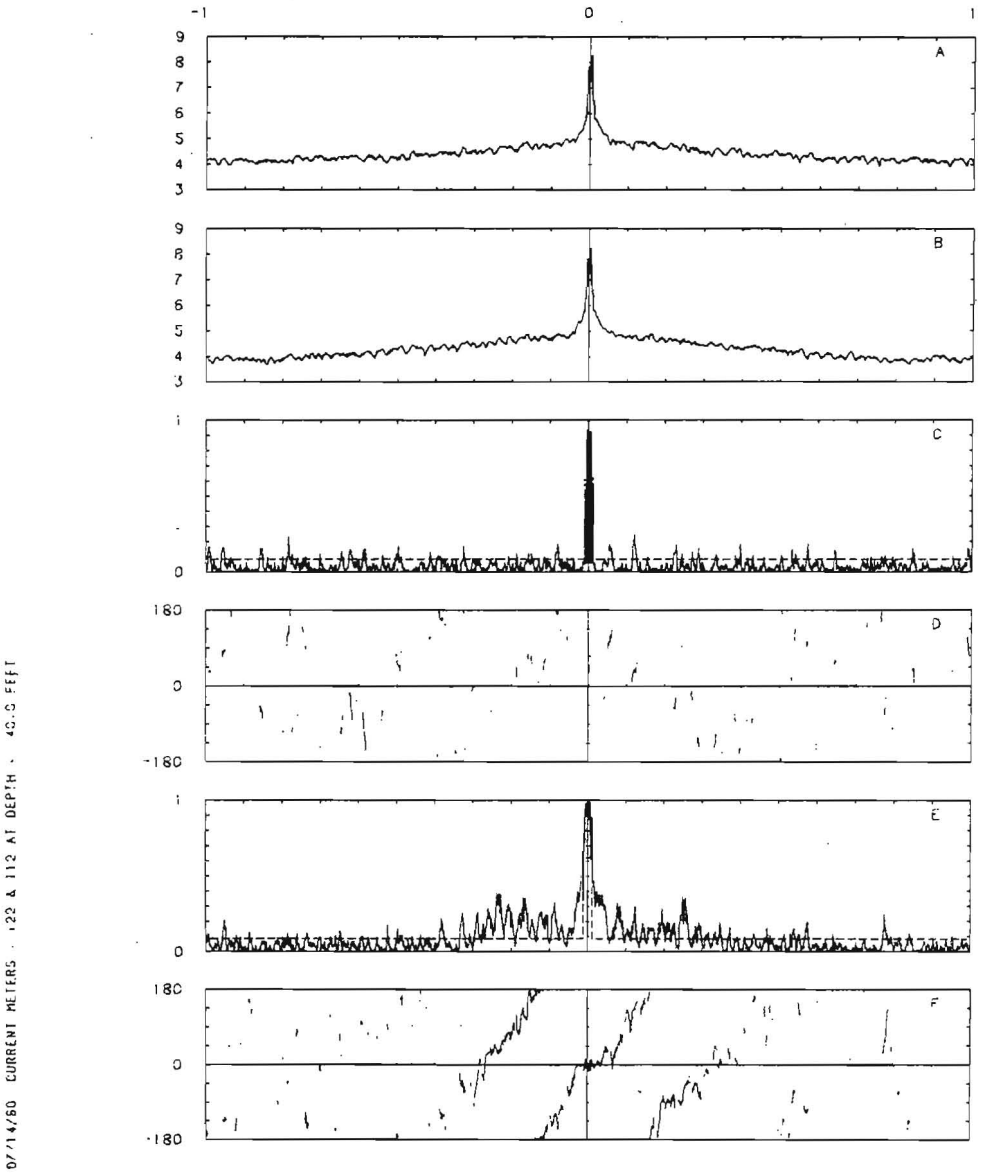

Figure 28. Rotational invariants for 11.4 day records beginning on 14 July, 1980 for meters deployed at 12.2 m: auto spectra for Meters #174122 and #174112 (Figures A and B), outer coherency squared and phase (Figures C and D), inner coherency squared and phase (Figures E and F). Degrees of freedom are 8.2 and 22.6 for periods less than and greater than 6 hours. Frequency scale is linear; values are normalized by the Nyquist frequency which is $4.17 \times 10^{-3} s^{-1}$.

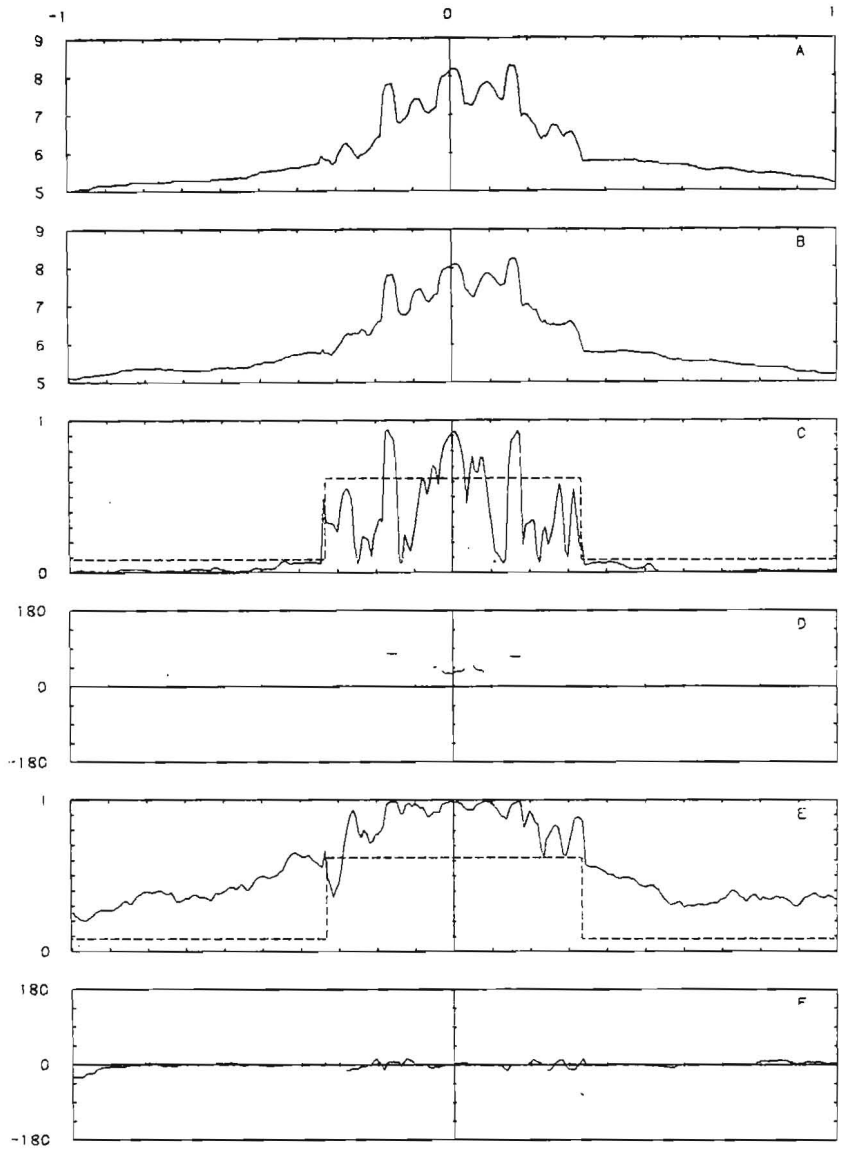

07/14/80 CURRENT METERS : 122 & 112 AT DEPTH = 40.0 FEET

Figure 29. Rotational invariants for 11.4 day records beginning on 14 July, 1980 for meters deployed at 12.2 m: auto spectra for Meters #174122 and #174112 (Figures A and B), outer coherency squared and phase (Figures C and D), inner coherency squared and phase (Figures E and F). Degrees of freedom are 8.2 and 22.6 for periods less than and greater than 6 hours. Frequency scale is linear; values are normalized by the Nyquist frequency which is $1.39 \times 10^{-4} s^{-1}$.

existence of phase lag increasing with frequency at periods shorter than 6 hours has been interpreted as a convection of "eddies" through the array. The convection velocity required to explain the phase relationships was much greater in magnitude than the mean flow although its direction was generally consistent with the principal axis directions of the semidiurnal and lower frequency current oscillations. Coherency estimates between pairs of instruments during winter discussed in the following sections show the lack of any coherency at supertidal frequencies presumably due to the reduced mean flow through the array. The occurrence of a phase lag between instruments at supertidal frequencies appears to depend on the existence of persistent mean flow through the array. The actual processes whereby eddies are convected through the array evidently results from an interaction of the tidal and lower frequency oscillations with the mean flow.

March 1981 Deployment

Rotational invariants were computed for the four Endeco 174 records available from this deployment. A common 22.8 day segment beginning on 27 February was extracted from current vector files for instruments 174183, 174181, 174122; only an 11.4 day segment beginning on 27 February could be extracted from the file for instrument 174107 because the record deteriorated. All of the files were from instruments at 4.6 m depth. The longer files contained 16,384 points and the shorter files contained 8192 points.

Mean values for the components of the current vectors resolved along 345°T and 45°T are presented in Table 7. The magnitude of vectors is approximately 25% of that of the mean vectors for the July deployment, and their direction varies from approximately 240°T to 248°T.

Figures 30 through 33 show the spectra, rotary coefficient, and the coherency squared and phase for each instrument. Note that the longer files were decimated to reduce the total number of points by a factor of 2. Their Nyquist frequency is, therefore, 0.125 minutes^{-1}. The spectra for the longer files (Figures 30 through 32) show significantly greater low frequency resolution than do the spectra estimated for summer deployment. Figure 30, for example, shows peaks at M_4, semidiurnal, inertial and diurnal periodicities. There is also a major peak at 2.2 days presumably related to meteorological forcing. The M_4 peak is especially pronounced in Figure 33.

Spectral and rotational characteristics estimated from the 3 long records (Figures 30 through 32) are in general quite similar. At subtidal frequencies including the powerful band centered on approximately 2.2 days the coherency squared (Figure D) is well above the 95% significance level; the phase (Figure E) is approximately constant at -24° and so the orientation of the principal axes is approximately +69°T which is exactly along the isobaths. The principal axes for both the diurnal and semidiurnal oscillations are quite stable; the principal axis orientation for both periods is nearly along the isobaths with at most a few degrees of cross isobath deflection.

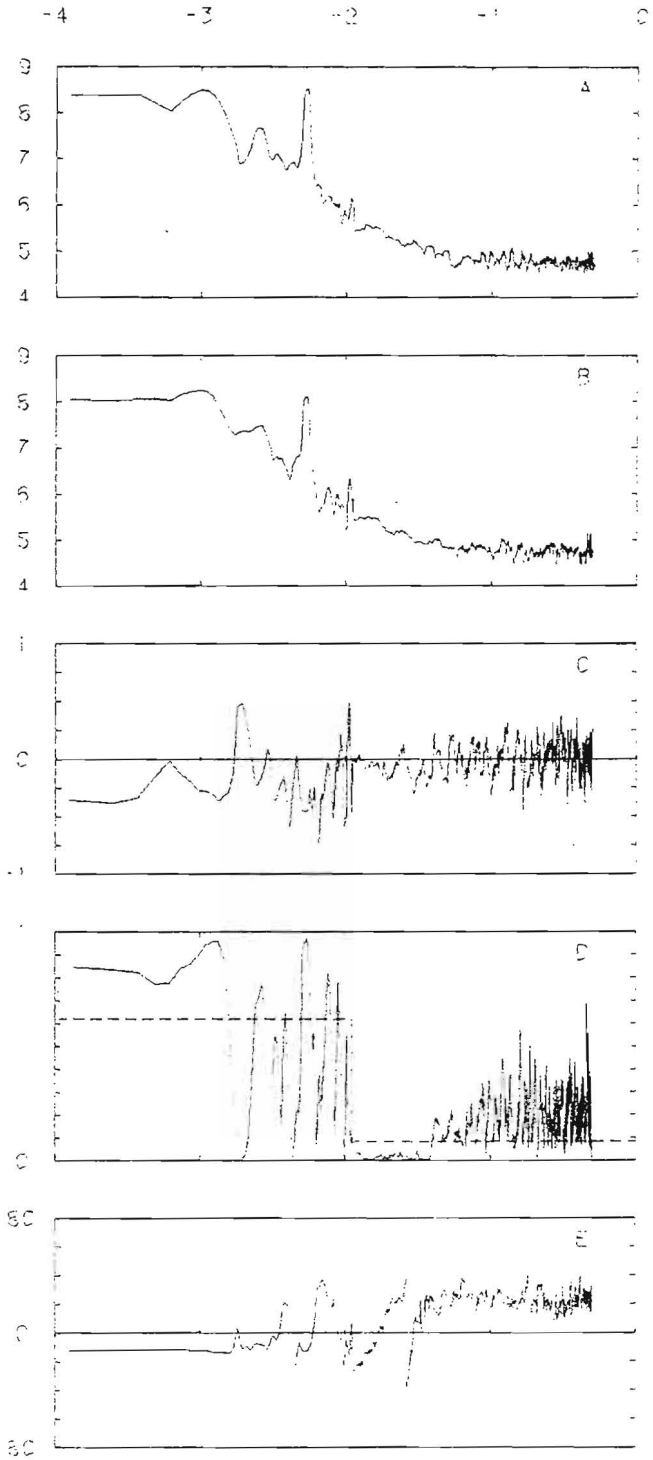

Figure 30.

Rotational invariants for a 22.8 day record beginning on 27 February, 1981 from Meter #174122 deployed at 4.6 m: auto spectrum for negative frequencies (Figure A); auto spectrum for positive frequencies (Figure B); rotary coefficient (Figure C); ellipse stability (Figure D); ellipse orientation (degrees) (Figure E). Degrees of freedom ar 8.2 and 82.6 for periods less than and greater than 6 hours. Frequency scale is logarithmic, values are normalized by the Nyquist frequency which is $4.17 \times 10^{-3} s^{-1}$.

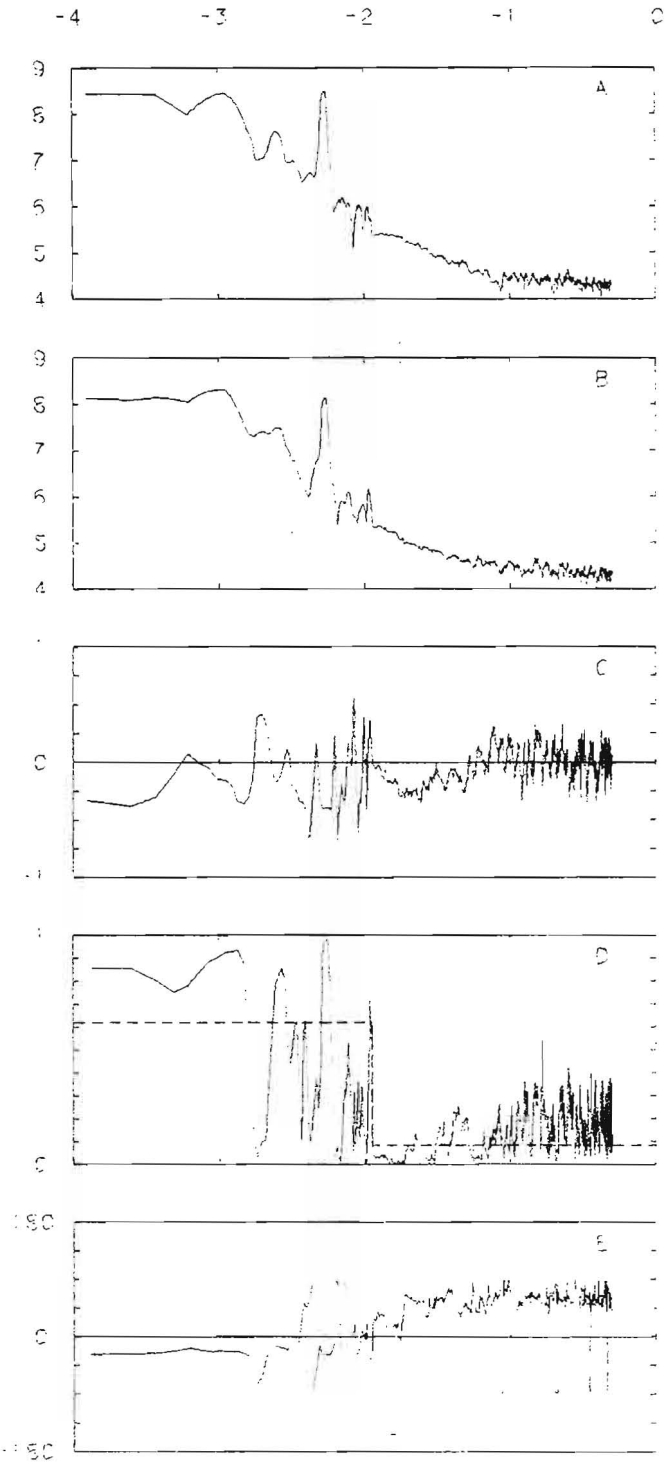

Figure 31.

Rotational invariants for a 22.8 day record beginning on 27 February, 1981 from Meter #174181 deployed at 4.6 m: auto spectrum for negative frequencies (Figure A); auto spectrum for positive frequencies (Figure B); rotary coefficient (Figure C); ellipse stability (Figure D); ellipse orientation (degrees) (Figure E). Degrees of freedom are 8.2 and 82.6 for periods less than and greater than 6 hours. Frequency scale is logarithmic, values are normalized by the Nyquist frequency which is $4.17 \times 10^{-3} s^{-1}$.

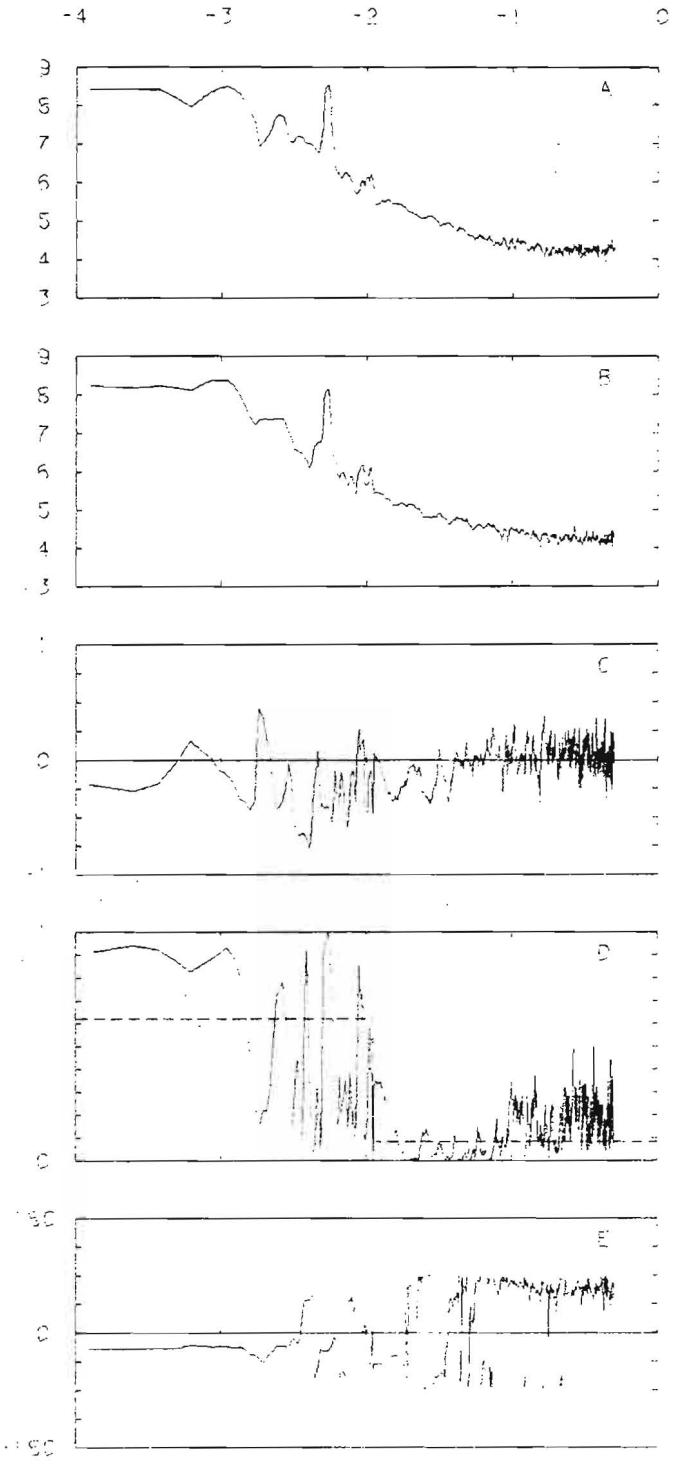

Figure 32.

Rotational invariants for a 22.8 day record beginning on 27 February, 1981 from Meter #174183 deployed at 4.6 m: auto spectrum for negative frequencies (Figure A); auto spectrum for positive frequencies (Figure B); rotary coefficient (Figure C); ellipse stability (Figure D); ellipse orientation (degrees) (Figure E). Degrees of freedom are 8.2 and 82.6 for periods less than and greater than 6 hours. Frequency scale is logarithmic, values are normalized by the Nyquist frequency which is $4.17 \times 10^{-3} s^{-1}$.

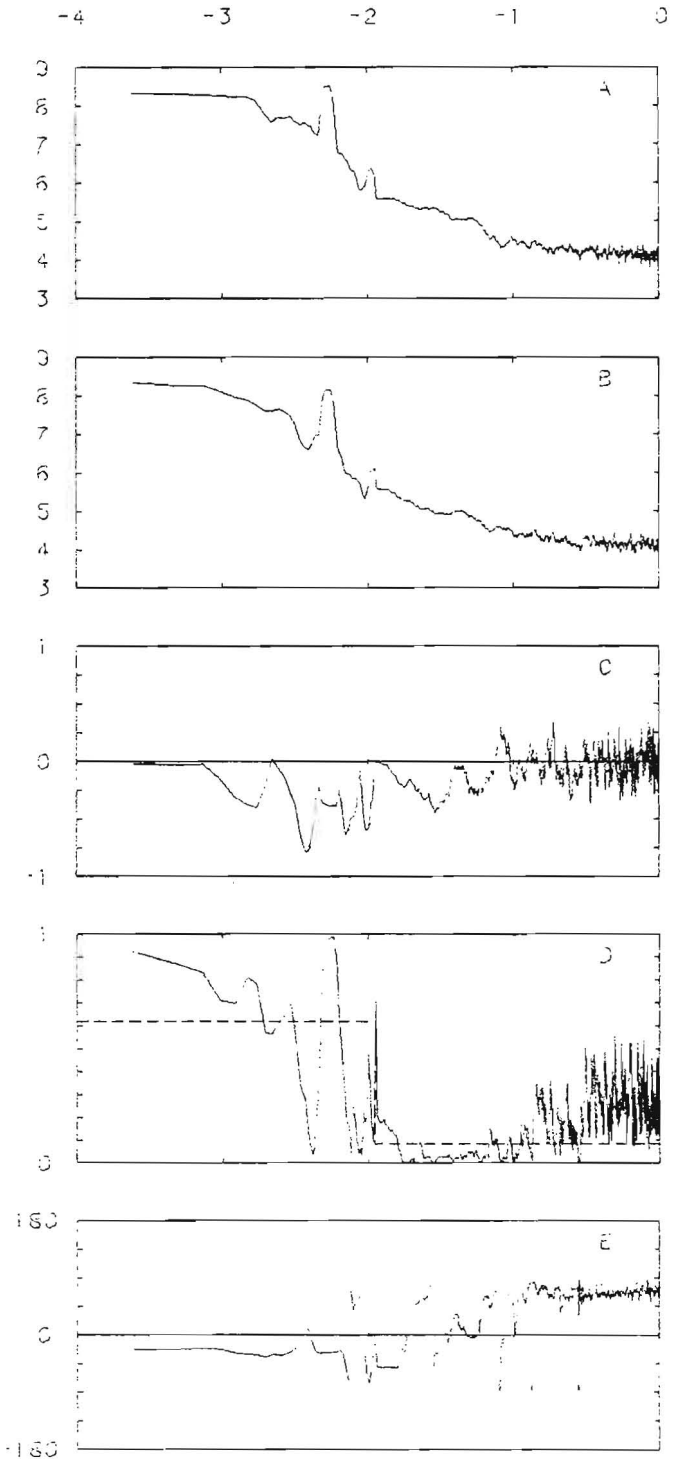

Figure 33.

Rotational invariants for an 11.4 day record beginning on 27 February, 1981 from Meter #174107 deployed at 4.6 m: auto spectrum for negative frequencies (Figure A); auto spectrum for positive frequencies (Figure B); rotary coefficient (Figure C); ellipse stability (Figure D); ellipse orientation (degrees) (Figure E). Degrees of freedom are 8.2 and 82.6 for periods less than and greater than 6 hours. frequency scale is lagarithmic, values are normalized by the Nyquist frequency which is $4.17 \times 10^{-3} s^{-1}$.

Oscillations with periods ranging from approximately 6 hours to 1.7 hours do not have a stable axis. At periods shorter than approximately 1.7 hours the oscillations do have stable axes; the phase for these oscillations is approximately constant at +60° and so the principal axis orientation is 345°T which is nearly in the cross isobath direction.

In summary, two of the most significant differences between the July deployment and the March deployment are a reduced mean flow and less cross isobath flow at subtidal frequencies during winter. At periods shorter than approximately 1.6 hours the principal axes for oscillations are oriented cross isobath for both July and March.

Coherencies computed for the six possible pairs of instruments for the March deployment are presented in Figures 34 through 45. Each coherency is again plotted on two frequency scales. Note that the shortest record length was limiting for these coherencies; all coherencies were computed for an 11.4 day record even though for three of the instruments 23 day records were available.

Coherencies for pairs of instruments at moorings B, C and E (Figure 8) tend to drop below the significance level for periods shorter than approximately 2 hours. This is in contrast to coherencies calculated for the same moorings (Figure 7) for the July deployment which drop below the significance level for periods shorter than approximately 13 minutes. Spatial separations for these three moorings were very similar for the March and July deployments. The absence of significant coherency at periods shorter than 2 hours for

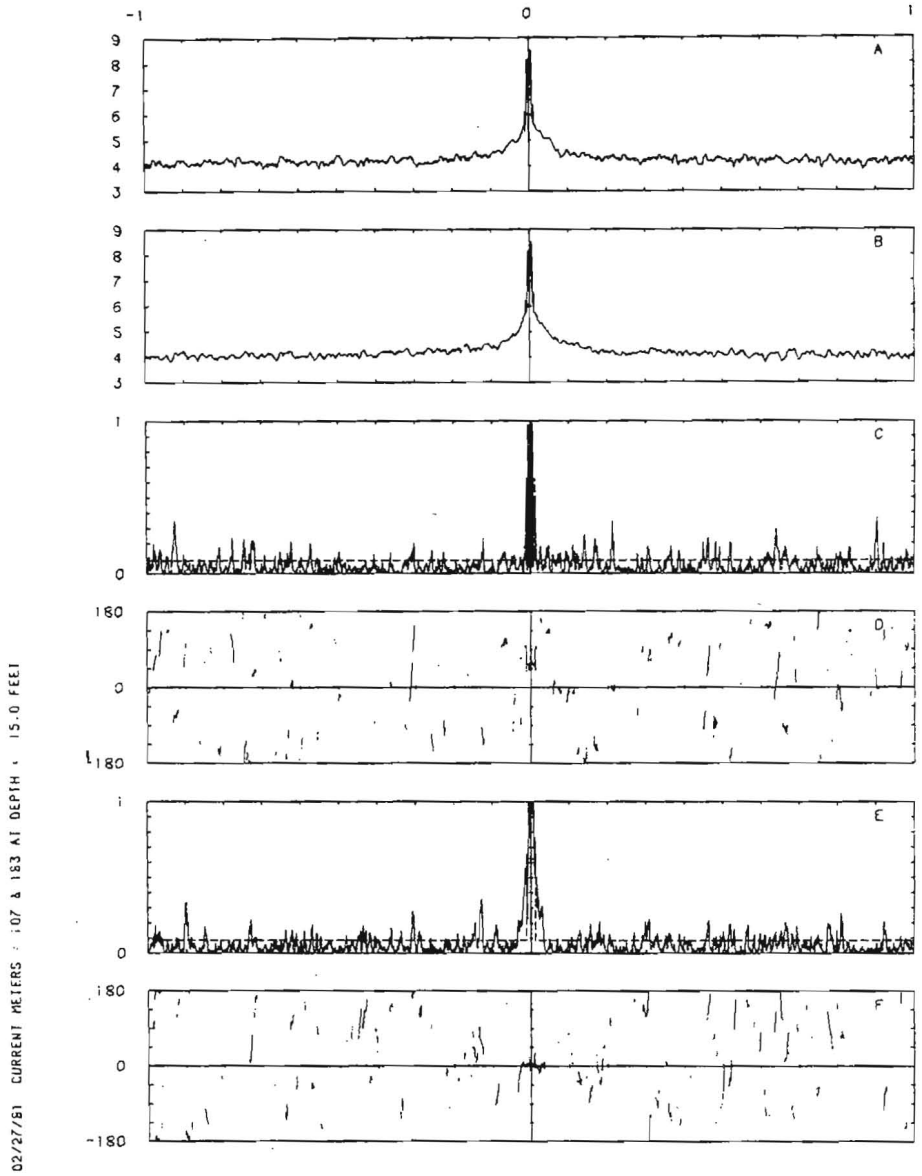

Figure 34. Rotational invariants for 11.4 day records beginning on 27 February, 1981 for meters deployed at 4.6 m: auto spectra for Meters #174107 and #174183 (Figures A and B), outer coherency squared and phase (Figures C and D), inner coherency squared and phase (Figures E and F). Degrees of freedom are 8.2 and 22.6 for periods less than and greater than 6 hours. Frequency scale is linear; values are normalized by the Nyquist frequency which is 4.17×10^{-3} $^{-1}$.

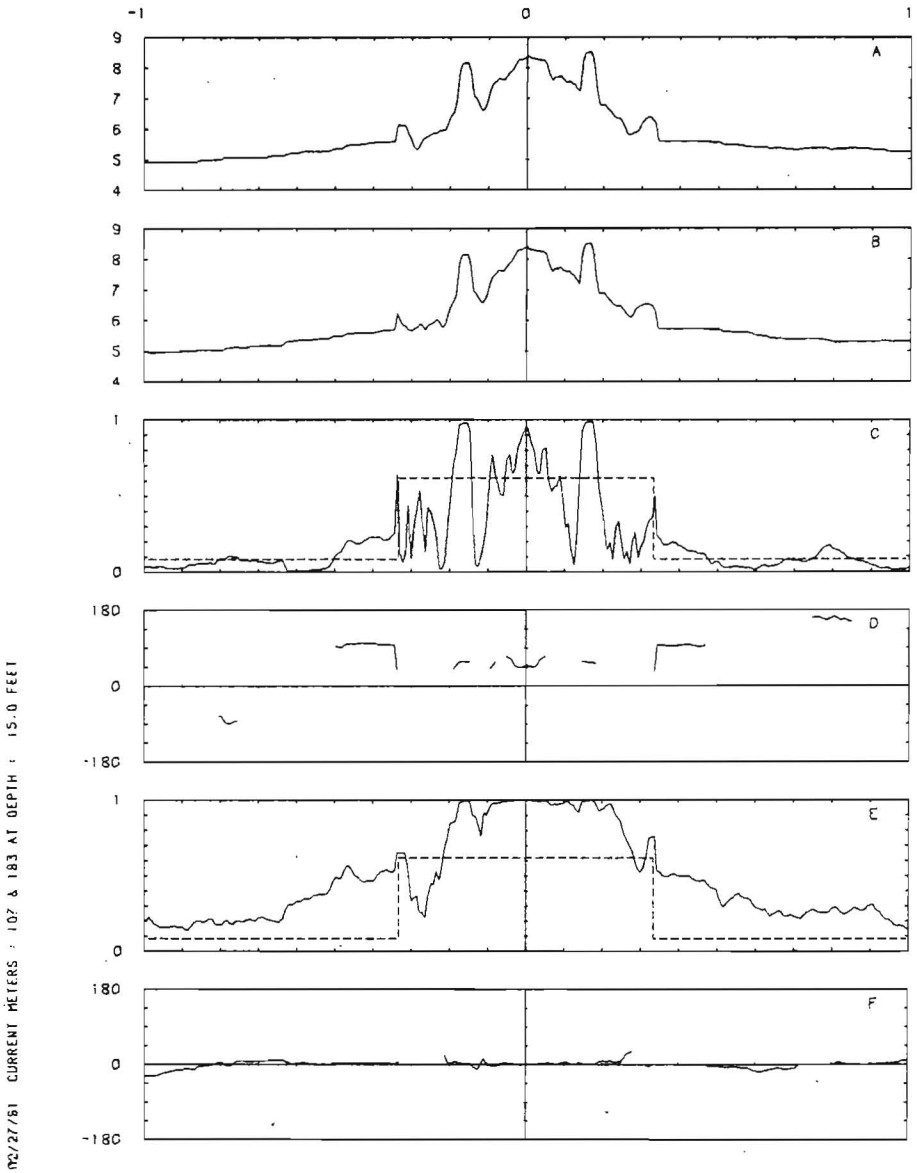

Figure 35. Rotational invariants for 11.4 day records beginning on 27 February, 1981 for meters deployed at 4.6 m: auto spectra for Meters #174107 and #174183 (Figures A and B), outer coherency squared and phase (Figures C and D), inner coherency squared and phase (Figures E and F). Degrees of freedom are 8.2 and 22.6 for periods less than and greater than 6 hours. Frequency scale is linear; values are normalized by the Nyquist frequency which is $1.39 \times 10^{-4} s^{-1}$.

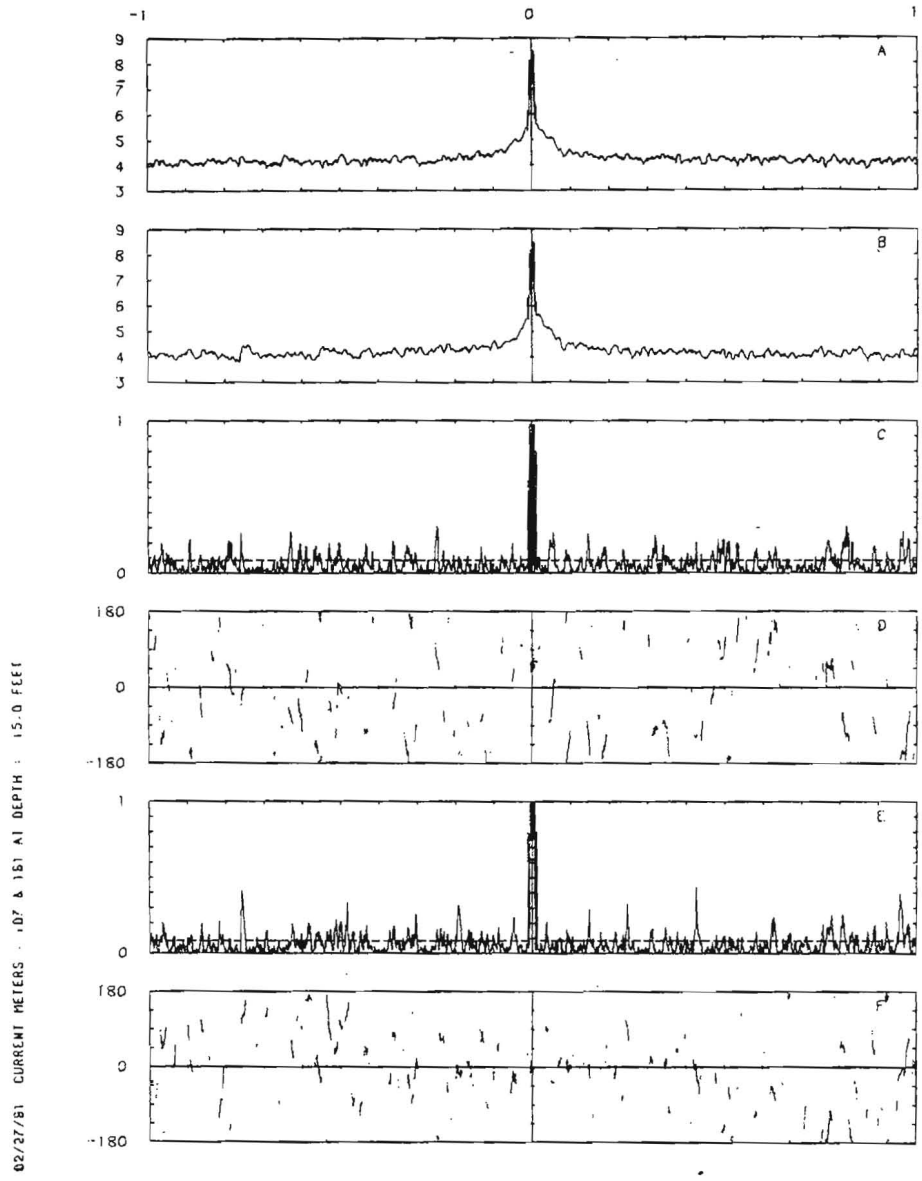

Figure 36. Rotational invariants for 11.4 day records beginning on 27 February, 1981 for meters deployed at 4.6 m: auto spectra for Meters #174107 and #174181 (Figures A and B), outer coherency squared and phase (Figures C and D), inner coherency squared and phase (Figures E and F). Degrees of freedom are 8.2 and 22.6 for periods less than and greater than 6 hours. Frequency scale is linear; values are normalized by the Nyquist frequency which is $4.17 \times 10^{-3} s^{-1}$.

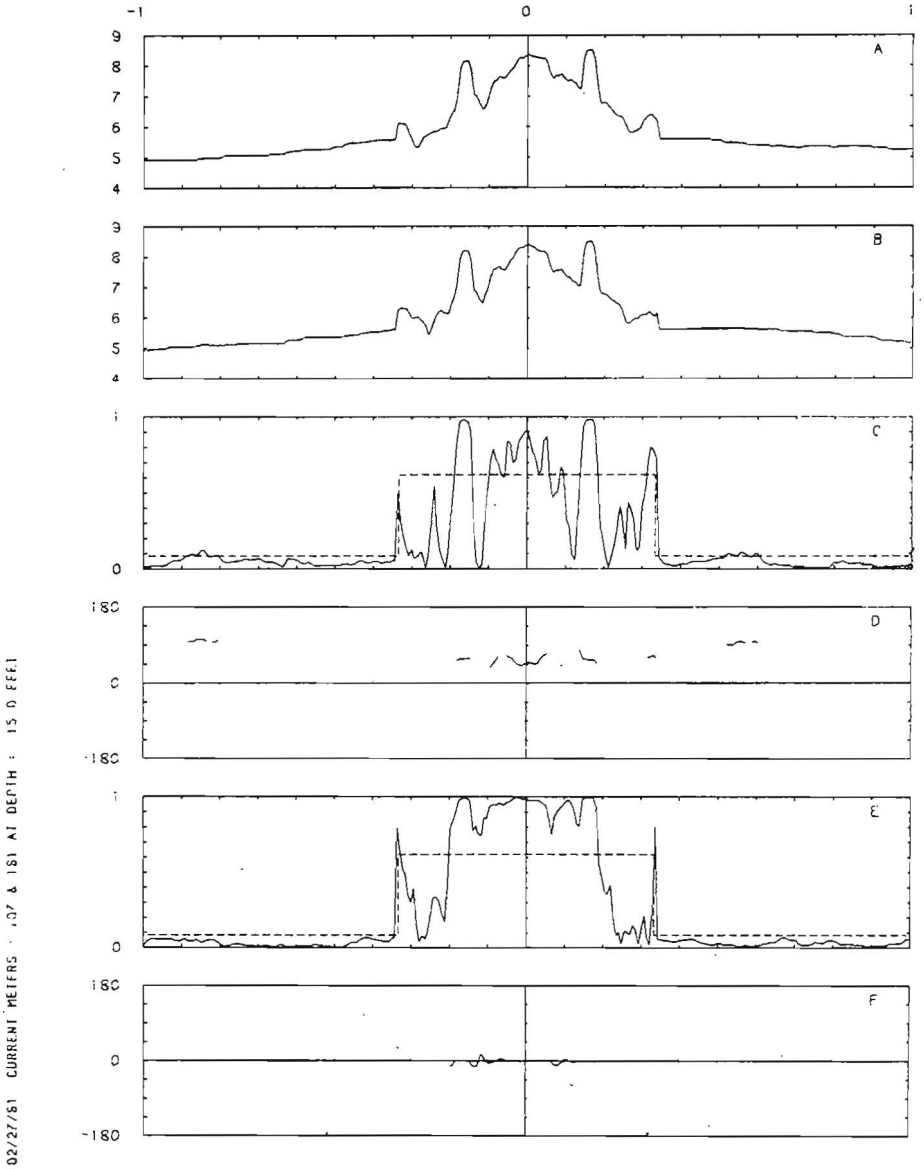

Figure 37. Rotational invariants for 11.4 day records beginning on 27 February, 1981 for meters deployed at 4.6 m: auto spectra for Meters #174107 and #174181 (Figures A and B), outer coherency squared and phase (Figures C and D), inner coherency squared and phase (Figures E and F). Degrees of freedom are 8.2 and 22.6 for periods less than and greater than 6 hours. Frequency scale is linear; values are normalized by the Nyquist frequency which is $1.39 \times 10^{-4} s^{-1}$.

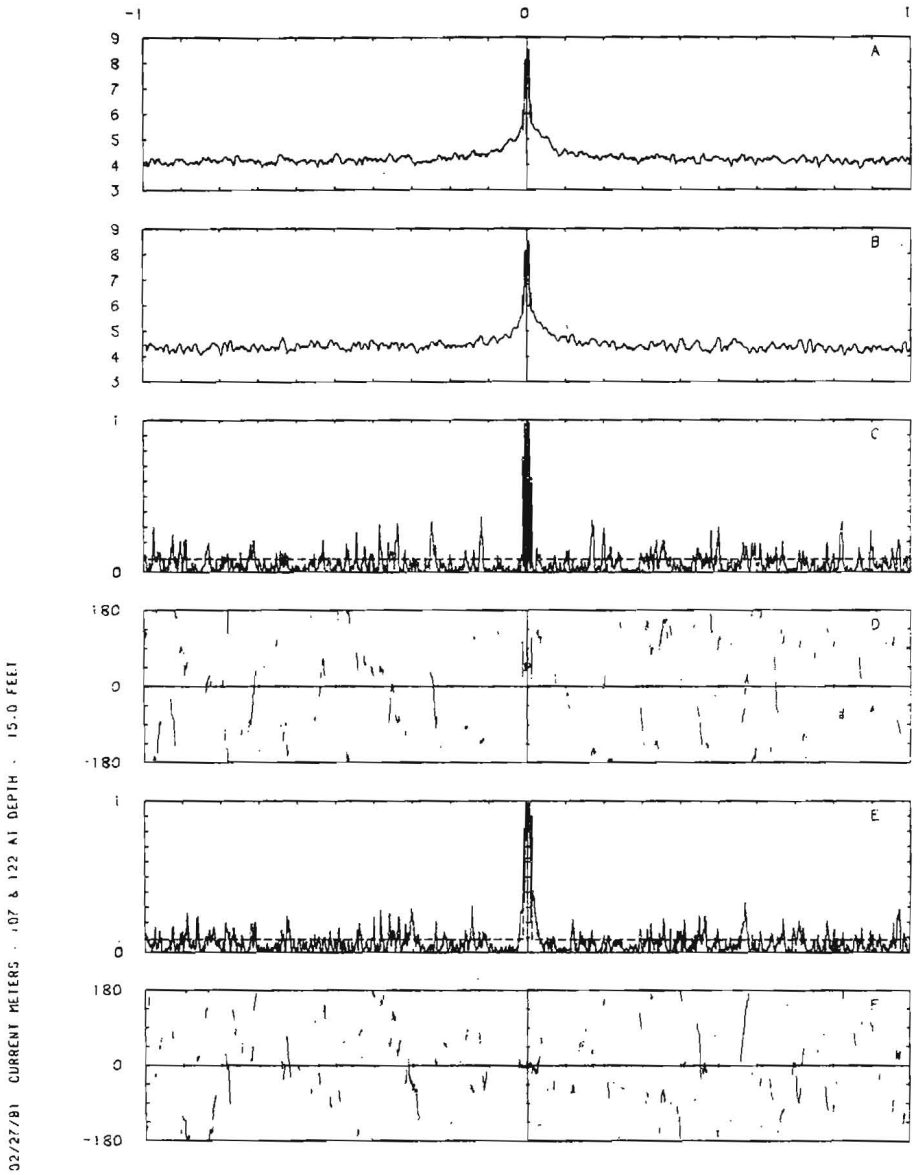

Figure 38. Rotational invariants for 11.4 day records beginning on 27 February, 1981 for meters deployed at 4.6 m: auto spectra for Meters #174107 and #174122 (Figures A and B), outer coherency squared and phase (Figures C and D), inner coherency squared and phase (Figures E and F). Degrees of freedom are 8.2 and 22.6 for periods less than and greater than 6 hours. Frequency scale is linear; values are normalized by the Nyquist frequency which is $4.17 \times 10^{-3} s^{-1}$.

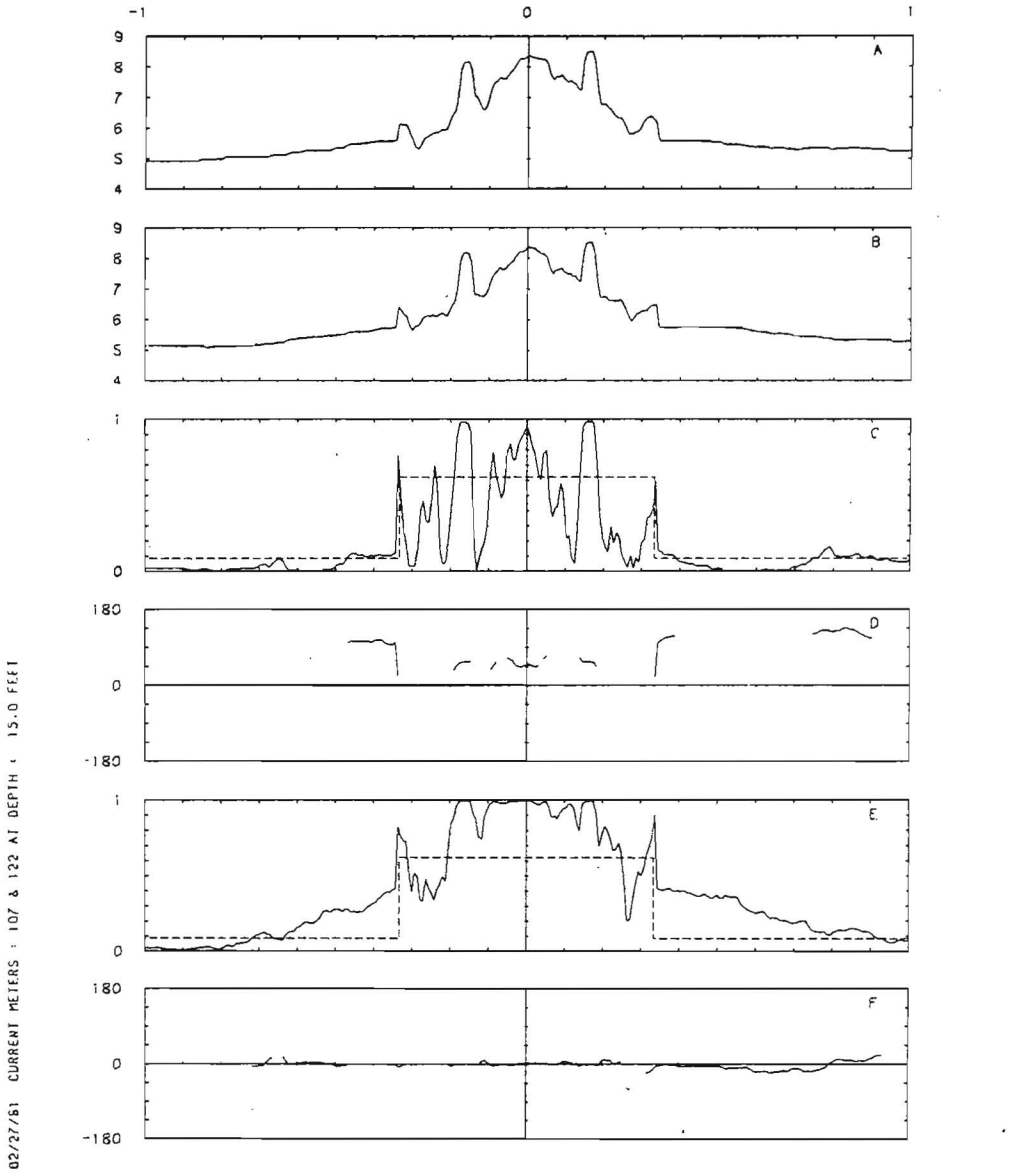

Figure 39. Rotational invariants for 11.4 day records beginning on 27 February, 1981 for meters deployed at 4.6 m: auto spectra for Meters #174107 and #174122 (Figures A and B), outer coherency squared and phase (Figures C and D), inner coherency squared and phase (Figures E and F). Degrees of freedom are 8.2 and 22.6 for periods less than and greater than 6 hours. Frequency scale is linear; values are normalized by the Nyquist frequency which is $1.39 \times 10^{-4} s^{-1}$.

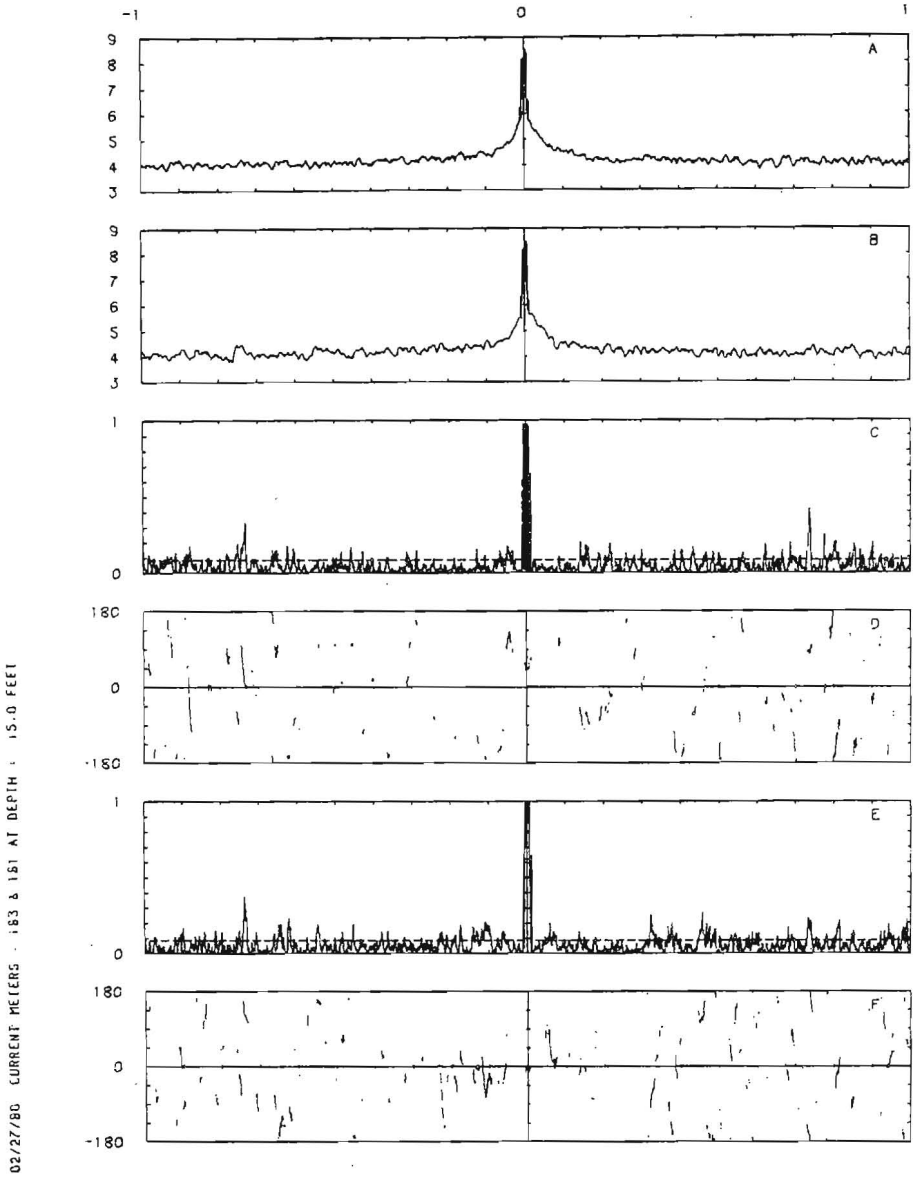

Figure 40. Rotational invariants for 11.4 day records beginning on 27 February, 1981 for meters deployed at 4.6 m: auto spectra for Meters #174183 and #174181 (Figures A and B), outer coherency squared and phase (Figures C and D), inner coherency squared and phase (Figures E and F). Degrees of freedom are 8.2 and 22.6 for periods less than and greater than 6 hours. Frequency scale is linear; values are normalized by the Nyquist frequency which is $4.17 \times 10^{-3} s^{-1}$.

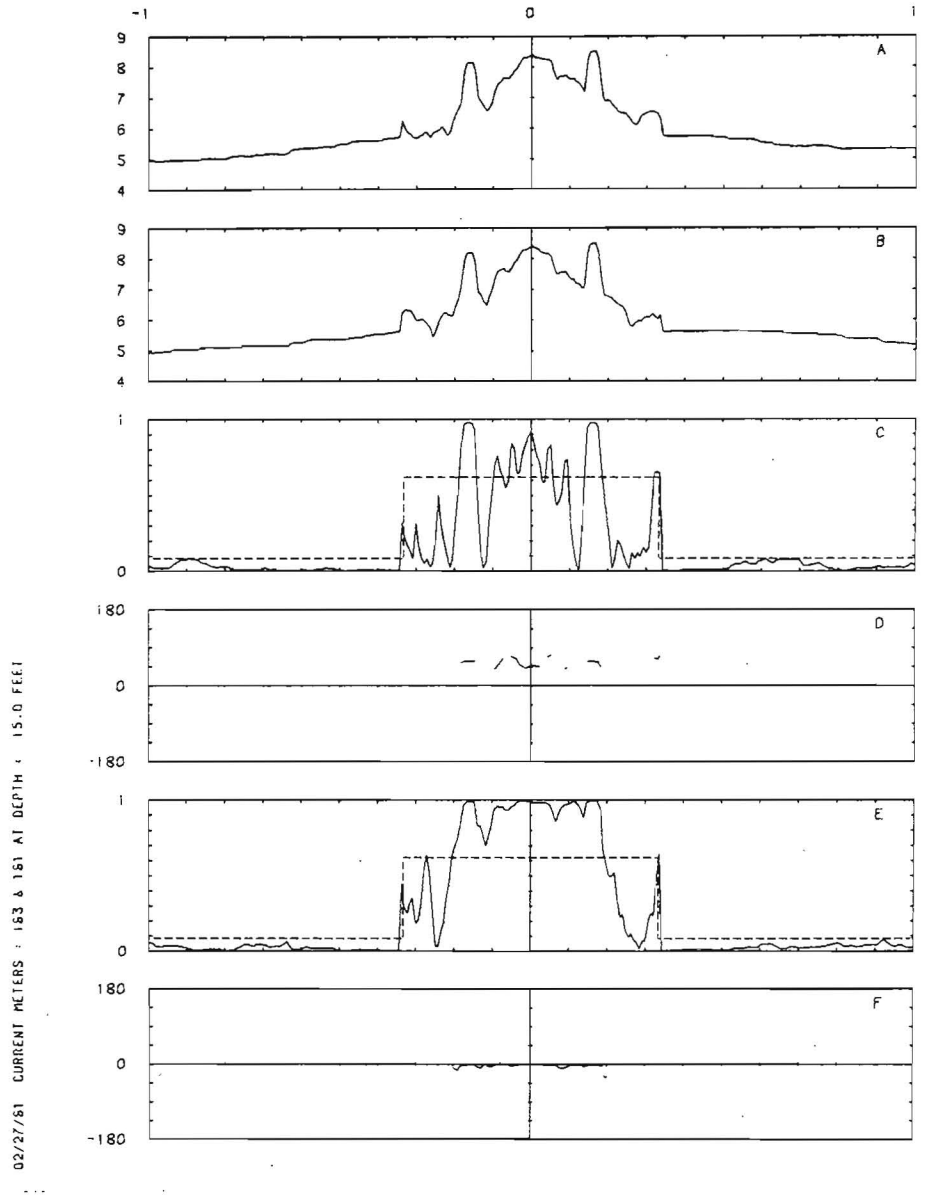

Figure 41. Rotational invariants for 11.4 day records beginning on 27 February, 1981 for meters deployed at 4.6 m: auto spectra for Meters #174183 and #174181 (Figures A and B), outer coherency squared and phase (Figures C and D), inner coherency squared and phase (Figures E and F). Degrees of freedom are 8.2 and 22.6 for periods less than and greater than 6 hours. Frequency scale is linear; values are normalized by the Nyquist frequency which is $1.39 \times 10^{-4} s^{-1}$.

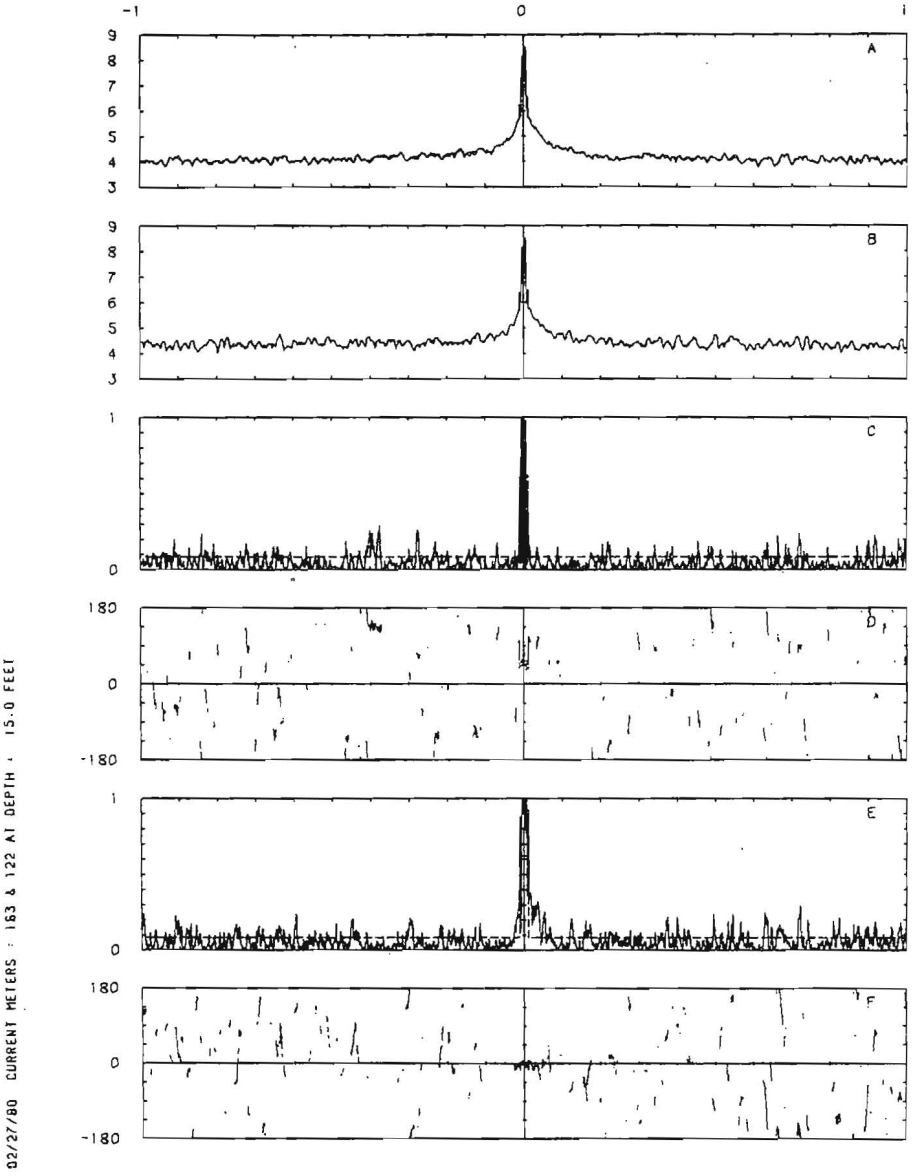

Figure 42. Rotational invariants for 11.4 day records beginning on 27 February, 1981 for meters deployed at 4.6 m: auto spectra for Meters 174183 and #174122 (Figures A and B), outer coherency squared and phase (Figures C and D), inner coherency squared and phase (Figures E and F). Degrees of freedom are 8.2 and 22.6 for periods less than and greater than 6 hours. Frequency scale is linear; values are normalized by the Nyquist frequency which is $4.17 \times 10^{-3} s^{-1}$.

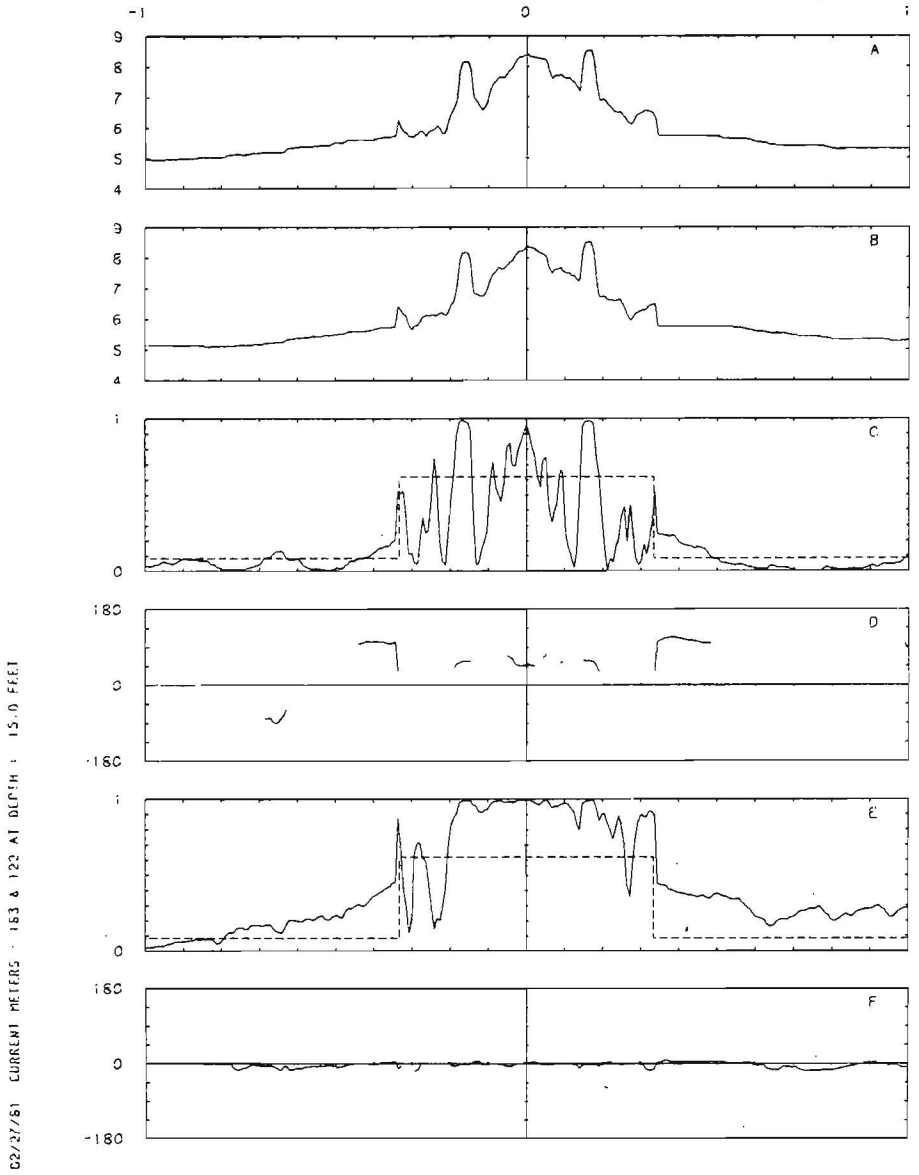

Figure 43. Rotational invariants for 11.4 day records beginning on 27 February, 1981 for meters deployed at 4.6 m: auto spectra for Meters #174183 and #174122 (Figures A and B), outer coherency squared and phase (Figures C and D), inner coherency squared and phase (Figures E and F). Degrees of freedom are 8.2 and 22.6 for periods less than and greater than 6 hours. Frequency scale is linear; values are normalized by the Nyquist frequency which is $1.39 \times 10^{-4} s^{-1}$.

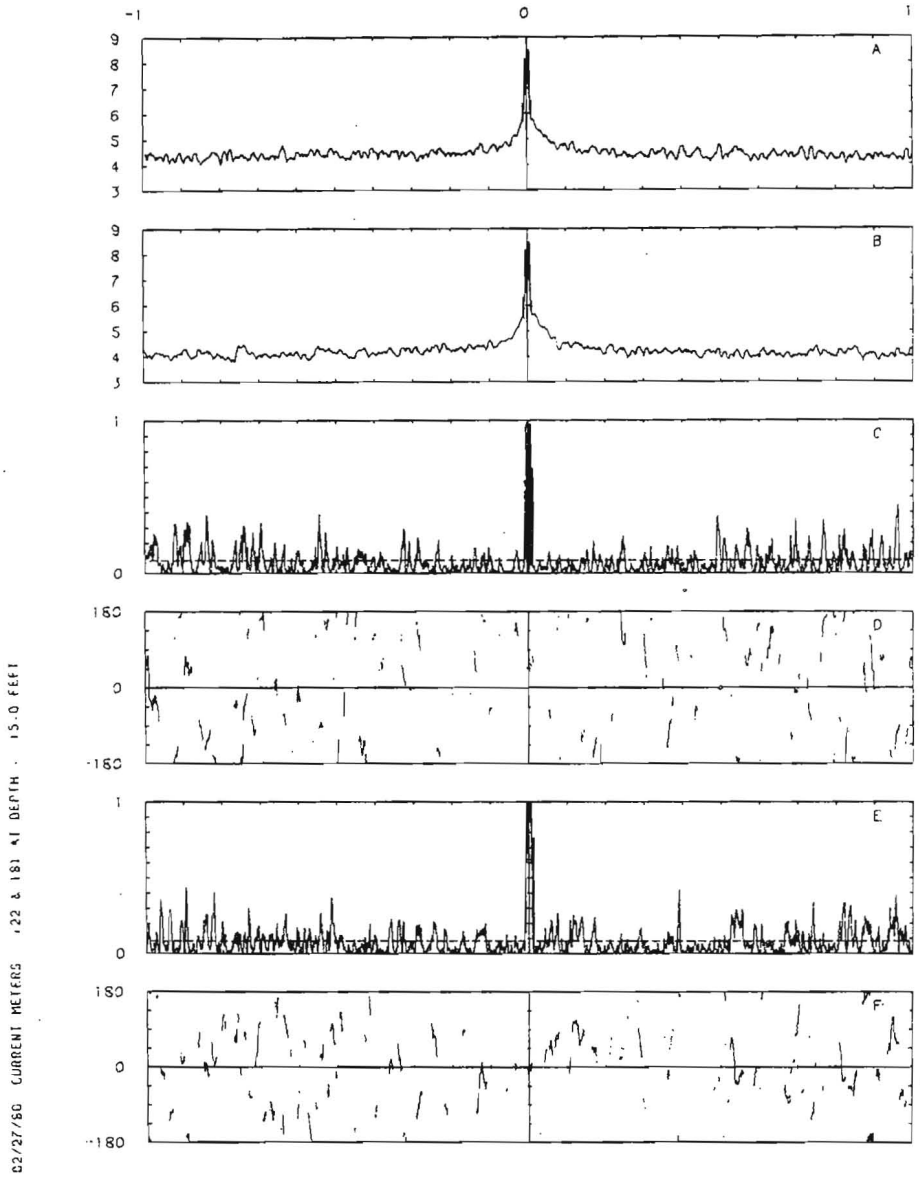

Figure 44. Rotational invariants for 11.4 day records beginning on 27 February, 1981 for meters deployed at 4.6 m: auto spectra for Meters #174122 and #174181 (Figures A and B), outer coherency squared and phase (Figures C and D), inner coherency squared and phase (Figures E and F). Degrees of freedom are 8.2 and 22.6 for periods less than and greater than 6 hours. Frequency scale is linear; values are normalized by the Nyquist frequency which is $4.17 \times 10^{-3} s^{-1}$.

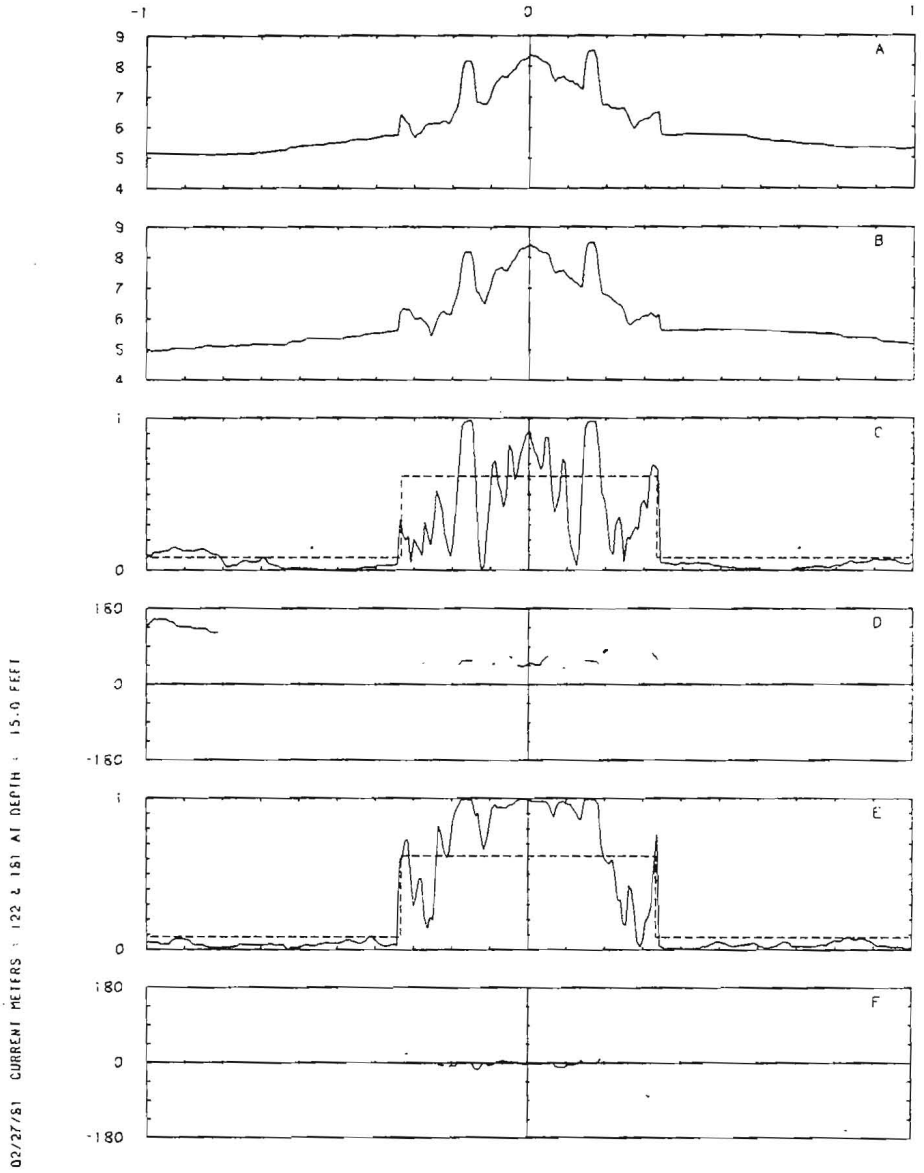

Figure 45. Rotational invariants for 11.4 day records beginning on 27 February, 1981 for meters deployed at 4.6 m: auto spectra for Meters #174122 and #174181 (Figures A and B), outer coherency squared and phase (Figures C and D), inner coherency squared and phase (Figures E and F). Degrees of freedom are 8.2 and 22.6 for periods less than and greater than 6 hours. Frequency scale is linear; values are normalized by the Nyquist frequency which is $1.39 \times 10^{-4} s^{-1}$.

instruments on moorings B, C and E during the March deployment could be explained by the substantially reduced mean flow. This would be consistent with our interpretation of these short period fluctuations of being due to convected disturbances. The coherency between fluctuations at mooring D and those at moorings B, C or E was usually not above the significance level for periods shorter than semidiurnal except for some coherency at periods near M_4. The relevance of these characteristics of the coherency to the calculation of horizontal velocity gradients from instruments in the March array will be discussed in the analysis section.

Vertical current shear

In addition to the rotary auto spectra and cross spectra (coherency) for instruments at a given depth which have been estimated for both the July and March deployments, we examined some very limited aspects of the vertical shear in horizontal currents for the July deployment only. The vertical shear in horizontal currents has an x-component, $\Delta u/\Delta z$, where u is the x-component of velocity (positive along 045°T) and z is the vertical coordinate (positive upward) and a y-component, $\Delta v/\Delta z$, where v is the y-component of velocity (positive along 345°T). These mean shear components are listed in Table 8 although these values must be viewed with extreme caution due to the uncertainty in the estimates of the mean currents. Figures 46 through 48 provide some information on the spectral and rotational characteristics of the vector with components $\Delta y/\Delta z$, $\Delta v/\Delta z$ for moorings B, C and E. The

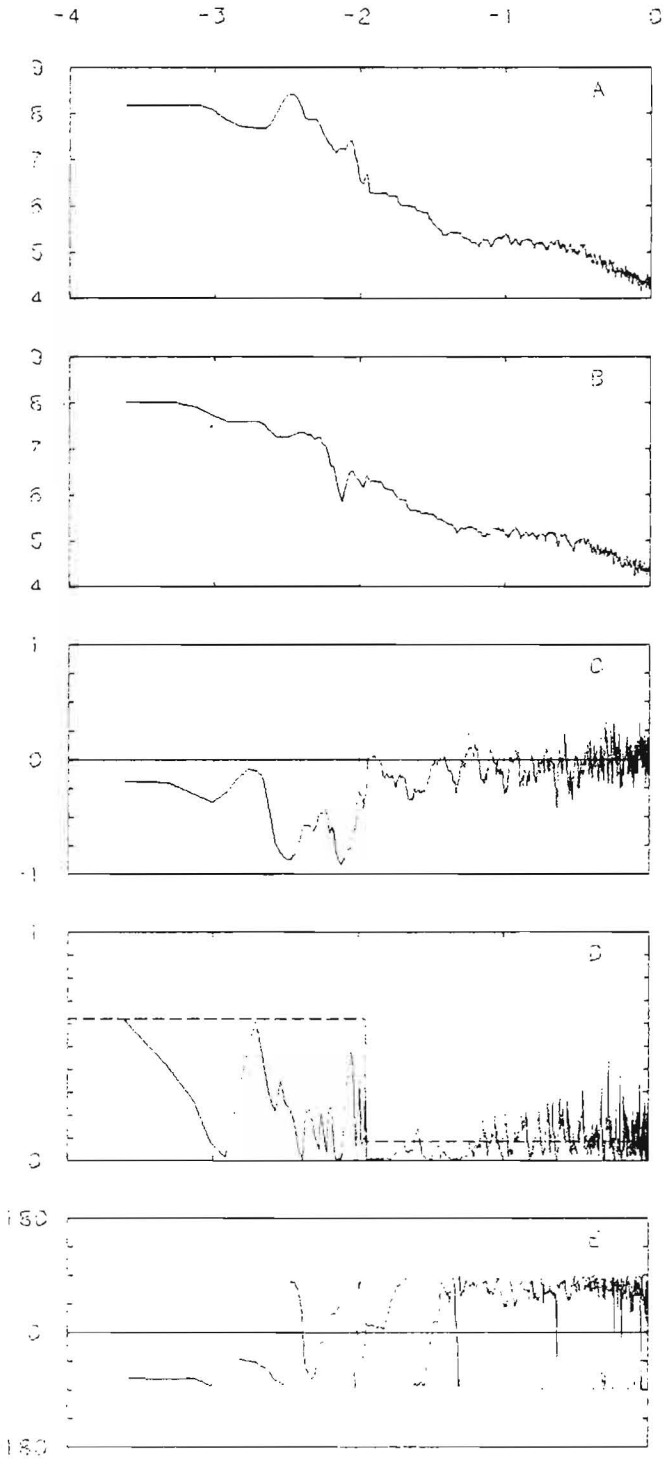

Figure 46.

Rotational invariants for vertical shear in horizontal current at mooring B for an 11.4 day record beginning on 14 July, 1980: auto spectrum for negative frequencies (Figure A); auto spectrum for positive frequencies (Figure B); rotary coefficient (Figure C); ellipse stability and ellipse orientation in degrees (Figures D and E). Degrees of freedom are 8.2 and 82.6 for periods less than and greater than 6 hours. Frequency scales is logarithmic; values are normalized by the Nyquist frequency which is $4.17 \times 10^{-3} s^{-1}$.

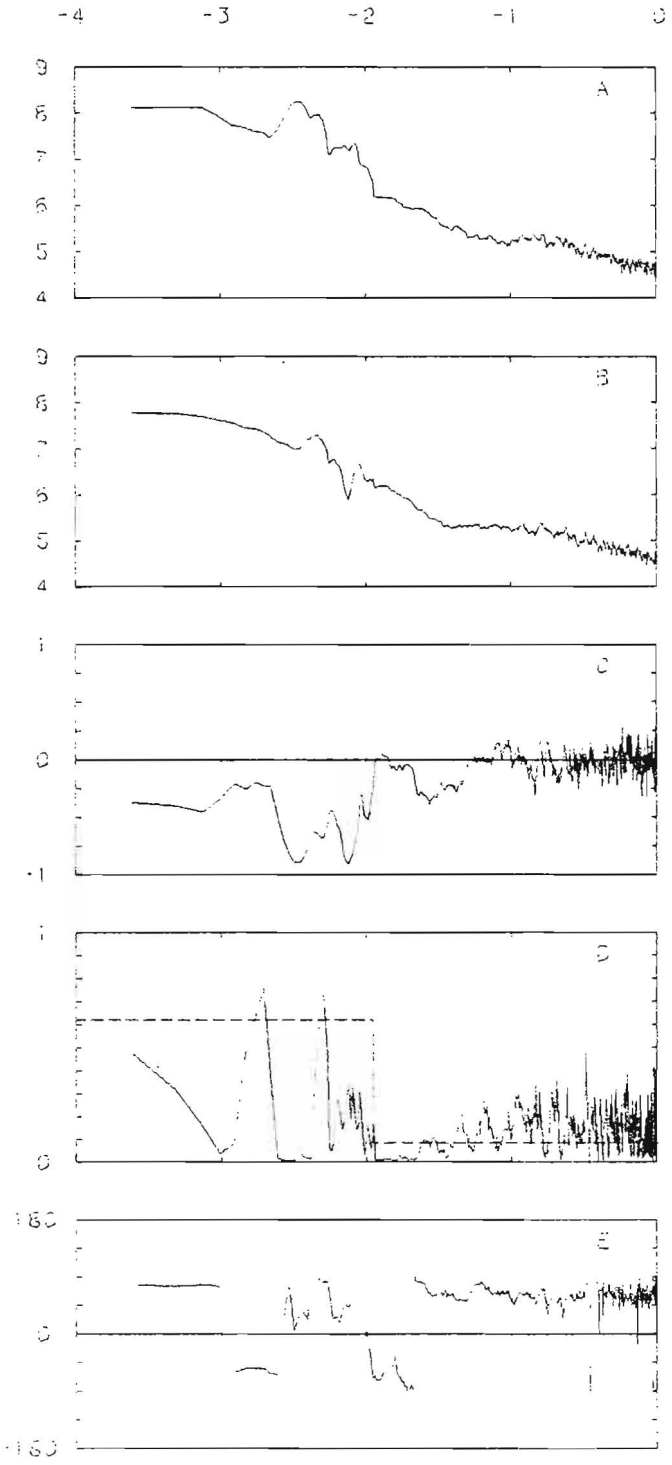

Figure 47.

Rotational invariants for vertical shear in horizontal current at mooring C for an 11.4 day record beginning on 14 July, 1980: auto spectrum for negative frequencies (Figure A); auto spectrum for positive frequencies (Figure B); rotary coefficient (Figure C); ellipse stability and ellipse orientation in degrees (Figures D and E). Degrees of freedom are 8.2 and 82.6 for periods less than and greater than 6 hours. Frequency scales is logarithmic; values are normalized by the Nyquist frequency which is $4.17 \times 10^{-3} s^{-1}$.

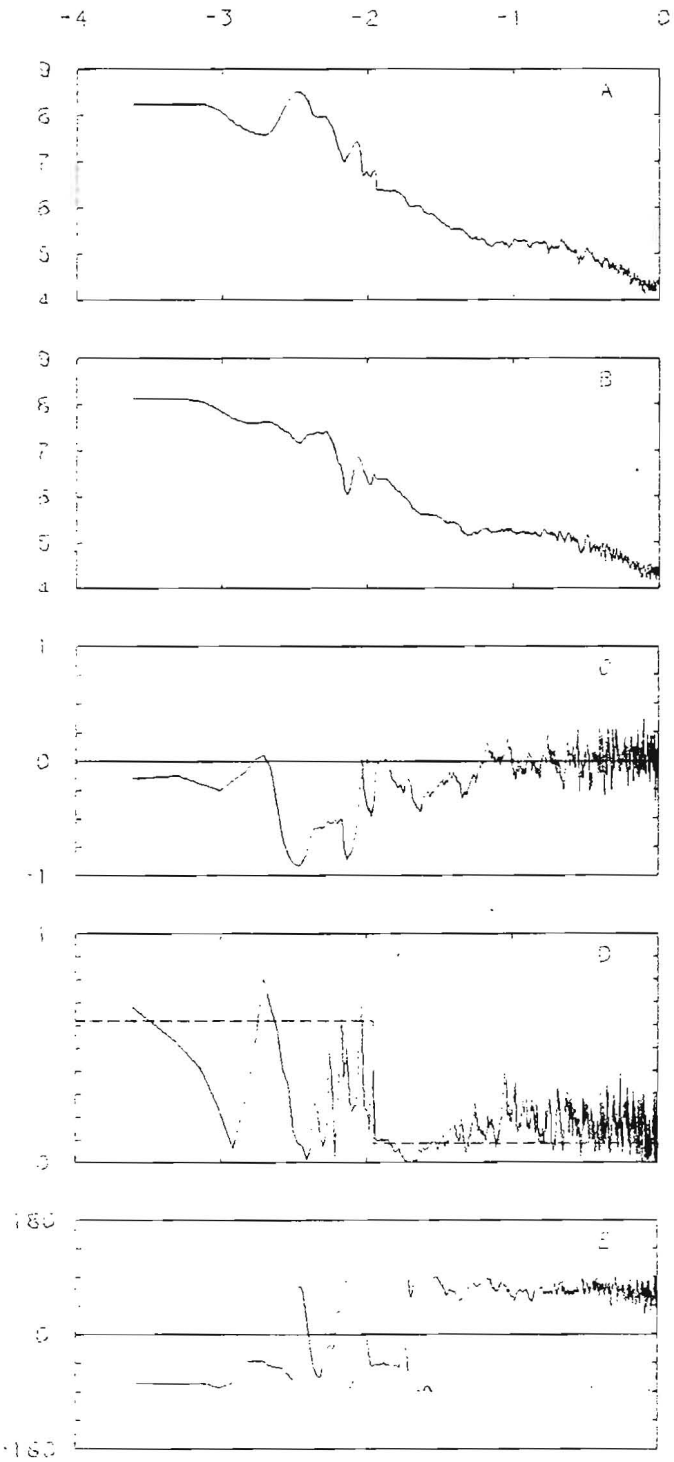

Figure 48.

Rotational invariants for vertical shear in horizontal current at mooring E for an 11.4 day record beginning on 14 July, 1980: auto spectrum for negative frequencies (Figure A); auto spectrum for positive frequencies (Figure B); rotary coefficient (Figure C); ellipse stability and ellipse orientation in degrees (Figure D and E). Degrees of freedom are 8.2 and 82.6 for periods less than and greater than 6 hours. Frequency scales is logarithmic; values are normalized by the Nyquist frequency which is $4.17 \times 10^{-3} s^{-1}$.

rotary spectra show clearly that fluctuations with periods centered on the inertial period have the maximum variance per frequency band. These fluctuations are represented by a clockwise rotating vector with a rotary coefficient of nearly minus one. At very low frequency there is also appreciable variance in the vertical shear; the phase at moorings E and C is approximately -72° and so the principal axis is approximately along 117°T. This shear would be the result of the veering of the principal axes with depth discussed earlier.

The Dye Studies

As noted earlier, dye was discharged continuously from a raft moored near current meter mooring "E" during the July, 1980 dye study, whereas the March, 1981 study consisted of 3 separate instantaneous releases. As a result, the sampling strategies differed markedly. During the July 1980 experiment the dye plume was crossed between 2 marker buoys placed perpendicular to the plume centerline, 10 or more times at up to 6 fixed distances from the dye raft. The data, therefore, consists of a series of individual cross-plume dye profiles at 3 depths at each section. The sections were located at various distances from the dye source. On the other hand, during the March 1981 experiments, the instantaneous patches were inventoried along a continuous track which crisscrossed the patch. These data consist of a series (up to 3) of horizontal dye concentration distributions at 3 depths for each release.

When dye is released into turbulent waters, such as our coastal waters, its diffusion may be studied in either a frame of reference moving with the center of mass, i.e., the centroid, or with reference to a fixed coordinate system. The former is referred to as "relative" diffusion and the latter as "absolute" diffusion (Csanady (1963)). Clearly, the instantaneous patch experiments must be studied from a relative frame of reference; the plume studies, however, can be studied from either a relative or an absolute frame or both. Absolute diffusion, of course, contains the meandering of the centroid of the plumes due to horizontal eddies larger than the scale of the plume as well as diffusion relative to the meandering centroid due to smaller scale eddies. Accordingly, our July experiments will be analyzed from both relative and absolute frames of reference; the March experiments from only a relative frame.

In the analysis that follows the following coordinate system has been adopted. For the July, 1980 experiments, the downstream or down-plume direction is denoted as the x-direction and is generally alongshore. The cross-plume direction is denoted as the y-direction. For the March, 1981 experiment, a local or natural system of coordinates is used. That is, the Y-direction is always the direction of the minor axis and the X-direction the major axis of the approximately elliptical patches.

It is useful in analyzing diffusion data to differentiate between several different kinds of time. They are:

t_a or $\overline{t_a}$, the age of the dye at a particular location,

t_p, the time since the dye discharge was initiated,

t_s, the sampling time or the time required to inventory the patch or to complete N runs at a particular section of a plume, and

t_v, an estimate of the time required for the dye to be uniformly mixed to a depth, H

Lateral Diffusion

July, 1980 Dye Study. Due to difficulties encountered in injecting the dye solution on 22 July (see footnote to Table 4a) and rough seas on 23 July, only the data taken on 24, 25, and 26 July were analyzed. To illustrate, Figure 49 shows the vertical variation of typical cross-plume dye profiles in units of $(C/q_d)10^9$ (ordinate) versus the lateral or cross-plume distance (abscissa) for selected sections and depths on 24, 25, and 26 July, 1980 from an *absolute* frame of reference. Figure 50 shows typical downstream distributions of cross-plume dye profiles at 0.9 m depth in units of $(C/q_d)10^9$ (ordinate) versus lateral or cross-plume distance (abscissa) on 24, 25, and 26 July, 1980, also from an *absolute* frame of reference. The solid curves represent individual profiles and the dashed curves the mean profile (absolute). Figures 51 and 52 shows the same information with respect to a *relative* frame of reference. That is, the individual profiles have been shifted so that their centroids coincide. The solid and dashed curves have the same meaning as before.

From these individual and mean profiles we have calculated the lateral or cross-plume variance, σ_y^2, from

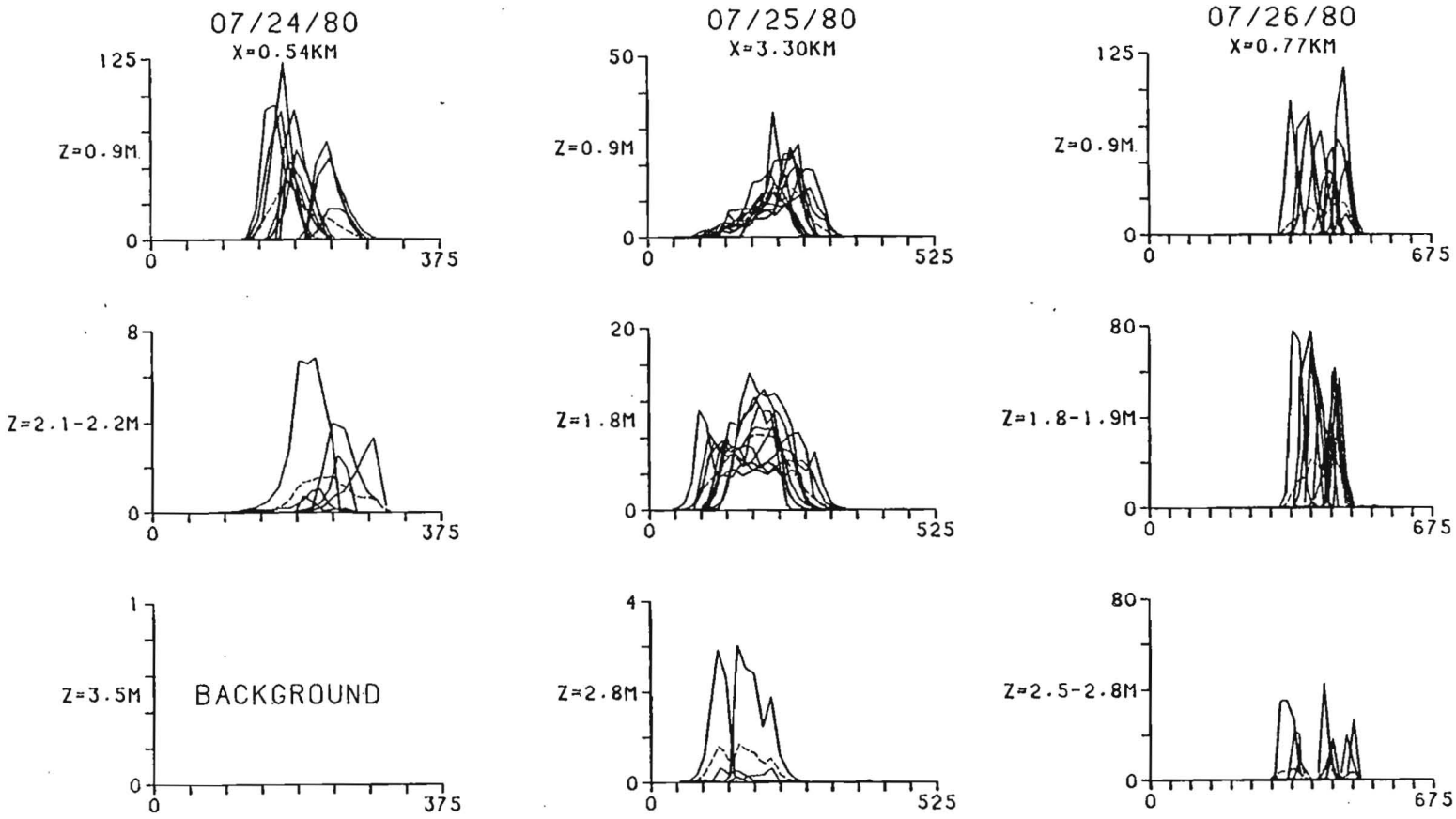

Figure 49. Vertical distribution of dye concentration in units of $(C/q_d)10^9$ (ordinate) versus lateral distance in meters (abscissa) for selected sections on 24, 25, and 26 July, 1980 from an absolute frame of reference.

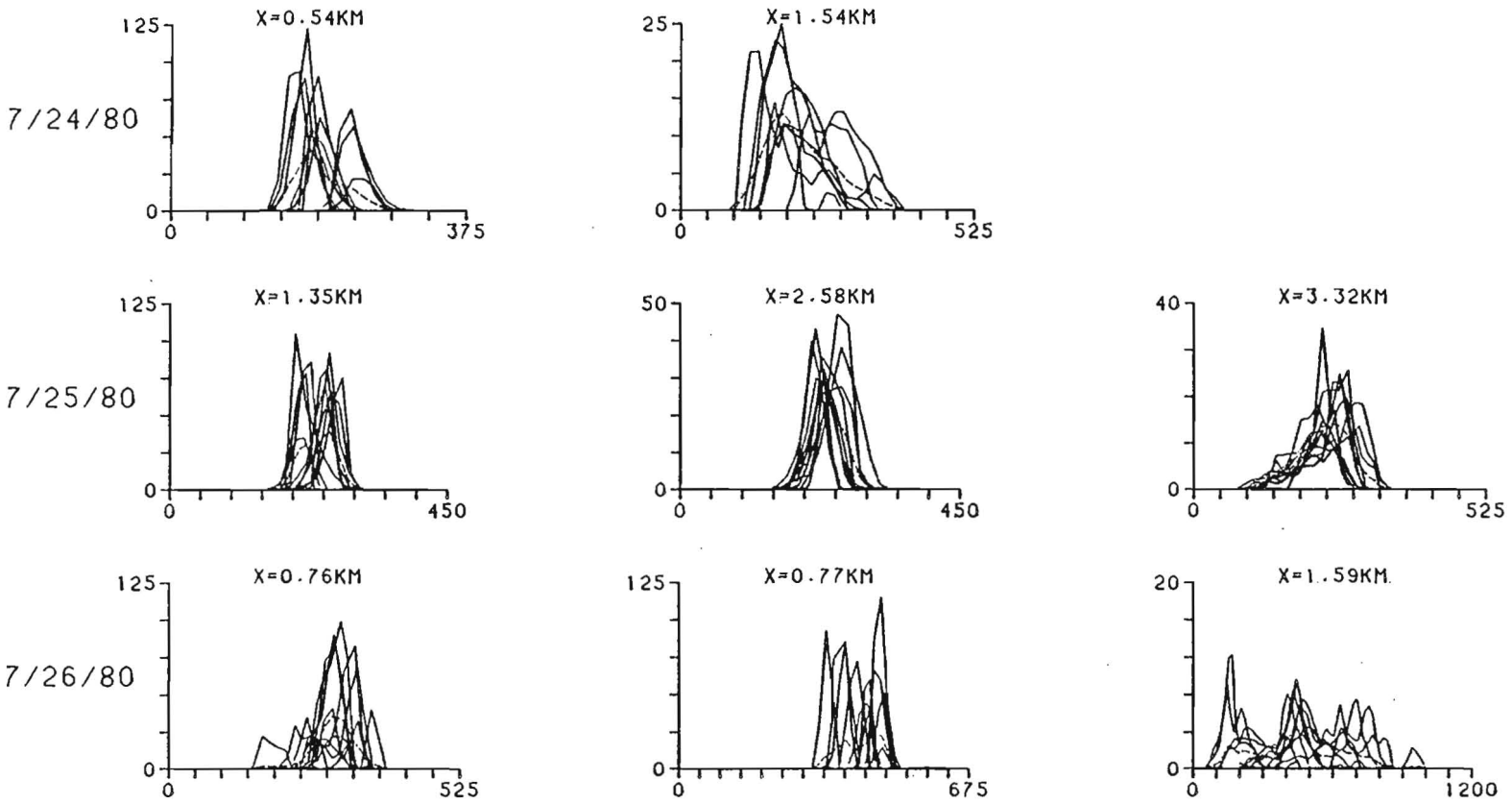

Figure 50. Downstream distribution of dye concentration at 0.9 m in units of $(C/q_d)10^9$ (ordinate) versus lateral distance in meters (abscissa) on 24, 25, and 26 July, 1980 from an absolute frame of reference.

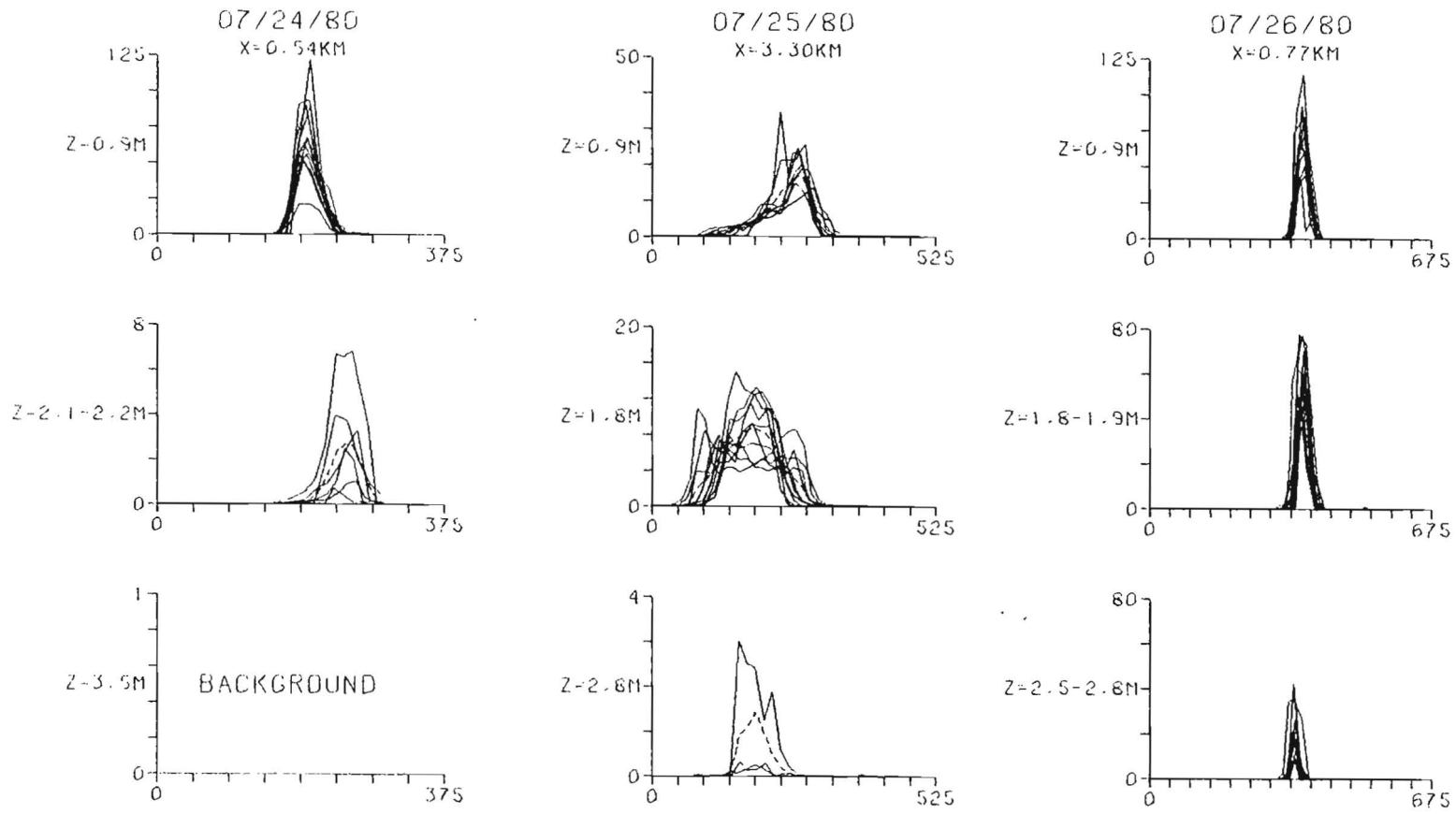

Figure 51. Vertical distribution of dye concentration in units of $(C/q_d)10^9$ (ordinate) versus lateral distance in meters (abscissa) for selected sections on 24, 25, and 26 July, 1980 from a frame of reference relative to the centroid.

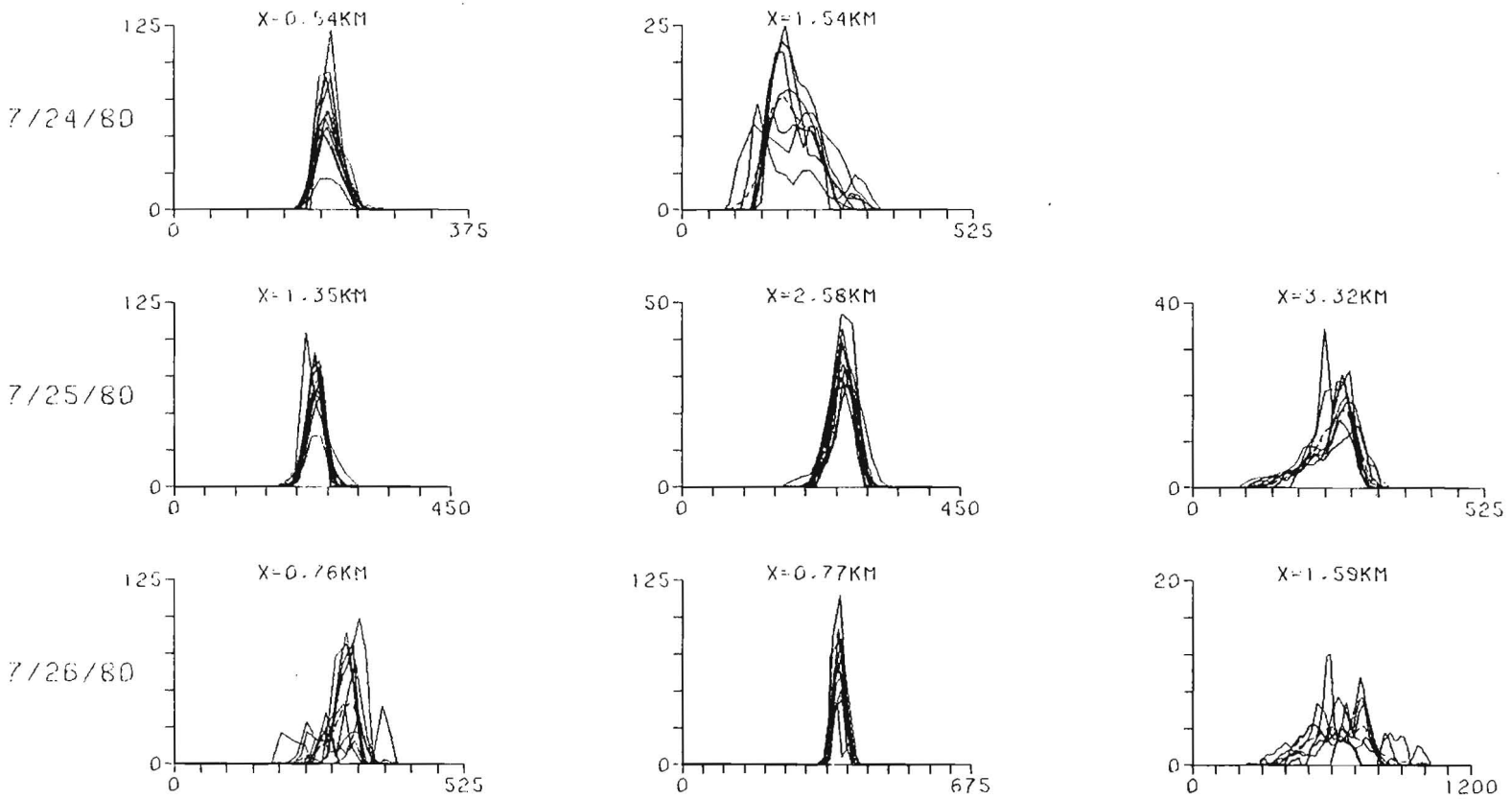

Figure 52. Downstream distribution of dye concentration at 0.9 m in units of $(C/q_d)10^9$ (ordinate) versus lateral distance in meters (abscissa) on 24, 25, and 26 July, 1980 from a frame of reference relative to the centroid.

$$\sigma_y^2 = \int_{-\infty}^{+\infty} C'(y-\bar{y})^2 dy / \int_{-\infty}^{+\infty} C' dy$$

where C' is the dye concentration in units of $(C/q_d)10^9$ and y is the cross-plume or lateral direction. Tables 9 through 11 list the calculated variances and ages for the individual runs by date, depth, and downstream distance (section). Missing runs are the result of the plume not being completely crossed at all levels, navigation failures or no dye (background). Table 12 lists the lateral or cross-plume variance for both relative and (absolute) mean dye concentration profiles for 24, 25, and 26 July, 1980 for depths between 0.9 and 4.2 m and downstream distances between 0.49 and 3.32 km. The data for a depth of 0.9 m are plotted on Figures 53 and 54 versus the average age appropriate for the section, i.e., the average of the ages in Tables 9 through 11. The profile ages, t_a, shown in Tables 9 through 11 were estimated from the 15 foot (4.6 m) current meter record from station "E" which was located in close proximity to the dye raft. See Figure 7. That is, a release time, t_{rel}, was estimated from

$$x = \int_{t_{obs}}^{t_{obs} - t_{rel}} (u^2+v^2)^{\frac{1}{2}} dt$$

where t_{obs} was the average local time of observation of the profile and x was the straight line distance between the dye raft and the center of the section where the profile was measured. The age, t_a, is given by $t_{obs} - t_{rel}$ and represents the time that a hypothetical, small, instantaneous patch of dye released at t_{obs} would take to

Table 9

The cross-plume variance, σ_y^2, and ages, t_a of the individual runs for 24 July, 1980 at depths of 0.9, 2.1-2.2, and 4.2 m.

$z = 0.9$ m

x = 0.49 km			x = 0.54 km			x = 1.54 km			x = 1.84 km		
Run#	σ_y^2, cm^2	t_a, m	Run#	σ_y^2, cm^2	t_a, m	Run#	σ_y^2, cm^2	t_a, m	Run#	σ_y^2, cm^2	t_a, m
–	No data at 0.9 m		35	2.57×10^6	54	47	1.55×10^7	178	–	No data at 0.9 m	
–			36	1.92×10^6	54	48	1.53×10^7	180	–		
–			37	1.59×10^6	56	49	1.91×10^7	186	–		
–			38	2.41×10^6	56	50	4.04×10^7	190	–		
–			39	2.48×10^6	56	51	5.03×10^7	196	–		
–			40	2.33×10^6	58	52	1.26×10^7	204	–		
–			41	2.40×10^6	58	53	1.41×10^7	212	–		
–			42	2.03×10^6	60	–	–	–	–		
–			43	2.37×10^6	62	–	–	–	–		
–			44	3.70×10^6	62	–	–	–	–		

$z = 2.1$-2.2 m

2	2.26×10^6	#	35	8.69×10^6	54	47	7.81×10^7	178	26	6.50×10^6	180
3	4.18×10^6	#	36	5.40×10^6	54	50	5.66×10^7	190	27	7.35×10^6	166
5	3.48×10^5	#	37	5.22×10^6	56	51	7.45×10^6	196	28	8.51×10^6	160
9	4.91×10^5	#	41	2.03×10^6	58	53	4.96×10^7	212	29	6.13×10^6	154
–	–	–	42	4.26×10^6	60	–		–	–	–	–
–	–	–	43	4.57×10^6	62	–		–	–	–	–

$z = 4.2$ m

3	7.52×10^6	#	–	Background		–	Background		29	6.15×10^7	154
4A	9.50×10^6	#	–			–			31	4.27×10^7	134
12	1.35×10^6	#	–			–			–	–	–

current reversing at approximate time of discharge.

Table 10

The cross-plume variance, σ_y^2, and ages, t_a, of the individual runs for 25 July, 1980 at depths of 0.9, 1.6-1.8, and 2.8 m.

z = 0.9 m

x = 0.52 km			x = 0.90 km			x = 0.98 km			x = 1.35 km			x = 2.58 km			x = 3.32 km		
Run#	σ_y^2, cm^2	t_a, m	Run#	σ_y^2, cm^2	t_a, m	Run#	σ_y^2, cm^2	t_a, m	Run#	σ_y^2, cm^2	t_a, m	Run#	σ_y^2, cm^2	t_a, m	Run#	σ_y^2, cm^2	t_a, m
2	8.03×10^5	38	12	1.36×10^6	54	52	5.31×10^6	44	22	4.51×10^6	76	32	2.01×10^6	120	42	7.93×10^6	162
3	3.16×10^5	36	14	2.97×10^6	54	53	6.05×10^6	44	23	2.14×10^6	76	33	4.13×10^6	120	43	1.27×10^7	162
4	5.97×10^5	34	15	4.74×10^6	54	54	1.38×10^6	44	24	3.96×10^6	74	34	3.05×10^6	120	44	1.51×10^7	160
5	1.13×10^6	36	16	5.62×10^6	52	-	-	-	25	1.27×10^6	74	35	3.02×10^6	120	45	1.60×10^7	160
6	9.45×10^5	34	17	2.10×10^6	52	-	-	-	26	1.81×10^6	74	36	2.81×10^6	120	46	2.58×10^7	158
9	1.17×10^6	34	18	1.37×10^7	52	-	-	-	27	3.18×10^6	74	37	3.59×10^6	120	47	3.09×10^7	158
10	1.09×10^6	34	19	7.39×10^5	50	-	-	-	28	2.59×10^6	74	38	2.92×10^6	100	48	3.41×10^7	156
11	6.60×10^6	32	20	7.15×10^5	52	-	-	-	29	2.80×10^6	72	39	4.12×10^6	100	49	2.12×10^7	156
-	-	-	21	4.25×10^6	52	-	-	-	30	4.34×10^6	72	40	3.95×10^6	100	50	1.59×10^7	154
									31	2.65×10^6	72	41	8.16×10^6	100	51	1.35×10^7	154

z = 1.6-1.8 m

-		-	12	4.27×10^6	54	52			23	7.91×10^6	76	32	6.39×10^6	120	42	1.33×10^7	162
-		-	14	6.23×10^6	54	53			26	3.17×10^6	74	33	6.67×10^6	120	43	1.15×10^7	162
-		-	15	1.96×10^6	54	54			28	1.59×10^7	74	34	3.20×10^6	120	44	2.26×10^7	160
-		-	-	-	-	55			29	1.03×10^6	72	35	5.48×10^6	120	45	3.35×10^7	160
-		-	-	-	-	56			30	3.94×10^7	72	36	3.83×10^6	120	46	3.55×10^7	158
-		-	-	-	-	57			31	1.92×10^7	72	37	3.19×10^6	120	47	5.76×10^7	158
-		-	-	-	-	58			-	-	-	38	4.58×10^6	100	48	4.69×10^7	156
-		-	-	-	-	59			-	-	-	39	6.55×10^6	100	49	2.35×10^7	156
-		-	-	-	-	60			-	-	-	40	1.22×10^7	100	50	1.81×10^7	154
-		-	-	-	-	61			-	-	-	41	1.10×10^7	100	51	9.86×10^6	154
-	No data at 1.6-1.8 m	-	-	-	-	62			-	-	-	-	-	-			

z = 2.8 m

-			12	2.21×10^6	54	-			-			-			42	8.63×10^6	162
-			14	6.89×10^5	53	-			-			-			43	3.24×10^6	162
-			16	2.40×10^7	52	-			-			-			45	6.35×10^7	160
-		Background	-	-	-	-		Background	-		Background	-		Background	46	1.78×10^7	158

Table 11

The cross-plume variance, σ_y^2, and ages, t_a, of the individual runs for 26 July, 1980 at depths of 0.9, 1.8-1.9 m, and 2.5-2.8 m.

z = 0.9 m

x = 0.76 km			x = 0.77 km			x = 1.14 km			x = 1.59 km		
Run#	σ_y^2, cm^2	t_a, m	Run#	σ_y^2, cm^2	t_a, m	Run#	σ_y^2, cm^2	t_a, m	Run#	σ_y^2, cm^2	t_a, m
12	4.90×10^6	98	34	3.01×10^6	66	1	3.42×10^6	110	23	9.72×10^7	224
13	2.37×10^7	100	35	6.50×10^6	66	2	1.15×10^7	112	24	2.28×10^8	228
14	4.40×10^7	102	36	3.21×10^7	64	3	1.48×10^7	114	25	1.33×10^8	230
15	2.07×10^7	102	37	3.53×10^6	62	4	2.82×10^7	116	26	2.67×10^8	230
16	2.03×10^7	102	38	1.38×10^6	60	–	–	–	27	1.34×10^8	230
17	3.26×10^7	102	39	1.08×10^7	60	–	–	–	28	1.96×10^8	228
18	1.24×10^7	104	40	1.16×10^7	58	–	–	–	29	1.24×10^8	226
19	3.53×10^6	108	41	2.68×10^7	58	–	–	–	30	1.81×10^8	224
20	1.48×10^7	108	42	7.86×10^6	58	–	–	–	31	1.71×10^8	220
21	2.21×10^7	110	43	1.33×10^7	58	–	–	–	–	–	–

z = 1.8-1.9 m

12	2.22×10^7	98	34	6.13×10^6	66	1	3.81×10^6	110	23	7.29×10^7	224
13	2.89×10^7	100	35	3.77×10^7	66	2	6.62×10^5	112	24	1.68×10^8	228
14	5.53×10^7	102	36	1.76×10^7	64	3	2.18×10^6	114	25	2.74×10^8	230
15	3.06×10^7	102	37	7.95×10^7	62	4	3.27×10^6	116	26	2.13×10^8	230
16	1.81×10^7	102	38	1.41×10^6	60	5	3.68×10^6	118	27	1.61×10^8	230
17	2.04×10^7	102	39	1.48×10^6	60	6	3.40×10^6	122	28	1.38×10^8	228
18	2.50×10^7	103	40	1.59×10^6	58	7	3.16×10^7	124	29	1.38×10^8	226
19	3.44×10^7	108	41	1.01×10^6	58	8	2.17×10^7	126	30	1.67×10^8	224
20	1.76×10^7	108	42	1.26×10^6	58	9	9.22×10^6	128	31	1.01×10^8	220
21	2.01×10^7	110	43	4.27×10^6	58	10	1.30×10^7	130	–	–	–
22	1.60×10^7	110	–	–	–	–	–	–	–	–	–

Table 11 (continued)

z = 2.5-2.8 km

x = 0.76 km			x = 0.77 km			x = 1.14 km			x = 1.59 km		
Run#	σ_y^2, cm^2	t_a, m	Run#	σ_y^2, cm^2	t_a, m	Run#	σ_y^2, cm^2	t_a, m	Run#	σ_y^2, cm^2	t_a, m
12	1.04×10^7	98	34	2.55×10^7	66	1	9.25×10^5	110	23	2.69×10^8	224
13	7.22×10^6	100	35	1.57×10^8	66	2	6.28×10^5	112	24	2.00×10^8	228
15	5.25×10^5	102	36	1.64×10^8	64	3	2.60×10^6	114	25	2.40×10^8	230
17	1.83×10^7	102	37	1.66×10^8	62	4	1.18×10^6	116	26	1.82×10^8	230
20	7.56×10^4	108	38	1.55×10^8	60	5	7.74×10^5	118	27	9.89×10^7	230
21	7.63×10^6	110	39	5.48×10^7	60	6	5.40×10^5	122	28	1.44×10^8	228
–	–	–	40	1.27×10^7	58	7	3.34×10^6	124	29	1.47×10^8	226
–	–	–	41	6.33×10^7	58	8	2.71×10^7	126	30	6.63×10^7	224
–	–	–	42	9.76×10^7	58	9	1.68×10^7	128	31	3.67×10^7	220
–	–	–	–	–	–	10	3.91×10^6	130	–	–	–
–	–	–	–	–	–	11	3.95×10^6	132	–	–	–

Table 12

Lateral or cross-plume variance of mean dye concentration profiles, $\sigma^2_{y,m}$, relative to the centroid and (unshifted (absolute)) for 24, 25, and 26 July, 1980.

7/24/80

x,km	z = 0.9 m	z = 2.2 m	z = 4.2 m
0.49	no data	2.99×10^6 (1.39×10^7)	9.55×10^6 (1.58×10^7)
0.54	3.04×10^6 (1.18×10^7)	6.19×10^6 (1.62×10^7)	background
1.54	2.76×10^7 (4.41×10^7)	6.78×10^7 (7.62×10^7)	background
1.84	no data	9.76×10^6 (2.30×10^7)	1.05×10^8 (1.08×10^8)

7/25/80

x,km	z = 0.9 m	z = 1.6-1.8 m	z = 2.8 m
0.52	1.79×10^6 (1.09×10^7)	no data	no data
0.90	5.96×10^6 (8.07×10^6)	8.25×10^6 (1.88×10^7)	3.06×10^7 (3.66×10^7)
0.98	7.10×10^6 (1.16×10^7)		background
1.35	3.85×10^6 (8.71×10^6)	8.36×10^6 (1.37×10^7)	background
2.58	4.89×10^6 (7.75×10^6)	7.74×10^6 (1.13×10^7)	background
3.32	2.17×10^7 (2.54×10^7)	3.12×10^7 (2.54×10^7)	1.41×10^7 (2.86×10^7)

7/26/80

x,km	z = 0.9 m	z = 1.8-1.9 m	z = 2.5-2.8 m
0.76	1.52×10^7 (1.77×10^7)	1.74×10^7 (3.45×10^7)	1.12×10^7 (1.86×10^7)
0.77	2.97×10^7 (2.50×10^7)	1.46×10^6 (1.63×10^7)	1.46×10^6 (4.35×10^7)
1.14	2.96×10^6 (5.45×10^6)	2.90×10^6 (2.12×10^7)	5.59×10^6 (4.17×10^7)
1.59	1.81×10^8 (4.21×10^8)	1.87×10^8 (4.19×10^8)	1.68×10^8 (4.84×10^8)

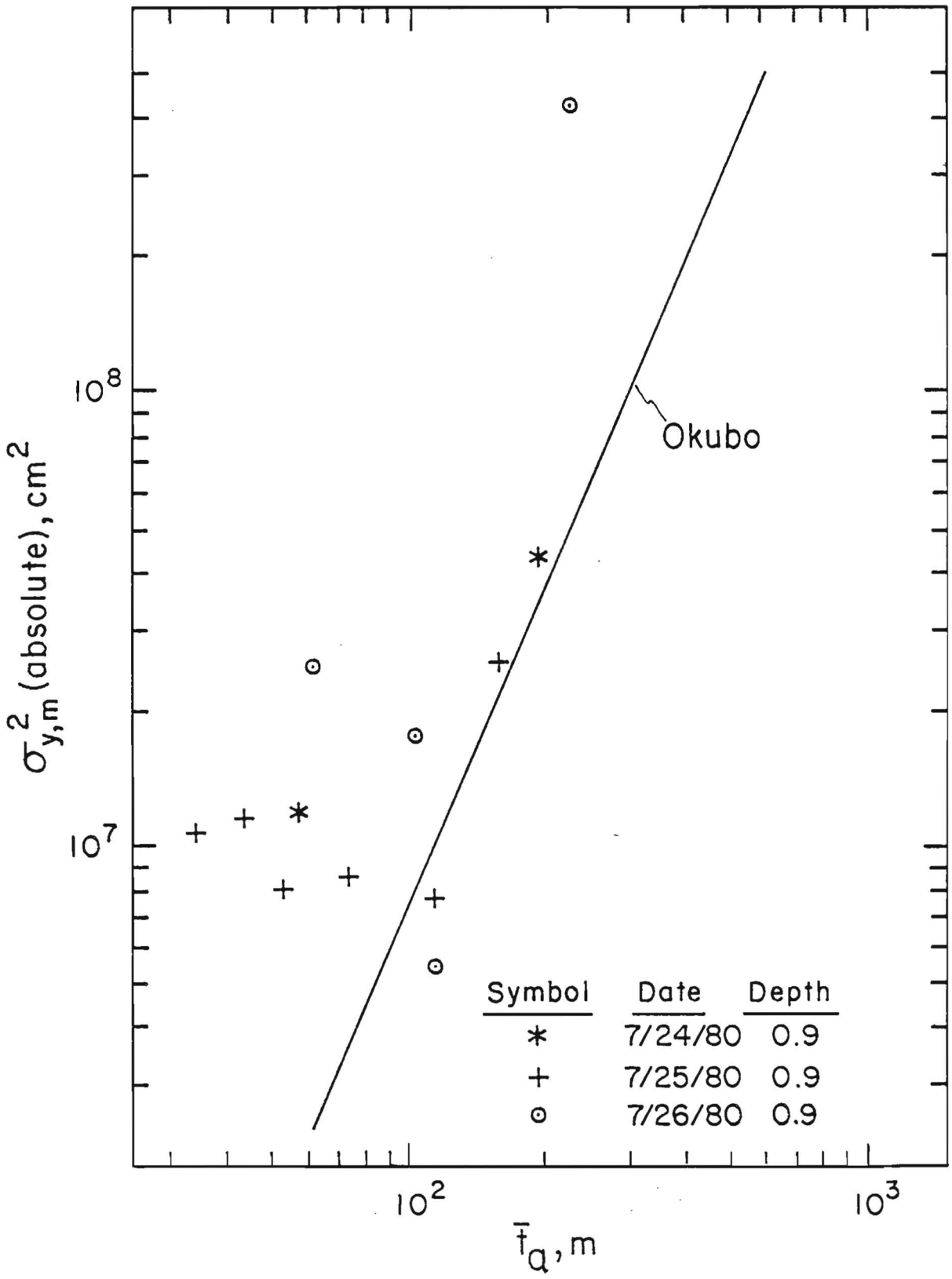

Figure 53. Lateral variance of the sectional mean dye concentration profiles (absolute) as a function of age, $\bar{t}_a$, for 24, 25, and 26 July, 1980.

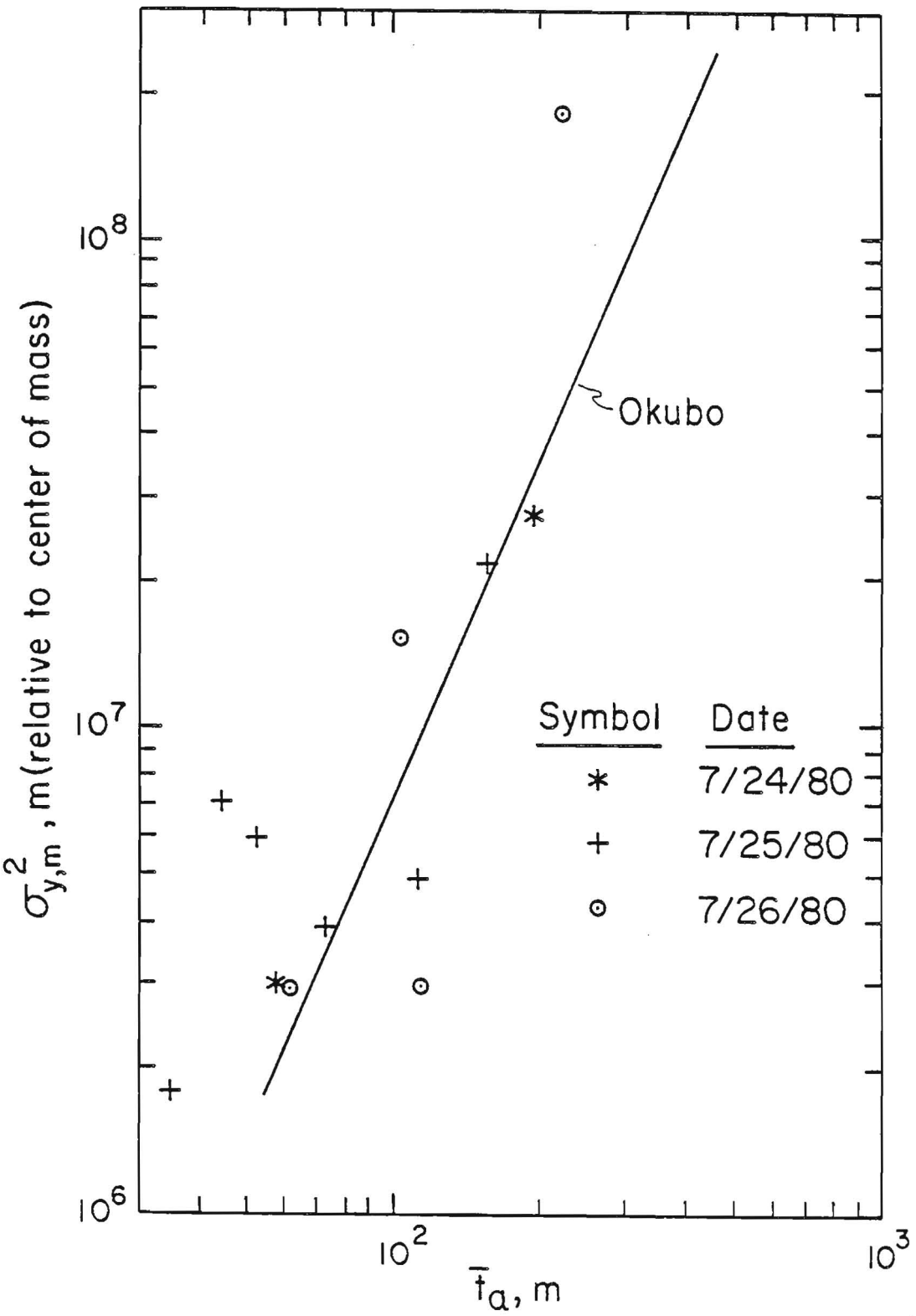

Figure 54. Lateral variance of the sectional mean dye concentration profiles relative to the centroid as a function of age, $\bar{t}_a$, for 24, 25 and 26 July, 1980.

reach the section located x km from the dye raft. It is assumed to represent the mean age of the dye in the measured profile. This method should not be used if a current reversal occurs between t_{obs} and t_{rel}. The only time this occurred during our study was at the section located at x = 0.49 km on 24 July, 1980.

A word of caution about Figure 53, the absolute lateral variance versus age. The data on this figure for ages less than 100 minutes are relatively constant and of the order of 10^7 cm^2. This is considered anomalous since it should approach a very small value as the source is approached, i.e., the age approaches zero. One possible explanation is the manner in which the dye raft was moored. Because of the exposed location and low freeboard of the dye raft, it was anchored so that it could swing freely although on a relatively short scope of anchor line. It can easily be shown that motion in a circle with a radius of 30 m would result in aliasing the absolute variance by $(30)^2$ or $\sim 10^7$ cm^2 if the period of the motion was shorter than the travel time, i.e., age, to a particular section. Support for this hypothesis is contained in Figures 13D and E. These figures show (as noted on page 50) that there were significant oscillations, stably oriented in the cross-isobath, cross-plume direction, of periods less than 100 minutes. There were no significant, stable oscillations with periods between 6 hours and 100 m. Although the power of these high frequency oscillations was low, it was probably sufficient to significantly alias the absolute variances at short times (< 100 m).

March 1981 Dye Study. Figures 55 through 72 show the horizontal distribution of dye tracer at various times and depths and the vertical distribution at the same times at representative cross-sections. Turbulent diffusion parameters, such as variances, have been inferred from these distributions as follows.

The concentration, $C(t,r_e)$, can usually be well described by the following generalized exponential distribution

$$C(t,r_e) = \frac{M\Gamma(4/m)m}{2\pi\sigma_{rc}^2 D(\Gamma(2/m))^2} \exp\{-(r_e/a\sigma_{rc})m\} \quad (1a)$$

$$= C(t,0) \exp\{-(r_e/a\sigma_{rc})^m\} \quad (1b)$$

where $a = \{\Gamma(2/m)/\Gamma(4/m)\}^{\frac{1}{2}}$; $C(t,0)$, the peak concentration $= M\Gamma(4/m)m/2\pi\sigma_{rc}^2 D(\Gamma(2/m))^2$; σ_{rc}^2 is the variance; m a positive number, and D the depth through which the dye is considered to be uniformly distributed. Taking the natural logarithm of both sides of equation (1b) twice, we have

$$\ell n[\ell n(C(t,r_e)/C(t,0))] = m\{\ell n(a\sigma_{rc}) - \ell n(r_e)\} \quad (2)$$

If we now planimeter the irregular areas within the various isolines of concentration on the horizontal distribution figures, calculate the equivalent circular radius, r_e, of these irregular areas from $(\text{area}/\pi)^{\frac{1}{2}}$, and plot $\ell n\{\ell n(C(t,r_e)/C(t,0)\}$ versus $\ell n\ r_e$, the slope of this regression line provides an estimate of m and its intercept a measure of σ_{rc} (given m from the slope).

Two special radially symmetric diffusion models for horizontal diffusion from an instantaneous vertical line source, M/D, are

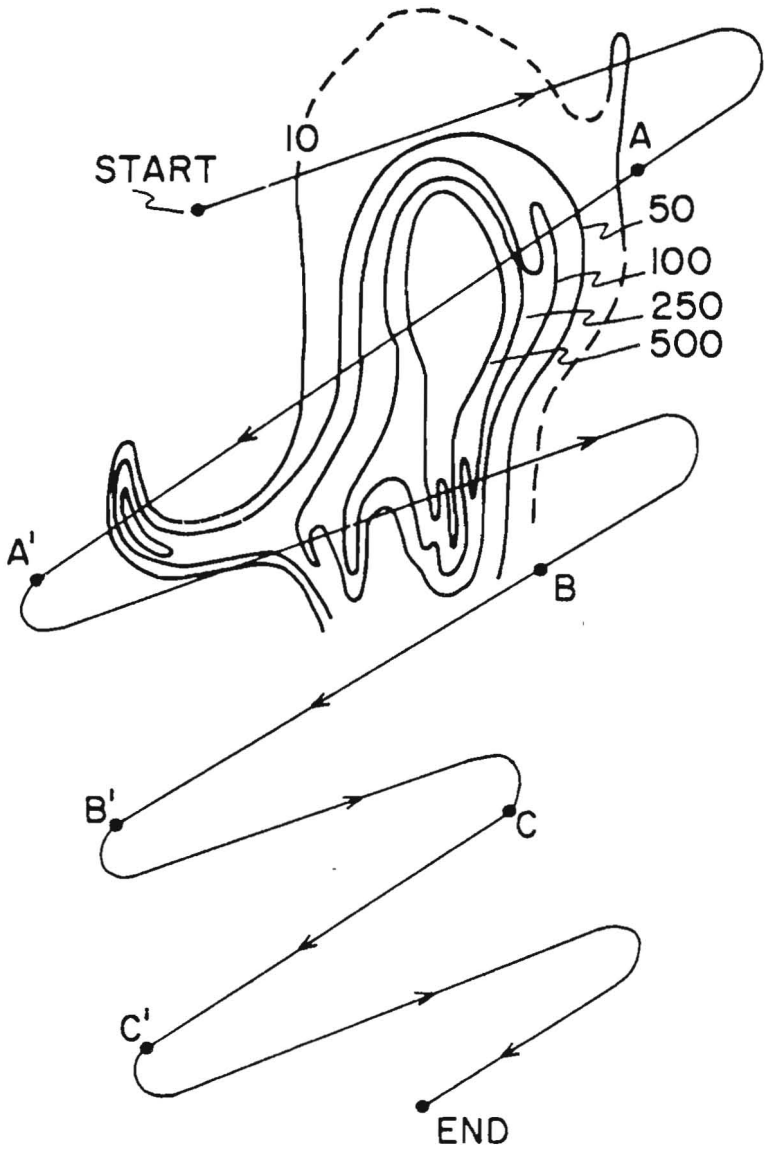

DISTRIBUTION OF RHODAMINE SOLUTION (RhWT)
AT 0.9 m ON 3/10/81 IN UNITS OF $(C/\Gamma)10^{10}$
PATCH AGE = 13212 s ; D.L. = DETECTABLE LIMIT

Scale: 1 to 40,000

Figure 55. Horizontal distribution of tracer at 0.9 m (3/10/81)

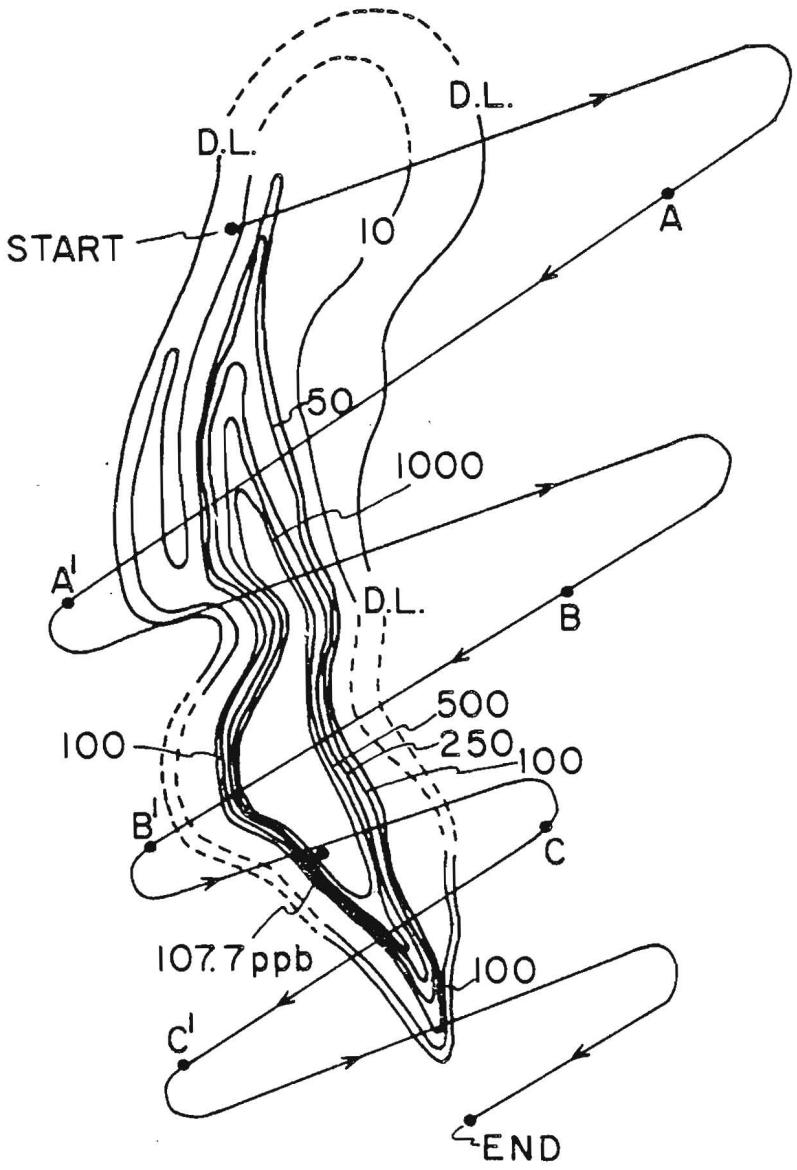

DISTRIBUTION OF RHODAMINE SOLUTION (RhWT)
AT 1.9m ON 3/10/81 IN UNITS OF $(C/\Gamma)10^{10}$
PATCH AGE = 13212s; D.L. = DETECTABLE LIMIT

Scale: 1 to 40,000

Figure 56. Horizontal distribution of tracer at 1.9 m (3/10/81)

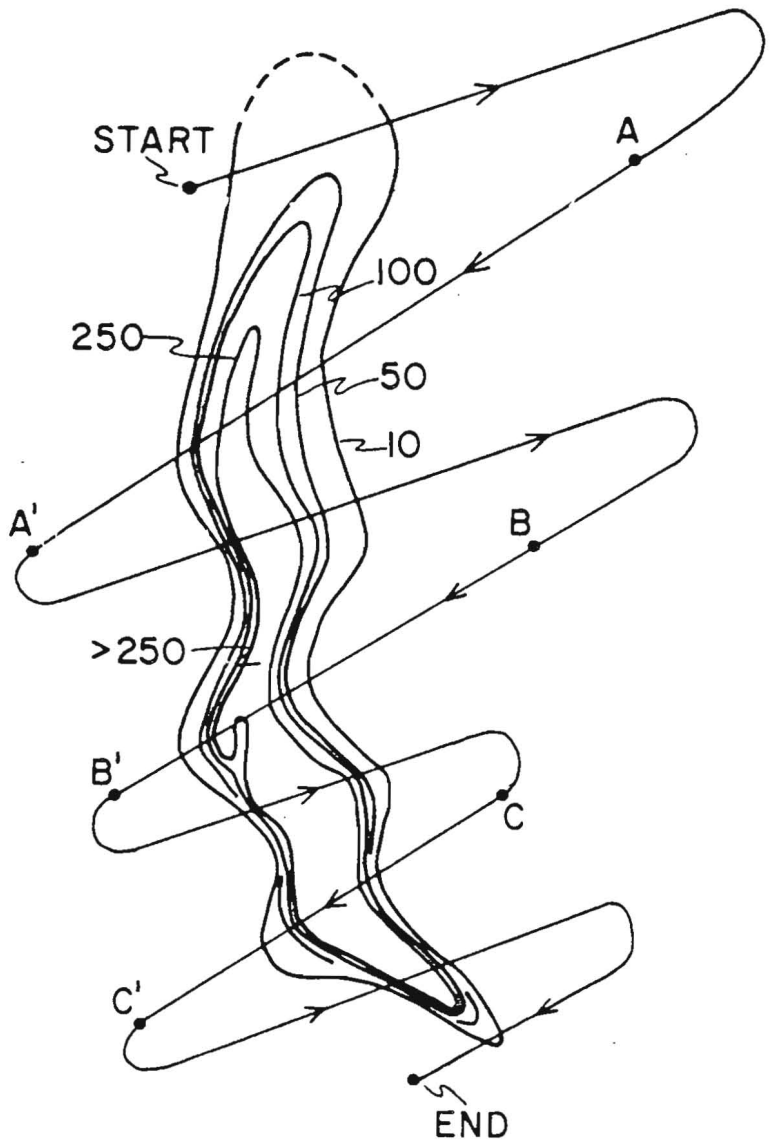

DISTRIBUTION OF RHODAMINE SOLUTION (RhWT)
AT 3.8m ON 3/10/81 IN UNITS OF $(C/\Gamma)10^{10}$
PATCH AGE = 13212s; D.L. = DETECTABLE LIMIT

Scale: 1 to 40,000

Figure 57. Horizontal distribution of tracer at 3.8 m (3/10/81).

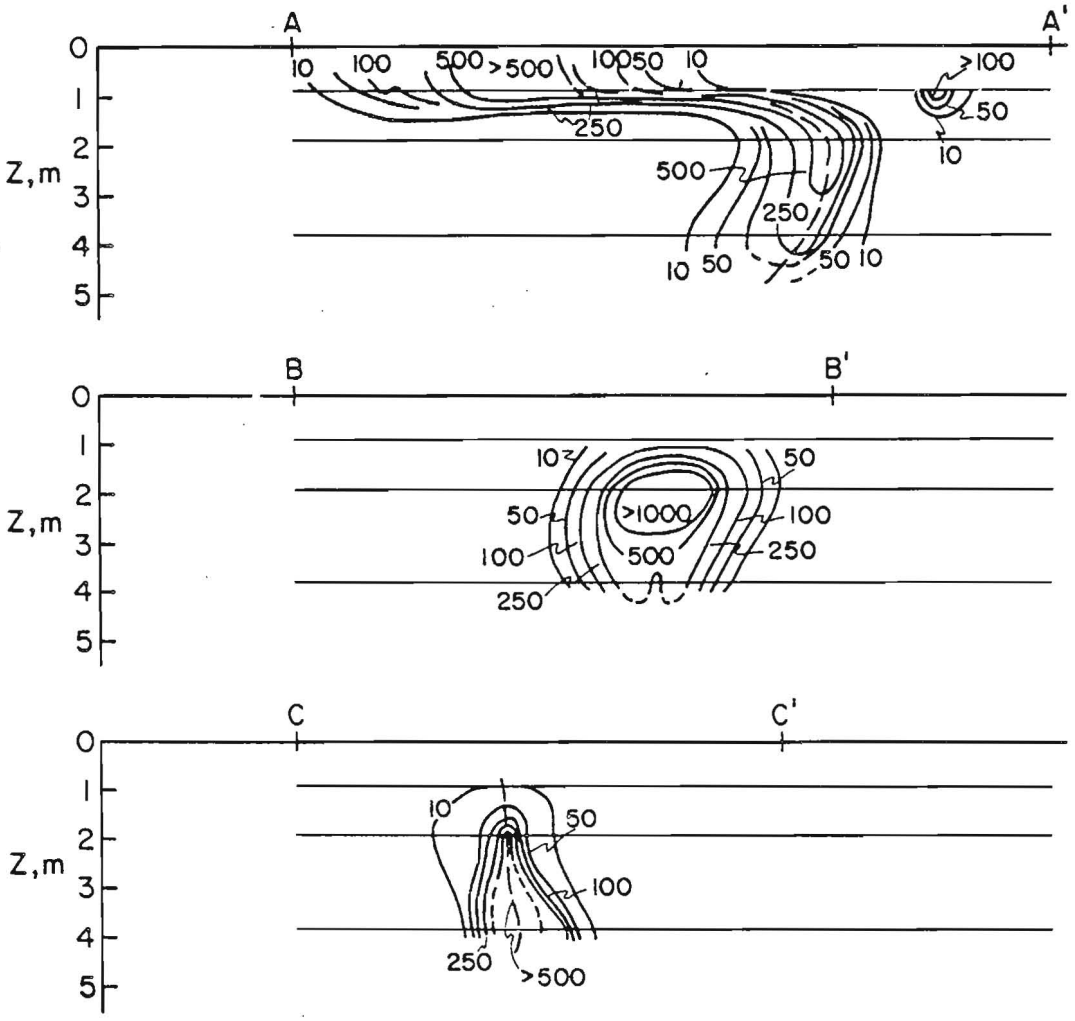

Figure 58. Vertical distribution of tracer at sections A-A', B-B', and C-C' (3/10/81).

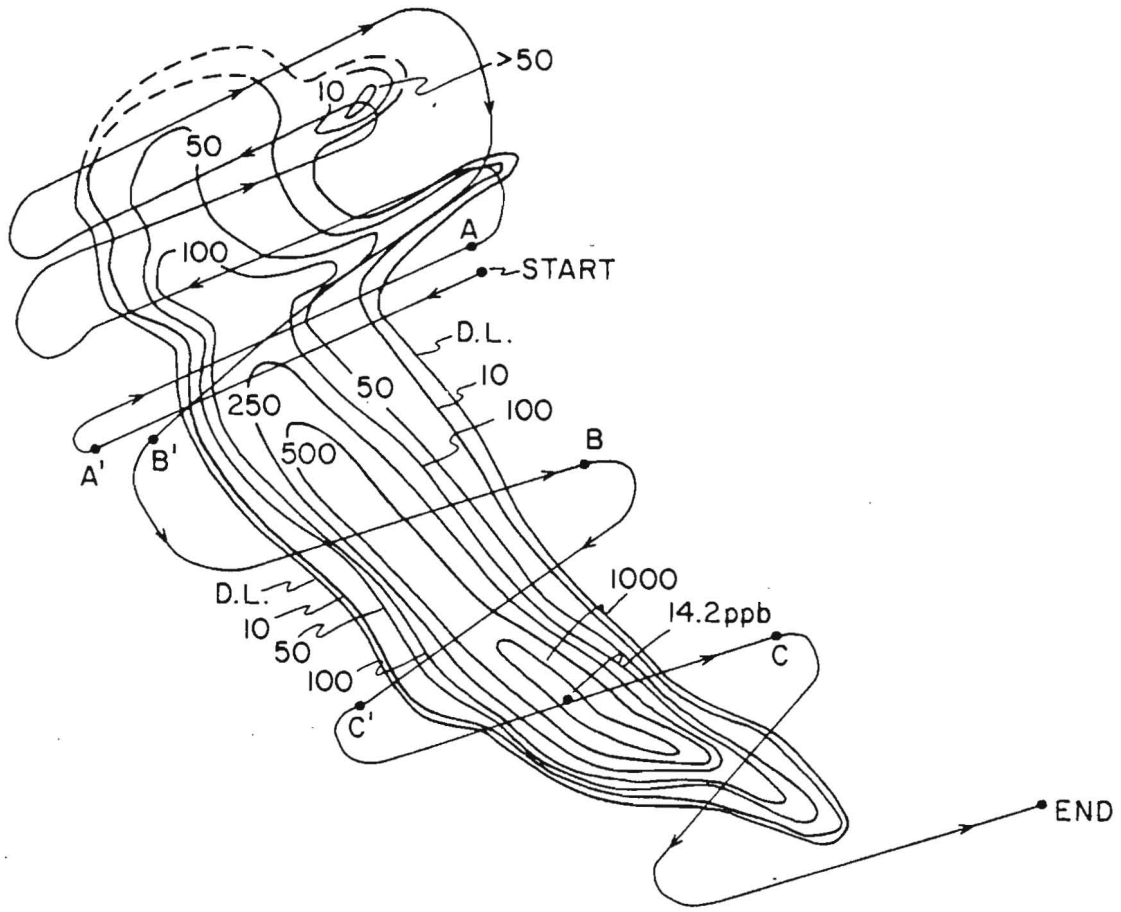

DISTRIBUTION OF RHODAMINE SOLUTION (RhWT)
AT 2.8m ON 3/10/81 IN UNITS OF $(C/\Gamma)10^{10}$
PATCH AGE = 21648s; D.L. = DETECTABLE LIMIT

Scale: 1 to 51,000

Figure 59. Horizontal distribution of tracer at 2.8 m (3/10/81).

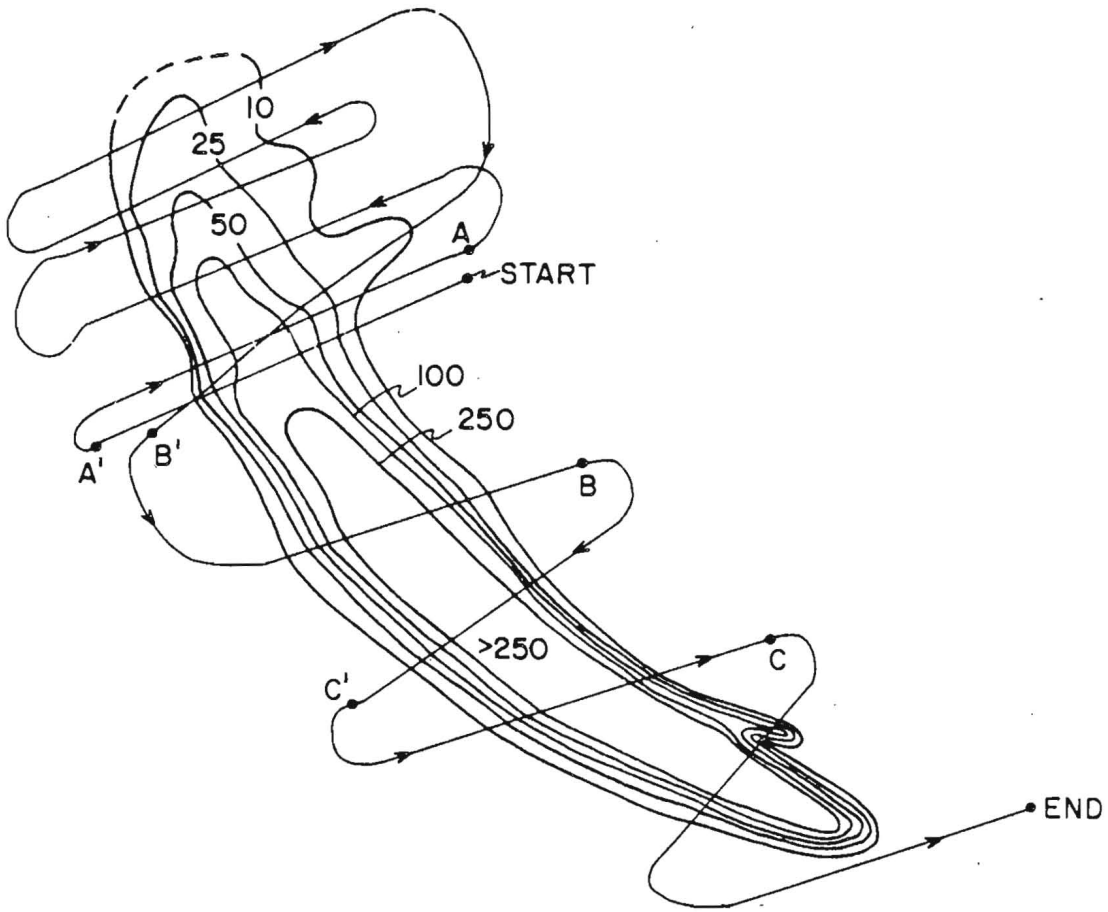

DISTRIBUTION OF RHODAMINE SOLUTION (RhWT)
AT 6.6 m ON 3/10/81 IN UNITS OF $(C/\Gamma)\,10^{10}$
PATCH AGE = 21648 s ; D.L. = DETECTABLE LIMIT

Scale: 1 to 51,000

Figure 60. Horizontal distribution of tracer at 6.6 m (3/10/81).

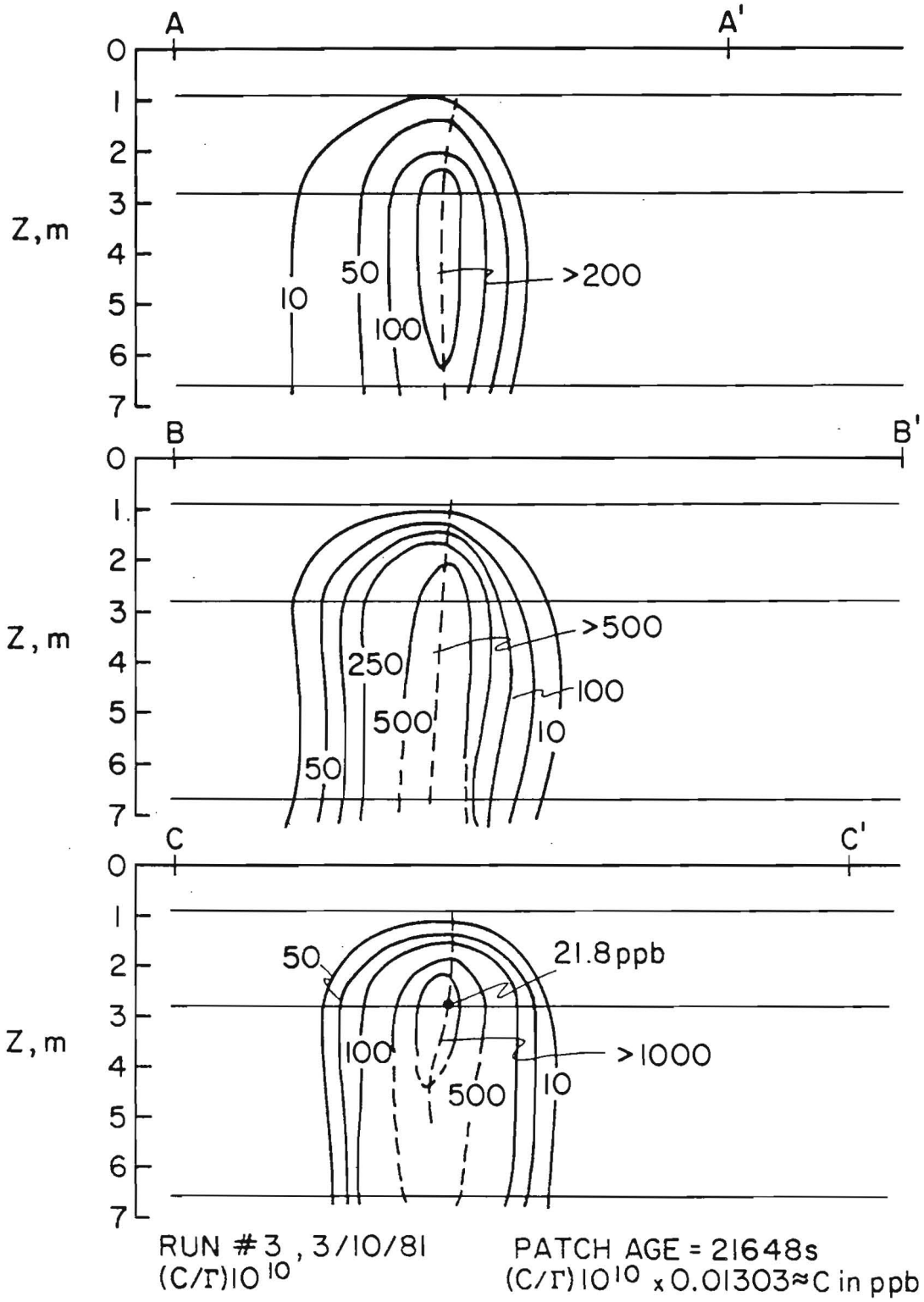

Figure 61. Vertical distribution of tracer at sections A-A', B-B', and C-C' (3/10/81).

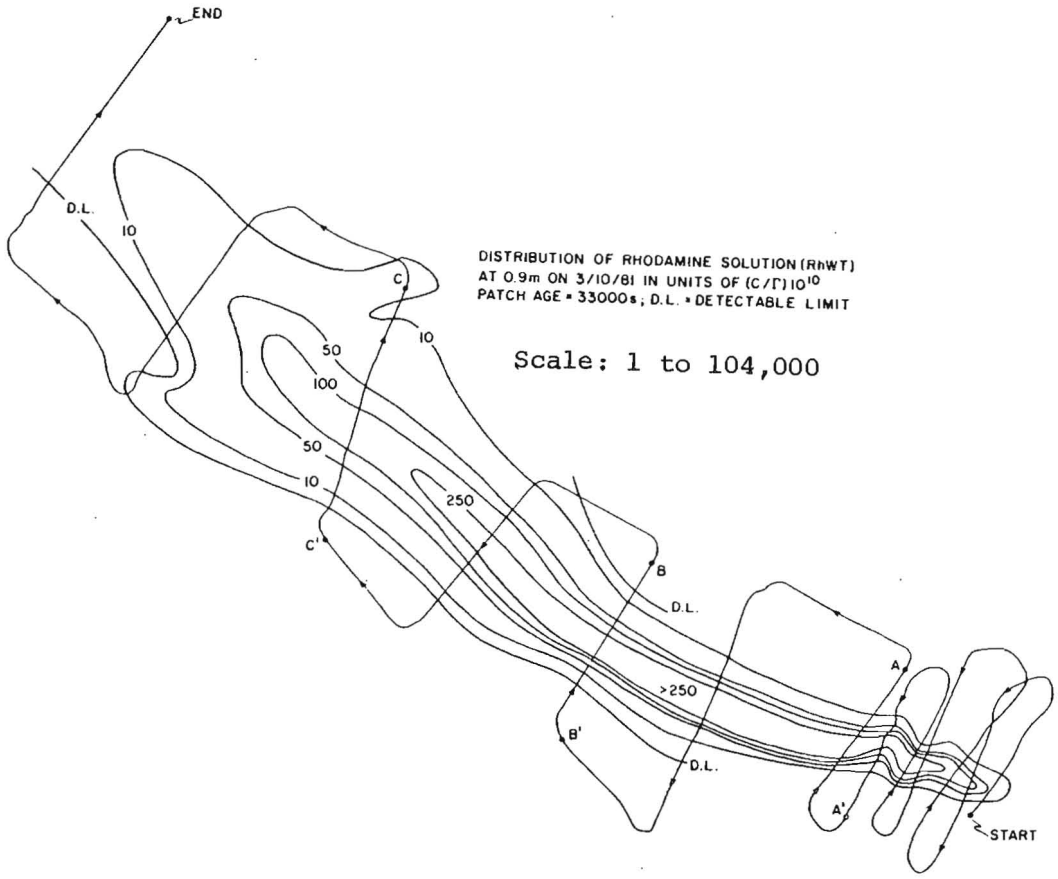

Figure 62. Horizontal distribution of tracer at 0.9 m (3/10/81).

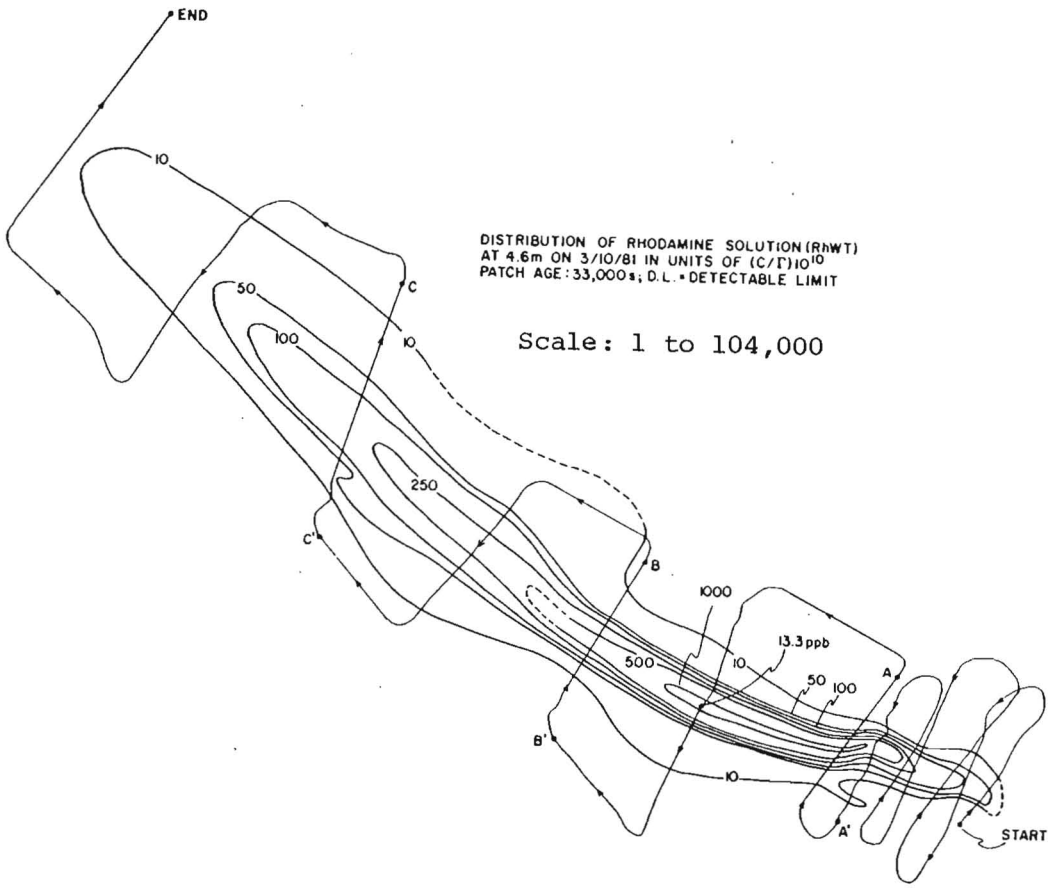

Figure 63. Horizontal distribution of tracer at 4.6 m (3/10/81).

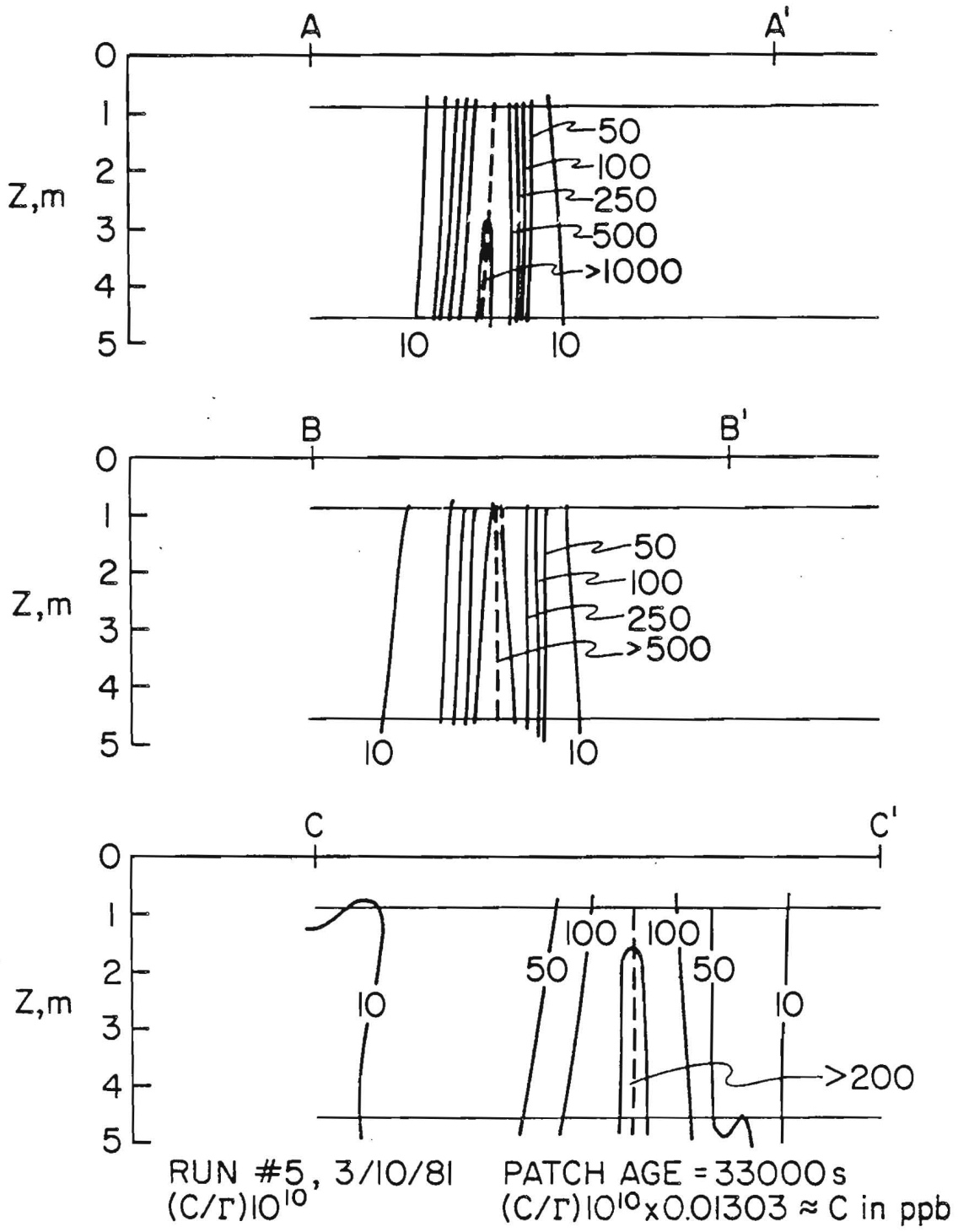

Figure 64. Vertical distribution of tracer at sections A-A', B-B', and C-C' (3/10/81).

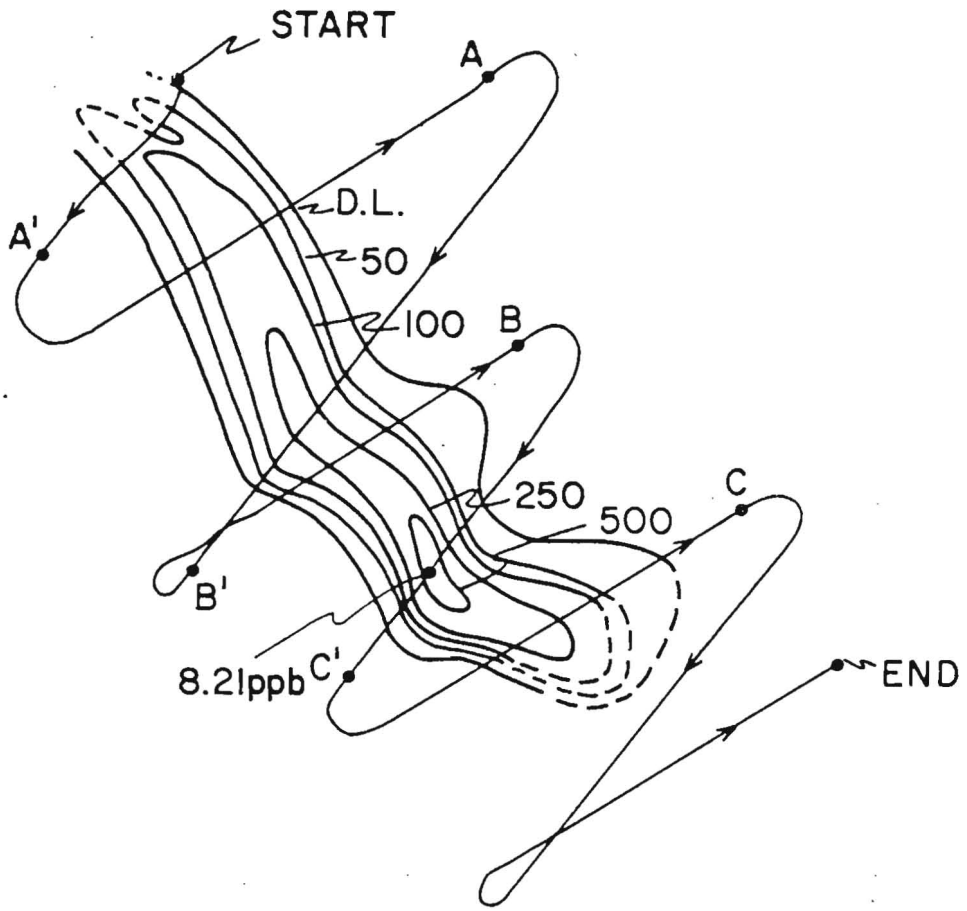

DISTRIBUTION OF RHODAMINE SOLUTION (RhWT)
AT 2.4 – 2.7m ON 3/12/81 IN UNITS OF (C/Γ)10^{10}
PATCH AGE = 12294s; D.L. = DETECTABLE LIMIT

Scale: 1 to 40,000

Figure 65. Horizontal distribution of tracer at 2.4–2.7 m (3/12/81).

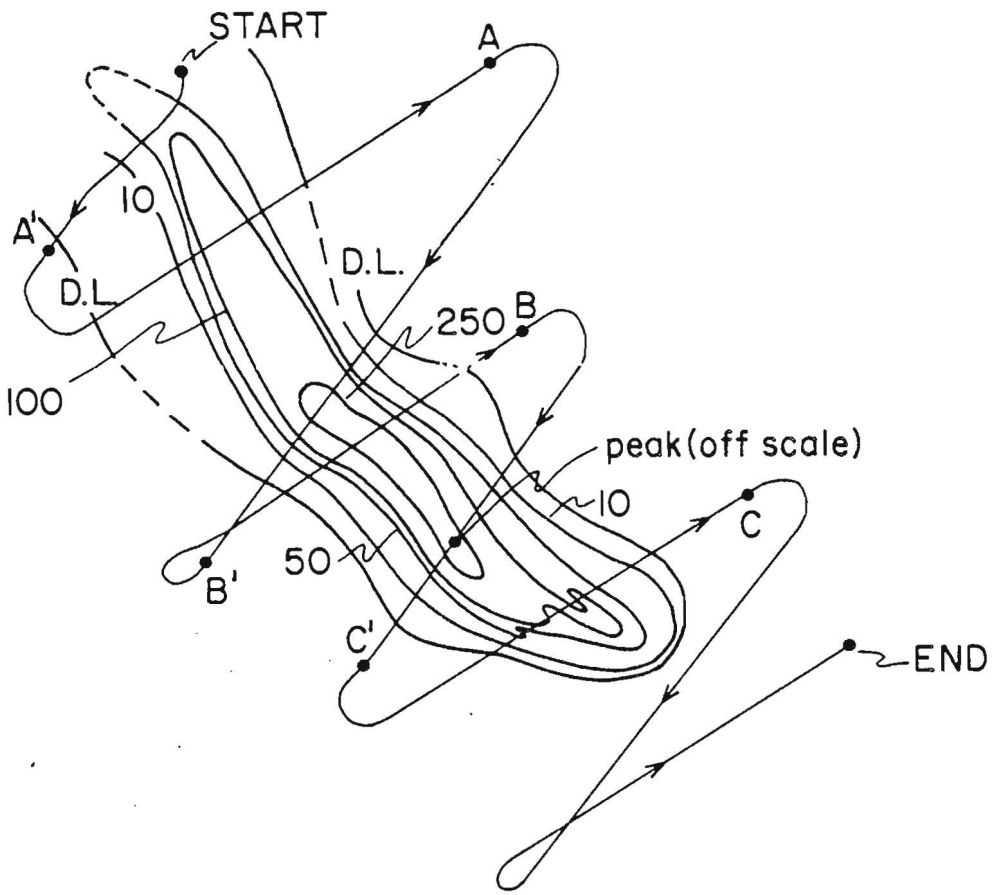

DISTRIBUTION OF RHODAMINE SOLUTION (RhWT)
AT 4.0 - 4.5m ON 3/12/81 IN UNITS OF $(C/\Gamma)10^{10}$
PATCH AGE = 12294 s; D.L. = DETECTABLE LIMIT

Scale: 1 to 40,000

Figure 66. Horizontal distribution of tracer at 4.0-4.5 m (3/12/81).

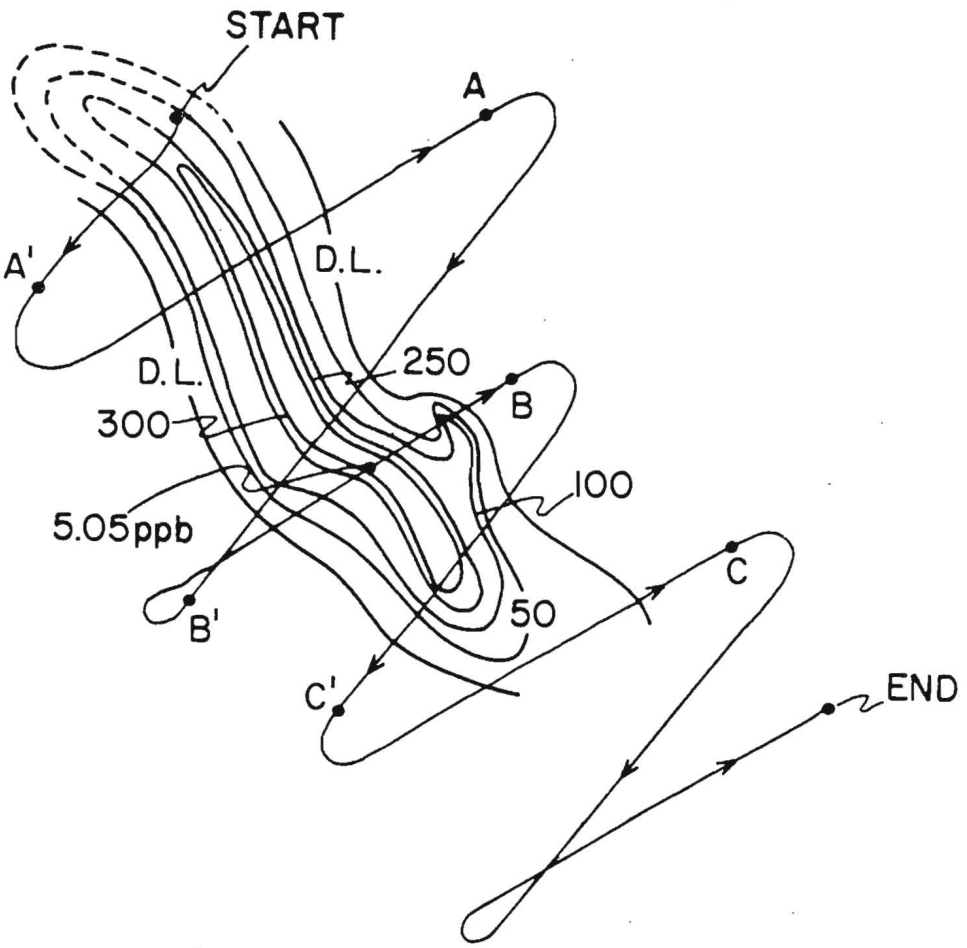

DISTRIBUTION OF RHODAMINE SOLUTION (RhWT)
AT 5.5 - 6.3m ON 3/12/81 IN UNITS OF $(C/\Gamma)10^{10}$
PATCH AGE = 12294s ; D.L. = DETECTABLE LIMIT

Scale: 1 to 40,000

Figure 67. Horizontal distribution of tracer at 5.5-6.3 m (3/12/81).

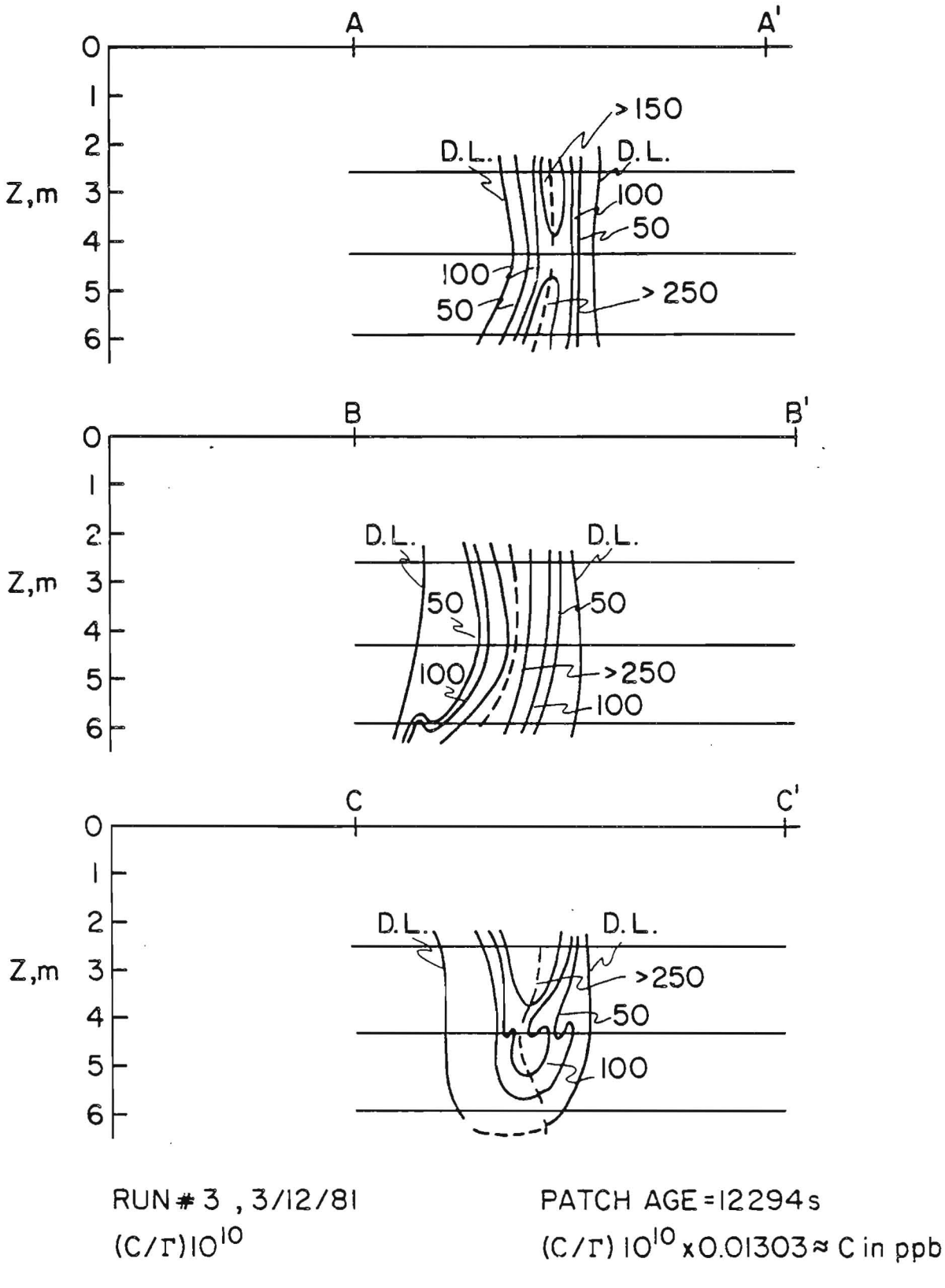

Figure 68. Vertical distribution of tracer at sections A-A', B-B', and C-C' (3/12/81).

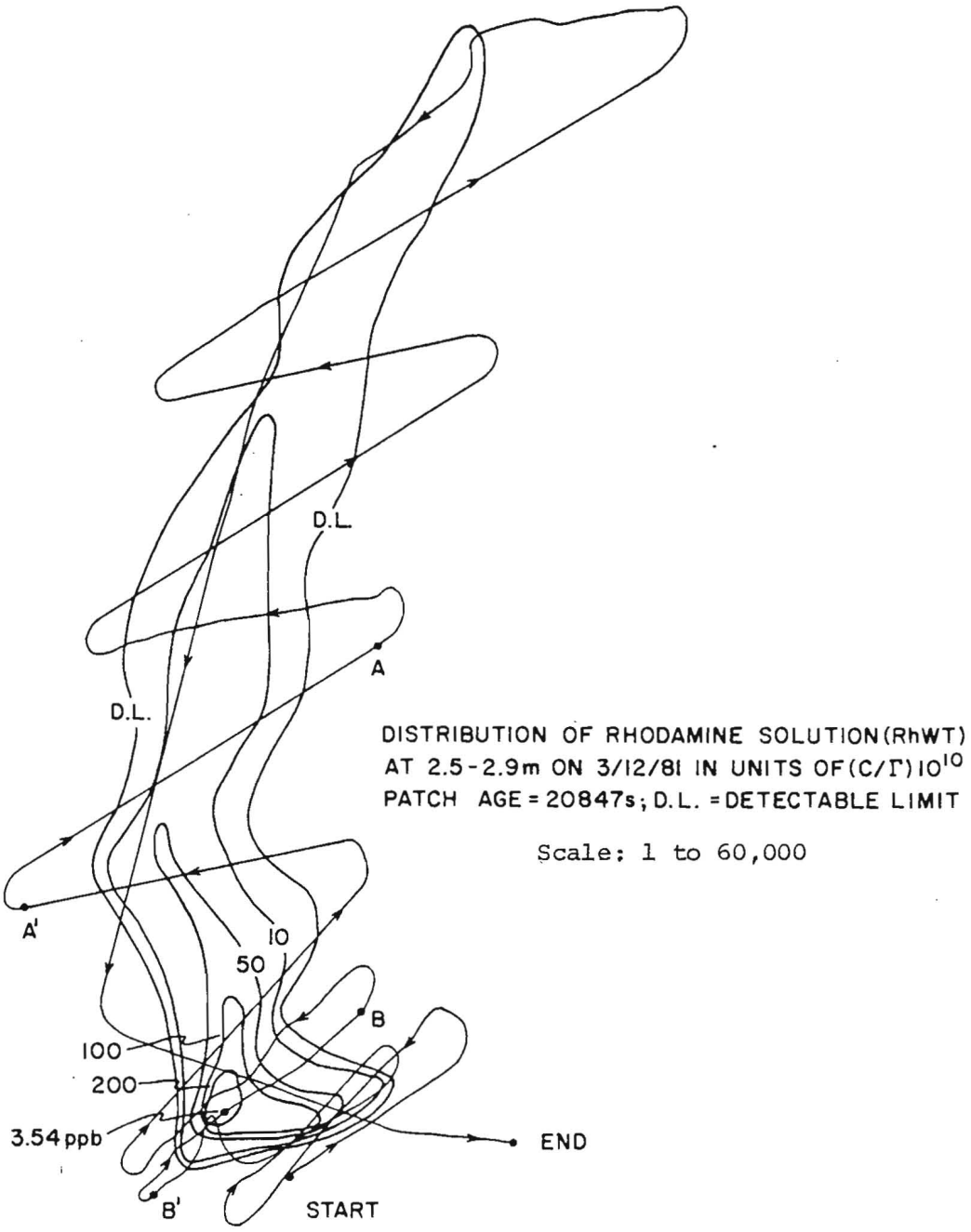

Figure 69. Horizontal distribution of tracer at 2.5-2.9 m (3/12/81).

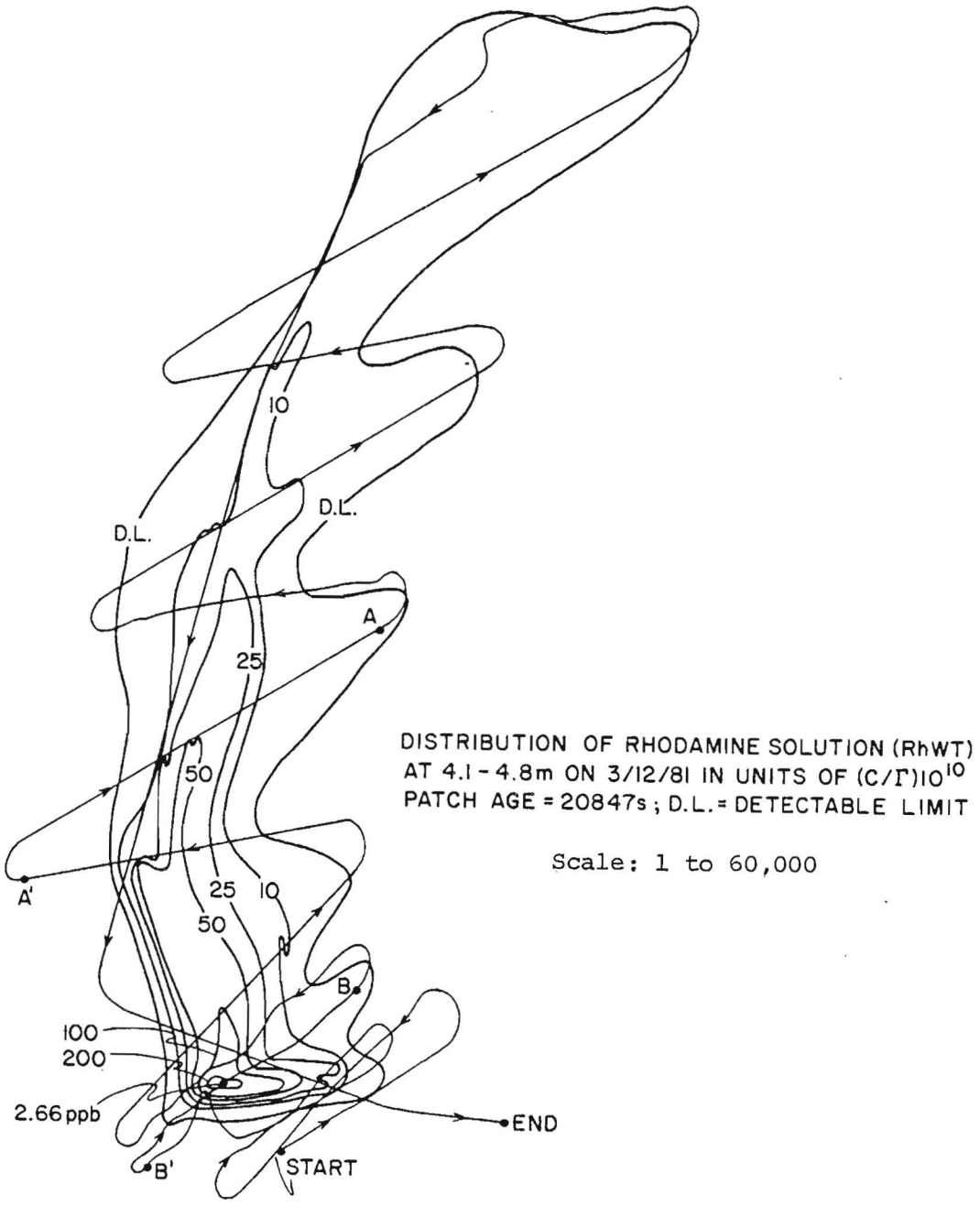

Figure 70. Horizontal distribution of tracer at 4.1-4.8 m (3/12/81).

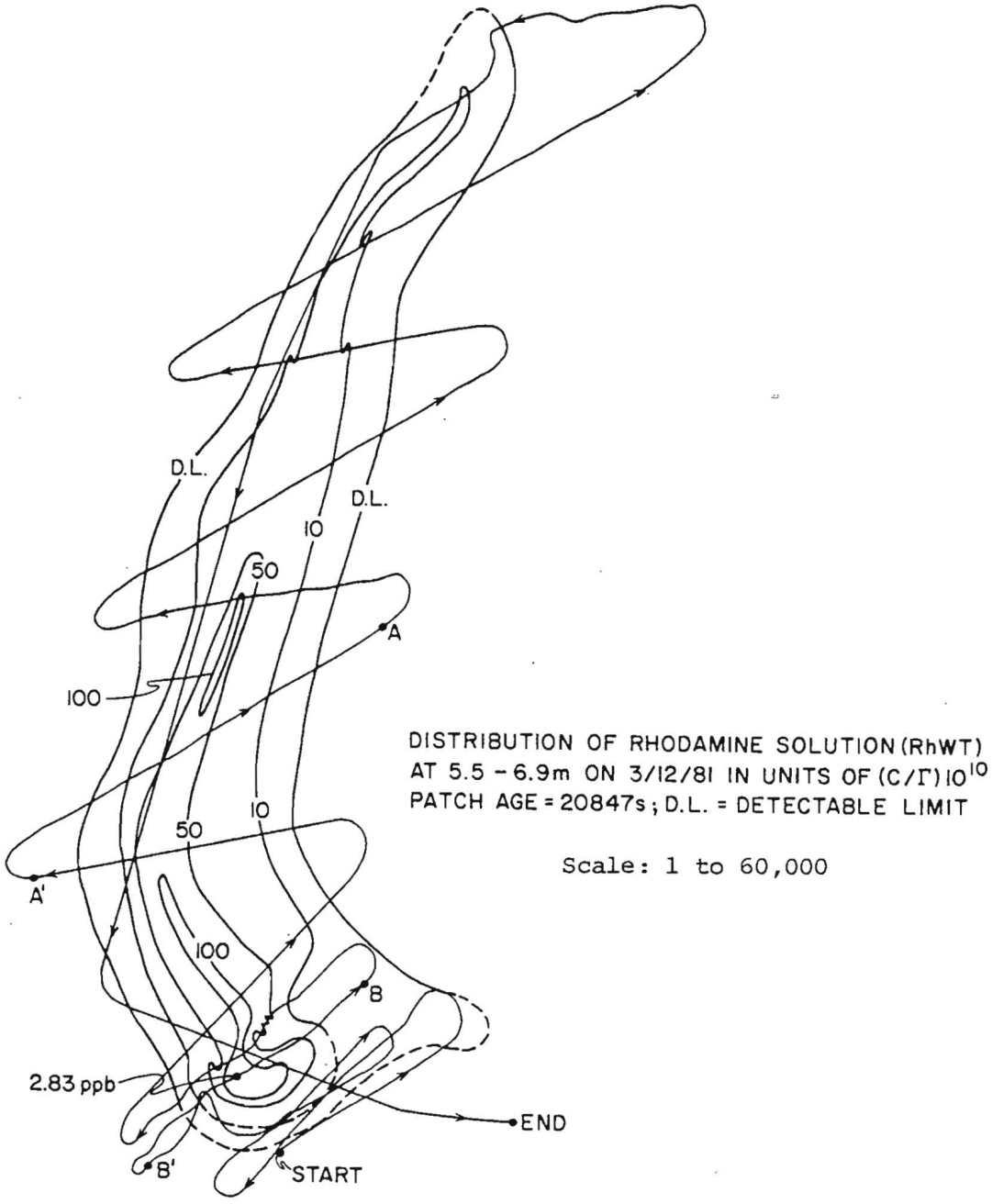

Figure 71. Horizontal distribution of tracer at 5.5-6.9 m (3/12/81).

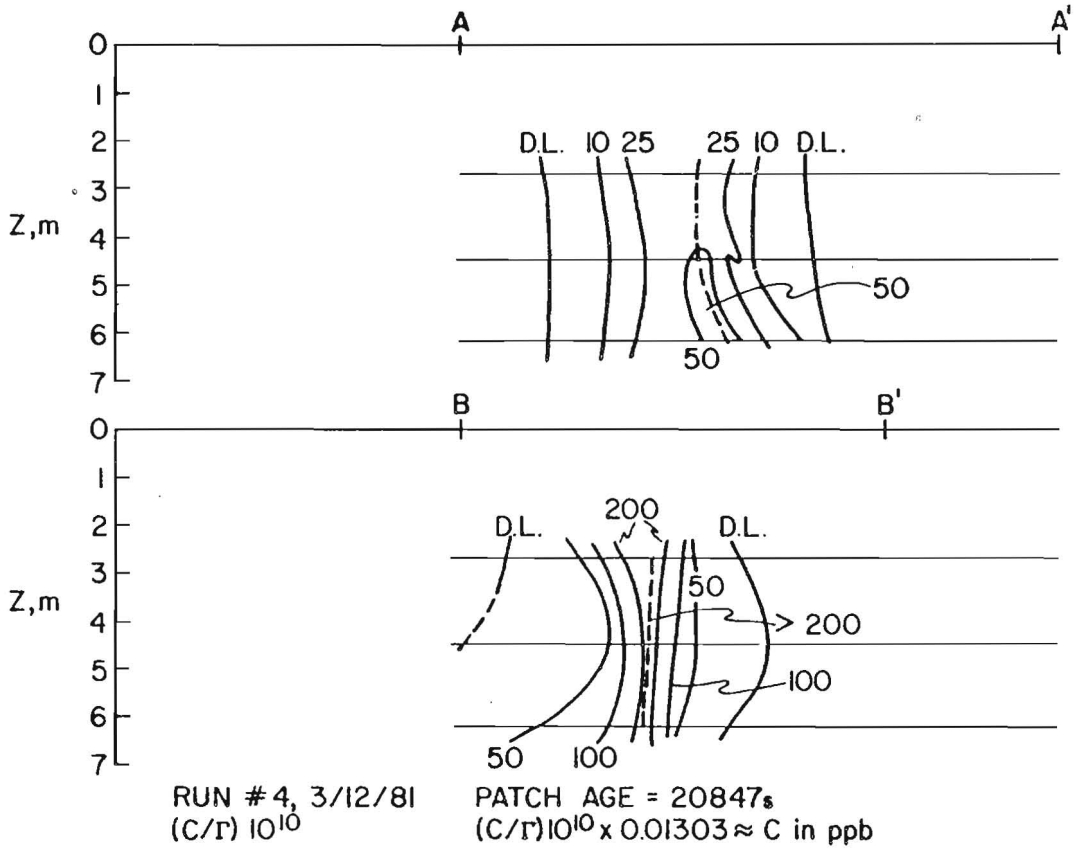

Figure 72. Vertical distribution of tracer at sections A-A' and B-B' (3/12/81).

directly obtainable from equation (1a). If we assume m = 1, then equation (1a) becomes

$$C(t,r_e) = \frac{6\ M/D}{2\pi\sigma_{rc}^2} \exp\{-r_e(6)^{\frac{1}{2}}/\sigma_{rc}\} \tag{3a}$$

$$= \frac{M/D}{2\pi P^2 t^2} \exp\{-r_e/Pt\} \tag{3b}$$

where $P \equiv \sigma_{rc}/t(6)^{\frac{1}{2}}$, a "diffusion velocity". On the other hand if m = 2, then equation (1a) gives

$$C(t,r_e) = \frac{M/D}{\pi\sigma_{rc}^2} \exp\{-(r_e/\sigma_{rc})^2\} \tag{4a}$$

$$= \frac{M/D}{\pi\omega^2 t^2} \exp\{-(r_e/\omega t)^2\} \tag{4b}$$

where $\omega \equiv \sigma_{rc}/t$, also a "diffusion velocity". Equation (3b) is known as the Joseph-Sendner solution (J-S) (Joseph and Sendner (1958)) and equation (4b) as the Okubo-Pritchard solution (O-P) (Okubo and Pritchard, unpublished note in Pritchard (1960)). By taking the natural logarithm of both sides of equations (3a) and (4a) we obtain

$$\ell n\ C(t,r_e) = \ell n\{C(t,0)\} - r_e/\sigma_{rc}(6)^{\frac{1}{2}} \tag{5a}$$

$$\ell n\ C(t,r_e) = \ell n\{C(t,0)\} - r_e^2/\sigma_{rc}^2 \tag{5b}$$

Early on in our analysis of the horizontal dye concentration distributions it became apparent that no single model adequately described all of our data. At times, a Gaussian model (O-P solution) seemed best while at other times the Joseph-Sendner (J-S) or the

generalized model (GEN) were required to account for the more peaked distributions. Accordingly, we calculated the variance of all patches by all three models and selected for our best estimate the variance provided by the model with the highest coefficient of determination. In some cases, the variance could not be calculated from the generalized solution since the peak concentration had not been sampled. The results of our analysis are given in Tables 13 and 14. The intercepts and slopes of equations (5a), (5b), and the ℓn of (1b) are designated by a_o and a_1, respectively. Figures 73 through 77 are summary plots of ℓn $C(t,r_e)$ versus either r_e^2 or r_e for each run and for all depths. Also shown on these figures for comparison are the best fit (all points) regression lines.

The data in Tables 13 and 14 have also been plotted as functions of patch age, $\bar{t}_a$, in Figures 78 and 79. Also shown on these figures for comparison is Okubo's empirical relationship between variance and diffusion time, i.e., age (Okubo (1971)).

The direction of the major axis of the patch relative to 069°T (the shoreline), θ, and the ratio of the minor axis to the major axis, ρ, an estimate of σ_Y/σ_X have been measured and are listed in Table 15.

Vertical Diffusion

As noted earlier, dye sampling was carried out simultaneously at 3 depths. Although this provided some information on the vertical extent of the dye plume, the data were not numerous enough to provide

Table 13

Analysis of Variance Summary for 3/10/81 Release

Run #2 ($\bar{t}_a$ = 13212s)

	z = 0.9 m	z = 1.9 m	z = 3.8 m	All Points
a_o:	2.567	4.938	4.565	4.786
a_1:	-1.287×10^{-4}	-1.319	-3.338×10^{-2}	-3.457×10^{-2}
σ^2_{rc} (cm^2):	7.77×10^{7}	4.04×10^{7}	5.38×10^{7}	5.02×10^{7}
r^2:	0.9986	0.9976	0.9953	0.9849
Solution:	O-P	GEN	J-S	J-S

Run #3 ($\bar{t}_a$ = 21648s)

	z = 0.9 m	z = 2.8 m	z = 6.6 m	All Points
a_o:	#	10.266	4.801	2.582
a_1:	#	-2.104	-2.518×10^{2}	6.244×10^{-2}
σ^2_{rc} (cm^2):	#	1.62×10^{8}	9.47×10^{7}	1.60×10^{8}
r^2:	#	0.9980	0.9997	0.9672
Solution:	#	GEN	J-S	O-P

All background

Run #5 ($\bar{t}_a$ = 33000s)

	z = 0.9 m	z = 4.6 m	All Points
a_o:	3.140	2.536	2.917
a_1:	-1.036	-2.59×10^{-5}	-9.435×10^{-3}
σ^2_{rc} (cm^2):	5.60×10^{8}	3.85×10^{8}	6.74×10^{8}
r^2:	0.9999	0.9911	0.9778
Solution:	J-S	O-P	J-S

Table 14

Analysis of Variance Summary for 3/12/81 Release

Run #3 ($\bar{t}_a$ = 12294s)

	z = 2.55 m	z = 4.25 m	z = 5.9 m	All Points
a_o:	5.616	1.839	11.106	1.935
a_1:	-1.188	-1.439×10^{-2}	-2.325	-1.242×10^{-2}
$\sigma^2_{rc}(cm^2)$:	1.89×10^{8}	2.90×10^{8}	1.16×10^{8}	3.89×10^{8}
r^2:	0.9940	0.9988	0.9996	0.8777
Solution:	GEN	J-S	GEN	J-S

Run #4 ($\bar{t}_a$ = 20847s)

	z = 2.7 m	z = 4.45 m	z = 6.2 m	All Points
a_o:	1.377	1.018	1.010	1.091
a_1:	-1.313×10^{-2}	-1.245×10^{-2}	1.017×10^{-2}	1.187×10^{-2}
$\sigma^2_{rc}(cm^2)$:	3.16×10^{8}	3.87×10^{8}	5.80×10^{8}	4.26×10^{8}
r^2:	0.9979	0.9935	0.9934	0.9710
Solution:	J-S	J-S	J-S	J-S

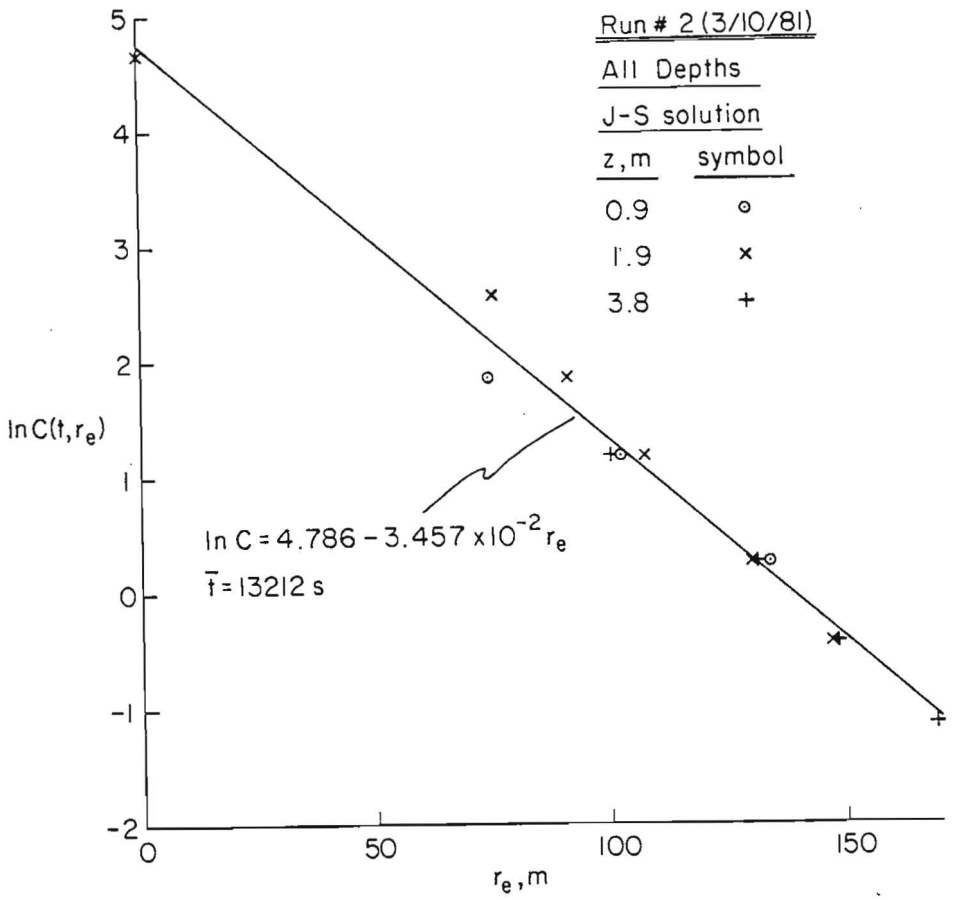

Figure 73. Dye concentrations, $C(t,r_e)$, plotted as a function of r_e for $t_a = 13212$s (10 III 81) and depths of 0.9, 1.9, and 3.8 m.

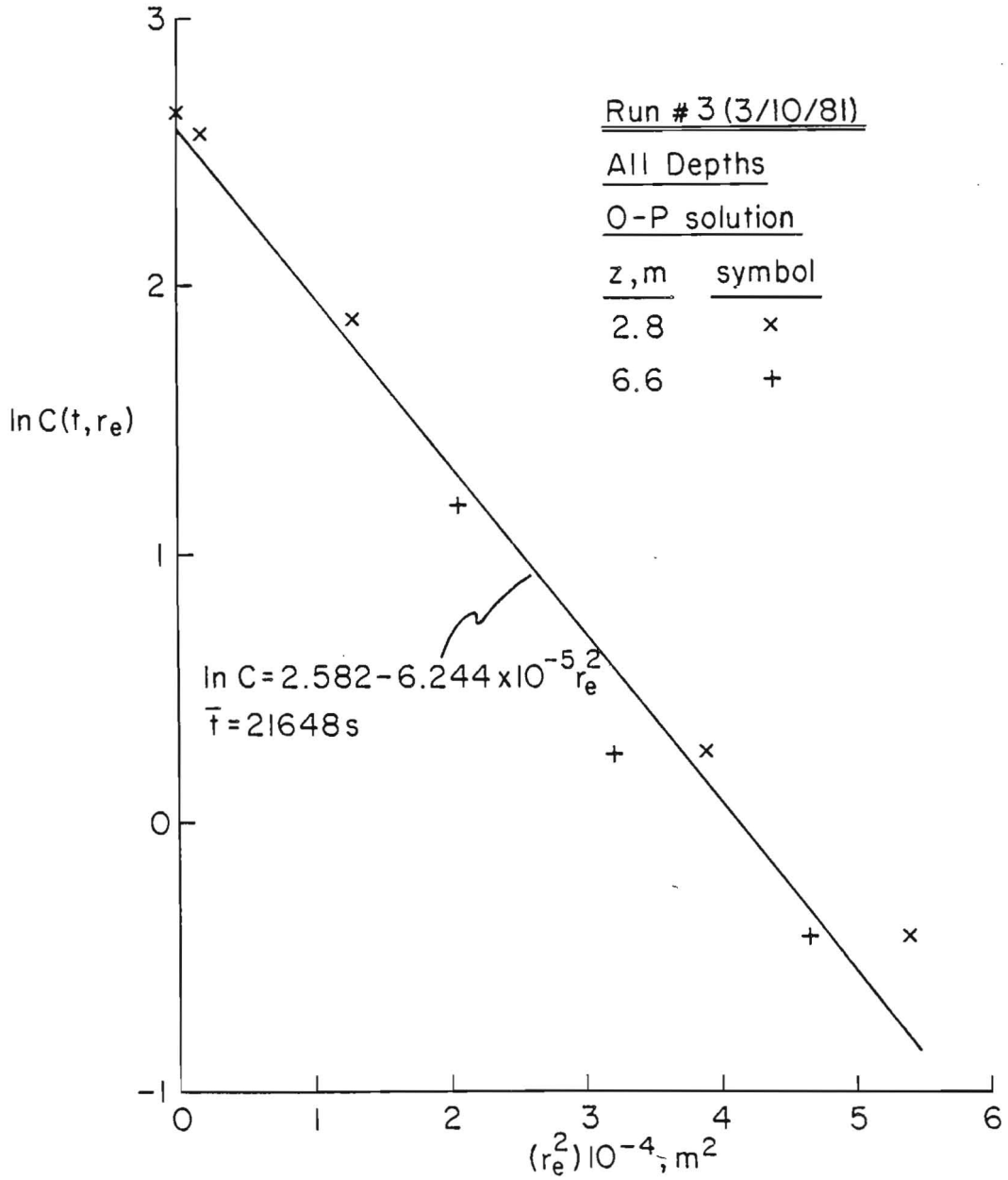

Figure 74. Dye concentrations, $C(t,r_e)$, plotted as a function of r_e^2 for t_a = 21648s (10 III 81) for depths of 2.8 and 6.6 m.

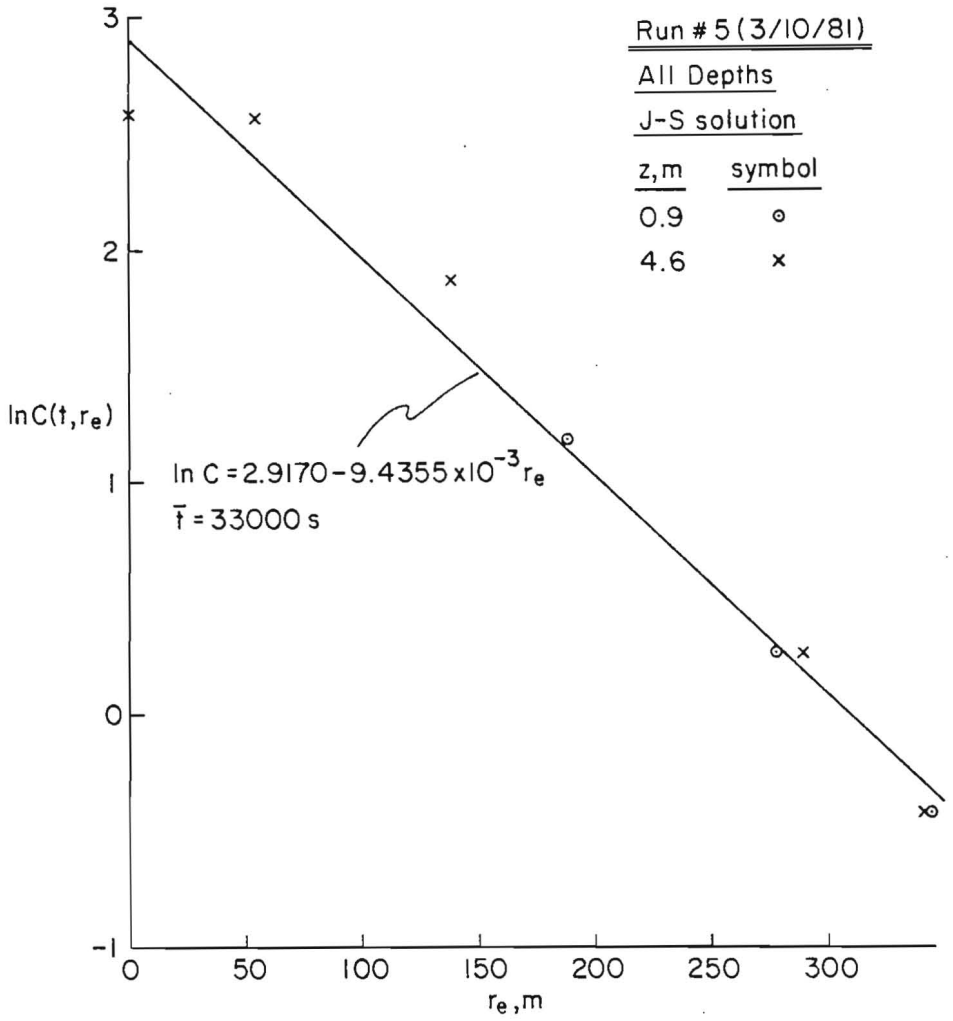

Figure 75. Dye concentrations, $C(t,r_e)$, plotted as a function of r_e for t_a = 33000s (10 III 81) for depths of 0.9 and 4.6 m.

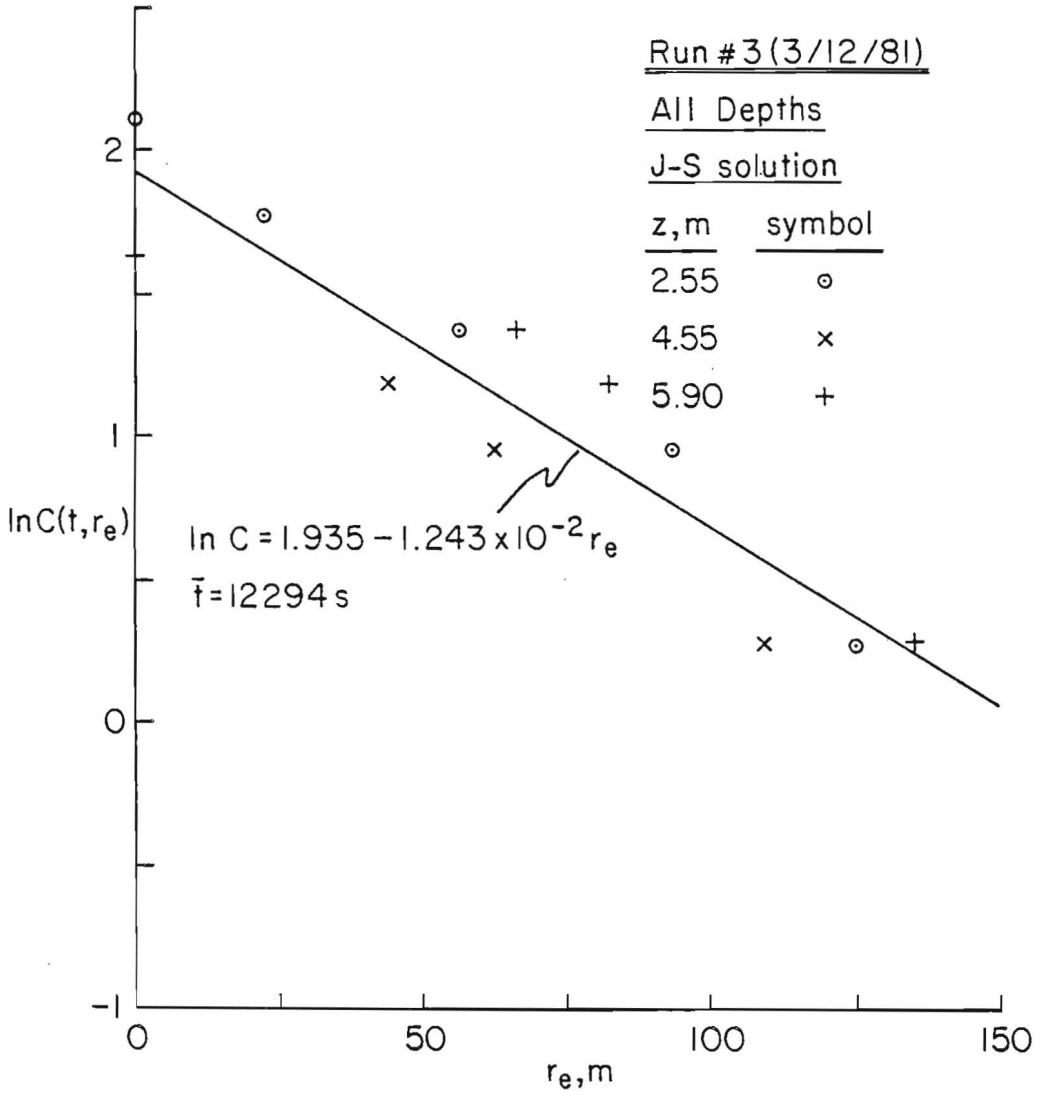

Figure 76. Dye concentrations, $C(t,r_e)$, plotted as a function of r_e for $t_a = 12294$s (12 III 81) for depths of 2.55, 4.55, and 5.90 m.

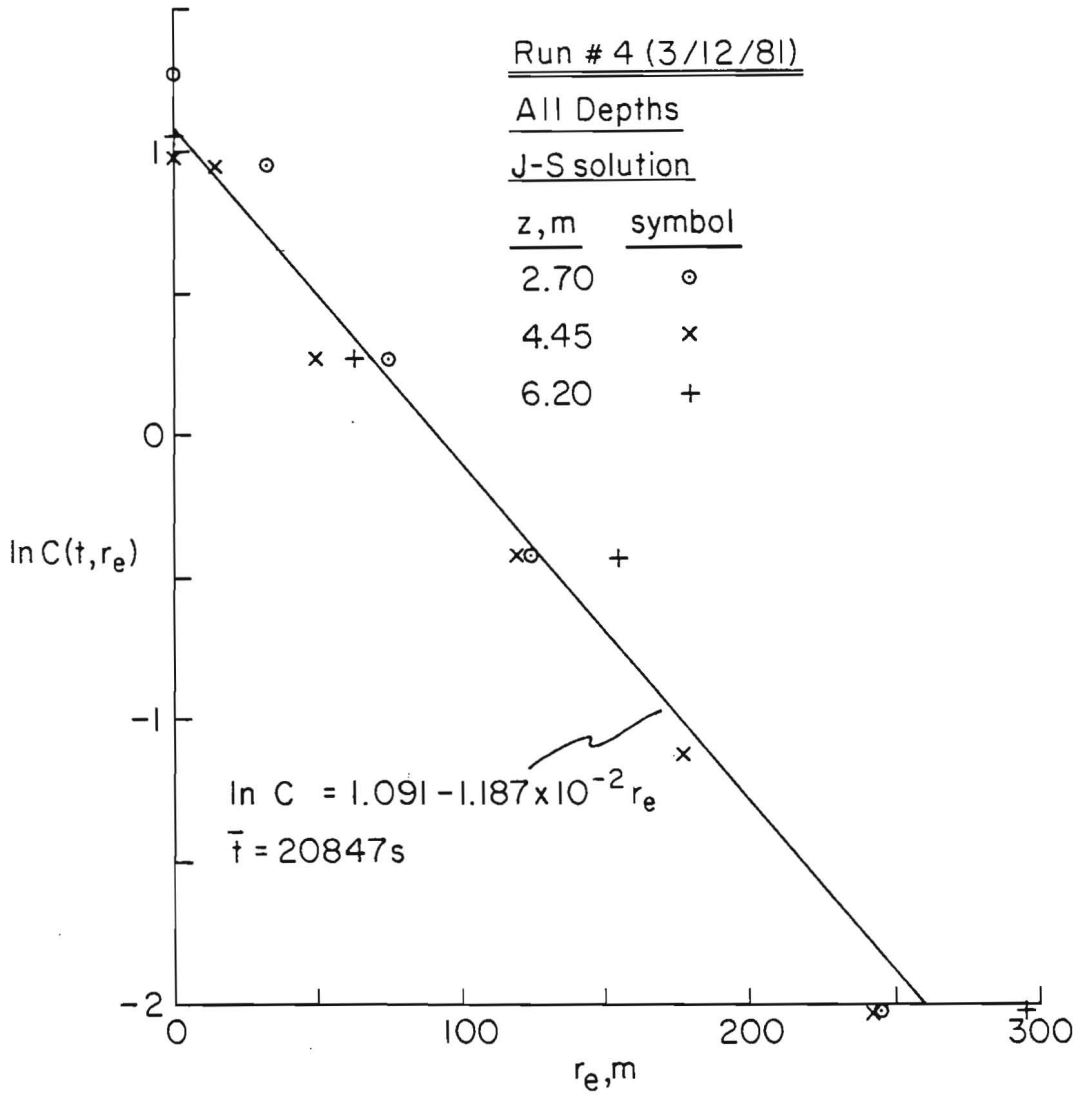

Figure 77. Dye concentrations, $C(t,r_e)$, plotted as a function of r_e for t_a = 20847s (12 III 81) for depths of 2.70, 4.45, and 6.20 m.

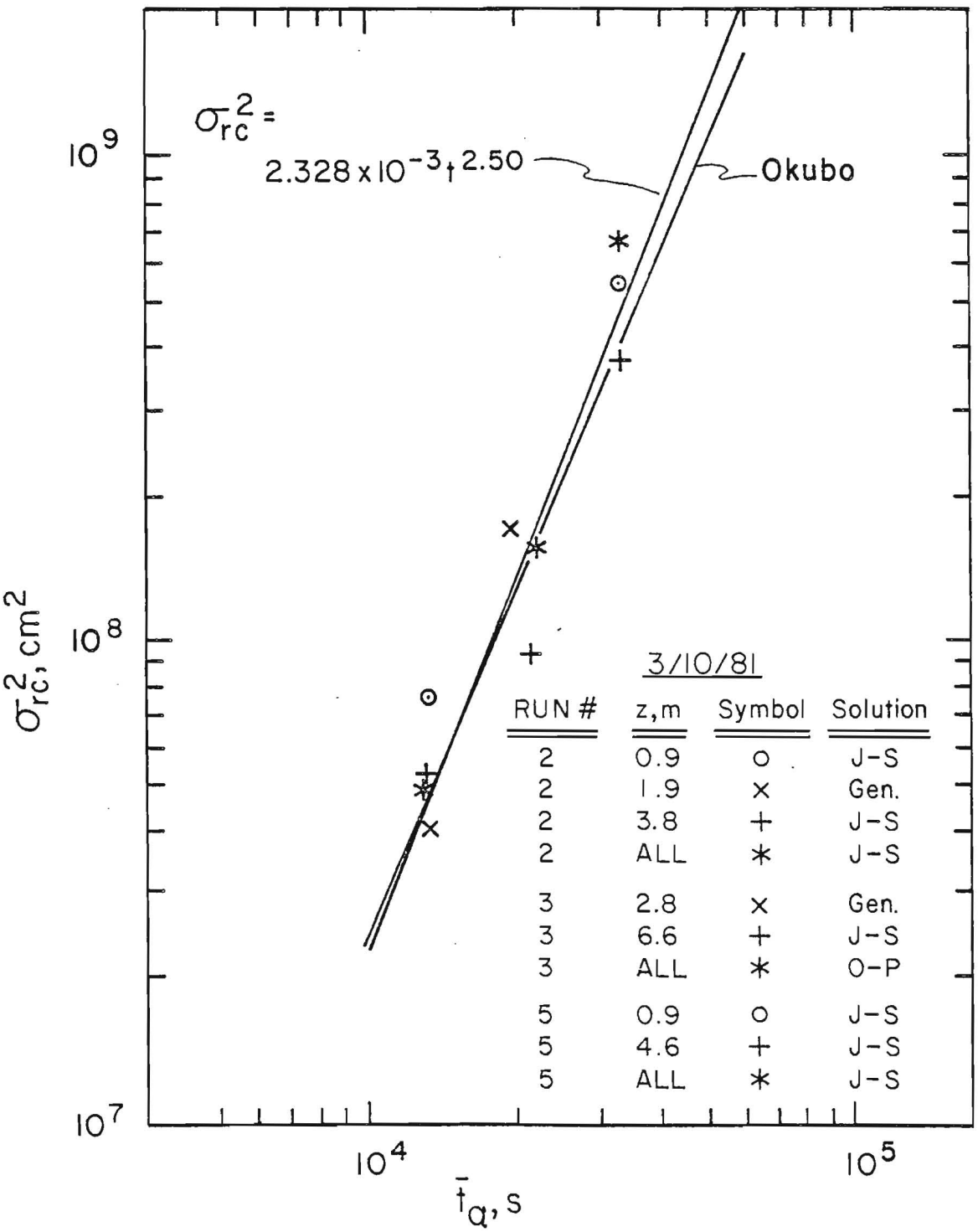

Figure 78. Radially symmetric variance, σ_{rc}^2, as a function of patch age, $\bar{t}_a$, for various depths on 3/10/81.

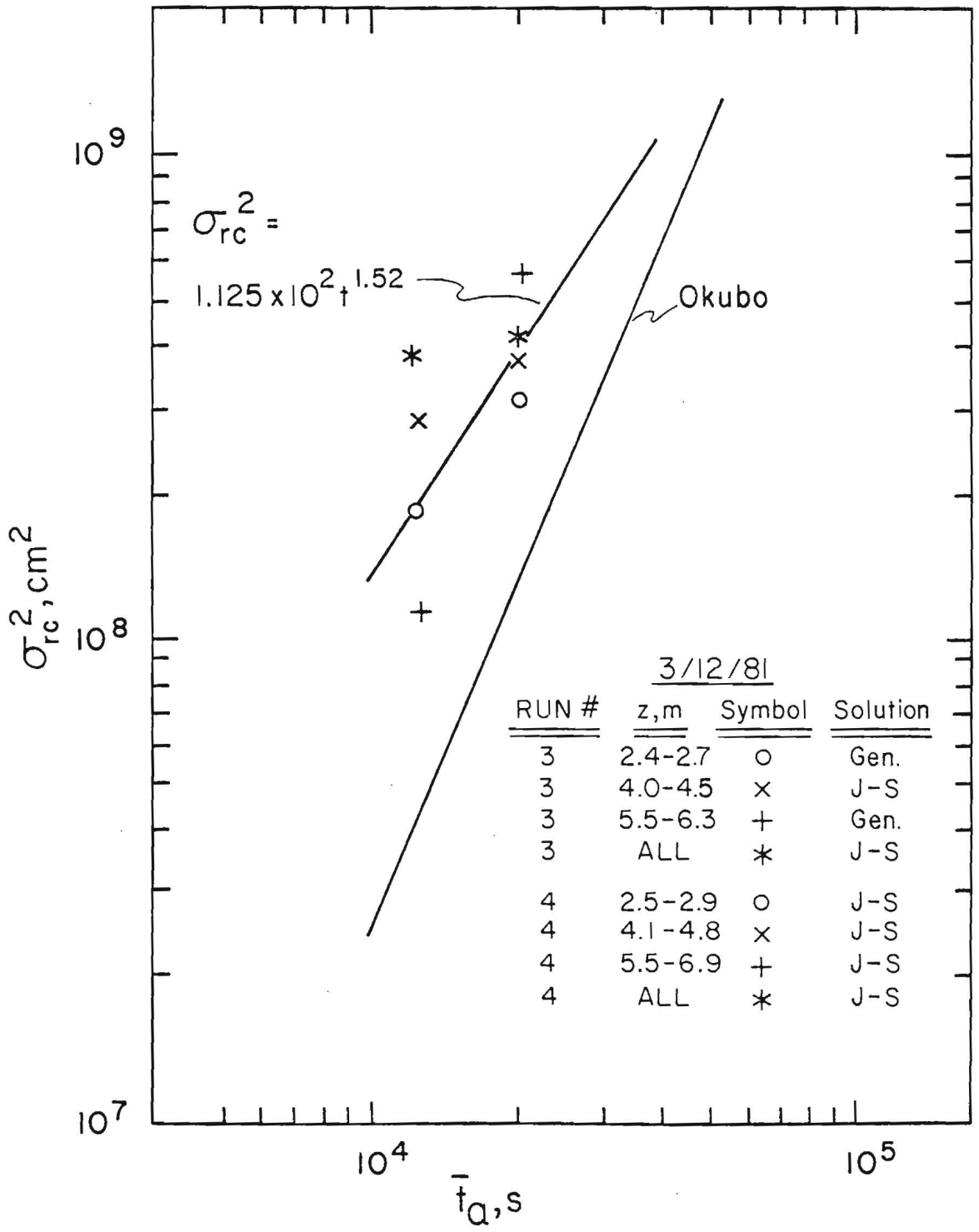

Figure 79. Radially symmetric variance, σ_{rc}^2, as a function of patch age, $\bar{t}_a$, for various depths on 3/12/81.

Table 15

The direction of the major axis relative to 069°T, θ, and the ratio of the minor axis to the major axis, ρ, as a function of age, $\bar{t}_a$, and depth, z.

Date	Run#	$\bar{t}_a$,s	z,m	$\rho \equiv \frac{\sigma_Y}{\sigma_X}$	θ,#°
3/10/81	2	13212	0.9	0.37	91.8
3/10/81	2	13212	1.9	1.17	106.9
3/10/81	2	13212	3.8	1.15	102.2
3/10/81	2	13212	All	-	-
3/10/81	3	21648	0.9	-	-
3/10/81	3	21648	2.8	0.19	136.2
3/10/81	3	21648	6.6	1.12	136 ± 17.5
3/10/81	3	21648	All	-	-
3/10/81	5	33000	0.9	0.083	151.2±12.7
3/10/81	5	33000	4.6	0.10	150.3±11.3
3/10/81	5	33000	All	-	-
3/12/81	3	12294	2.55	0.20	134.2±17.8
3/12/81	3	12294	4.25	0.18	130.6±13.4
3/12/81	3	12294	5.9	0.23	126
3/12/81	3	12294	All	-	-
3/12/81	4	20847	2.7	0.12	86.8±18.75
3/12/81	4	20847	4.45	0.13	77.3±20.3
3/12/81	4	20847	6.2	0.13	95.5±24.6
3/12/81	4	20847	All	-	-

#Counter clockwise relative to 069°T

reliable quantitative information on vertical structure. As a result we have estimated the vertical variances of our dye patches and plumes from measurements of the peak concentration and lateral variance as follows.

Equation (4b), the Okubo-Pritchard diffusion model, is appropriate for an instantaneous release of dye, i.e., a patch. From equation (4b) we have for the peak concentration, C(t,o)

$$C(t,0) = \frac{M}{\pi \sigma_{rc}^2 D} \tag{6}$$

Equation (6) can be converted to a non-uniform vertical distribution by requiring that

$$C(t,0)D = C(t,o) \int_0^\infty \exp(-\frac{z^2}{2\sigma_z^2}) dz \tag{7}$$

or that

$$D = \sqrt{\frac{\pi}{2}}\, \sigma_z \tag{8}$$

Equation (6) then becomes on rearranging

$$\sigma_z = \frac{\sqrt{2}}{\pi^{3/2} \sigma_{rc}^{\ 2} (C(t,o)/M)} \tag{9}$$

for a patch.

Assuming that a continuous source can be considered as a supposition of a large number of instantaneous releases, it can be shown (Carter and Okubo (1966)) that integration of equation (4b) over time gives for the peak concentration of the steady state portion of a plume whose source is discharging dye at a rate

(mass per unit time) of q

$$C(x,o,t) = \frac{q}{\sqrt{\pi}\ \omega x\ D} \tag{10}$$

where ω and D have the same meanings as before and x is the downstream distance from the source taken along the centerline of the meandering plume. Converting equation (10) to a non-uniform vertical distribution as before and noting that

$$\omega = \sigma_{rc}/t\ ,$$

$$\sigma_{rc}^2 = 2\sigma_y\sigma_x \text{ (Okubo (1971))},$$

$$U = \sqrt{u^2+v^2}\ , \text{ and}$$

$$x = Ut$$

we have

$$C(x,o,o,t) = \frac{q}{\pi\sigma_y\sigma_z U} \tag{11}$$

assuming that $\sigma_x = \sigma_y$. Rearranging equation (11) results in

$$\sigma_z = \frac{1}{\pi\sigma_y U(C(x,o,o,t)/q)} \tag{12}$$

for plumes.

σ_z^2, the vertical variance, has been calculated from equation (9) for the patch releases (March, 1981 dye study) and from equation (12) for the plumes (July, 1980 dye study). The results are tabulated in Tables 16a and 16b, respectively and are also presented on Figure 80.

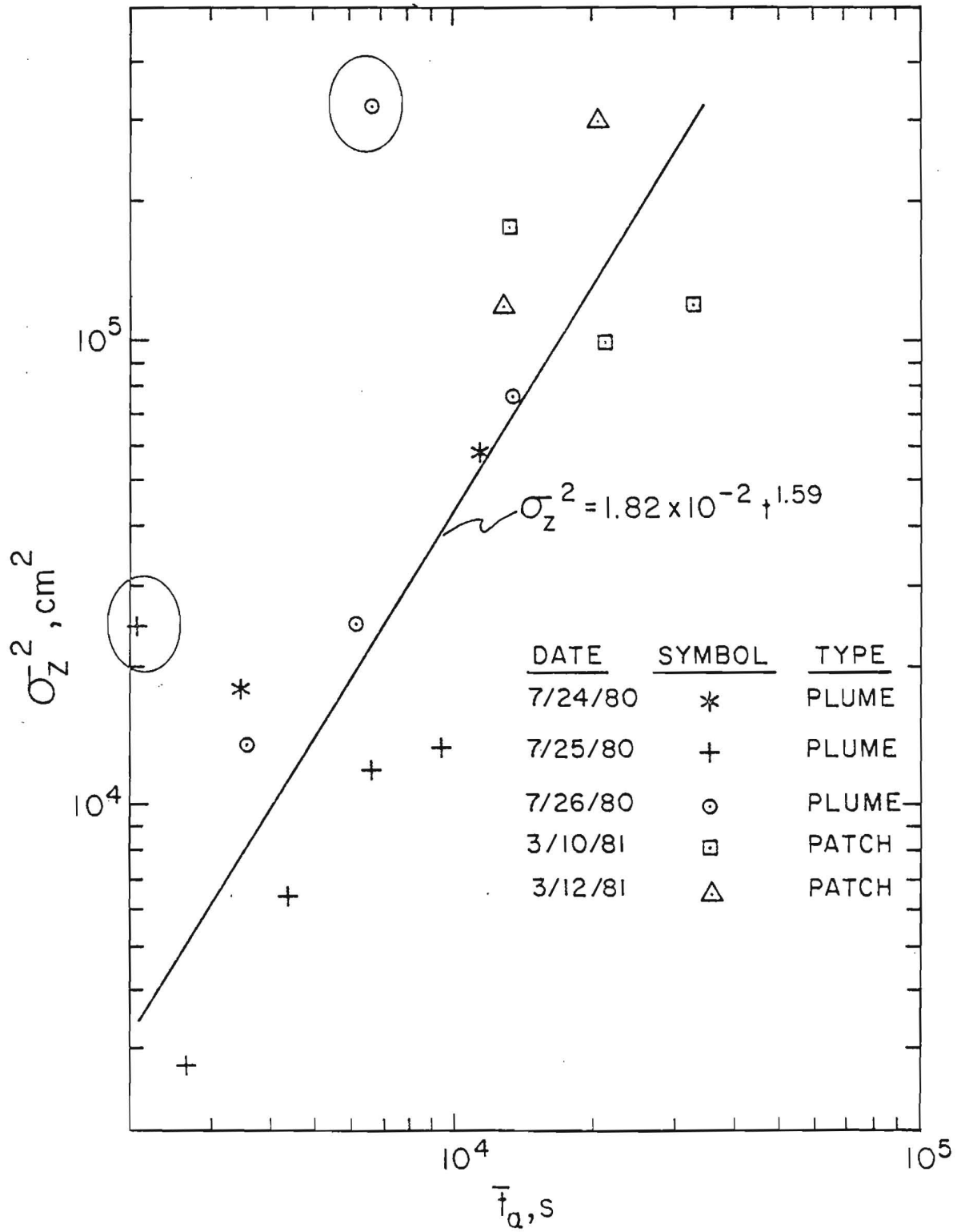

Figure 80. Vertical variance, σ_z^2, for the various sections (plumes) and runs (patches) as a function of age, $\bar{t}_a$, for 24, 25, and 26 July, 1980 and 10 and 12 March, 1981.

Table 16a

Vertical variance, σ_z^2, for the patch experiments as a function of age, $\bar{t}_a$.

Date	Run#	M,g	$(C(t,o)/M)10^{11}, g^{-1}$	$\sigma_{rc}{}^2, cm^2$	$\bar{t}_a$,s	σ_z^2, cm^2
3/10/81	2	7107.5	1.515	4.04×10^7	13212	1.72×10^5
3/10/81	3	7107.5	0.498	1.62×10^8	21648	9.91×10^4
3/10/81	5	7107.5	0.196	3.85×10^8	33000	1.19×10^5
3/12/81	3	2403.2	3.416	1.89×10^8	12294	1.55×10^5
3/12/81	4	2403.2	1.473	3.16×10^8	20847	2.98×10^5

Table 16b

Vertical variance, σ_z^2, for the plume experiments as a function of age, $\bar{t}_a$.

Date	Section	$(C/q)10^9, s\,g^{-1}$	$U, cm\,s^{-1}$	$\sigma_{y,m}$, cm	$\bar{t}_a$,s	σ_z^2, cm^2
7/24/80	5	44.47	15.51	3.44×10^3	3.45×10^3	1.80×10^4
7/24/80	6	15.11	13.38	6.64×10^3	1.15×10^4	5.62×10^4
7/25/80	(1)	24.85	24.75	3.30×10^3	2.09×10^3	2.46×10^4
7/25/80	2	74.26	28.63	2.84×10^3	3.14×10^3	2.78×10^3
7/25/80	3	44.04	30.53	2.95×10^3	4.43×10^3	6.44×10^3
7/25/80	4	29.14	35.83	2.78×10^3	6.72×10^3	1.20×10^4
7/25/80	5	15.61	35.06	5.04×10^3	9.48×10^3	1.33×10^4
7/26/80	(1)	14.41	16.76	2.34×10^3	6.78×10^3	3.19×10^5
7/26/80	2	39.93	12.31	4.21×10^3	6.17×10^3	2.44×10^4
7/26/80	3	4.75	11.89	2.05×10^4	1.34×10^4	7.55×10^4
7/26/80	4	25.83	21.09	5.00×10^3	3.60×10^3	1.36×10^4

NOTE: (C/q) and σ_y,m are sectional means from an absolute frame of reference which have been unbiased by multiplication by N/N-1 where N is the number of runs per section. Date circled were not included in the regression analysis.

It should be noted in Figure 80 that the winter (patch) and summer (plume) estimates of σ_z^2 have been combined for purposes of calculating the regression of σ_z^2 on age, $\bar{t}_a$, even though the estimates of σ_z^2 made from the summer experiments utilized peak concentration and lateral variances relative to an absolute frame of reference whereas the winter (patch) releases provided estimates from a relative frame. In addition if our assumption that σ_y equals σ_x was not correct, our estimate of σ_z for the plumes would be in error by the ratio of σ_y to σ_x; too small if $\sigma_y < \sigma_x$ and too large if $\sigma_y > \sigma_x$.

One can estimate the time at which the vertical growth becomes inhibited by either the pycnocline (summer) or the bottom (winter) as follows. Since

$$\tfrac{1}{2} \frac{d\sigma_z^2}{dt} \equiv K_z, \text{ and} \tag{13}$$

$$\sigma_z^2 = 1.82\times10^{-2} t^{1.59}, \text{ then} \tag{14}$$

$$K_z = 1.45\times10^{-2}\ t^{0.59} \tag{15}$$

A first order estimate of the time required for the plume or patch to mix vertically to the pycnocline depth in summer or the bottom in winter can be estimated from (15) if it is assumed that this time, t_v, is given by

$$t_v = \frac{H^2}{2K_z(t)} \tag{16}$$

where H is the depth of the bottom or pycnocline. From (15) and (16) we obtain

$$H = \sqrt{2.90\times10^{-2} t^{1.59}} \tag{17}$$

Tabulating we have

H,m	t_v,s	K_z,$cm^2 s^{-1}$ (Eq. (15))
0.41	10^3	0.85
2.58	10^4	3.32
16.1	10^5	12.92
100.3	10^6	50.28

These calculations suggest the upper layer (6-12 m) during summer would have been well mixed after 8 to 19 hours and after 2.5 days during winter (bottom depth $\approx$ 30 m).

The Drogue Studies

With the exception of Experiment #2 (see Table 5), all the LEDS cluster experiments were subjected to the following analysis. Experiment #2 had low quality data due to the availability of only one boat for tracking and deploying drogues and hence the data has not been processed.

First, time series of the fundamental statistics of each cluster experiment were evaluated. They are the centroid position, $(\bar{x},\bar{y})$, variances about the centroid in the x and y direction, (σ_x^2,σ_y^2), and covariance, σ_{xy}^2, of the x and y position coordinates relative to the centroid. From these the components of variance in a principal axes coordinate system (σ_X^2,σ_Y^2) relative to which the covariance vanishes, were calculated. Also calculated was the angle (θ) that the principal axes were rotated in an anticlockwise sense relative to the initial

coordinate system (069°T/339°T). The resulting drogue statistics are shown in Table 17.

From σ_X^2 and σ_Y^2 the following parameters were calculated: The equivalent radially symmetric cluster variance, σ_{rc}^2, where

$$\sigma_{rc}^2 = 2\sigma_X\sigma_Y, \tag{18}$$

The cluster area, A, defined as the area of the ellipse with major and minor axes oriented along the principal axes and where the border of the ellipse marks the 95% confidence interval, that is

$$A = 4\pi\sigma_X\sigma_Y, \text{ and} \tag{19}$$

The cluster elongation, ρ^{-1} defined as

$$\rho^{-1} = \sigma_X/\sigma_Y \geq 1 \tag{20}$$

Also calculated were the gross diffusivities in the x and y directions, K_x, K_y and the cross diffusivity, K_{xy}. They are defined by

$$\begin{aligned} K_x &= \tfrac{1}{2}\frac{\Delta\sigma_x^2}{\Delta t}, \\ K_y &= \tfrac{1}{2}\frac{\Delta\sigma_y^2}{\Delta t}, \text{ and} \\ K_{xy} &= \frac{\Delta\sigma_x\sigma_y}{\Delta t} \end{aligned} \tag{21}$$

where the increments in $\sigma_{x,y,xy}^2$ are evaluated for a time interval of 6 min except for Experiments 10 and 11, for which a 10 minute interval was taken. In Table 18 we show the result of evaluating the parameters, σ_{rc}^2, ρ^{-1}, K_x, K_y and K_{xy}. Note that K_x and K_y often

Table 17

Drogue statistics ($\bar{x}$,$\bar{y}$: centroids, σ_x^2, σ_y^2: variances in x and y directions, σ_{xy}^2: covariance, σ_X^2, σ_Y^2: variances in principal axes, θ: angle of orientation of principal axes) for Experiments 1, 3, 4S, 4L, 5S, 5L, 6S, 6L, 8S, 8D, 10, 11, 12.

EXPERIMENT 1

t	$\bar{x}$ (m)	$\bar{y}$ (m)	σ_x^2 (m²)	σ_{xy}^2 (m²)	σ_y^2 (m²)	σ_X^2 (m²)	σ_Y^2 (m²)	θ (degree)
0	968	-6625	6799	-897	618	6926	491	-8.1
1	840	-6614	6572	-936	704	6718	558	-8.8
2	713	-6601	7018	-839	781	7129	670	-7.5
3	583	-6589	7331	-1071	784	7501	613	-9.1
4	456	-6574	7440	-1202	964	7656	748	-10.2
5	336	-6559	6601	-1134	1122	6826	897	-11.2
6	214	-6544	6483	-1528	1358	6904	937	-15.4
7	93	-6526	6389	-1697	1691	6938	1142	-17.9
8	-29	-6508	6429	-1882	2037	7125	1341	-20.3
9	-148	-6489	6149	-2050	2364	7046	1467	-23.6
10	-261	-6469	5786	-2027	2470	6746	1510	-25.4
11	-372	-6449	5740	-2187	2724	6889	1575	-27.7
12	-482	-6427	5898	-2547	3113	7409	1603	-30.7
13	-590	-6402	5850	-2797	3565	7728	1686	-33.9
14	-696	-6375	5785	-2999	4043	8037	1791	-36.9
15	-795	-6348	5526	-3219	4724	8370	1881	-41.5
16	-893	-6321	5784	-3245	5184	8743	2225	-42.4
17	-985	-6293	6344	-3719	5349	9599	2094	-41.2
18	-1078	-6261	6802	-4086	5648	10352	2098	-41.0
19	-1169	-6229	6930	-4249	5996	10737	2188	-41.9
20	-1253	-6196	6704	-4343	6388	10892	2200	-44.0
21	-1329	-6162	6268	-4090	6700	10580	2388	-46.5

(t interval: 6 min)

EXPERIMENT 3

t	$\bar{x}$ (m)	$\bar{y}$ (m)	σ_x^2 (m^2)	σ_{xy}^2 (m^2)	σ_y^2 (m^2)	σ_X^2 (m^2)	σ_Y^2 (m^2)	θ (degree)
0	2088	-6229	635	357	304	863	76	32.6
1	2060	-6225	603	338	292	820	75	32.7
2	2036	-6220	417	245	270	599	88	36.7
3	2016	-6211	353	213	326	553	126	43.2
4	2001	-6210	352	218	306	548	109	42.0
5	1978	-6207	398	195	245	531	112	34.3
6	1946	-6202	483	177	263	581	165	29.1
7	1918	-6210	593	190	264	680	177	24.6
8	1885	-6219	637	263	290	779	148	28.3
9	1849	-6220	684	200	238	761	161	21.0
10	1815	-6223	787	170	318	842	263	18.0
11	1782	-6225	791	184	217	845	162	16.4
12	1747	-6226	835	212	281	907	209	18.7
13	1712	-6230	865	198	328	930	263	18.2
14	1678	-6235	909	179	383	964	328	17.2
15	1639	-6235	802	225	397	902	297	24.0
16	1584	-6224	756	256	387	887	256	27.1
17	1531	-6226	781	197	525	888	418	28.5
18	1482	-6229	957	205	462	1031	388	19.8
19	1427	-6227	965	246	455	1065	355	22.0
20	1364	-6216	1068	259	406	1157	317	19.0
21	1305	-6209	1265	243	462	1332	394	15.6
22	1245	-6208	1286	238	561	1357	490	16.7
23	1190	-6215	1419	176	670	1458	630	12.6
24	1132	-6218	1512	219	610	1562	560	13.0
25	1067	-6213	1411	355	579	1542	448	20.2
26	1005	-6212	1511	341	754	1642	623	21.0
27	948	-6221	1611	334	815	1733	693	20.0
28	890	-6229	1640	360	697	1762	576	18.7

(t interval: 6 min)

EXPERIMENT 3 (Continued)

t	$\bar{x}$ (m)	$\bar{y}$ (m)	σ_x^2 (m^2)	σ_{xy}^2 (m^2)	σ_y^2 (m^2)	σ_X^2 (m^2)	σ_Y^2 (m^2)	θ (degree)
29	828	-6228	1776	266	566	1832	510	11.9
30	763	-6225	1669	436	806	1850	624	22.6
31	696	-6231	1581	478	890	1826	646	27.1
32	631	-6244	1463	659	1020	1936	546	35.7
33	566	-6262	1322	672	915	1821	417	36.6
34	495	-6273	1668	526	921	1940	649	27.3
35	422	-6284	1820	373	822	1943	699	18.4
36	339	-6287	1844	417	786	1988	642	19.1
37	242	-6281	1803	375	764	1924	643	17.9
38	154	-6287	1920	491	765	2101	585	20.2
39	70	-6302	2073	472	880	2237	716	19.2
40	-13	-6319	2196	416	1062	2332	926	18.1
41	-95	-6336	2261	350	1221	2368	1114	17.0
42	-180	-6352	2506	329	1188	2583	1111	13.3
43	-264	-6370	2708	100	1004	2714	998	3.4
44	-355	-6373	2607	243	956	2642	921	8.2
45	-453	-6378	2677	167	917	2693	901	5.4
46	-548	-6384	3013	108	1270	3020	1263	3.5
47	-639	-6397	3583	112	964	3588	960	2.4
48	-731	-6408	3928	30	1168	3928	1168	.6
49	-828	-6427	3989	-37	1186	3989	1185	-.7
50	-920	-6449	3832	-243	1447	3857	1423	-5.8
51	-1011	-6484	3800	-762	1786	4056	1530	-18.6
52	-1100	-6519	4185	-452	1726	4265	1646	-10.1
53	-1193	-6544	3583	-499	1598	3701	1479	-13.3
54	-1286	-6568	3780	-343	1422	3829	1373	-8.1
55	-1384	-6585	3835	-421	1321	3903	1253	-9.3
56	-1481	-6597	3695	-400	1178	3757	1116	-8.8
57	-1576	-6612	3593	-560	1350	3725	1218	-13.3

(t interval: 6 min)

EXPERIMENT 3 (Continued)

t	$\bar{x}$ (m)	$\bar{y}$ (m)	σ_x^2 (m^2)	σ_{xy}^2 (m^2)	σ_y^2 (m^2)	σ_X^2 (m^2)	σ_Y^2 (m^2)	θ (degree)
58	-1673	-6622	3854	-985	1420	4203	1072	-19.5
59	-1773	-6628	4211	-1145	1513	4631	1092	-20.2
60	-1871	-6632	4172	-984	1577	4503	1246	-18.6
61	-1968	-6639	4039	-1141	1663	4498	1203	-21.9
62	-2055	-6661	4534	-1724	2167	5442	1260	-27.8
63	-2142	-6686	5145	-1781	1923	5936	1133	-23.9
64	-2230	-6705	5086	-1424	1522	5585	1023	-19.3
65	-2319	-6720	4386	-1342	1778	4953	1211	-22.9
66	-2406	-6732	4732	-1461	1686	5319	1099	-21.9
67	-2498	-6723	4497	-1524	1258	5101	654	-21.6
68	-2604	-6664	4336	-1575	1021	4965	392	-21.8
69	-2709	-6608	4981	-2882	2417	6853	545	-33.0
70	-2804	-6580	6793	-6182	7081	13121	754	-45.7
71	-2883	-6593	6806	-6207	7146	13186	766	-45.8
72	-2965	-6609	6639	-6397	7643	13558	725	-47.2
73	-3044	-6629	6621	-6663	8330	14193	758	-48.7
74	-3124	-6652	6729	-6752	8535	14444	820	-48.8
75	-3203	-6674	6978	-6774	8397	14498	877	-48.0
76	-3277	-6692	6917	-6702	8074	14223	769	-47.5
77	-3344	-6694	7091	-7774	10198	16572	717	-50.7
78	-3412	-6712	6233	-8062	12651	18119	765	-55.9
79	-3483	-6742	6016	-7991	13308	18446	878	-57.3
80	-3550	-6771	5710	-7590	12754	17599	865	-57.4
81	-3618	-6797	5761	-7457	12144	17063	842	-56.6
82	-3681	-6818	5756	-7398	12377	17171	962	-57.1
83	-3746	-6834	5827	-7977	14036	18902	960	-58.6
84	-3808	-6851	5732	-7929	13940	18764	908	-58.7

(t interval: 6 min)

EXPERIMENT 3 (Continued)

t	$\bar{x}$ (m)	$\bar{y}$ (m)	σ_x^2 (m^2)	σ_{xy}^2 (m^2)	σ_y^2 (m^2)	σ_X^2 (m^2)	σ_Y^2 (m^2)	θ (degree)
85	-3864	-6873	5405	-6895	11825	16221	1009	-57.5
86	-3919	-6892	5418	-6781	11799	16103	1114	-57.6
87	-3975	-6898	5492	-7410	13439	17874	1057	-59.1
88	-4032	-6904	5574	-8075	15299	19863	1010	-60.5
89	-4089	-6911	5660	-8763	17345	22035	971	-61.8
90	-4144	-6910	5846	-8694	16558	21414	991	-60.8
91	-4192	-6910	6331	-8613	15628	20767	1192	-59.2
92	-4235	-6907	5540	-8999	18319	22966	892	-62.7
93	-4277	-6914	5788	-11040	25718	30626	881	-66.0
94	-4317	-6933	5205	-11392	30358	34750	813	-68.9
95	-4361	-6954	5384	-12158	33650	38160	874	-69.6
96	-4403	-6978	4906	-11014	31102	35117	890	-70.0
97	-4443	-7002	4722	-10582	29978	33825	874	-70.0
98	-4482	-7033	4074	-8705	24416	27633	858	-69.7

(t interval: 6 min)

EXPERIMENT 4S

t	$\bar{x}$ (m)	$\bar{y}$ (m)	σ_x^2 (m^2)	σ_{xy}^2 (m^2)	σ_y^2 (m^2)	σ_X^2 (m^2)	σ_Y^2 (m^2)	θ (degree)
0	1932	-6450	220	-0	179	220	179	-.2
1	1809	-6439	221	-2	194	221	194	-4.0
2	1684	-6428	196	-25	197	221	171	-45.6
3	1557	-6423	169	-31	251	262	158	-71.5
4	1427	-6412	200	-41	209	245	163	-47.9
5	1302	-6391	187	-39	212	241	158	-53.7
6	1177	-6380	167	-43	255	273	149	-67.9
7	1052	-6352	141	-24	281	285	137	-80.5
8	926	-6342	113	-35	354	359	108	-81.9
9	801	-6328	111	-8	381	381	110	-88.3
10	672	-6311	105	7	322	323	104	88.2
11	539	-6279	79	36	320	325	74	81.8
12	405	-6242	68	43	483	487	63	84.1
13	273	-6221	85	60	649	655	79	84.0
14	152	-6197	54	12	617	617	54	88.7
15	29	-6174	64	82	698	708	54	82.7
16	-104	-6140	86	107	581	603	64	78.3
17	-240	-6100	80	60	676	682	74	84.4

(t interval: 6 min)

EXPERIMENT 4L

t	$\bar{x}$ (m)	$\bar{y}$ (m)	σ_x^2 (m^2)	σ_{xy}^2 (m^2)	σ_y^2 (m^2)	σ_X^2 (m^2)	σ_Y^2 (m^2)	θ (degree)
0	1844	-6460	80688	2580	58490	80984	58194	6.5
1	1722	-6446	81794	1276	57338	81860	57272	3.0
2	1600	-6432	83216	-745	55454	83236	55434	-1.5
3	1476	-6417	83802	-2742	54253	84055	54000	-5.3
4	1352	-6402	84781	-4954	53828	85555	53055	-8.9
5	1227	-6384	86770	-7845	54223	88563	52431	-12.9
6	1101	-6362	88496	-9224	54275	90824	51947	-14.2
7	976	-6338	89646	-9710	52441	92028	50060	-13.8
8	853	-6316	89091	-9097	50932	91148	48874	-12.7
9	729	-6293	87977	-8963	50878	90029	48826	-12.9
10	603	-6265	87881	-11691	51851	91342	48390	-16.5
11	477	-6236	87203	-14678	52443	92572	47075	-20.1
12	350	-6206	86280	-16514	50826	92781	44325	-21.5
13	222	-6174	85707	-17673	51439	93188	43957	-22.9
14	93	-6140	85152	-18329	54379	93697	45835	-25.0
15	-36	-6106	84827	-19434	57275	94873	47229	-27.3

(t interval: 6 min)

EXPERIMENT 5S

t	$\bar{x}$ (m)	$\bar{y}$ (m)	σ_x^2 (m^2)	σ_{xy}^2 (m^2)	σ_y^2 (m^2)	σ_X^2 (m^2)	σ_Y^2 (m^2)	θ (degree)
0	2100	-6466	943	-46	136	945	133	-3.3
1	1958	-6441	984	-110	158	998	143	-7.5
2	1813	-6413	1007	-131	136	1027	117	-8.4
3	1672	-6382	960	-151	154	987	126	-10.3
4	1531	-6352	902	-142	150	928	124	-10.3
5	1391	-6330	962	-174	194	1000	156	-12.2
6	1249	-6304	987	-133	158	1008	137	-8.9
7	1105	-6277	982	-133	166	1004	145	-9.0
8	961	-6250	990	-133	179	1011	158	-9.1
9	817	-6226	999	-173	225	1036	188	-12.0
10	674	-6199	956	-107	207	971	192	-8.0
11	532	-6173	1043	-208	254	1094	202	-13.9
12	388	-6145	1004	-169	211	1038	177	-11.5
13	244	-6114	1005	-199	297	1057	245	-14.7
14	101	-6086	1073	-237	288	1139	222	-15.6
15	-40	-6058	1071	-234	315	1137	248	-15.9
16	-179	-6029	1068	-247	347	1145	270	-17.2
17	-318	-6001	1108	-252	414	1190	332	-18.0

(t interval: 6 min)

EXPERIMENT 5L

t	$\bar{x}$ (m)	$\bar{y}$ (m)	σ_x^2 (m²)	σ_{xy}^2 (m²)	σ_y^2 (m²)	σ_X^2 (m²)	σ_Y^2 (m²)	θ (degree)
0	2108	-6481	50539	-6844	63331	66302	47568	-66.5
1	1966	-6458	50560	-8011	63359	67213	46706	-64.3
2	1826	-6432	50843	-9695	64029	69160	45711	-62.1
3	1684	-6405	51166	-10338	63974	69731	45409	-60.9
4	1542	-6378	51464	-11809	64661	71590	44535	-59.6
5	1400	-6354	51981	-12853	65064	72944	44101	-58.5
6	1258	-6327	53017	-13245	65490	73893	44613	-57.6
7	1115	-6301	54253	-13389	66291	74952	45592	-57.1
8	973	-6278	54908	-13409	65698	74757	45849	-56.0
9	831	-6253	55719	-13836	65409	75224	45904	-54.6
10	690	-6227	57013	-14425	65998	76614	46398	-53.6
11	548	-6201	58333	-15025	66652	78083	46902	-52.7
12	406	-6176	59138	-15674	67421	79491	47067	-52.4
13	265	-6150	59878	-16269	67757	80557	47078	-51.8
14	122	-6122	61673	-16788	67525	81640	47558	-49.9
15	-19	-6094	63413	-17397	67497	82971	47938	-48.3
16	-158	-6067	64189	-17738	67467	83642	48015	-47.6
17	-297	-6040	65580	-17980	66851	84206	48224	-46.0

(t interval: 6 min)

EXPERIMENT 6S

t	$\bar{x}$ (m)	$\bar{y}$ (m)	σ_x^2 (m^2)	σ_{xy}^2 (m^2)	σ_y^2 (m^2)	σ_X^2 (m^2)	σ_Y^2 (m^2)	θ (degree)
0	1984	-6134	594	271	261	746	109	29.2
1	1927	-6069	606	272	290	762	133	29.9
2	1871	-6007	630	313	335	828	137	32.4
3	1819	-5943	692	309	341	872	161	30.2
4	1770	-5880	746	334	367	941	172	30.2
5	1725	-5818	805	401	457	1068	194	33.3
6	1682	-5756	761	407	463	1046	178	34.9
7	1644	-5691	768	391	424	1023	168	33.1
8	1611	-5623	799	374	416	1028	187	31.4

(t interval: 6 min)

EXPERIMENT 6L

t	$\bar{x}$ (m)	$\bar{y}$ (m)	σ_x^2 (m^2)	σ_{xy}^2 (m^2)	σ_y^2 (m^2)	σ_X^2 (m^2)	σ_Y^2 (m^2)	θ (degree)
0	1991	-6163	29460	4239	12705	30471	11694	13.4
1	1936	-6097	30238	4551	13321	31385	12175	14.1
2	1884	-6033	30756	4944	13692	32085	12363	15.0
3	1833	-5969	31877	5411	13990	33387	12481	15.6
4	1784	-5906	32645	5837	14195	34336	12504	16.2
5	1739	-5843	33476	6120	14145	35251	12370	16.2
6	1697	-5780	33448	6362	13894	35336	12006	16.5
7	1659	-5718	33551	6488	13621	35477	11694	16.5

(t interval: 6 min)

EXPERIMENT 8S

t	$\bar{x}$ (m)	$\bar{y}$ (m)	σ_x^2 (m^2)	σ_{xy}^2 (m^2)	σ_y^2 (m^2)	σ_X^2 (m^2)	σ_Y^2 (m^2)	θ (degree)
0	1920	-6652	4191	1174	4605	5590	3206	50.0
1	1838	-6660	4437	1345	4883	6023	3297	49.7
2	1756	-6665	4091	1235	4735	5689	3136	52.3
3	1673	-6666	4292	1251	4320	5557	3055	45.3
4	1587	-6668	4418	1392	4449	5826	3041	45.3
5	1497	-6671	4344	1195	4183	5461	3066	43.1
6	1407	-6667	4651	1275	3940	5619	2972	37.2
7	1318	-6663	4512	1154	3849	5381	2980	37.0
8	1232	-6661	4696	1243	4161	5699	3157	38.9
9	1140	-6665	4854	1459	4298	6061	3090	39.6
10	1050	-6663	4393	1446	4143	5719	2817	42.5
11	959	-6660	4261	1420	4034	5571	2723	42.7
12	869	-6655	4464	1335	3773	5498	2739	37.7

(t interval: 6 min)

EXPERIMENT 8D

t	$\bar{x}$ (m)	$\bar{y}$ (m)	σ_x^2 (m^2)	σ_{xy}^2 (m^2)	σ_y^2 (m^2)	σ_X^2 (m^2)	σ_Y^2 (m^2)	θ (degree)
0	1963	-6657	1277	1246	3926	4420	783	68.4
1	1890	-6667	1247	1225	4028	4491	785	69.3
2	1820	-6674	1426	1314	3964	4522	868	67.0
3	1749	-6683	1855	1415	3979	4686	1147	63.4
4	1670	-6692	1875	1245	4024	4594	1304	65.4
5	1590	-6699	1821	1227	4024	4571	1273	66.0
6	1509	-6699	1820	1107	3955	4425	1350	67.0
7	1427	-6702	1677	594	4009	4152	1535	76.5
8	1346	-6710	1752	701	4247	4431	1569	75.3
9	1263	-6718	2033	760	4246	4482	1798	72.8
10	1178	-6722	2183	636	4436	4604	2015	75.3
11	1092	-6723	2317	451	4477	4567	2227	78.7
12	1011	-6722	2655	228	4657	4683	2629	83.6
13	933	-6722	2776	107	5062	5067	2771	87.3

(t interval: 6 min)

EXPERIMENT 10

t	$\bar{x}$ (m)	$\bar{y}$ (m)	σ_x^2 (m^2)	σ_{xy}^2 (m^2)	σ_y^2 (m^2)	σ_X^2 (m^2)	σ_Y^2 (m^2)	θ (degree)
0	2933	-6495	863	-169	555	937	481	-23.9
1	2942	-6486	977	-214	651	1084	545	-26.4
2	2960	-6474	1213	-284	726	1344	595	-24.7
3	2984	-6463	1492	-366	786	1648	630	-23.0
4	3015	-6453	1597	-389	869	1766	700	-23.5
5	3053	-6445	1657	-410	928	1841	744	-24.2
6	3098	-6441	1906	-464	1026	2105	826	-23.3
7	3150	-6440	2001	-478	1071	2203	869	-22.9
8	3204	-6439	2185	-516	1131	2395	920	-22.2
9	3261	-6443	2244	-561	1200	2488	956	-23.5
10	3318	-6450	2251	-637	1283	2567	967	-26.4
11	3373	-6458	2287	-737	1365	2696	956	-29.0
12	3428	-6468	2414	-836	1398	2884	928	-29.4
13	3482	-6480	2496	-893	1429	3002	923	-29.6
14	3533	-6496	2397	-915	1457	2956	898	-31.4
15	3579	-6509	2233	-828	1401	2744	890	-31.7
16	3627	-6523	2083	-770	1382	2579	886	-32.8
17	3675	-6535	2231	-801	1392	2716	907	-31.2
18	3725	-6552	2379	-848	1387	2865	900	-29.8
19	3775	-6572	2610	-964	1357	3133	834	-28.5
20	3823	-6594	2805	-1058	1309	3352	761	-27.4
21	3870	-6618	2971	-1165	1342	3578	735	-27.5
22	3913	-6643	3121	-1251	1344	3766	698	-27.3
23	3952	-6667	3273	-1257	1277	3880	670	-25.8
24	3985	-6690	3546	-1305	1224	4132	638	-24.2
25	4015	-6713	3868	-1363	1185	4439	614	-22.7
26	4040	-6737	4096	-1410	1144	4661	578	-21.8
27	4058	-6762	4408	-1547	1096	5018	486	-21.5
28	4067	-6786	4699	-1718	1106	5388	417	-21.9
29	4066	-6807	5158	-1866	1097	5885	370	-21.3
30	4056	-6826	5585	-1919	1080	6292	374	-20.2
31	4038	-6841	6219	-2120	1110	6984	345	-19.8

(t interval: 10 min)

EXPERIMENT 11

t	$\bar{x}$ (m)	$\bar{y}$ (m)	σ_x^2 (m^2)	σ_{xy}^2 (m^2)	σ_y^2 (m^2)	σ_X^2 (m^2)	σ_Y^2 (m^2)	θ (degree)
0	217	-6751	603	-119	293	643	252	-18.8
1	149	-6771	688	-155	315	744	258	-19.9
2	87	-6795	767	-186	389	843	313	-22.3
3	31	-6816	826	-247	491	957	361	-27.9
4	-13	-6832	885	-328	637	1112	410	-34.7
5	-49	-6845	955	-386	746	1251	451	-37.4
6	-79	-6858	1063	-449	855	1419	498	-38.5
7	-101	-6872	1175	-475	971	1559	587	-38.9
8	-118	-6884	1285	-505	1115	1712	687	-40.2
9	-130	-6897	1353	-541	1275	1857	772	-42.9
10	-135	-6910	1385	-549	1379	1931	833	-44.9
11	-133	-6924	1396	-542	1462	1973	886	-46.7
12	-124	-6938	1429	-564	1571	2069	932	-48.6
13	-108	-6953	1519	-547	1622	2120	1021	-47.7
14	-86	-6968	1604	-523	1639	2145	1098	-46.0
15	-57	-6982	1620	-484	1636	2112	1143	-45.5
16	-31	-6996	1633	-458	1663	2106	1190	-45.9
17	12	-7012	1787	-322	1664	2054	1397	-39.6
18	48	-7027	1815	-195	1663	1947	1530	-34.3
19	85	-7042	1780	-128	1664	1863	1582	-32.8
20	124	-7058	1763	-87	1756	1847	1672	-43.9
21	165	-7076	1851	-86	1884	1955	1780	-50.3
22	209	-7095	1917	-103	2003	2072	1848	-56.3
23	255	-7115	1971	-94	2057	2118	1910	-57.2
24	302	-7137	2038	-93	2065	2146	1957	-49.1
25	351	-7161	2103	-124	2129	2241	1991	-48.0

(t interval: 10 min)

EXPERIMENT 11 (Continued)

t	$\bar{x}$ (m)	$\bar{y}$ (m)	σ_x^2 (m^2)	σ_{xy}^2 (m^2)	σ_y^2 (m^2)	σ_X^2 (m^2)	σ_Y^2 (m^2)	θ (degree)
26	399	-7186	2190	-180	2150	2351	1989	-41.9
27	446	-7211	2280	-235	2179	2470	1989	-38.9
28	494	-7237	2385	-268	2194	2575	2004	-35.2
29	537	-7263	2530	-344	2166	2737	1959	-31.1
30	576	-7290	2707	-410	2138	2922	1923	-27.6
31	610	-7317	2892	-492	2171	3141	1922	-26.9
32	643	-7344	3120	-610	2243	3433	1929	-27.1
33	674	-7370	3389	-766	2333	3791	1931	-27.7
34	702	-7395	3638	-897	2459	4122	1975	-28.3
35	724	-7418	4010	-1050	2595	4569	2037	-28.0
36	742	-7440	4340	-1218	2740	4997	2083	-28.4

(t interval: 10 min)

EXPERIMENT 12

t	$\bar{x}$ (m)	$\bar{y}$ (m)	σ_x^2 (m^2)	σ_{xy}^2 (m^2)	σ_y^2 (m^2)	σ_X^2 (m^2)	σ_Y^2 (m^2)	θ (degree)
0	1000	-6502	9390	-35	1228	9391	1228	-.2
1	950	-6473	10211	-107	1368	10213	1366	-.7
2	905	-6445	10769	-112	1536	10770	1535	-.7
3	868	-6416	11153	-73	1735	11154	1735	-.4
4	837	-6384	11663	-32	2000	11663	2000	-.2
5	814	-6349	11963	31	2304	11964	2304	.2
6	798	-6312	12136	73	2575	12137	2574	.4
7	791	-6274	12406	47	2784	12407	2784	.3
8	791	-6236	12843	-93	2952	12844	2951	-.5
9	796	-6199	13362	-434	3156	13380	3138	-2.4
10	805	-6164	13924	-623	3355	13960	3318	-3.4
11	818	-6128	15178	-856	3595	15241	3533	-4.2
12	836	-6093	16159	-994	3920	16239	3840	-4.6
13	858	-6059	17277	-1271	4205	17400	4083	-5.5
14	888	-6024	18001	-1567	4490	18181	4310	-6.5
15	925	-5987	18530	-2006	4739	18816	4453	-8.1
16	966	-5951	19220	-2520	4851	19649	4422	-9.7
17	1013	-5918	19748	-3174	4936	20400	4285	-11.6

(t interval: 10 min)

TABLE 18

Equivalent radially symmetric cluster area ($2\sigma_X\sigma_Y$), elongation (ρ^{-1}), and diffusivities ($K_x = \frac{1}{2}\Delta(\sigma_x^2)/\Delta t$, $K_y = \frac{1}{2}\Delta(\sigma_y^2)/\Delta t$, $K_{xy} = \Delta(\sigma_x\sigma_y)/\Delta t$) for drogue Experiments 1, 3, 4S, 4L, 5S, 5L, 6S, 6L, 8S, 8D, 10, 11, 12. The value of the diffusivity is significant only for the first three numbers.

EXPERIMENT 1

t	$2\sigma_X\sigma_Y$ (m^2)	ρ^{-1}	K_x (m^2s^{-1})	K_y (m^2s^{-1})	K_{xy} (m^2s^{-1})
0	.368739+004	3.76			
1	.387367+004	3.47	-.289474+000	.939494-001	.258726+000
2	.437254+004	3.26	.570821+000	.155655+000	.692867+000
3	.428831+004	3.50	.517264+000	-.800003-001	-.116974+000
4	.478450+004	3.20	.214392+000	.187017+000	.689140+000
5	.494774+004	2.76	-.115161+001	.206924+000	.226735+000
6	.508692+004	2.71	.108254+000	.561754-001	.193292+000
7	.562959+004	2.46	.462386-001	.284818+000	.753709+000
8	.618239+004	2.31	.260641+000	.276425+000	.767785+000
9	.643067+004	2.19	-.109720+000	.175198+000	.344832+000
10	.638238+004	2.11	-.416684+000	.587768-001	-.670696-001
11	.658787+004	2.09	.197747+000	.910105-001	.285405+000
12	.689137+004	2.15	.722517+000	.381262-001	.421531+000
13	.721977+004	2.14	.443586+000	.116223+000	.456107+000
14	.758703+004	2.12	.428710+000	.144993+000	.510084+000
15	.793543+004	2.11	.462153+000	.125482+000	.483884+000
16	.882189+004	1.98	.518674+000	.478355+000	.123120+001
17	.896704+004	2.14	.118892+001	-.182228+000	.201594+000
18	.932056+004	2.22	.104545+001	.535863-002	.490999+000
19	.969496+004	2.22	.535450+000	.125603+000	.520001+000
20	.979031+004	2.23	.215230+000	.159811-001	.132426+000
21	.100534+005	2.10	-.434145+000	.261614+000	.365399+000

(t interval: 6 min)

EXPERIMENT 3

t	$2\sigma_X\sigma_Y$ (m^2)	ρ^{-1}	K_x (m^2s^{-1})	K_y (m^2s^{-1})	K_{xy} (m^2s^{-1})
0	.512028+003	3.37	-.607537-001	-.110531-002	-.218889-001
1	.496268+003	3.30	-.306239+000	.177242-001	-.518443-001
2	.458940+003	2.61	-.637809+001	.533643-001	.968898-001
3	.528701+003	2.09	-.727775-002	-.234915-001	-.541811-001
4	.489690+003	2.24	-.241562-001	.358996-002	-.301696-002
5	.487518+003	2.18	.702396-001	.737775-001	.183363+000
6	.619539+003	1.88	.137500+000	.163463-001	.103009+000
7	.693706+003	1.96	.136445+000	-.402381-001	-.209707-001
8	.678607+003	2.29	.242510-001	.188023-001	.310902-001
9	.700992+003	2.17	.112297+000	.140908+000	.333174+000
10	.940877+003	1.79	.425616-002	-.139459+000	-.277589+000
11	.741013+003	2.28	.112297+000	.140908+000	.333174+000
12	.870456+003	2.08	.425616-002	-.139459+000	-.277589+000
11	.741013+003	2.28	.865144-001	.643403-001	.179782+000
12	.870456+003	2.08	.314798-001	.752509-001	.164669+000
13	.989018+003	1.88	.479234-001	.903245-001	.188682+000
14	.112487+004	1.71	-.868366-001	-.436121-001	-.125627+000
15	.103442+004	1.74	-.204209-001	-.563419-001	-.112784+000
16	.953213+003	1.86	.102654-002	.225202+000	.368755+000
17	.121872+004	1.46	.198301+000	-.413562-001	.648903-001
18	.126544+004	1.63	.474107-001	-.459417-001	-.488947-001
19	.123023+004	1.73	.127918+000	-.531316-001	-.262417-001
20	.121134+004	1.91	.243521+000	.106640+000	.329744+000
21	.144876+004	1.84	.347135-001	.133449+000	.253012+000
22	.163092+004	1.66	.140209+000	.194994+000	.397971+000
23	.191746+004	1.52	.144435+000	-.975864-001	-.648423-001
24	.187078+004	1.67	-.280517-001	-.155135+000	-.288565+000
25	.166301+004	1.85	.138948+000	.242689+000	.500058+000
26	.202305+004	1.62	.126126+000	.975918-001	.235051+000
27	.219229+004	1.58	.399007-001	-.163685+000	-.247910+000
28	.201379+004	1.75	.971507-001	-.904466-001	-.111204+000
29	.193373+004	1.89			

(t interval: 6 min)

EXPERIMENT 3 (Continued)

t	$2\sigma_X\sigma_Y$ (m^2)	ρ^{-1}	K_x (m^2s^{-1})	K_y (m^2s^{-1})	K_{xy} (m^2s^{-1})
29	.193373+004	1.89	.258057-001	.157655+000	.298692+000
30	.214878+004	1.72	-.338872-001	.306353-001	.322067-001
31	.217197+004	1.68	.153213+000	-.138242+000	-.159537+000
32	.205711+004	1.88	-.159922+000	-.180402+000	-.437894+000
33	.174182+004	2.09	.165721+000	.323181+000	.698428+000
34	.224469+004	1.73	.416440-002	.686154-001	.118940+000
35	.233033+004	1.67	.628655-001	-.789813-001	-.985979-001
36	.225934+004	1.76	-.894530-001	.122511-002	-.491165-001
37	.222397+004	1.73	.245417+000	-.807150-001	-.106717-001
38	.221629+004	1.90	.189424+000	.182696+000	.437643+000
39	.253139+004	1.77	.132325+000	.291442+000	.566324+000
40	.293915+004	1.59	.495580-001	.261168+000	.429486+000
41	.324838+004	1.46	.298796+000	-.459092-002	.193481+000
42	.338768+004	1.53	.181582+000	-.155864+000	-.132539+000
43	.329225+004	1.65	-.100549+000	-.108091+000	-.240783+000
44	.311889+004	1.69	.713528-001	-.269752-001	-.446256-002
45	.311568+004	1.73	.453646+000	.503138+000	.109830+001
46	.390645+004	1.55	.788794+000	-.422081+000	-.271822+000
47	.371074+004	1.93	.472697+000	.289068+000	.795100+000
48	.428321+004	1.83	.849842-001	.245710-001	.914012-001
49	.434902+004	1.83	-.184048+000	.329894+000	.466717+000
50	.468506+004	1.65	.277176+000	.149026+000	.413277+000
51	.498261+004	1.63	.290819+000	.160316+000	.439174+000
52	.529882+004	1.61	-.784099+000	-.230938+000	-.859851+000
53	.467973+004	1.58	.178354+000	-.147398+000	-.129762+000
54	.458630+004	1.67	.102617+000	-.167574+000	-.227858+000
55	.442224+004	1.77	-.203405+000	-.189304+000	-.453611+000
56	.409564+004	1.83	-.442336-001	.140735+000	.227339+000
57	.425933+004	1.75	.663718+000	-.202661+000	-.205125-001
58	.424456+004	1.98	.594337+000	.288468-001	.352522+000
59	.449837+004	2.06	-.176777+000	.213315+000	.332409+000
60	.473771+004	1.90			

(t interval: 6 min)

EXPERIMENT 3 (Continued)

t	$2\sigma_X\sigma_Y$ (m^2)	ρ^{-1}	K_x (m^2s^{-1})	K_y (m^2s^{-1})	K_{xy} (m^2s^{-1})
60	.473771+004	1.90	-.711085-002	-.591286-001	-.117064+000
61	.465342+004	1.93	.131036+001	.780981-001	.809706+000
62	.523641+004	2.08	.686134+000	-.176411+000	-.701693-001
63	.518589+004	2.29	-.487655+000	-.151928+000	-.562187+000
64	.478111+004	2.34	-.876737+000	.261032+000	.163578+000
65	.489889+004	2.02	.508048+000	-.156124+000	-.883917-001
66	.483525+004	2.20	-.303627+000	-.618061+000	-.164294+001
67	.365233+004	2.79	-.188366+000	-.364091+000	-.119905+001
68	.278901+004	3.56	.262270+001	.213093+000	.149528+001
69	.386562+004	3.55	.870465+001	.290115+000	.336796+001
70	.629055+004	4.17	.901672-001	.169910-001	.923564-001
71	.635704+004	4.15	.516763+000	-.578956-001	-.123238+000
72	.626831+004	4.33	.882642+000	.462045-001	.403912+000
73	.655913+004	4.33	.347743+000	.863382-001	.449505+000
74	.688277+004	4.20	.754666-001	.788067-001	.343797+000
75	.713031+004	4.07	-.382447+000	-.149604+000	-.716808+000
76	.661421+004	4.30	.326361+001	-.727953-001	.385975+000
77	.689211+004	4.81	.214776+001	.674143-001	.770081+000
78	.744657+004	4.87	.454403+000	.156708+000	.835957+000
79	.804846+004	4.58	-.117618+001	-.184820-001	-.342678+000
80	.780173+004	4.51	-.743931+000	-.319240-001	-.308942+000
81	.757929+004	4.50	.149941+000	.166513+000	.760333+000
82	.812673+004	4.23	.240432+001	-.196652-002	.546566+000
83	.852026+004	4.44	-.191812+000	-.720767-001	-.366374+000
84	.825647+004	4.55	-.353236+001	.140054+000	-.229106+000
85	.809151+004	4.01	-.164594+000	.145791+000	.526862+000
86	.847085+004	3.80	.246070+001	-.792942-001	.308551+000
87	.869301+004	4.11	.276148+001	-.648971-001	.369297+000
88	.895890+004	4.43	.301675+001	-.547862-001	.404282+000
89	.924998+004	4.76	-.862322+000	.279200-001	-.518333-001
90	.921266+004	4.65	-.898694+000	.279890+000	.102727+001
91	.995230+004	4.17			

(t interval: 6 min)

EXPERIMENT 3 (Continued)

t	$2\sigma_X\sigma_Y$ (m^2)	ρ^{-1}	K_x (m^2s^{-1})	K_y (m^2s^{-1})	K_{xy} (m^2s^{-1})
91	.995230+004	4.17	.305456+001	-.416530+000	-.124665+001
92	.905471+004	5.07	.106384+002	-.161879-001	.185140+001
93	.103877+005	5.90	.572881+001	-.948390-001	.333178+000
94	.106276+005	6.54	.473514+001	.853726-001	.128152+001
95	.115503+005	6.61	-.422561+001	.228345-001	-.508727+000
96	.111840+005	6.28	-.179429+001	-.223732-001	-.426920+000
97	.108766+005	6.22	-.860110+001	-.228319-001	-.158167+001
98	.973784+004	5.68			

(t interval: 6 min)

EXPERIMENT 4S

t	$2\sigma_X\sigma_Y$ (m^2)	ρ^{-1}	K_x (m^2s^{-1})	K_y (m^2s^{-1})	K_{xy} (m^2s^{-1})
0	.397148+003	1.11	.773721-003	.212501-001	.238343-001
1	.414308+003	1.07	.646607-003	-.326903-001	-.354373-001
2	.388794+003	1.14	.561538-001	-.173642-001	.252976-001
3	.407008+003	1.29	-.228097-001	.728388-002	-.900746-002
4	.400523+003	1.23	-.639013-002	-.690352-002	-.136853-001
5	.390669+003	1.23	.445067-001	-.128598-001	.178274-001
6	.403505+003	1.35	.170592-001	-.174808-001	-.122367-001
7	.394694+003	1.45	.102047+000	-.399193-001	-.195295-002
8	.393288+003	1.82	.307296-001	.348418-002	.231054-001
9	.409924+003	1.86	-.809869-001	-.826786-002	-.597309-001
10	.366918+003	1.76	.367652-002	-.419206-001	-.782088-001
11	.310608+003	2.09	.225188+000	-.151989-001	.562051-001
12	.351075+003	2.78	.233509+000	.214016-001	.143044+000
13	.454067+003	2.89	-.535825-001	-.347654-001	-.125505+000
14	.363704+003	3.39	.126946+000	.389613-003	.375473-001
15	.390738+003	3.63	-.145513+000	.134809-001	.149904-002
16	.391817+003	3.08	.108916+000	.139873-001	.783962-001
17	.448262+003	3.04			

(t interval: 6 min)

EXPERIMENT 4L

t	$2\sigma_X\sigma_Y$ (m^2)	ρ^{-1}	K_x (m^2s^{-1})	K_y (m^2s^{-1})	K_{xy} (m^2s^{-1})
0	.137300+006	1.18			
1	.136942+006	1.20	.121725+001	-.128123+001	-.496571+000
2	.135854+006	1.23	.191092+001	-.255298+001	-.151114+001
3	.134744+006	1.25	.113671+001	-.199093+001	-.154228+001
4	.134745+006	1.27	.208344+001	-.131350+001	.193414-002
5	.136286+006	1.30	.417812+001	-.866060+000	.213949+001
6	.137375+006	1.32	.314001+001	-.672403+000	.151375+001
7	.135748+006	1.36	.167241+001	-.262131+001	-.226062+001
8	.133489+006	1.37	-.122137+001	-.164605+001	-.313741+001
9	.132602+006	1.36	-.155443+001	-.668016-001	-.123245+001
10	.132966+006	1.37	.182337+001	-.606316+000	.506779+000
11	.132027+006	1.40	.170808+001	-.182656+001	-.130470+001
12	.128258+006	1.45	.289935+000	-.381858+001	-.523491+001
13	.128005+006	1.46	.566040+000	-.510821+000	-.351400+000
14	.131066+006	1.43	.706337+000	.260714+001	.425103+001
15	.133877+006	1.42	.163328+001	.193718+001	.390494+001

(t interval: 6 min)

EXPERIMENT 5S

t	$2\sigma_X\sigma_Y$ (m^2)	ρ^{-1}	K_x (m^2s^{-1})	K_y (m^2s^{-1})	K_{xy} (m^2s^{-1})
0	.710192+003	2.66			
			.734079-001	.137945-001	.642580-001
1	.756458+003	2.64			
			.395304-001	-.370999-001	-.895385-001
2	.691990+003	2.97			
			-.549530-001	.136832-001	.203018-001
3	.706607+003	2.79			
			-.821984-001	-.361506-002	-.397193-001
4	.678009+003	2.74			
			.100057+000	.447847-001	.155770+000
5	.790164+003	2.53			
			.107400-001	-.266626-001	-.657287-001
6	.742839+003	2.71			
			-.568855-002	.105993-001	.262095-001
7	.761710+003	2.64			
			.103611-001	.181483-001	.508855-001
8	.798347+003	2.53			
			.349172-001	.427242-001	.118371+000
9	.883574+003	2.35			
			-.910119-001	.563242-002	-.267202-001
10	.864336+003	2.25			
			.171505+000	.138315-001	.106641+000
11	.941117+003	2.33			
			-.775850-001	-.351599-001	-.116103+000
12	.857524+003	2.42			
			.262479-001	.943731-001	.222706+000
13	.101787+004	2.08			
			.113997+000	-.320403-001	-.169435-001
14	.100567+004	2.27			
			-.323794-002	.368136-001	.795415-001
15	.106294+004	2.14			
			.106500-001	.302455-001	.685251-001
16	.111228+004	2.06			
			.625717-001	.864277-001	.202064+000
17	.125777+004	1.89			

(t interval: 6 min)

EXPERIMENT 5L

t	$2\sigma_X\sigma_Y$ (m^2)	ρ^{-1}	K_x (m^2s^{-1})	K_y (m^2s^{-1})	K_{xy} (m^2s^{-1})
0	.112318+006	1.18			
			.126472+001	-.119656+001	-.361263+000
1	.112058+006	1.20			
			.270480+001	-.138174+001	.548201+000
2	.112453+006	1.23			
			.792437+000	-.419817+000	.123542+000
3	.112542+006	1.24			
			.258176+001	-.121420+001	.537736+000
4	.112929+006	1.27			
			.188109+001	-.602394+000	.703868+000
5	.113436+006	1.29			
			.131814+001	.711496+000	.193993+001
6	.114833+006	1.29			
			.147089+001	.135900+001	.289077+001
7	.116914+006	1.28			
			-.271311+000	.357384+000	.245249+000
8	.117091+006	1.28			
			.648541+000	.758030-001	.604175+000
9	.117526+006	1.28			
			.193004+001	.685817+000	.238443+001
10	.119242+006	1.29			
			.204024+001	.701177+000	.248734+001
11	.121033+006	1.29			
			.195690+001	.228987+000	.180773+001
12	.122335+006	1.30			
			.147962+001	.147359-001	.115403+001
13	.123166+006	1.31			
			.150458+001	.666590+000	.202195+001
14	.124621+006	1.31			
			.184886+001	.528594+000	.210221+001
15	.126135+006	1.32			
			.931128+000	.105703+000	.845905+000
16	.126744+006	1.32			
			.783628+000	.291541+000	.978391+000
17	.127449+006	1.32			

(t interval: 6 min)

EXPERIMENT 6S

t	$2\sigma_X\sigma_Y$ (m^2)	ρ^{-1}	K_x (m^2s^{-1})	K_y (m^2s^{-1})	K_{xy} (m^2s^{-1})
0	.570691+003	2.61	.226556-001	.333960-001	.924605-001
1	.637263+003	2.39	.920650-001	.500843-002	.500982-001
2	.673334+003	2.46	.603457-001	.333051-001	.104885+000
3	.748851+003	2.33	.963763-001	.156772-001	.778841-001
4	.804927+003	2.34	.175893+000	.304071-001	.146316+000
5	.910275+003	2.35	-.305380-001	-.222894-001	-.659526-001
6	.862789+003	2.42	-.318325-001	-.133063-001	-.455473-001
7	.829995+003	2.46	.680387-002	.258846-001	.650315-001
8	.876818+003	2.34			

(t interval: 6 min)

EXPERIMENT 6L

t	$2\sigma_X\sigma_Y$ (m^2)	ρ^{-1}	K_x (m^2s^{-1})	K_y (m^2s^{-1})	K_{xy} (m^2s^{-1})
0	.377532+005	1.61	.126877+001	.667833+000	.186325+001
1	.390947+005	1.61	.971891+000	.261889+000	.102550+001
2	.398330+005	1.61	.180856+001	.163667+000	.137981+001
3	.408265+005	1.64	.131892+001	.312768-001	.852611+000
4	.414404+005	1.66	.126993+001	-.185253+000	.449413+000
5	.417640+005	1.69	.118354+000	-.505309+000	-.790344+000
6	.411949+005	1.72	.196205+000	-.433258+000	-.635406+000
7	.407374+005	1.74			

(t interval: 6 min)

EXPERIMENT 8D

t	$2\sigma_X\sigma_Y$ (m^2)	ρ^{-1}	K_x (m^2s^{-1})	K_y (m^2s^{-1})	K_{xy} (m^2s^{-1})
0	.372081+004	2.38	.982096-001	.274514-002	.477415-001
1	.375518+004	2.39	.426910-001	.115512+000	.288069+000
2	.396259+004	2.28	.228883+000	.387437+000	.936951+000
3	.463719+004	2.02	-.128087+000	.218495+000	.359531+000
4	.489606+004	1.88	-.320200-001	-.430670-001	-.981884-001
5	.482536+004	1.89	-.202566+000	.106082+000	.870906-001
6	.488807+004	1.81	-.379604+000	.257164+000	.223544+000
7	.504902+004	1.64	.387742+000	.469366-001	.311236+000
8	.527311+004	1.68	.703998-001	.317795+000	.560643+000
9	.567677+004	1.58	.169091+000	.302610+000	.576792+000
10	.609206+004	1.51	-.503141-001	.293760+000	.397833+000
11	.637850+004	1.43	.160839+000	.558193+000	.887514+000
12	.701751+004	1.33	.533078+000	.197977+000	.662761+000
13	.749470+004	1.35			

(t interval: 6 min)

EXPERIMENT 8S

t	$2\sigma_X\sigma_Y$ (m^2)	ρ^{-1}	K_x (m^2s^{-1})	K_y (m^2s^{-1})	K_{xy} (m^2s^{-1})
0	.846660+004	1.32			
			.602329+000	.126491+000	.619806+000
1	.891286+004	1.35			
			-.463988+000	-.223917+000	-.646003+000
2	.844774+004	1.35			
			-.184018+000	-.112625+000	-.288329+000
3	.824015+004	1.35			
			.373729+000	-.188678-001	.247733+000
4	.841851+004	1.38			
			-.506437+000	.344460-001	-.325743+000
5	.818398+004	1.33			
			.218585+000	-.130130+000	-.149151-001
6	.817324+004	1.37			
			-.330373+000	.100607-001	-.229357+000
7	.800810+004	1.34			
			.442385+000	.246822+000	.660884+000
8	.848394+004	1.34			
			.502615+000	-.926904-001	.239217+000
9	.865617+004	1.40			
			-.475467+000	-.380363+000	-.873864+000
10	.802699+004	1.42			
			-.204816+000	-.129675+000	-.328593+000
11	.779041+004	1.43			
			-.102353+000	.219129-001	-.407063-001
12	.776110+004	1.42			

(t interval: 6 min)

EXPERIMENT 10

t	$2\sigma_X\sigma_Y$ (m^2)	ρ^{-1}	K_x ($m^2 s^{-1}$)	K_y ($m^2 s^{-1}$)	K_{xy} ($m^2 s^{-1}$)
0	.134249+004	1.40	.121889+000	.533738-001	.161756+000
1	.153660+004	1.41	.216925+000	.418466-001	.209818+000
2	.178838+004	1.50	.253077+000	.294666-001	.208152+000
3	.203816+004	1.62	.987576-001	.584354-001	.155258+000
4	.222447+004	1.59	.627109-001	.365873-001	.975007-001
5	.234147+004	1.57	.220108+000	.679617-001	.246589+000
6	.263738+004	1.60	.812335-001	.360472-001	.108422+000
7	.276749+004	1.59	.160454+000	.420899-001	.167564+000
8	.296856+004	1.61	.773167-001	.304026-001	.969733-001
9	.308493+004	1.61	.654928-001	.933173-002	.555284-001
10	.315157+004	1.63	.107368+000	-.921051-002	.496872-001
11	.321119+004	1.68	.157084+000	-.238388-001	.502678-001
12	.327151+004	1.76	.984228-001	-.403685-002	.479886-001
13	.332910+004	1.80	-.386893-001	-.206089-001	-.586675-001
14	.325870+004	1.81	-.176581+000	-.666487-002	-.110821+000
15	.312571+004	1.76	-.137438+000	-.326396-002	-.850542-001
16	.302365+004	1.71	.114171+000	.174084-001	.963587-001
17	.313928+004	1.73	.124293+000	-.552156-002	.610398-001
18	.321252+004	1.78	.223141+000	-.555967-001	.166042-001
19	.323245+004	1.94	.182879+000	-.604225-001	-.311673-001
20	.319505+004	2.10	.188317+000	-.218259-001	.405406-001
21	.324370+004	2.21	.156742+000	-.309527-001	-.842133-003
22	.324269+004	2.32	.948918-001	-.236637-001	-.158330-001
23	.322369+004	2.41	.209611+000	-.266283-001	.187433-001
24	.324618+004	2.55	.255819+000	-.196788-001	.462769-001
25	.330171+004	2.69	.185471+000	-.296815-001	-.148720-001
26	.328387+004	2.84	.297097+000	-.770970-001	-.134263+000
27	.312275+004	3.21	.308592+000	-.577146-001	-.105281+000
28	.299641+004	3.60	.413883+000	-.386196-001	-.368896-001
29	.295215+004	3.99	.338952+000	.280176-002	.951204-001
30	.306629+004	4.10	.576965+000	-.234559-001	.335240-001
31	.310652+004	4.50			

(t interval: 10 min)

EXPERIMENT 11

t	$2\sigma_X\sigma_Y$ (m^2)	ρ^{-1}	K_x (m^2s^{-1})	K_y (m^2s^{-1})	K_{xy} (m^2s^{-1})
0	.805646+003	1.60			
			.840461-001	.504244-002	.593167-001
1	.876826+003	1.70			
			.823263-001	.456449-001	.125492+000
2	.102742+004	1.64			
			.948433-001	.395615-001	.122691+000
3	.117464+004	1.63			
			.129474+000	.416221-001	.147221+000
4	.135131+004	1.65			
			.115311+000	.336353-001	.125332+000
5	.150171+004	1.67			
			.140606+000	.396529-001	.150343+000
6	.168212+004	1.69			
			.116048+000	.740216-001	.192694+000
7	.191335+004	1.63			
			.127950+000	.832611-001	.213281+000
8	.216929+004	1.58			
			.120438+000	.704470-001	.187195+000
9	.239392+004	1.55			
			.619833-001	.513973-001	.119310+000
10	.253710+004	1.52			
			.346344-001	.440339-001	.893374-001
11	.264430+004	1.49			
			.800761-001	.379745-001	.110326+000
12	.277669+004	1.49			
			.431714-001	.744141-001	.138485+000
13	.294287+004	1.44			
			.201149-001	.638568-001	.104790+000
14	.306862+004	1.40			
			-.272633-001	.380876-001	.327116-001
15	.310788+004	1.36			
			-.454318-002	.387252-001	.486935-001
16	.316631+004	1.33			
			-.440856-001	.172697+000	.184430+000
17	.338762+004	1.21			
			-.884367-001	.110624+000	.537309-001
18	.345210+004	1.13			
			-.706691-001	.432677-001	-.159892-001
19	.343291+004	1.09			
			-.132646-001	.750518-001	.677214-001
20	.351418+004	1.05			
			.903940-001	.902172-001	.180813+000
21	.373116+004	1.05			
			.970192-001	.568045-001	.151938+000
22	.391348+004	1.06			
			.383587-001	.516697-001	.908837-001
23	.402254+004	1.05			
			.233348-001	.388979-001	.630659-001
24	.409822+004	1.05			
			.797762-001	.285256-001	.105752+000
25	.422512+004	1.06			

(t interval: 10 min)

EXPERIMENT 11 (Continued)

t	$2\sigma_X\sigma_Y$ (m^2)	ρ^{-1}	K_x (m^2s^{-1})	K_y (m^2s^{-1})	K_{xy} (m^2s^{-1})
25	.422512+004	1.06	.913136-001	-.187691-002	.829993-001
26	.432472+004	1.09	.991842-001	-.290248-003	.897785-001
27	.443246+004	1.11	.871231-001	.132086-001	.923624-001
28	.454329+004	1.13	.135696+000	-.380537-001	.731713-001
29	.463110+004	1.18	.153874+000	-.296085-001	.917110-001
30	.474115+004	1.23	.182777+000	-.129954-002	.143941+000
31	.491388+004	1.28	.243080+000	.651711-002	.194604+000
32	.514741+004	1.33	.298483+000	.146192-002	.220268+000
33	.541173+004	1.40	.275407+000	.363636-001	.245285+000
34	.570607+004	1.44	.372535+000	.518779-001	.329526+000
35	.610150+004	1.50	.357298+000	.378440-001	.292182+000
36	.645212+004	1.55			

(t interval: 10 min)

EXPERIMENT 12

t	$2\sigma_X\sigma_Y$ (m^2)	ρ^{-1}	K_x (m^2s^{-1})	K_y (m^2s^{-1})	K_{xy} (m^2s^{-1})
0	.679065+004	2.77			
1	.747083+004	2.73	.685072+000	.115531+000	.566814+000
2	.813214+004	2.65	.464677+000	.140646+000	.551094+000
3	.879712+004	2.54	.319620+000	.166284+000	.554151+000
4	.965905+004	2.41	.424124+000	.221084+000	.718272+000
5	.105000+005	2.28	.250616+000	.253337+000	.700827+000
6	.111790+005	2.17	.144584+000	.225229+000	.565839+000
7	.117537+005	2.11	.224732+000	.174660+000	.478869+000
8	.123125+005	2.09	.364549+000	.139108+000	.465640+000
9	.129590+005	2.07	.446685+000	.155891+000	.538771+000
10	.136125+005	2.05	.483286+000	.150502+000	.544564+000
11	.146749+005	2.08	.106723+001	.178445+000	.885357+000
12	.157941+005	2.06	.832115+000	.256492+000	.932712+000
13	.168566+005	2.06	.967082+000	.201899+000	.885357+000
14	.177049+005	2.05	.650629+000	.189881+000	.706958+000
15	.183061+005	2.06	.529279+000	.118473+000	.501021+000
16	.186415+005	2.11	.694170+000	-.259132-001	.279497+000
17	.186983+005	2.18	.625670+000	-.113982+000	.472662-001

(t interval: 6 min)

exhibit negative values although the cluster area generally increased with time. Since the x and y axes do not necessarily coincide with the principal axes of the drogue cluster, the variances in those directions may not always increase with time.

Following Okubo and Ebbesmeyer (1976), time series of the mean velocity, horizontal divergence (γ), relative vorticity (η), stretching deformation rate (α), and shearing deformation rate (h) were computed. Observations of the x,y coordinates of each drogue were used to calculate u,v speeds of n drogues simultaneously at m times by in place differentiation of the position coordinates.

$$x_i(k),\ y_i(k) \qquad i = 1,2,3,\ldots n$$
$$u_i(k),\ v_i(k) \qquad k = 1,2,3,\ldots m$$

Next the u_i, v_i speeds of each drogue at each time were expanded in Taylor series about the centroid located at $\bar{x}(k)$, $\bar{y}(k)$:

$$u_i(k) = \bar{u}(k) + \frac{\partial \bar{u}(k)}{\partial x}[x_i(k) - \bar{x}(k)] + \frac{\partial \bar{u}(k)}{\partial y}[y_i(k) - \bar{y}(k)] + u_i''(k)$$
$$v_i(k) = \bar{v}(k) + \frac{\partial \bar{v}(k)}{\partial x}[x_i(k) - \bar{x}(k)] + \frac{\partial \bar{v}(k)}{\partial y}[y_i(k) - \bar{y}(k)] + v_i''(k) \qquad (22)$$

where

$$\bar{x}(k) = \frac{1}{n}\sum_{i=1}^{n} x_i(k), \qquad \bar{y}(k) = \frac{1}{n}\sum_{i=1}^{n} y_i(k)$$

and $\frac{\partial \bar{u}}{\partial x}$, $\frac{\partial \bar{u}}{\partial y}$, $\frac{\partial \bar{v}}{\partial x}$, $\frac{\partial \bar{v}}{\partial y}$ are linear velocity gradients evaluated at the centroid, and u_i'', v_i'' are the turbulent speeds.

The velocity gradients and mean velocities were calculated from

the above equations using linear regression techniques. Rather than presenting the velocity gradients as such we chose to use the following parameters which have more physical meaning:

Horizontal divergence: $\gamma(k) = \frac{\partial \bar{u}}{\partial x} + \frac{\partial \bar{v}}{\partial y}$,

Relative vorticity: $\eta(k) = \frac{\partial \bar{v}}{\partial x} - \frac{\partial \bar{u}}{\partial y}$,

Stretching deformation rate: $\alpha(k) = \frac{\partial \bar{u}}{\partial x} - \frac{\partial \bar{v}}{\partial y}$, and

Shearing deformation rate: $h(k) = \frac{\partial \bar{v}}{\partial x} + \frac{\partial \bar{u}}{\partial y}$

Table 19 shows the results of the velocity-gradient parameter computations. By and large these absolute values range from $10^{-4}s^{-1}$ to $10^{-6}s^{-1}$ as far as the order of magnitude is concerned. On the average, the velocity gradient field is characterized by positive divergence. In particular, for the entire period of Experiments #1 and 11 the flow was predominantly divergent. As will be discussed later, the current meter records also reveal predominant divergence in the experimental area.

Three drogue experiments (#4,5,6) in which a small cluster of 8 drogues was surrounded by a larger cluster of 8 drogues were carried out during the July 1980 LEDS experiments. All drogues were set at 10 ft depths. Figure 81 shows velocity gradient parameters for the large and small clusters of Experiment #6 as a function of time. Clearly the velocity gradients show similar trends for both the large and small scale clusters, with the magnitude being much

Table 19

Velocity gradient parameters obtained from drifter observation, Experiments 1, 3, 4S, 4L, 5S, 5L, 6S, 6L, 8S, 8D, 10, 11, 12.

EXPERIMENT 1

t	divergence (s^{-1})	shearing (s^{-1})	stretching (s^{-1})	vorticity (s^{-1})
0	.1639-004	-.6978-004	-.2671-003	-.2621-005
1	.2447-003	.4647-004	-.2001-003	.4521-004
2	.1227-003	-.3585-004	.2075-004	.2086-004
3	.1458-003	-.1344-003	-.9008-004	.5694-004
4	.1971-003	-.1438-003	-.4043-003	.2349-003
5	.8823-004	-.2138-003	-.3418-003	.1668-003
6	.1840-003	-.1559-003	-.2772-003	.4506-004
7	.2699-003	-.5981-004	-.3234-003	.9112-004
8	.1848-003	-.9901-004	-.3031-003	.1284-003
9	.3945-004	-.8791-004	-.2593-003	.1308-003
10	.3509-004	-.4135-004	-.1522-003	.2574-004
11	.1049-003	-.1198-003	-.1333-003	.1432-004
12	.1293-003	-.1296-003	-.1771-003	.4428-004
13	.1330-003	-.8218-004	-.2710-003	.1421-003
14	.1357-003	-.8848-004	-.4200-003	.3064-003
15	.1659-003	.3620-004	-.2964-003	.1487-003
16	.2066-003	-.9525-005	.1305-003	-.1440-003
17	.7255-004	-.1473-003	.8668-004	-.4385-004
18	.1091-003	-.5358-004	-.3172-004	.2209-004
19	.6943-004	-.1420-004	-.1282-003	.4972-004
20	.5263-004	.6652-004	-.1558-003	.1473-004
21	.9965-004	.2437-003	-.7660-004	-.1416-003

(t interval: 6 min)

EXPERIMENT 3

t	divergence (s^{-1})	shearing (s^{-1})	stretching (s^{-1})	vorticity (s^{-1})
0	-.5648-003	.5386-003	.3265-003	-.9419-005
1	.1795-004	-.5689-003	.8421-004	.5227-003
2	-.2186-003	-.3127-003	-.3168-003	.3866-003
3	.2063-003	-.3314-003	.8592-006	.2558-003
4	.1272-003	-.1967-003	.3413-003	.4944-005
5	.9667-004	-.1974-003	.3402-003	.1636-003
6	.5000-003	-.2904-003	.2843-003	.1084-003
7	.2153-003	.2281-003	.3974-004	-.2564-003
8	.8444-004	-.1234-004	.1315-003	-.3109-004
9	.4432-003	-.5333-003	.5585-004	.1775-003
10	.5879-004	-.1536-004	.1095-003	-.7223-004
11	-.8686-004	.1327-003	.1498-003	-.4920-004
12	.4062-003	-.2124-003	-.1830-003	.1926-003
13	.3628-003	-.2960-003	-.1266-003	.2178-003
14	.4517-004	-.1778-004	-.1081-003	.1852-003
15	-.2442-003	.2634-003	-.1018-003	-.7885-005
16	.2823-003	-.2503-003	-.1748-003	.2414-003
17	.3713-003	-.3245-003	.1737-003	.3911-003
18	.1676-005	.7041-004	.2902-003	.9110-004
19	-.5836-004	.7902-004	.2211-003	.1104-003
20	.2389-003	-.2761-003	.2960-003	.4110-003
21	.4084-003	-.2849-003	-.3226-004	.3084-003
22	.3770-003	-.1551-003	-.2064-003	-.9270-004
23	.1854-003	.5553-004	-.2309-004	-.3070-003
24	-.1781-003	.3501-003	.1086-003	-.1806-003
25	.1090-003	.1233-003	-.1334-003	.2111-004
26	.3767-003	-.1588-003	-.1448-003	.2212-004
27	-.5227-005	.5373-004	.8676-004	-.8478-004
28	-.1984-003	.9140-004	.2586-003	-.2501-003
29	.1130-003	.7036-004	-.1037-003	-.1796-004
30	.1650-003	.1376-003	-.3375-003	.9766-004
31	-.7415-004	.2896-003	-.2005-003	-.1199-004
32	-.3042-003	.3836-003	-.1258-003	-.2466-004
33	.1000-003	-.1546-003	.7095-004	-.2029-003
34	.4310-003	-.4691-003	.7987-004	-.2153-003
35	.2131-005	-.7300-004	.1257-003	-.1224-003
36	-.6632-004	.6727-004	.1881-005	-.1176-003
37	-.5805-004	.1479-003	.7387-004	-.8161-004

(t interval: 6 min)

EXPERIMENT 3 (Continued)

t	divergence (s^{-1})	shearing (s^{-1})	stretching (s^{-1})	vorticity (s^{-1})
38	.2241-003	.2224-004	-.3753-004	-.3622-004
39	.3985-003	-.1837-003	-.1790-003	-.2483-004
40	.3430-003	-.2014-003	-.1831-003	.2129-004
41	.1847-003	-.8235-004	.6029-006	-.7559-004
42	.1680-004	-.1101-003	.2162-003	-.2136-003
43	-.1131-003	.8531-004	.1388-003	-.3359-003
44	-.8430-004	.8982-004	.4590-004	-.6552-004
45	.3137-003	-.1082-003	-.9034-004	-.2871-004
46	.2296-003	-.1740-004	.1719-003	-.5607-004
47	.1534-003	-.1580-003	.2228-003	.1578-003
48	.2012-003	-.7429-004	-.6780-004	-.1067-004
49	.1358-003	-.1473-003	-.1729-003	.1039-005
50	.1933-003	-.3068-003	-.2462-003	-.1373-003
51	.1738-003	-.9175-005	-.3304-004	-.1373-003
52	-.8943-004	.1129-003	.2859-004	.5896-005
53	-.2121-003	.8269-004	.8206-004	-.1322-003
54	-.6567-004	.6972-004	.1912-003	-.1174-003
55	-.1662-003	-.1555-004	.1419-003	-.8031-004
56	-.4733-004	-.4306-004	-.4092-004	-.9610-004
57	.6111-004	-.2609-003	-.3377-004	-.9057-004
58	.5202-004	-.2753-003	.1050-003	-.3476-004
59	.1604-003	.4080-004	-.5441-004	.5965-004
60	-.2189-004	.1529-003	-.4376-004	-.2045-003
61	.1465-003	-.1139-003	.7196-004	-.4042-003
62	.1914-003	-.1925-003	.1716-003	-.1090-003
63	-.1165-003	-.1990-004	.2345-003	.1378-003
64	-.6935-004	.1223-003	-.1269-003	.5392-004
65	.1058-004	.2024-004	-.9061-004	-.6403-004
66	-.4523-003	-.7843-004	.5727-003	-.3841-003
67	-.8788-003	-.3074-004	.1022-002	-.8240-003
68	-.8026-004	-.2836-003	.3298-003	-.6005-003
69	.1157-002	-.6909-003	-.8984-003	-.1299-004
70	.6910-003	-.1777-003	-.5055-003	.7899-004
71	.2975-005	-.4462-004	.5846-004	-.1461-003
72	.5413-004	-.3606-004	-.1792-003	.5440-004
73	.1295-003	.4767-004	-.4582-004	-.1709-004
74	.1137-003	.7201-004	.9980-004	-.6760-004

(t interval: 6 min)

EXPERIMENT 3 (Continued)

t	divergence (s^{-1})	shearing (s^{-1})	stretching (s^{-1})	vorticity (s^{-1})
75	-.6948-004	-.5946-004	.1112-003	-.6441-004
76	-.1072-003	-.3011-003	.8539-004	-.2567-003
77	.1986-003	-.1079-003	-.8248-004	-.3406-003
78	.2367-003	.1552-003	-.1924-003	-.6042-004
79	.6910-004	.1237-003	-.9658-005	-.1106-004
80	-.9054-004	-.1843-004	.8220-004	-.5886-004
81	.5795-004	.7527-004	.6248-004	-.8043-005
82	.1697-003	.6216-004	-.7503-004	.1562-005
83	-.8869-005	-.6861-004	-.1398-003	.3577-004
84	-.6277-004	.1708-003	-.2378-004	.1576-003
85	.5252-004	.2707-003	.5782-004	.1236-003
86	.1047-003	-.1533-004	-.4832-004	-.4250-004
87	.7701-004	-.1980-003	-.8566-004	-.1625-003
88	.8640-004	-.1768-003	-.1026-003	-.1367-003
89	.1519-004	.1734-004	-.1739-003	.1611-003
90	.5779-004	.2781-003	-.1757-003	.4600-003
91	.4919-005	-.8795-005	-.1726-003	.6350-004
92	.6305-004	-.2944-003	-.4318-003	-.1479-003
93	.2340-003	.1737-003	-.6570-003	.3482-003
94	.1441-003	.2504-003	-.4625-003	.3525-003
95	.7312-004	.3589-003	-.2379-003	.3984-003
96	-.7975-004	.2816-003	-.1253-003	.2909-003
97	-.1970-003	-.1077-003	.2751-003	-.2601-003
98	-.4055-003	-.1667-003	.6116-003	-.5141-003

(t interval: 6 min)

EXPERIMENT 4S

t	divergence (s^{-1})	shearing (s^{-1})	stretching (s^{-1})	vorticity (s^{-1})
0	.2134-003	.1550-003	-.7642-004	.6218-004
1	-.1814-004	-.1884-003	-.1501-003	.9413-005
2	-.1833-004	-.1986-003	-.3617-003	-.9085-004
3	.2926-004	-.1111-003	-.1137-005	-.1581-003
4	-.5699-004	-.8747-004	.2094-003	-.1270-003
5	.7029-005	-.5107-004	-.2300-003	-.1553-003
6	.3487-004	.1203-003	-.3718-003	-.4889-004
7	-.7008-004	-.9824-004	-.4563-003	-.2836-003
8	.4836-004	-.1354-003	-.3201-003	-.5247-003
9	-.7279-004	.2566-004	.5057-004	-.4048-003
10	-.4002-003	.7213-004	-.1307-003	-.4276-003
11	-.2772-004	.8748-004	-.6831-003	-.3068-003
12	.5372-003	-.1255-003	-.4564-003	-.1932-003
13	.3947-004	-.4901-003	-.3354-003	-.4380-003
14	-.2368-003	-.3565-003	-.3932-003	-.5777-003
15	.7772-004	-.8908-004	.8849-004	-.5431-003
16	.2656-003	-.4978-003	.1351-003	-.4200-003
17	.4917-003	-.6564-003	-.4101-003	.9768-004

EXPERIMENT 4L

t	divergence (s^{-1})	shearing (s^{-1})	stretching (s^{-1})	vorticity (s^{-1})
0	-.3440-006	-.3632-004	.3456-004	-.5590-005
1	-.1444-004	-.7020-004	.5844-004	.2162-004
2	-.2259-004	-.8950-004	.5488-004	.4376-004
3	-.1131-004	-.9412-004	.3283-004	.4315-004
4	.1613-004	-.1039-003	.2565-004	.1427-004
5	.2632-004	-.8282-004	.2530-004	.5924-005
6	-.5552-005	-.4037-004	.4518-004	.1369-004
7	-.4031-004	-.9209-005	.4589-004	.2447-004
8	-.3281-004	-.4354-005	.5271-006	.5501-004
9	-.4605-005	-.6344-004	-.2537-004	.4123-004
10	-.5777-005	-.1164-003	-.2264-004	.5568-005
11	-.5028-004	-.1046-003	.8966-005	-.8896-005
12	-.4391-004	-.7533-004	.1795-005	.1784-004
13	.3093-004	-.4699-004	-.7460-004	.7555-004
14	.6242-004	-.3694-004	-.1022-003	.8191-004
15	.5543-004	-.4714-004	-.8598-004	.5522-004

(t interval: 6 min)

EXPERIMENT 5S

t	divergence (s^{-1})	shearing (s^{-1})	stretching (s^{-1})	vorticity (s^{-1})
0	.3342-003	-.5030-003	-.2246-003	.1144-003
1	-.1389-005	-.1836-003	.7410-004	-.3412-004
2	-.1021-003	-.1423-003	.5002-004	.2232-004
3	-.3026-004	-.8468-004	-.1462-003	.7257-004
4	.1676-003	-.4000-004	-.1749-003	.3567-004
5	.1129-003	.3118-004	.1031-004	.2616-004
6	-.5390-004	-.4069-004	.4868-004	.1847-003
7	.1043-003	-.1610-003	-.1538-003	.2565-003
8	.2129-003	-.1759-003	-.2431-003	.1895-003
9	.1094-003	.1505-003	-.1189-003	-.9503-004
10	.9607-004	-.3234-004	-.3345-004	-.3532-004
11	-.3211-004	-.3655-003	-.3738-004	.3448-003
12	.1351-003	.1591-004	-.1919-003	.5511-004
13	.2076-003	-.4558-004	-.1108-003	-.5959-004
14	.5315-004	-.1043-003	-.9061-005	.8976-004
15	.1306-003	-.2121-005	-.1489-003	.4939-004
16	.2435-003	.2079-004	-.2076-003	.4831-004
17	.4679-003	.1727-003	-.2476-003	.2150-005

EXPERIMENT 5L

t	divergence (s^{-1})	shearing (s^{-1})	stretching (s^{-1})	vorticity (s^{-1})
0	-.1511-004	-.3879-004	-.4956-005	.6623-004
1	.1853-005	-.6241-004	-.1318-004	.6031-004
2	.5754-005	-.4970-004	-.7534-005	.4971-004
3	.6140-005	-.4725-004	-.3293-005	.2161-004
4	.1073-004	-.5550-004	-.6378-005	.2179-004
5	.2304-004	-.2191-004	-.3120-005	.6435-004
6	.4219-004	.4463-005	.3007-006	.7331-004
7	.2721-004	.6156-005	.1332-004	.3979-004
8	.7240-005	-.6880-005	.2313-004	.2037-004
9	.2532-004	-.1534-004	.1676-004	.2601-004
10	.4086-004	-.1505-004	.1137-004	.3018-004
11	.3550-004	-.1704-004	.2488-005	.3208-004
12	.2412-004	-.1883-004	-.2905-005	.3758-004
13	.2600-004	-.1644-004	.2267-004	.2086-004
14	.3301-004	-.1537-004	.4037-004	.7091-005
15	.2328-004	-.1302-004	.1976-004	.3170-004
16	.1444-004	-.7334-005	.1776-004	.4558-004
17	.1625-004	-.3197-005	.4488-004	.3684-004

(t interval: 6 min)

EXPERIMENT 6S

t	divergence (s^{-1})	shearing (s^{-1})	stretching (s^{-1})	vorticity (s^{-1})
0	.2827-003	-.2703-003	-.1439-003	-.1913-004
1	.2438-003	-.4924-004	-.1192-003	.5330-004
2	.2134-003	-.9732-004	.1240-003	.2197-003
3	.2559-003	-.1994-003	.2094-003	.3056-003
4	.2750-003	-.5922-004	.1047-003	.3321-003
5	.8159-004	.4162-004	.7600-004	.3026-003
6	-.1081-003	-.2064-004	.1983-003	.2588-003
7	.1183-004	-.1701-003	.2609-003	.2618-003
8	.3162-003	-.3839-003	.2452-003	.3979-003

(t interval: 6 min)

EXPERIMENT 6L

t	divergence (s^{-1})	shearing (s^{-1})	stretching (s^{-1})	vorticity (s^{-1})
0	.1197-003	.1609-004	-.3945-004	-.1062-004
1	.7419-004	.1319-004	-.9809-005	.4172-004
2	.6025-004	.1901-004	.1922-004	.5532-004
3	.5515-004	.2265-004	.3165-004	.4738-004
4	.3145-004	.9094-005	.4621-004	.6333-004
5	-.8313-005	.4713-005	.5381-004	.7003-004
6	-.3495-004	.1820-005	.5099-004	.7005-004
7	-.2591-004	-.1720-004	.5857-004	.7834-004

(t interval: 6 min)

EXPERIMENT 8S

t	divergence (s^{-1})	shearing (s^{-1})	stretching (s^{-1})	vorticity (s^{-1})
0	.2854-003	.1328-003	.1163-003	.2928-003
1	-.2616-005	.1902-004	-.2674-004	.4216-004
2	-.1069-003	-.1375-006	.5185-004	-.3510-004
3	-.6899-005	.5137-004	.7015-004	-.8726-004
4	-.7179-005	-.1493-004	.3727-005	-.8784-004
5	-.4263-004	-.2920-004	.1331-003	.4340-004
6	-.3113-004	.1316-005	.7567-004	-.2996-004
7	.5338-004	-.1492-004	-.7442-004	-.1500-003
8	.1070-003	.6545-004	-.1940-004	.7693-005
9	-.7409-004	.8541-004	-.4360-004	.2041-006
10	-.1487-003	.4252-004	-.9426-004	-.1413-003
11	-.4728-004	-.2410-004	.7466-004	.1761-006
12	.2964-004	-.9319-004	.3192-003	.2425-003

(t interval: 6 min)

EXPERIMENT 8D

t	divergence (s^{-1})	shearing (s^{-1})	stretching (s^{-1})	vorticity (s^{-1})
0	-.3518-003	.2129-003	-.3216-003	.2453-003
1	.9666-004	.3008-005	.8399-004	.1473-004
2	.3169-003	-.8768-004	.2849-003	-.6153-004
3	.3280-003	-.1853-003	.2535-003	.3323-004
4	.5135-004	-.9980-004	.1527-004	.3493-004
5	-.6850-005	-.5773-004	.1089-005	.4909-005
6	.7092-004	-.3165-003	-.6641-006	.3386-004
7	.9487-004	-.2511-003	-.5243-004	-.7436-004
8	.1664-003	.6070-005	.7328-004	-.6861-004
9	.2026-003	-.5749-004	.1436-003	.5455-004
10	.1658-003	-.1702-003	.6394-004	-.2775-004
11	.1932-003	-.1850-003	.1065-003	.2071-004
12	.2249-003	-.1375-003	.4771-004	.2162-004
13	.1420-003	-.9147-004	-.1552-003	-.1278-003

(t interval: 6 min)

EXPERIMENT 10

t	divergence (s^{-1})	shearing (s^{-1})	stretching (s^{-1})	vorticity (s^{-1})
0	.2125-003	-.3557-004	-.1052-003	.2328-004
1	.2370-003	-.7497-004	.1315-004	.8089-004
2	.2375-003	-.8487-004	.7853-004	.9754-004
3	.1774-003	-.5491-004	.4049-005	.1055-003
4	.1184-003	-.1675-004	-.5341-004	.8363-004
5	.1451-003	-.1486-004	-.7974-005	.4763-004
6	.1367-003	-.1135-004	.1587-005	.4656-004
7	.9948-004	-.5069-005	.8312-005	.2834-004
8	.8942-004	-.2096-004	-.6106-005	.2569-004
9	.4960-004	-.6265-004	-.5775-004	.6506-004
10	.3033-004	-.9338-004	-.6308-004	.7059-004
11	.3624-004	-.7703-004	-.4099-005	.1380-004
12	.2930-004	-.5338-004	.2906-004	-.1149-004
13	-.4495-005	-.4930-004	-.4438-004	.6207-004
14	-.5942-004	-.2379-004	-.8898-004	.9952-004
15	-.6637-004	.9369-005	-.1027-003	.1286-003
16	.1410-004	.2505-005	-.1194-004	.5119-004
17	.5352-004	.2921-005	.8187-004	-.6082-004
18	.2439-004	-.6269-004	.8480-004	-.6810-006
19	-.4357-005	-.9487-004	.9953-004	.1647-004
20	.1586-005	-.8704-004	.6643-004	.1722-004
21	.1075-004	-.1015-003	.3752-005	.8742-004
22	-.7480-005	-.7344-004	.2275-004	.8544-004
23	.3040-005	-.4456-004	.6596-004	.5935-004
24	.1265-004	-.7667-004	.5796-004	.9769-004
25	.1469-004	-.9513-004	.3051-004	.1259-003
26	-.4907-004	-.1889-003	.2940-004	.1807-003
27	-.7825-004	-.2651-003	.2541-004	.2150-003
28	-.4498-004	-.2945-003	-.3759-004	.2854-003
29	.1587-004	-.2403-003	-.6568-004	.3006-003
30	.5097-004	-.2373-003	-.8007-004	.3025-003
31	.1516-005	-.4133-003	-.7932-004	.4129-003

(t interval: 6 min)

EXPERIMENT 11

t	divergence (s^{-1})	shearing (s^{-1})	stretching (s^{-1})	vorticity (s^{-1})
0	.3635-004	.2123-003	.9251-004	.2159-003
1	.2166-003	-.8991-004	-.6162-004	.1156-003
2	.2445-003	-.8111-004	-.1376-003	.8875-004
3	.2344-003	-.1147-003	-.1817-003	.1067-003
4	.2042-003	-.8630-004	-.1552-003	.1214-003
5	.1826-003	-.5286-004	-.9708-004	.1159-003
6	.2054-003	.1206-004	-.5155-004	.5639-004
7	.2136-003	.4837-004	-.4867-004	.3476-004
8	.1845-003	.2963-004	-.7223-004	.3972-004
9	.1292-003	.2483-004	-.6458-004	.1910-004
10	.8356-004	.3113-004	-.4185-004	-.5594-005
11	.7541-004	.2017-004	-.3801-004	-.9106-005
12	.8960-004	.2907-004	.2394-005	-.2657-004
13	.8348-004	.4977-004	.4212-004	-.3090-004
14	.4403-004	.4686-004	.2362-004	-.2879-005
15	.2363-004	.4110-004	-.9920-005	.3343-004
16	.7340-004	.1010-003	.3066-004	.4381-005
17	.7481-004	.1433-003	.5140-004	-.2472-004
18	.1035-004	.9444-004	-.3291-005	.1162-004
19	.1398-004	.5158-004	-.3732-004	.3951-004
20	.6971-004	.2304-004	-.3829-004	.5091-004
21	.8963-004	-.1931-005	-.2259-004	.5185-004
22	.6218-004	.7152-006	-.1227-004	.4251-004
23	.3798-004	.6471-005	.1167-004	.3393-004
24	.4111-004	-.1031-004	.1002-004	.5168-004
25	.4571-004	-.3173-004	.1008-004	.4468-004
26	.3993-004	-.3954-004	.2217-004	.2355-004
27	.4134-004	-.2914-004	.2660-004	.6919-005
28	.3698-004	-.3516-004	.4605-004	.2519-006
29	.3536-004	-.4619-004	.6179-004	.1337-004
30	.4927-004	-.4425-004	.5278-004	.1588-004
31	.6908-004	-.5473-004	.3704-004	.2005-004
32	.8035-004	-.6931-004	.3509-004	.1644-004
33	.8554-004	-.6075-004	.2830-004	.1225-005
34	.1003-003	-.4463-004	.3334-004	-.1487-004
35	.1022-003	-.4736-004	.3395-004	-.8229-005
36	.8603-004	-.5841-004	.1020-004	.2204-004

(t interval: 6 min)

EXPERIMENT 12

t	divergence (s^{-1})	shearing (s^{-1})	stretching (s^{-1})	vorticity (s^{-1})
0	.1678-003	-.1602-003	-.2765-005	.1672-003
1	.1508-003	-.7654-004	-.3912-004	.8864-004
2	.1380-003	-.2374-004	-.6555-004	.3992-004
3	.1438-003	-.7131-005	-.7758-004	.2709-004
4	.1477-003	-.4005-006	-.8890-004	.1905-004
5	.1210-003	.6664-005	-.8798-004	.7917-005
6	.9360-004	-.2013-004	-.6314-004	.3265-004
7	.8061-004	-.6030-004	-.3312-004	.6542-004
8	.8157-004	-.1007-003	-.2155-004	.8150-004
9	.8321-004	-.1076-003	-.2239-004	.9427-004
10	.1040-003	-.1038-003	-.6441-005	.1156-003
11	.1234-003	-.9816-004	-.1265-004	.1239-003
12	.1153-003	-.1046-003	-.2234-004	.1342-003
13	.9484-004	-.1177-003	-.2441-004	.1385-003
14	.6897-004	-.1169-003	-.3101-004	.1197-003
15	.4313-004	-.1316-003	-.1618-004	.1189-003
16	.1825-004	-.1550-003	-.3068-005	.1307-003
17	-.8483-005	-.1844-003	-.5269-005	.1400-003

(t interval: 6 min)

greater for the small cluster than the large cluster. The small cluster velocity gradients fluctuate more rapidly with time than those of the large cluster, as might be expected.

In the Taylor series (equation (22)) we have assumed that the velocity gradients were uniform within the group of drogues and that the second-and higher-order terms were turbulence. This form views the spectrum of oceanic turbulence as separable into two major parts; the large scale eddies that appear as shears of the mean velocity, and the small scale eddies responsible for eddy diffusion.

In the real ocean the spectrum of oceanic turbulence contains a wide range of eddy scales and is not easily separable in this way. This means that the second-and higher-order velocity gradients are not truly random, but more or less deterministic. This situation is demonstrated in Figure 82a,b,c, and d, where as an example, the drogue cluster of Experiment #12 was broken into subclusters of 3 drogues, and the velocity-gradient parameters (equation 23) calculated for the subclusters. The values were then plotted at the centroid position of each triad and contoured; for demonstration purposes we have only shown in Figure 82a,b,c, and d the zero-value contours dividing positive and negative regions of the parameters. Clearly these local values are not uniform, nor are they chaotic. The contours show that the velocity field changes greatly but somewhat smoothly in space and time.

Since position, not velocity, is the quantity measured in the drogue dispersion study, a purely Lagrangian analysis should be more

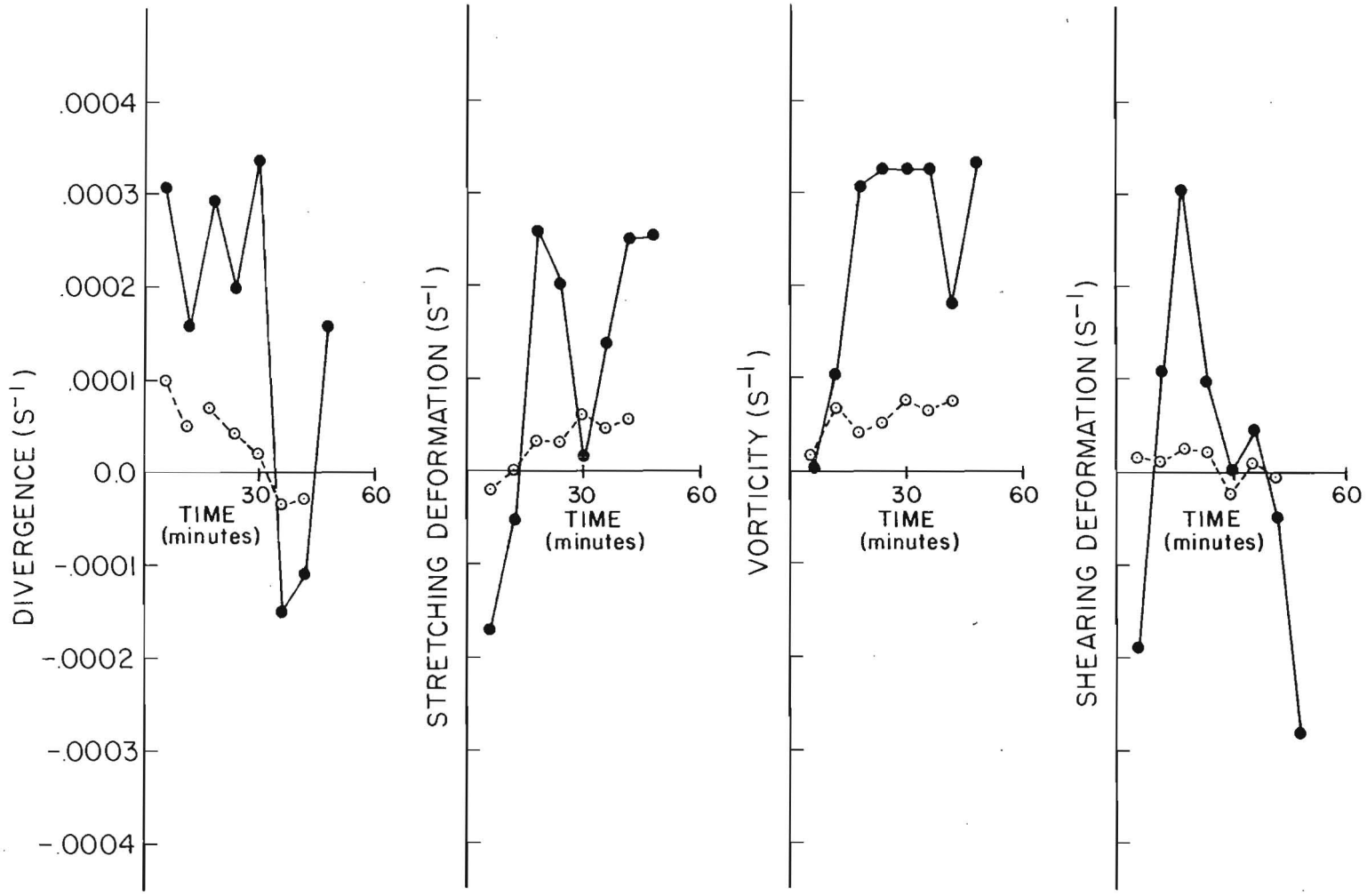

Figure 81. Velocity gradient parameters: divergence, stretching deformation, vorticity, shearing deformation. The solid line indicates data from a small cluster, and the hatched line indicates data from a larger cluster in Experiment #6.

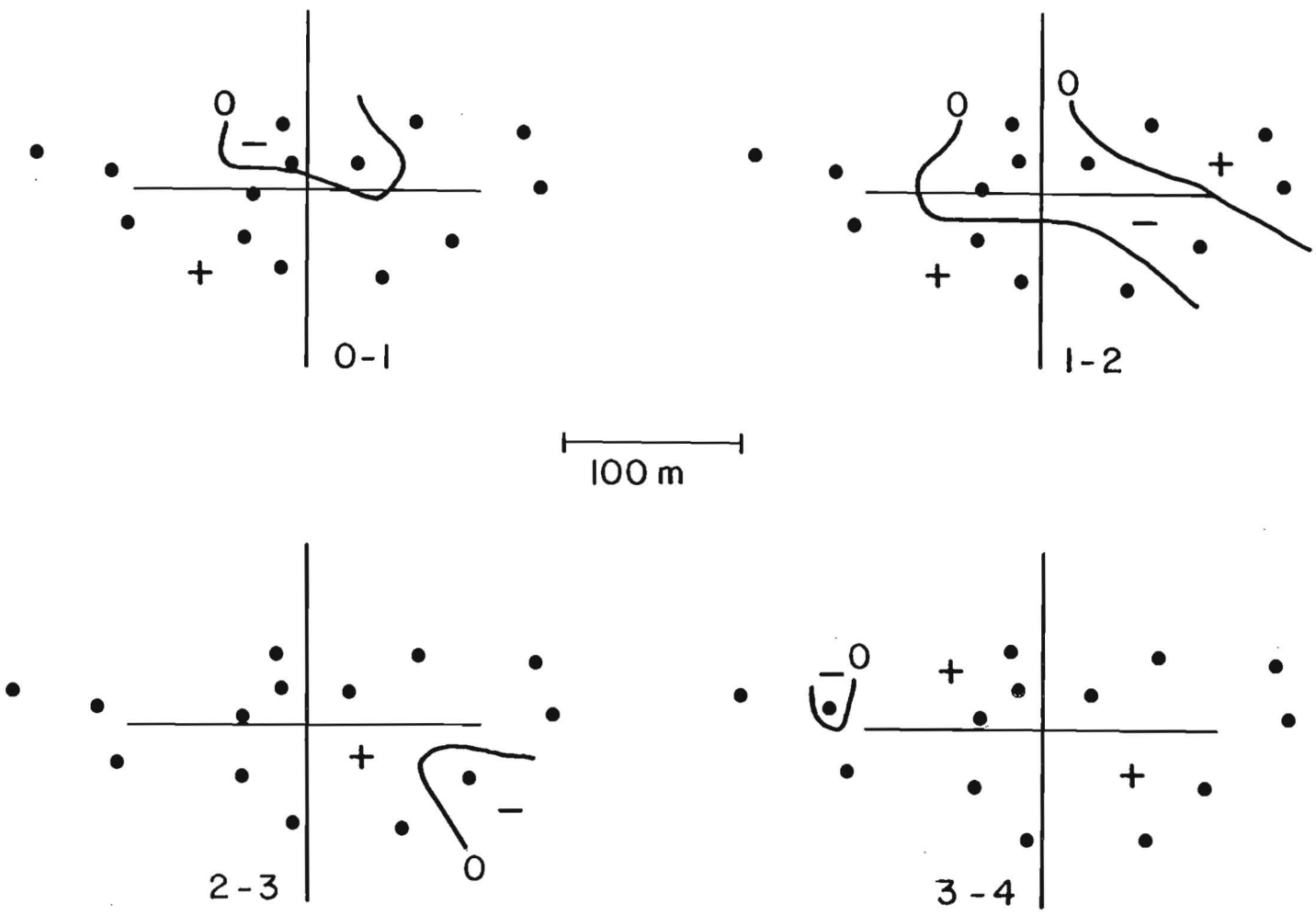

Figure 82a. Local divergence field obtained by subclusters of 3 drogues in Experiment 12 with triad centroids indicated by solid black circles. Time intervals between which the divergence field is calculated are indicated on each plot, e.g., 0-1.

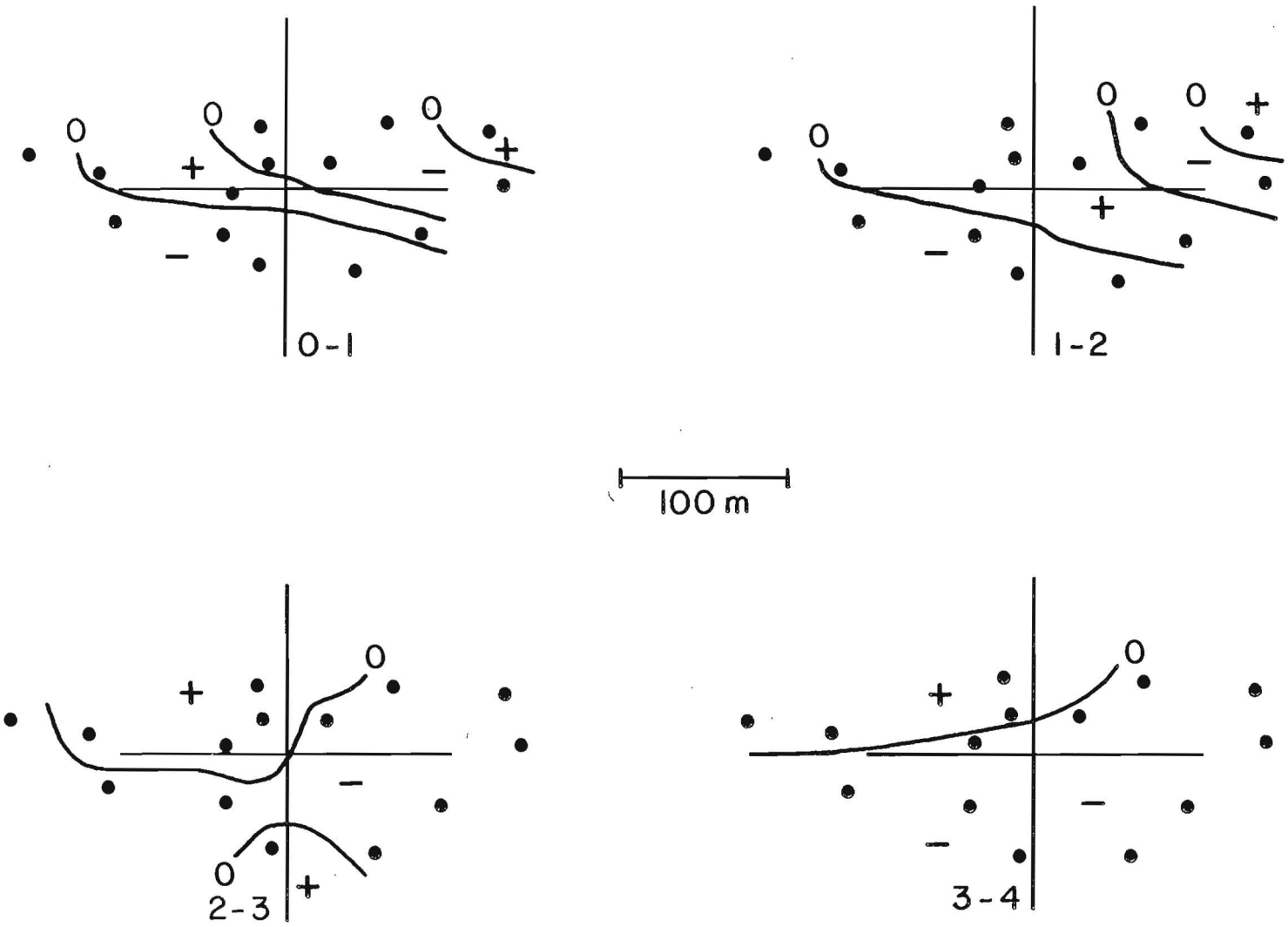

Figure 82b. Local stretching deformation rate field obtained by subclusters of 3 drogues in Experiment 12 with triad centroids indicated by solid black circles. Time intervals between which the stretching deformation rate field is calculated are indicated on each plot.

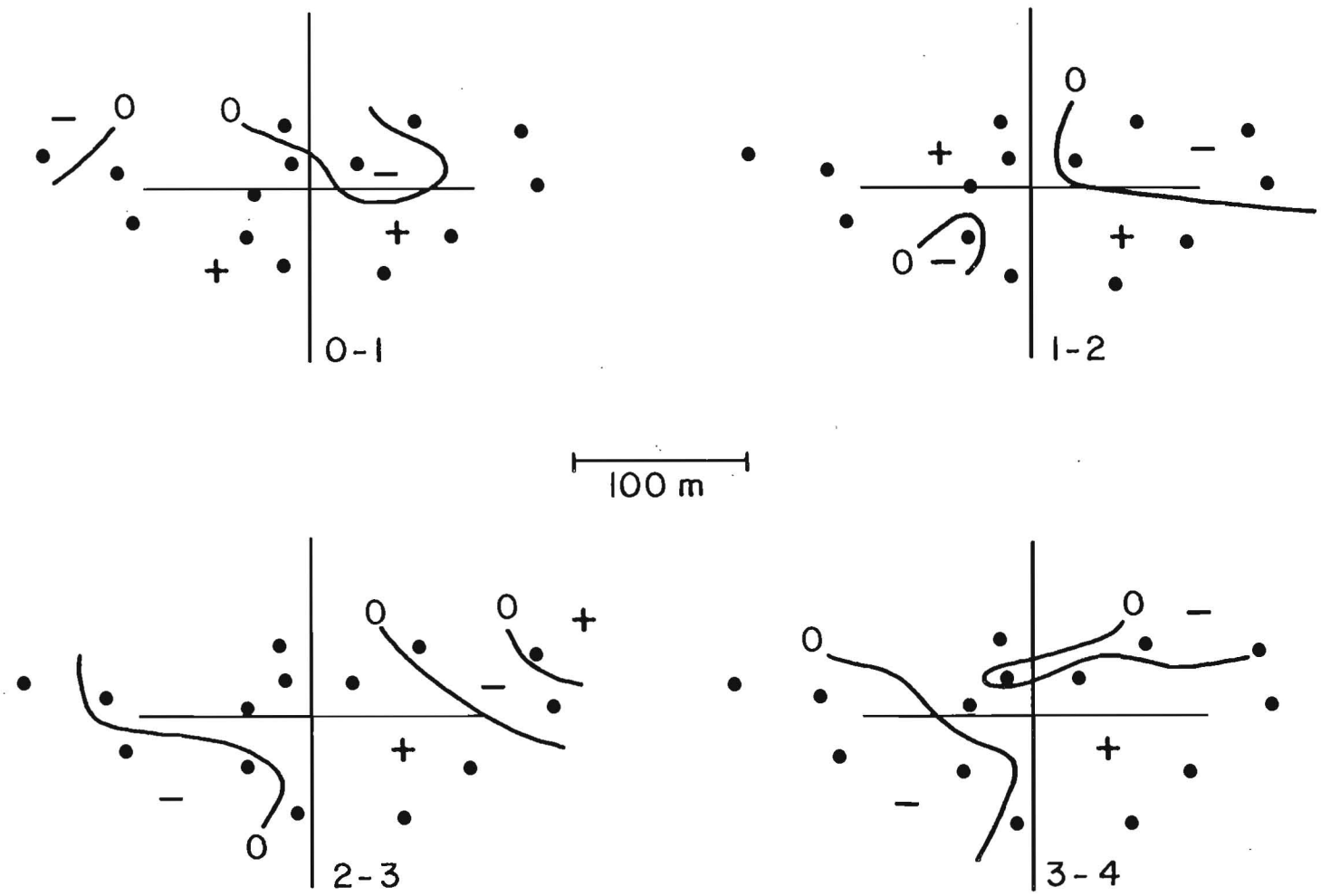

Figure 82c. Local vorticity field obtained by subclusters of 3 drogues in Experiment 12 with triad centroids indicated by solid black circles. Time intervals between which the vorticity field is calculated are indicated on each plot, e.g., 0-1.

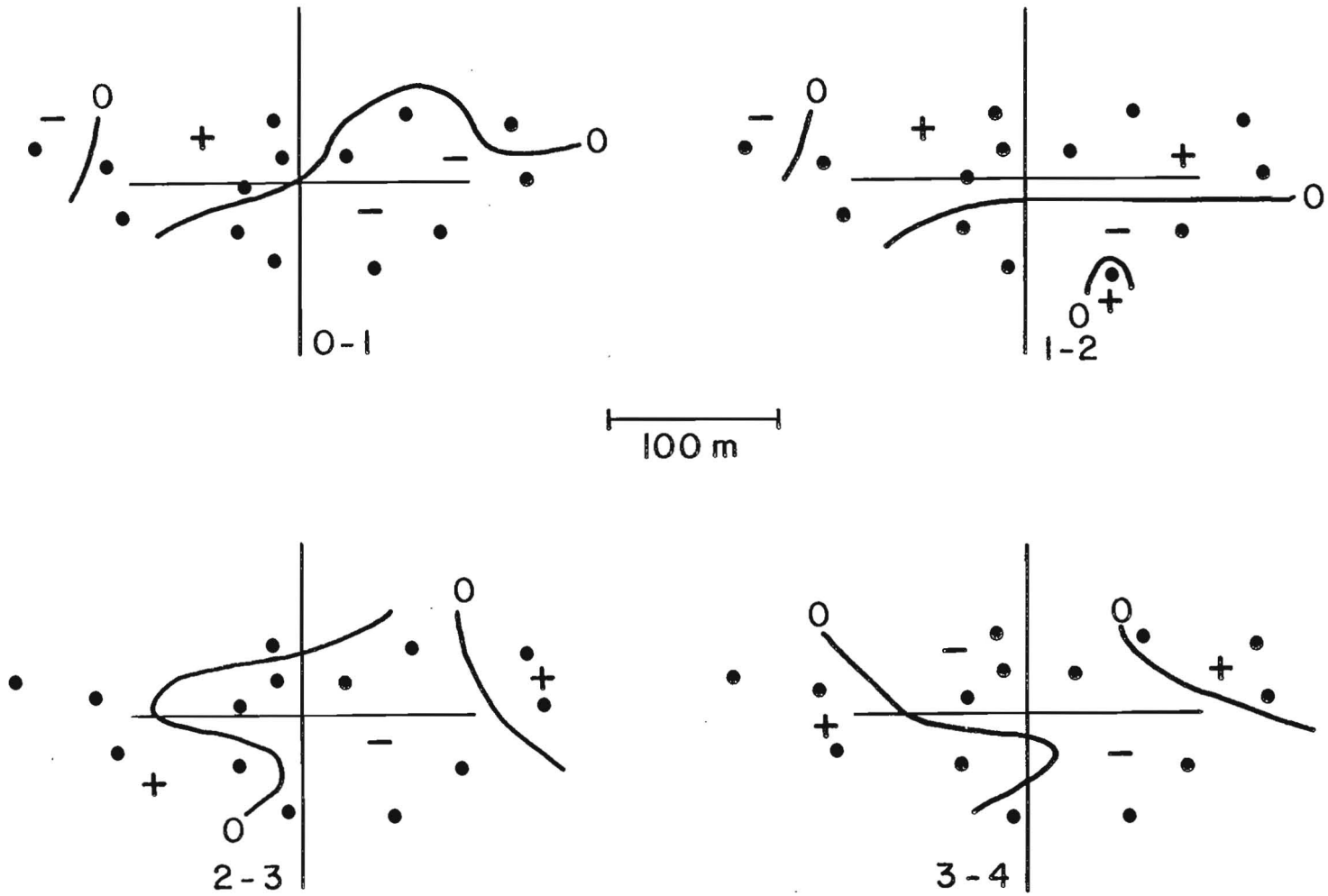

Figure 82d. Local shearing deformation rate field obtained by subclusters of 3 drogues in Experiment 12 with triad centroids indicated by solid black circles. Time intervals between which the shearing deformation rate field is calculated are indicated on each plot.

appropriate. Along this line of thought, Okubo, Ebbesmeyer and Helseth (1976a) developed methods to determine Lagrangian deformations and turbulence statistics from current followers. According to them, the drogue positions, $x_i(t)$, $y_i(t)$, at t can be expanded in terms of the initial positions, i.e., the Lagrangian coordinates (a_i, b_i) as

$$x_i(\underset{\sim}{a}_i, t) = x(\bar{a}, t) + \left(\frac{\partial x}{\partial a}\right)_0 (a_i - \bar{a}) + \left(\frac{\partial x}{\partial b}\right)_0 (b_i - \bar{b}) + x_i''(\underset{\sim}{a}_i, t)$$

$$y_i(\underset{\sim}{a}_i, t) = y(\bar{a}, t) + \left(\frac{\partial y}{\partial a}\right)_0 (a_i - a) + \left(\frac{\partial y}{\partial b}\right)_0 (b_i - \bar{b}) + y_i''(\underset{\sim}{a}_i, t) \qquad (24)$$

where $\underset{\sim}{a}_i = (a_i, b_i)$; $\underset{\sim}{\bar{a}} = (\bar{a}, \bar{b})$, the initial centroid; $\left(\frac{\partial x}{\partial a}\right)_0$ etc, the Lagrangian first-order deformations at t evaluated at $\bar{a}, \bar{b}$; x_i'' and y_i'' are second-and higher-order displacements. In the above expressions (equation (24)), we assume that the first-order deformation field is uniform within the group of drogues and that the second-and higher-order (deformation) terms are considered as random. Thus this formulation is based on the same concept of the oceanic turbulence spectrum as was used in the velocity expansion formulas.

The following Lagrangian diffusivity matrix can be defined from the higher-order terms x_i'', y_i'' as

$$\begin{pmatrix} K_{11} & K_{12} \\ K_{21} & K_{22} \end{pmatrix} = \begin{pmatrix} \frac{1}{n} \sum_{i=1}^{n} x_i'' \dot{x}_i'' & \frac{1}{n} \sum_{i=1}^{n} x_i'' \dot{y}_i'' \\ \frac{1}{n} \sum_{i=1}^{n} y_i'' \dot{x}_i'' & \frac{1}{n} \sum_{i=1}^{n} y_i'' \dot{y}_i'' \end{pmatrix} \qquad (25)$$

The components of the diffusivity tensor have been evaluated according to equation (25) and are presented in Table 20. It is

TABLE 20

Observed cluster area (A_{obs}), area calculated from linear Lagrangian deformations (A_J), area calculated from deformations and diffusivity (A_{JK}), Lagrangian diffusivity matrix (K_{11}, K_{12}, K_{21}, K_{22}), for Experiments 1, 3, 4S, 4L, 5S, 5L, 6S, 6L, 8S, 8D, 10, 11, 12.

EXPERIMENT 1

t	A_{obs} (m^2)	A_J (m^2)	A_{JK} (m^2)	K_{11} ($m^2 s^{-1}$)	K_{12} ($m^2 s^{-1}$)	K_{21} ($m^2 s^{-1}$)	K_{22} ($m^2 s^{-1}$)
0	23095.9						
2	27423.3	27022.4	27519.	.6301-001	-.2953-001	-.3115-001	.1545-001
4	30046.4	28519.2	29990.	-.1609-001	-.4642-002	-.8102-002	.3384-001
6	31944.8	29945.8	31877.	.1471-002	.1601-002	.5276-002	.5071-002
8	38831.1	36053.8	38904.	.4575-001	-.1397-001	-.4156-002	.1288-001
10	40084.7	37045.7	40113.	.2661-001	-.7175-002	-.8988-002	.4201-002
12	43281.3	39767.3	43272.	.5219-001	.3465-002	.7650-002	.3815-002
14	47657.9	43487.7	47643.	.7805-001	-.4500-001	-.2828-001	.2160-001
16	55416.2	48524.9	54605.	.4798+000	-.1538+000	-.1596+000	.6216-001
18	58546.1	50997.3	57647.	.8274-001	-.5691-001	-.4467-001	.3515-001
20	61505.9	53217.0	60468.	.1150-001	-.6284-002	.1024-002	.2011-002

(t interval: 6 min)

EXPERIMENT 3

t	A_{obs} (m^2)	A_J (m^2)	A_{JK} (m^2)	K_{11} ($m^2 s^{-1}$)	K_{12} ($m^2 s^{-1}$)	K_{21} ($m^2 s^{-1}$)	K_{22} ($m^2 s^{-1}$)
0	3182.7						
2	2862.0	1268.6	1473.	-.2799-001	.3350-002	.4360-002	.1285-002
4	3049.0	1011.0	1728.	.3092-001	.4079-002	-.2273-002	.7172-002
6	3862.7	1161.4	1906.	.2574-001	-.5817-002	-.3356-002	.7591-002
8	4237.9	1069.9	2583.	.1737-001	.1440-002	.2545-003	.1050-001
10	5887.9	1402.7	3807.	.1157-001	-.7595-002	-.5074-003	.1669-001
12	5429.1	1252.3	3517.	.1651-001	.3713-002	-.1375-002	-.4807-003
14	7044.1	1588.7	4720.	.1208-001	.7044-002	.4840-002	.5005-002
16	5982.9	1290.0	3931.	.4974-002	-.1970-002	-.4347-002	.1674-001
18	7940.7	1677.7	5351.	.8176-002	.3369-002	-.1571-003	-.1242-002
20	7580.7	1563.1	5134.	.9741-002	-.3967-002	-.1014-002	.9266-002
22	10216.8	2077.7	7037.	-.3202-002	-.7475-003	-.3125-002	.3114-002
24	11743.0	2312.4	8301.	.1595-001	-.1329-002	.2352-002	-.2856-002
26	12690.0	2447.3	8924.	.5179-002	-.1192-002	-.7366-002	.2280-002
28	12619.5	2423.1	8900.	.2732-002	-.1329-002	-.2199-002	.4073-002
30	13492.7	2474.5	9536.	.6277-002	-.1974-002	.1665-001	.2565-001
32	12908.7	2260.5	9090.	.4505-002	-.2202-001	-.6351-002	.6147-001
34	14093.4	2426.9	9845.	.1144-001	-.1110-001	-.3861-002	.3112-001
36	14173.7	2416.1	9900.	.8031-002	.3935-002	.1057-001	.9891-002
38	13895.0	2304.4	9494.	.6045-002	.9093-002	-.1128-001	.3306-001
40	18453.1	3009.8	13071.	.1270-001	-.8314-002	-.7390-002	.2181-001
42	21272.6	3432.1	15161.	.7412-002	.1200-002	-.2127-001	.1844-001
44	19596.8	3099.3	13930.	-.1145-001	.1154-001	-.5657-002	.8682-002
46	24517.3	3736.8	17400.	.3490-001	-.6641-002	-.1631-001	-.4023-002
48	26887.4	3908.5	19232.	-.1697-001	.2802-001	-.1538-001	-.6520-002
50	29422.1	4114.3	21274.	.1045+000	-.6955-001	-.2389-001	.2793-001
52	33269.3	4559.9	24266.	.4536-001	-.1219-001	-.5370-002	.2347-001
54	28786.1	3902.7	20848.	.2192-001	-.2525-001	-.2764-002	.2522-001
56	25707.9	3436.4	18455.	-.1220-002	-.1163-002	-.5826-002	.1226-001
58	26634.2	3511.6	19171.	.4183-001	-.4143-001	-.2561-001	-.4430-002

(t interval: 6 min)

EXPERIMENT 3 (Continued)

t	A_{obs} (m^2)	A_J (m^2)	A_{JK} (m^2)	K_{11} ($m^2 s^{-1}$)	K_{12} ($m^2 s^{-1}$)	K_{21} ($m^2 s^{-1}$)	K_{22} ($m^2 s^{-1}$)
60	29730.2	3755.3	22059.	.1244+000	-.8182-001	-.1264+000	.1171+000
62	32863.8	4111.5	24484.	-.3503-001	.2338-001	-.5826-002	.2132-001
64	30006.8	3652.7	22391.	-.1905-001	-.5792-002	.2323-001	.1279-001
66	30337.5	3658.3	22644.	.3794-002	-.1998-001	-.3407-002	.6927-002
68	17437.2	1891.9	11699.	.8575-001	-.2328+000	-.1457+000	.3974+000
70	39485.2	2525.6	37849.	.1580+000	-.4533+000	-.4256+000	.1303+001
72	39329.6	2499.5	37691.	.5950-002	-.1955-002	-.3588-002	.6768-003
74	43199.3	2729.5	41430.	.4023-002	-.4837-003	-.4350-003	.1937-001
76	41462.6	2566.1	39171.	-.2245-002	-.4900-002	-.7449-002	.1868-001
78	46719.5	2847.1	44473.	.2301-002	-.4774-001	.1910-003	.1283-001
80	48950.3	2959.1	46748.	-.1815-003	-.3015-002	-.8218-002	.8020-002
82	50982.9	3064.3	48567.	.4388-002	-.2911-001	.6452-002	.2444-001
84	51817.0	3041.8	48704.	.2718-002	.2247-001	.1778-001	.1741+000
86	53201.1	3027.1	49686.	.7034-002	-.2376-001	-.2371-002	.4011-001
88	56203.8	3163.7	52545.	.9866-002	-.3463-001	-.3455-001	.1709+000
90	57809.9	3206.2	53524.	.6535-002	.8273-002	-.2205-001	.1149+000
92	56858.2	3032.7	52188.	.2248-002	-.6996-001	.1897-001	-.8393-001
94	66738.8	3348.9	63534.	.1400+000	-.5524+000	-.5007+000	.2044+001
96	70202.6	3453.7	66913.	.1583-001	-.1269-001	-.2909-001	.6439-001

(t interval: 6 min)

EXPERIMENT 4S

t	A_{obs} (m^2)	A_J (m^2)	A_{JK} (m^2)	K_{11} ($m^2 s^{-1}$)	K_{12} ($m^2 s^{-1}$)	K_{21} ($m^2 s^{-1}$)	K_{22} ($m^2 s^{-1}$)
0	2487.1						
2	2436.2	2387.2	2427.	.1909-002	-.2996-002	.3070-002	.4274-003
4	2509.9	2435.1	2485.	.2610-002	-.1500-002	-.1365-002	.1877-002
6	2533.2	2402.9	2483.	.6124-003	-.1663-002	.4605-002	.8733-002
8	2471.2	2294.5	2377.	.1279-002	.9259-004	.1886-002	.2908-002
10	2300.4	2104.6	2222.	-.1218-002	-.2533-002	-.1201-002	.1937-002
12	2203.9	1917.8	2063.	.2626-002	.3341-003	.2272-002	.3444-002
14	2284.9	1935.3	2101.	.2481-002	.1137-002	.8931-002	.5232-002
16	2460.7	2032.7	2245.	.2583-002	-.2834-002	-.9813-003	.4371-002

(t interval: 6 min)

EXPERIMENT 4L

t	A_{obs} (m^2)	A_J (m^2)	A_{JK} (m^2)	K_{11} ($m^2 s^{-1}$)	K_{12} ($m^2 s^{-1}$)	K_{21} ($m^2 s^{-1}$)	K_{22} ($m^2 s^{-1}$)
0	862495.0						
2	853592.5	853105.1	853487.	.1889-001	-.1523-001	-.2074-001	.5480-001
4	846623.7	845870.0	846447.	.1093-001	.1337-002	.2311-003	.1260-001
6	863150.9	862197.0	862930.	.1552-001	-.9999-002	-.3672-002	.2317-001
8	838731.1	837005.9	838219.	.2169-001	-.4204-001	-.1376-001	.7533-001
10	835444.0	832979.7	834745.	.3870-001	-.3301-001	-.2189-001	.3105-001
12	805863.9	802909.6	804991.	.1255-001	.9732-002	-.1122-001	.5895-001
14	823507.8	819690.2	822598.	.3335-001	-.2813-001	-.3381-001	.4084-001

(t interval: 6 min)

EXPERIMENT 5S

t	A_{obs} (m^2)	A_J (m^2)	A_{JK} (m^2)	K_{11} ($m^2 s^{-1}$)	K_{12} ($m^2 s^{-1}$)	K_{21} ($m^2 s^{-1}$)	K_{22} ($m^2 s^{-1}$)
0	4434.7						
2	4342.8	4212.5	4361.	.3792-002	-.9364-003	-.5197-002	.3312-002
4	4249.5	4061.8	4259.	.2448-002	-.6437-003	.2970-003	.3003-002
6	4656.1	4387.5	4661.	.1896-002	.2178-002	.5954-003	.3706-002
8	5013.2	4711.9	5013.	-.8750-003	.1834-003	-.3222-003	.5711-003
10	5422.0	5040.1	5441.	.3004-002	.4995-002	.1126-002	.2150-002
12	5372.1	4944.5	5378.	-.2067-003	.4326-004	.2562-002	.2422-002
14	6302.2	5770.0	6300.	.7010-004	.2054-003	-.6442-003	-.1991-003
16	6976.3	6331.0	6946.	.9812-003	-.3708-002	-.2479-003	.5752-002

(t interval: 6 min)

EXPERIMENT 5L

t	A_{obs} (m^2)	A_J (m^2)	A_{JK} (m^2)	K_{11} ($m^2 s^{-1}$)	K_{12} ($m^2 s^{-1}$)	K_{21} ($m^2 s^{-1}$)	K_{22} ($m^2 s^{-1}$)
0	705562.4						
2	706556.4	706345.4	706492.	.1562-001	.9054-003	.7296-002	-.5789-002
4	709546.8	709020.2	709413.	.3100-001	-.3491-001	-.9218-002	.1357-001
6	721509.5	720608.0	721326.	.2673-001	-.1620-001	-.4511-001	.2881-001
8	735703.6	734696.0	735518.	.1752-003	-.4142-002	-.1290-002	.3787-002
10	749219.1	748124.1	749024.	.1429-002	.3272-002	.1725-002	.1078-001
12	768647.4	767449.8	768444.	.6908-002	-.4673-002	-.1197-001	.1546-001
14	783011.6	781657.5	782791.	-.1760-002	-.4525-002	.7534-002	.6578-002
16	796351.0	794859.3	796111.	.2152-002	.7506-002	-.3527-002	.6851-002

(t interval: 6 min)

EXPERIMENT 6S

t	A_{obs} (m^2)	A_J (m^2)	A_{JK} (m^2)	K_{11} ($m^2 s^{-1}$)	K_{12} ($m^2 s^{-1}$)	K_{21} ($m^2 s^{-1}$)	K_{22} ($m^2 s^{-1}$)
0	3570.4						
2	4220.9	4133.1	4260.	.4154-002	.2586-003	-.1984-002	-.2311-002
4	5038.4	4785.8	5152.	.5456-002	.4074-002	.4899-002	.8652-002
6	5404.5	4998.1	5497.	.1412-001	-.1084-002	-.2491-003	.1706-002

(t interval: 6 min)

EXPERIMENT 6L

t	A_{obs} (m^2)	A_J (m^2)	A_{JK} (m^2)	K_{11} ($m^2 s^{-1}$)	K_{12} ($m^2 s^{-1}$)	K_{21} ($m^2 s^{-1}$)	K_{22} ($m^2 s^{-1}$)
0	237145.0						
2	250265.2	250035.5	250240.	.3976-002	.1635-001	.9486-002	.9835-002
4	260364.2	260003.0	260346.	.7078-002	.4335-002	-.2378-002	-.9141-003
6	258821.2	258343.4	258752.	.9004-003	-.3733-002	-.3554-002	.1326-002

(t interval: 6 min)

EXPERIMENT 8S

t	A_{obs} (m^2)	A_J (m^2)	A_{JK} (m^2)	K_{11} ($m^2 s^{-1}$)	K_{12} ($m^2 s^{-1}$)	K_{21} ($m^2 s^{-1}$)	K_{22} ($m^2 s^{-1}$)
0	53170.1						
2	53064.3	52849.7	52998.	.1317-001	-.2555-002	.1332-001	.2415-002
4	52890.9	52598.6	52804.	.5953-002	-.9445-003	.1525-002	-.2649-002
6	51336.1	50862.0	51144.	.9833-002	.1633-001	.7758-003	.1040-001
8	53297.2	52746.2	53076.	.1793-002	.3455-002	.2406-002	.7986-003
10	50424.8	49859.2	50215.	.4024-002	.1165-002	.2697-002	-.3399-003

(t interval: 6 min)

EXPERIMENT 8D

t	A_{obs} (m^2)	A_J (m^2)	A_{JK} (m^2)	K_{11} ($m^2 s^{-1}$)	K_{12} ($m^2 s^{-1}$)	K_{21} ($m^2 s^{-1}$)	K_{22} ($m^2 s^{-1}$)
0	23369.0						
2	24888.3	23910.8	24739.	.2811-001	-.3271-001	-.6092-001	.2901-001
4	30759.1	28062.7	31860.	.1918-001	-.2113-001	.3767-003	.2613-001
6	30709.9	27720.7	31707.	.2832-001	-.2017-001	-.3487-001	.2118-001
8	33125.2	29290.4	34169.	.3921-001	-.2865-001	-.4805-001	.3742-001
10	38274.9	33360.7	39572.	.2109-001	-.1970-001	.1480-001	.3497-001
12	44082.8	38250.0	45534.	.3605-001	-.2900-002	-.1485-001	.8227-002

(t interval: 6 min)

EXPERIMENT 10

t	A_{obs} (m^2)	A_J (m^2)	A_{JK} (m^2)	K_{11} ($m^2 s^{-1}$)	K_{12} ($m^2 s^{-1}$)	K_{21} ($m^2 s^{-1}$)	K_{22} ($m^2 s^{-1}$)
0	8404.9						
2	11219.5	10981.7	11386.	.2508-001	.3377-002	-.6322-003	.2968-002
4	13963.6	13381.3	14304.	.8369-002	.7000-002	.5114-002	.1039-001
6	16550.6	15775.5	16982.	.3480-002	.1297-002	-.5729-003	.2270-002
8	18625.2	17618.2	19131.	.9120-002	.8459-003	.1831-002	.2934-002
10	19792.7	18615.4	20334.	.4422-002	.1330-002	.2091-002	.9542-002
12	20539.7	19058.5	21096.	.4360-002	-.1511-002	-.6196-002	.2545-002
14	20456.6	18856.7	20973.	.1045-001	-.8929-002	-.6291-002	.7540-002
16	18970.5	17347.0	19357.	.1381-001	-.4847-002	-.7169-002	.2752-002
18	20166.7	18302.7	20602.	.5796-002	-.4699-002	-.4376-002	.4652-002
20	20070.2	18119.7	20474.	.3804-002	-.2598-003	-.4244-003	.3333-002
22	20346.5	18193.7	20736.	.6693-002	-.3450-002	-.1901-002	.1027-001
24	20359.9	17945.4	20701.	-.1904-002	.1155-002	-.2833-003	.8188-002
26	20596.7	17792.5	20891.	.4790-002	.2208-002	-.5471-002	.4229-002
28	18791.0	15922.0	18887.	.2967-003	-.4378-002	-.1218-003	.1456-001
30	19211.1	15792.3	19126.	.9441-002	-.1752-002	-.4765-002	.1097-001

(t interval: 10 min)

EXPERIMENT 11

t	A_{obs} (m^2)	A_J (m^2)	A_{JK} (m^2)	K_{11} ($m^2 s^{-1}$)	K_{12} ($m^2 s^{-1}$)	K_{21} ($m^2 s^{-1}$)	K_{22} ($m^2 s^{-1}$)
0	5033.3						
2	6415.8	6029.0	6549.	.5031-002	.1728-002	-.5606-004	.1332-001
4	8463.1	7714.2	8806.	.1321-001	-.3634-002	-.2123-002	.6075-002
6	10558.9	9451.1	11094.	.6152-002	.4125-002	.5882-002	.1039-001
8	13613.1	12045.6	14423.	.3940-002	-.1971-002	.3267-002	.5012-002
10	15916.2	13915.8	16926.	.6686-002	-.2678-002	-.4408-002	.1110-001
12	17420.8	15173.2	18524.	.1625-002	.7038-003	-.8010-003	.2924-002
14	19260.9	16712.3	20481.	.1375-002	.1619-003	-.2989-004	.2909-002
16	19870.8	17091.1	21044.	-.2778-003	.1306-002	.2404-002	.5222-002
18	21677.7	18476.4	23042.	.4316-002	.1484-002	-.1776-002	.5291-002
20	22053.9	18712.6	23422.	.3104-002	-.6124-003	-.3729-003	.8193-002
22	24572.2	20750.7	26122.	.3416-002	-.1487-002	-.3276-002	.1201-001
24	25719.1	21581.4	27338.	.4933-002	-.5232-002	-.6535-002	.1447-001
26	27149.1	22686.7	28865.	.2922-002	-.8318-003	.1738-002	.9934-002
28	28534.4	23744.6	30332.	.2933-002	.2951-002	.2607-002	.1026-001
30	29765.6	24688.8	31631.	.3744-002	.1960-002	.1076-002	.4332-002
32	32317.2	26720.8	34353.	.3737-002	.1358-002	.1374-002	.5400-002
34	35825.8	29538.3	38092.	.3415-002	.2999-002	.2423-003	.5955-002

(t interval: 10 min)

EXPERIMENT 12

t	A_{obs} (m^2)	A_J (m^2)	A_{JK} (m^2)	K_{11} ($m^2 s^{-1}$)	K_{12} ($m^2 s^{-1}$)	K_{21} ($m^2 s^{-1}$)	K_{22} ($m^2 s^{-1}$)
0	42609.9						
2	51073.9	50291.2	51396.	.1446-001	-.5934-002	-.5026-002	.2400-001
4	60663.1	59416.4	61175.	.2321-001	-.7322-002	.2250-002	.1033-001
6	70217.6	68458.2	70945.	.9315-002	-.4990-002	-.6468-002	.1521-001
8	77342.3	75167.3	78213.	.1772-001	.3872-002	.8146-003	.1035-001
10	85490.6	82758.0	86528.	.1857-001	.1103-001	.7474-002	.1013-001
12	99203.5	95674.1	100536.	.1614-001	.1004-001	.8134-002	.1717-001
14	111220.3	106823.0	112790.	.1283-001	.4454-002	.7396-002	.1943-001
16	117106.1	111989.1	118769.	.1800-001	.1016-001	.1564-001	.1431-001

(t interval: 10 min)

seen that K_{11} and K_{22} components are usually positive as required for diffusivity, while the K_{12} and K_{21} components fluctuate above and below zero. The values of K_{11} and K_{22} are much smaller than those of the gross diffusivities (K_x,K_y) simply because K_{11} and K_{22} represent the small-scale (genuine) diffusivity.

If the advection-diffusion equation is written in a Lagrangian coordinate system then its solution yields the following expressions for the three primary characteristics of the cluster dispersion (Okubo *et al.*, 1976b):

Variance along the major principal axis:

$$\sigma_X^2(t) = B_1+B_3 + [(B_3-B_1)^2 + 4B_2^2]^{\frac{1}{2}}, \tag{26}$$

Variance along the minor principal axis:

$$\sigma_Y^2(t) = B_1+B_3 - [(B_3-B_1)^2 + 4B_2^2]^{\frac{1}{2}}, \text{ and} \tag{27}$$

Orientation of the principal axes:

$$\theta(t) = \tfrac{1}{2} \tan^{-1}[2B_2(B_3-B_1)^{-1}]. \tag{28}$$

where B_i are expressed in terms of initial variances, initial correlation coefficient of drogue positions, Lagrangian deformations, and Lagrangian diffusivities (Okubo *et al.* (1976b)).

The drogue cluster area, A, can be calculated from σ_X^2 and σ_Y^2 also using the formula $A = 4\pi\sigma_X\sigma_Y$. In Table 20[#] we also show the cluster area thus calculated (A_{JK}), the area actually observed (A_{obs}), and the area calculated using only the deformations having neglected the diffusivities (A_J). Clearly the deformations alone give reasonable values but consistently underestimate area. The inclusion of the diffusivity improves the area estimate.

[#] In Table 20 A_J and A_{JK} were calculated from $A = 4\pi\sigma_X\sigma_Y$ using equations (26) and (27); A_{obs} is also calculated from $A = 4\pi\sigma_X\sigma_Y$ but using measured valus of σ_X and σ_Y from the drogue clusters.

Aerial Photography

These are approximately 240 separate exposures for 22, 25 and 26 July, 1980 that are available for analysis. On 24 July, 1980 the scheduled flights were flown but no photographs resulted, presumably due to defective film. Approximately 25 composites were constructed from the prints; six are shown in Figures 83 through 85 for illustration purposes. Quantitatively, the plumes appear to spread linearly with downstream distance, at least for travel times less than several hours. However, the relationship between the visible boundary and the cross-plume standard deviation, σ_y, should not be linear throughout the plume, at least for a plume that is laterally Gaussian. For this simple case, it can be shown that where the peak concentration is greater by a factor of e than the half-width of the visible boundary, the plume width will be greater than σ_y and where it is less than e, the visible boundary will be less than σ_y. We intend to investigate this relationship in more detail at a later time.

Qualitatively, Figures 83 through 85 show the complex lateral and longitudinal structure of the plumes which, of course, only reflects the complicated processes which produce them. Featherlike striations aligned in the direction of the wind can be seen, apparently due to Langmuir cells. The effect of the larger scale eddies in producing meandering can be seen by comparing the two photographs for 26 July, 1980. In the upper left hand corner of the composite for 1040, 25 July, 1980, a cluster of eight drogues

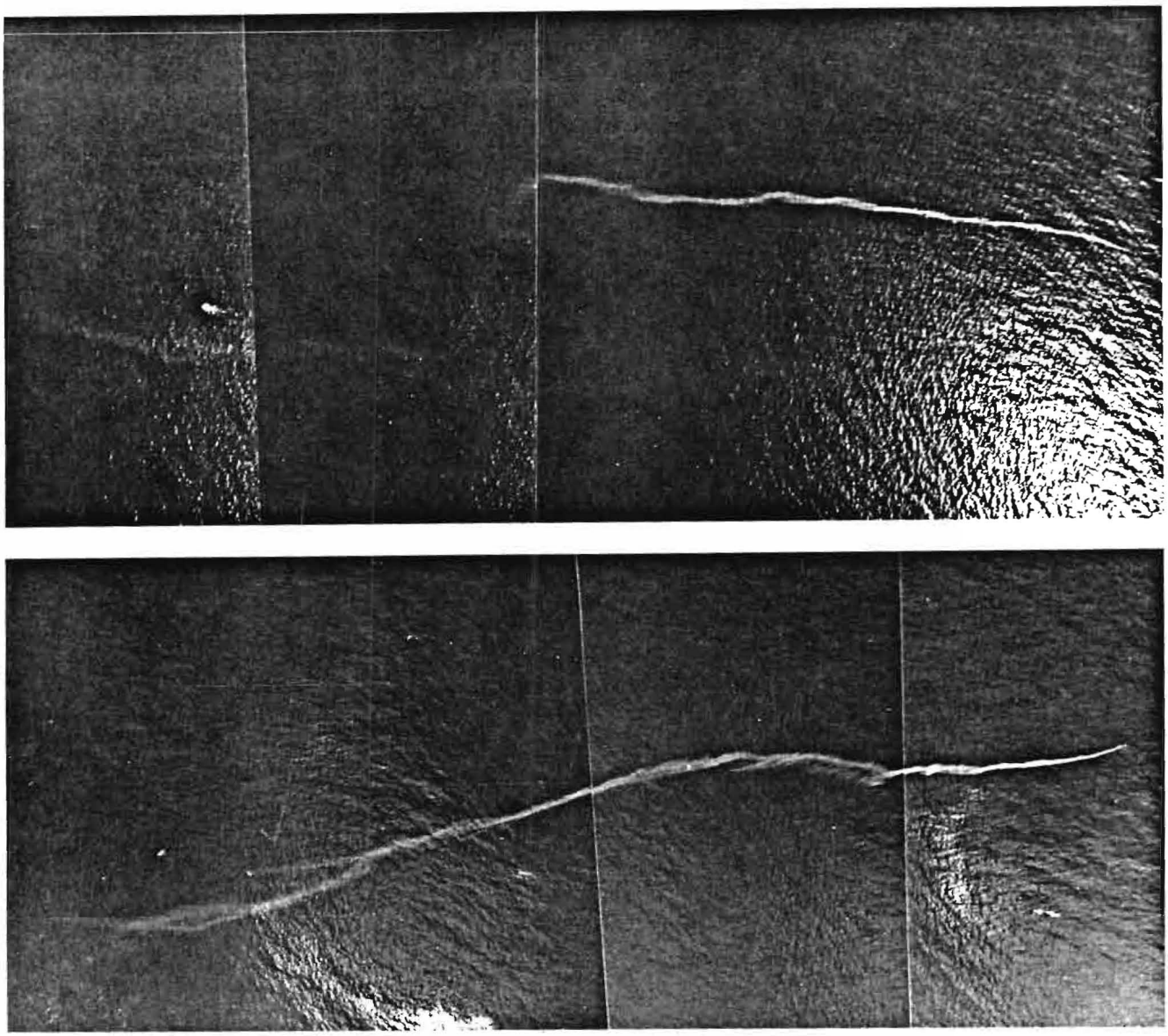

Figure 83. Aerial photographs of dye plume at 0945 (upper) and at 1030 (lower) on July 22, 1980. Altitude = 3000 feet.

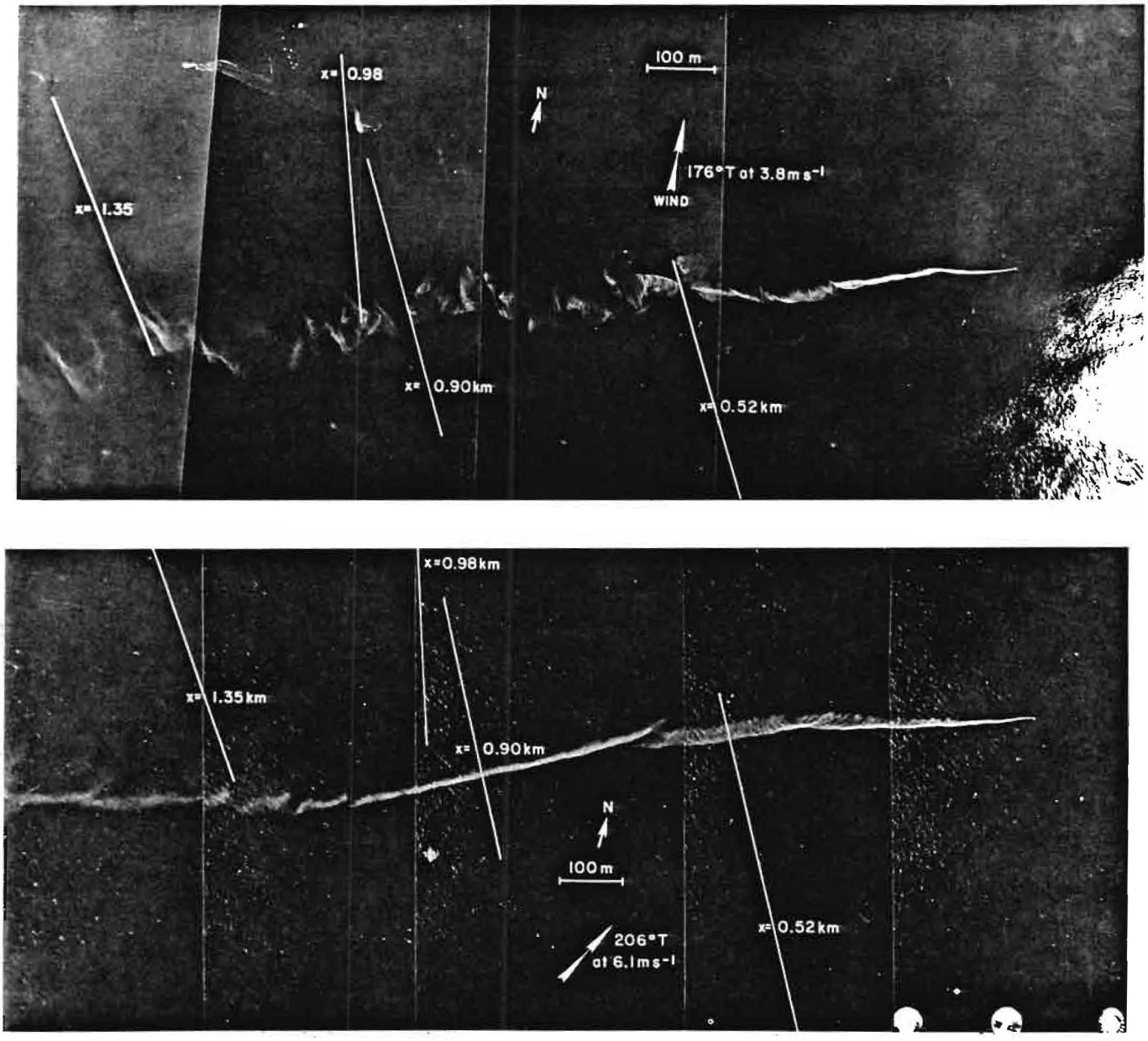

Figure 84. Aerial photographs of dye plume at 1040 and an altitude of 1850 feet (upper) and at 1618 and an altitude of 2000 feet (lower) on July 25, 1980. Note the cluster of 8 drogues in the upper left hand corner of the 1040 photograph.

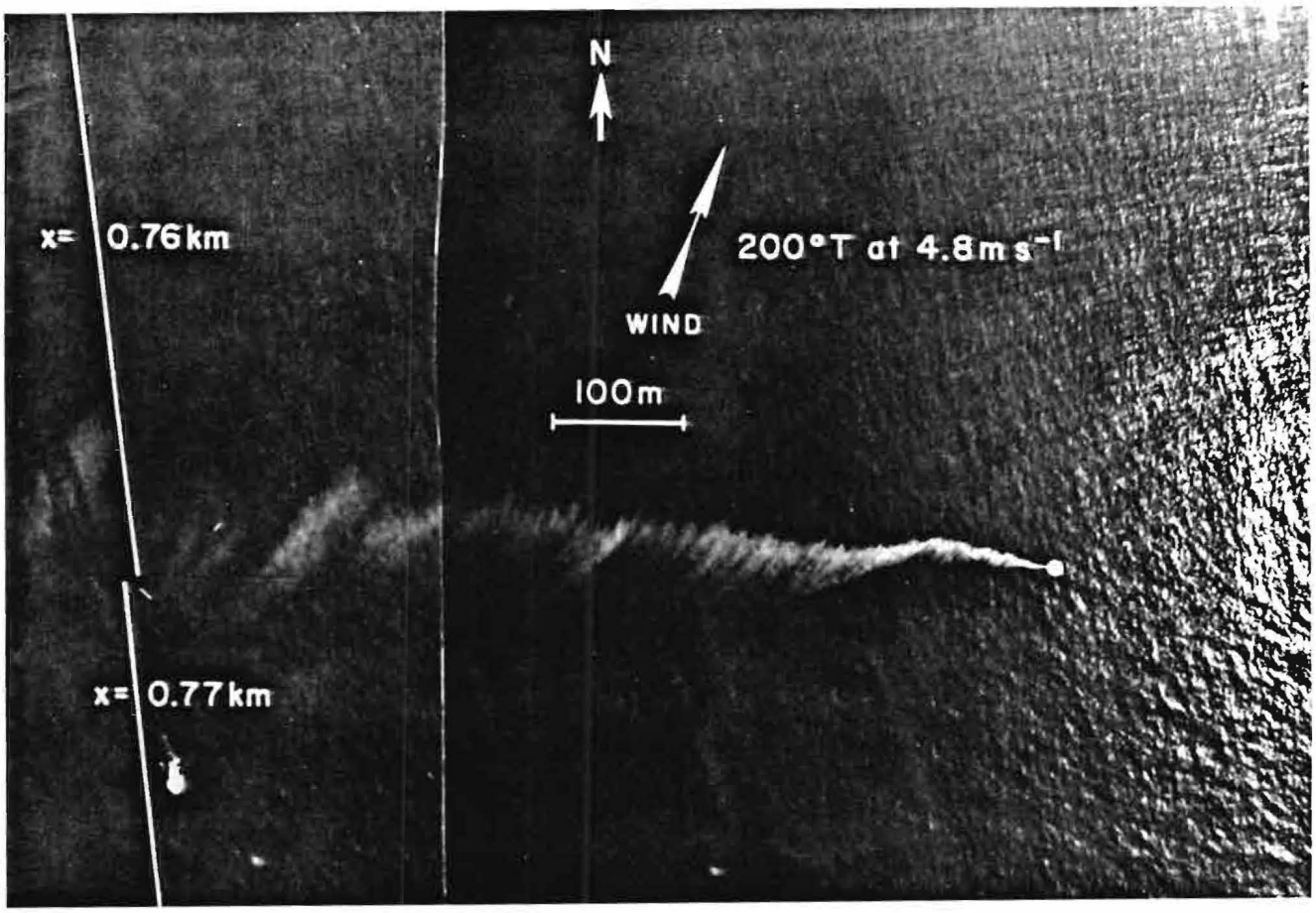

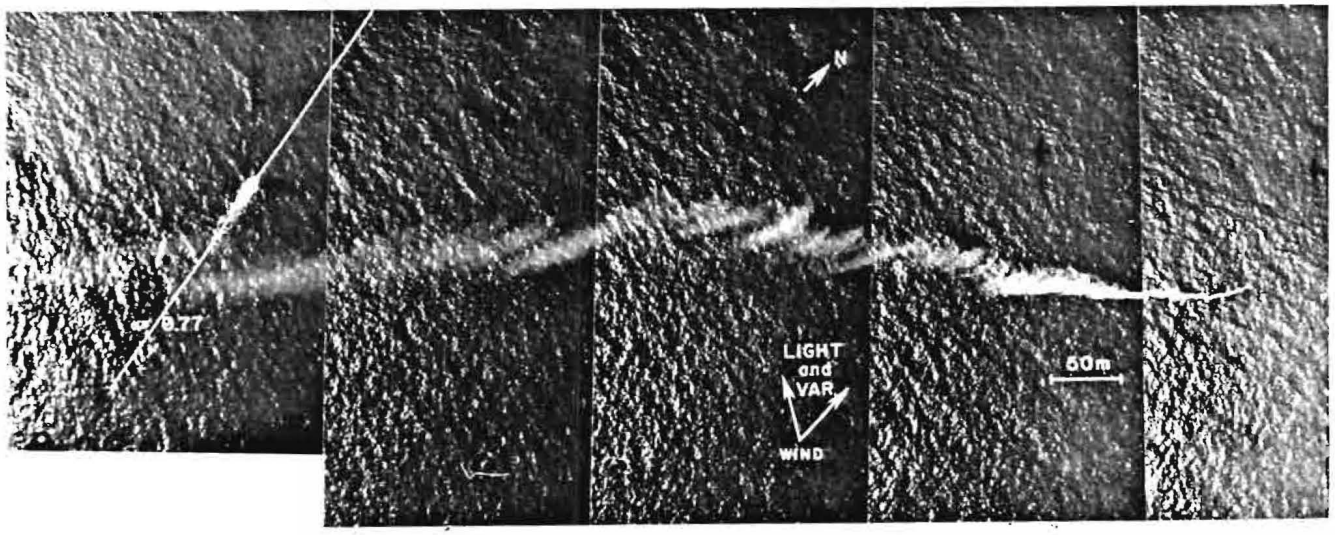

Figure 85. Aerial photographs of the dye plume at 1003 and an altitude of 2000 feet (upper) and at 1405 and an altitude of 1000 feet (lower) on July 26, 1980.

can be seen (Drogue Experiment 4, Table 5). Under the microscope, the current followers at 10 feet (3.05 m) can be seen. This composite clearly shows the complicated structure responsible for the variation in the variance of consecutive crossings at the same section.

A detailed quantitative analysis of representative portions of the photograph negatives has been initiated. This analysis, based on scanning the negatives with a scanning microdensitometer, has two objectives. The first objective is to provide details of the concentration field by means of a correlation analysis between the optical densities obtained from the densitometer and the *in situ* dye concentrations obtained from the fluorometers. The second objective, once the first objective is achieved, will be to calculate detailed statistics of the scale dependence (eddy size) of the variance of the concentration field by means of a FFT technique which transforms the 2-dimensional image into wave number space.

A portion of one photograph has already been scanned on the microdensitometer and has provided 140,000 measures of the optical density for a rectangle 280 m long (down-plume) by 100 m wide (cross-plume). The data was initially stored in a microcomputer connected to the densitometer and has been transmitted to the main computer (UNIVAC 1100) for processing. Final processing to achieve the aforementioned objectives now awaits acquisition of the necessary software for processing digitized image data. The software package is known as the IBIS/VICAR software system and is obtainable on a lease basis (10 years) from the University of Georgia. It is

anticipated that funds will be available for this purpose in the near future. Results of the analysis will be the subject of a separate report.

ANALYSIS AND DISCUSSION OF RESULTS

Preface

The peak or maximum concentration in a plume or patch of tracer is often used as a measure of diffusion. However, care must be exercised in doing so. The observation of the maximum concentration involves not only a great deal of uncertainty but also the peak concentration can be sensitive to the loss of dye tracer due to adsorption on suspended particles, photochemical decay, etc. On the other hand, the variance of particle displacement is certainly a more suitable measure of the spread of the substance. So long as dye losses obey the law of the first-order kinetics, the value of the variance computed from the data uncorrected for losses will be the same as that from corrected data. As a result, the variance is one of the most stable parameters of diffusion. From the relationship between the variance, σ^2, and the time of diffusion, t, an apparent diffusivity, K_a, can be computed,

$K_a = \frac{1}{2} \sigma^2/t$ for one-dimensional case, and

$K_a = \frac{1}{4} \sigma^2/t$ for two-dimensional radially symmetric patch (Okubo (1971))

The variance of particle displacement is also considered to be a most convenient characteristic in the theory of turbulent diffusion. Thus Taylor (1921) formulated the variance in terms of the velocity autocorrelation of particle movement.

In addition, when we speak of oceanic diffusion it is crucial to make a distinction between the diffusion from an instantaneous source and the diffusion from a continuous (fixed) source.

For an instantaneous release the diffusion is classified as *relative diffusion*, in which we are concerned with the spread of substance about the centroid of particles as the patch moves around. In other words only eddies whose scales are equal to less than the patch size and whose periods are equal to or less than the time of diffusion, contribute appreciably to the relative diffusion, while eddies whose scales are larger than the patch should be regarded as a mean flow and thus they contribute little to the relative diffusion. As a patch spreads, the division between the part of eddying motion assignable to the mean flow and the part assignable to relative diffusion tends toward larger scales. Therefore the amplitude of the mean flow tends to decrease while the rate of relative diffusion tends to increase with time.

For a continuous release, on the other hand, the diffusion is classified either as *relative* or *absolute diffusion* (Csanady (1963)), depending upon how we observe or sample the plume of substance. When our attention is focused on a meandering single plume which is observed instantaneously or for a very short duration of time, the lateral spread of the plume may be regarded as relative diffusion because the diffusion relative to the meandering center line is due primarily to smaller scale eddies. On the other hand, when we are concerned with a superposition of many meandering plumes with respect

to an absolute frame of reference, e.g., the position of the source of release or a fixed direction of mean flow, the lateral spread of substance of the overall plume may be regarded as absolute diffusion. Thus absolute diffusion contains the meandering of the center of gravity of individual plumes due to eddies larger than the scale of the plume as well as diffusion relative to the meandering center of gravity due to small scale eddies (Frenkiel (1953); Gifford (1959)).

Absolute diffusion can be studied theoretically by one-particle analysis and relative diffusion can be studied by two-particle analysis (Batchelor and Townsend (1956)). Since in principle the entire spectrum of eddies contribute to absolute diffusion, the velocity autocorrelation function of dispersing particles may be assumed to be stationary, and Taylor's theory for variance can be used as the foundation for one-particle analysis. For two-particle analysis, on the other hand, the autocorrelation function of particle velocity relative to the moving center of gravity cannot be assumed to be stationary. As a result Taylor's theory needs certain modifications if applyed to relative diffusion.

In this section we will first intercompare the time behavior of variance derived from the dye patch studies with that from drogue dispersion followed by comparisons of the drogue areas, i.e., a measure of horizontal variance, with the integrated divergence, i.e., a parameter of velocity gradients relevant to drogue dispersion obtained from current meter records. Finally we will compare the characteristics of relative diffusion observed in dye plume studies

with those derived from current meter records and velocity gradient parameters derived from current meter records and drogue trajectories.

Variances in Dye and Drogue Dispersion

Although some diffusion studies have been made to compare the results of dye diffusion with that of drogue dispersion (Ahn (1974); Ichiye *et al.* (1981); Yanagi *et al.* (1982)), none of them really achieved a proper comparison simply because in most studies the two types of diffusion experiments were not carried out at the same time and place.

In the LEDS winter experiments we attempted three sets of comparison experiments, one each on March 10, 11, and 12, 1981. Unfortunately, the March 11 dye patch sank soon after release, presumably due to a localized convergence, so no comparison is available for that day. On March 12 no drogue tracking was possible due to adverse weather conditions, although the dye study data were successfully obtained. Thus only one set of data is available for comparison, that of March 10.

There is one problem in analyzing these data. That is, the initial dimensions of the dye patch and of the drogue cluster were very different; the release of dye was more or less as a point-source, whereas the drogues were initially in the form of a cluster, i.e., a type of finite source. Therefore, a correction for the difference in initial size is necessary for a proper comparison of diffusion characteristics.

Obviously a group of drogues cannot initially occupy a point in space. Accordingly, we consider it is appropriate to adjust the dye diffusion data to the same initial size as the drogue cluster. This practice is analogous to the correction of dye study data to a point source release (Okubo (1971)).

Let σ_o^2 be the (radially symmetric) horizontal variance associated with the initial distribution of a dye patch. Then the variance σ^2 of the dye diffusion dispersing from an initial size may be given by

$$\sigma^2(t) = \sigma_o^2 + \sigma_{rc}^2(t) \tag{29}$$

where $\sigma_{rc}^2(t)$ denotes the variance of dye from an initial point source (Figure 78). For comparison σ_o^2 is taken as the initial variance of the drogue cluster.

In Figure 86 we show the time behaviors of the radially symmetric variances of dye patch and drogue cluster with the same initial variance. As expected, the dye diffuses faster than the drogues. For diffusion times ranging from 2 to 5 hours, the horizontal variance for dye is seen to be $2 \sim 5$ times the horizontal variance of drogues. The larger ratio is observed at the larger diffusion time. However, after 5 hours or so, the variance for both cases tends to approach a t^2 relation and the ratio of the two variances remains almost constant. The t^2 relation of variance suggests that the primary mechanism of dispersion of dye and drogues may be due to the combined effect of velocity shear and small-scale diffusion (Carter and Okubo (1965)).

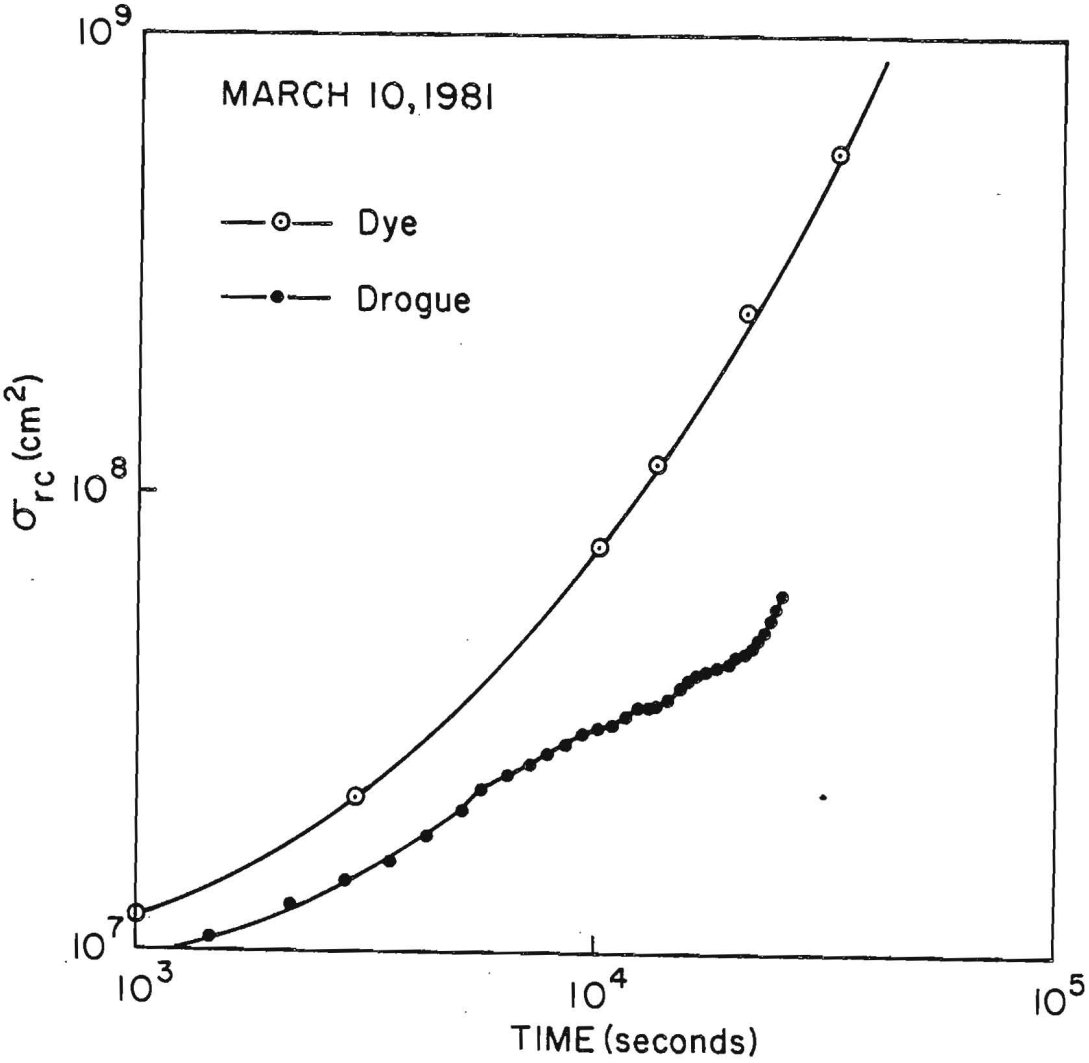

Figure 86. Time behavior of radially symmetric variance of a dye patch (March 10 release) and a drogue cluster (Experiment 11) with the same initial variance.

To quickly review the model in Carter and Okubo (1965), consider the following basic equation of shear diffusion.

$$\frac{\partial S}{\partial t} + (V_o - \Omega_y Y - \Omega_z Z)\frac{\partial S}{\partial x} = A_x \frac{\partial^2 S}{\partial x^2} + A_y \frac{\partial^2 S}{\partial y^2} + A_z \frac{\partial^2 S}{\partial z^2} \tag{30}$$

Where $S(t,x,y,z)$ represents the concentration of tracer, V_o is the mean velocity, Ω_y and Ω_z are respectively the horizontal and vertical shears, A_x, A_y and A_z are, respectively, eddy diffusivities in the x, y, and z directions with the x-axis directed in the mean flow, y-axis lateral, and z-axis vertically downward.

Solving (30) subject to an instantaneous point-source release, Carter and Okubo (1965) obtained, among others, expressions for σ_{rc}^2. Thus for small values of t, i.e., $t << t_c \equiv \{12\ A_x/(\Omega_y^2 A_y + \Omega_z^2 A_z)\}^{\frac{1}{2}}$,

$$\sigma_{rc}^2 = 2(A_x A_y)^{\frac{1}{2}} t \tag{31}$$

and for large values of t, i.e., $t >> t_c$,

$$\sigma_{rc}^2 = \left(\frac{4}{3}\Omega_y^2 A_y + \frac{1}{3}\Omega_z^2 A_y A_z\right)^{\frac{1}{2}} t^2 \tag{32}$$

The small time behavior of σ_{rc}^2 is independent of shears, while the large time behavior depends not only on eddy diffusivities but also on the horizontal and vertical shears.

Now a dye patch is subject to a shear effect due to both horizontal and vertical shears because a dye mixes both horizontally and vertically, while a drogue cluster is subject only to the horizontal shear effect because a drogue responds only to horizontal flows. As a result, the variance of a dye patch is expected to be

larger than that of a drogue cluster. Thus from (32) the ratio of the variances for large t is given by

$$\frac{\sigma^2(\text{dye})}{\sigma^2(\text{drogue})} \approx \frac{\sigma^2_{rc}(\text{dye})}{\sigma^2_{rc}(\text{drogue})} = \{(\tfrac{4}{3}\,\Omega_y^2 A_y + \tfrac{1}{3}\,\Omega_z^2 A_z)/\tfrac{4}{3}\,\Omega_y^2 A_y\}^{\frac{1}{2}}$$

$$= (1 + \tfrac{1}{4}\,\frac{\Omega_z^2}{\Omega_y^2}\,\frac{A_z}{A_y})^{\frac{1}{2}} \qquad (33)$$

From the values of the parameters (Ω_y, Ω_z, A_y, A_z) we can estimate the ratio of the variances. Typically

$$\Omega_y = 10^{-5}\ \text{sec}^{-1}$$

$$\Omega_z = 10^{-3}\ \text{sec}^{-1}$$

$$A_y = 10^3\ \text{cm}^2\ \text{sec}^{-1}$$

$$A_z = 10\ \ \text{cm}^2\ \text{sec}^{-1}$$

These values* give

$$\frac{\sigma^2(\text{dye})}{\sigma^2(\text{drogue})} = 5.1 \qquad (34)$$

Using the t^2 region of σ^2 in Figure 86 the observed ratio of the variances is obtained as

$$\frac{\sigma^2(\text{dye})}{\sigma^2(\text{drogue})} = 5.7 \qquad (35)$$

The agreement between the observed and calculated values of the variance ratio is very good.

---

*These values of the parameters yield

$$t_c = 1.1 \times 10^4\ \text{sec},$$

which justifies the use of the large time behavior of variance in equation (33).

A Comparison of Drogue Cluster Area with Integrated Divergence

The areas of drogue clusters are often used to estimate the horizontal divergence (Chew and Berberian (1971); Reed (1971); Kawai (1982)). The method is based on the intuitive relationship

$$\frac{1}{A}\frac{dA}{dt} = \frac{\partial \bar{u}}{\partial x} + \frac{\partial \bar{v}}{\partial y} \equiv \gamma \tag{36}$$

where A represents the area determined from a drogue cluster and $\bar{u}$ and $\bar{v}$ are horizontal velocities in x and y directions (069°T/339°T). Reed (1971) pointed out that some part of the change in drogue area may result from turbulence at scales smaller than the drogue separations. No quantitative estimate of the turbulence effect has been made previously. Integrating (36) we obtain

$$\frac{A(t)}{A(0)} = \exp \int_0^t \gamma \, dt' \tag{37}$$

Okubo, Ebbesmeyer and Sanderson (1983) (in preparation), using the Lagrangian advection-diffusion equation (see page 210), obtain the following reaction

$$\frac{A(t)}{A(0)} = \exp \int_0^t \gamma \, dt' [1 + \sigma_a^{-2}\sigma_b^{-2}\{2(\sigma_b^2 B_1 + \sigma_a^2 B_3) + 4B_1 B_3 - B_2^2\}^{\frac{1}{2}}] \tag{38}$$

where σ_a^2 and σ_b^2 are initial variances of drogue displacements in x and y directions and B_1, B_2, B_3 are given previously (page 210). Equation (38) provides an estimate of the turbulence effect.

Taking the logarithm of (38) and differentiating with respect to time we obtain

$$\frac{1}{A}\frac{dA}{dt} = \gamma + \tfrac{1}{2}\,\ell n[1 + \sigma_a^{-2}\sigma_b^{-2}\{2(\sigma_b^2 B_1 + \sigma_a^2 B_3) + 4B_1B_3 - B_2^2\}] \qquad (39)$$

Thus the second term on the right-hand side of (39) represents the part of the change in drogue area due to the combined action of deformations and turbulence. In practice (39) may be approximated by

$$\frac{1}{A}\frac{dA}{dt} = \gamma + \{\sigma_a^{-2}K_{11}(0) + \sigma_b^{-2}K_{22}(0)\}t \qquad (40)$$

for small values of elapsed time, $t << \sigma_a^2/K_{11}(0)$, $\sigma_b^2/K_{22}(0)$. K_{11} and K_{22} are the Lagrangian diffusivities previously defined (page 199). Typically for our experiments, $\sigma^2_{a,b} \sim 10^8$ cm^2, $K_{ii} \sim 10^2$ cm^{2}s^{-1} initially for small clusters and $\sigma^2_{a,b} \sim 10^{10}$ cm^2, $K_{ii} \sim 10^3$ cm^{2}s^{-1} for large clusters (Table 20), which gives t (critical) $\sim 10^6$ sec and 10^7 sec, respectively. This justifies the use of (37) in our experimental data. Note that in (37), A represents a Lagrangian quantity and γ represents an Eulerian quantity. Thus for proper comparison we must select data in such a way that both Lagrangian and Eulerian measurements were made in the same locality and over approximately the same time intervals.

On 11 March, 1981 (Experiment #12) a cluster of 20 drifters remained in the vicinity of our array of current meters for a few hours (see Figure 87). Also the drogues and current meters were at the same depth (15 feet). Unfortunately, however, there was a spatial scale difference in the drogue and current meter observations. The drogue cluster occupied a much larger spatial domain than the current meter array. Because the magnitudes of the velocity gradients,

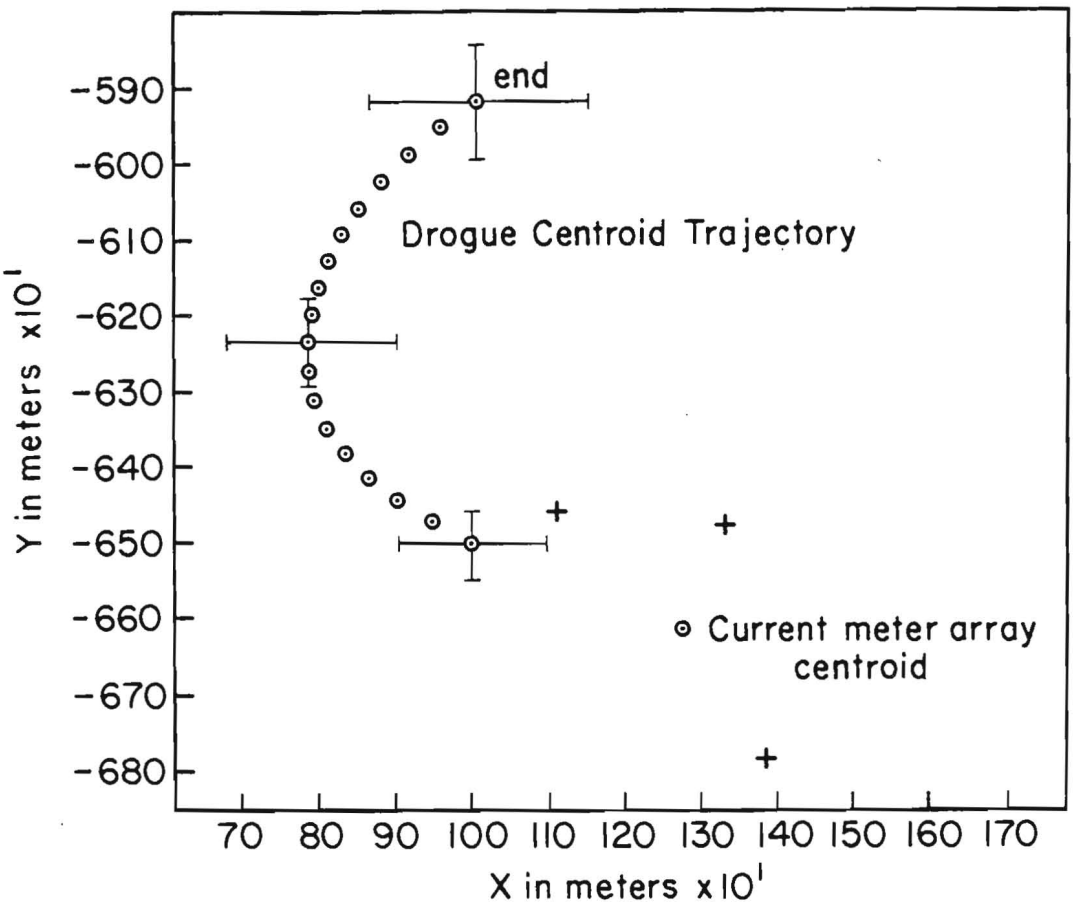

Figure 87. Relative positions of the drogue centroid trajectory (⊙) for Experiment #12 (3/11/81) and the current meter array (+).

e.g., the divergence, depends upon the length scale over which they are measured (see Figure 81), we must take into account this scale dependence of divergence in using (37).

Let

$$\gamma = \gamma\{t, A(t)\} \tag{41}$$

(41) states that divergence depends not only upon time but also upon area, a measure of spatial scales. Substituting (41) into (37) we have

$$\frac{1}{A(t)} \frac{dA(t)}{dt} = \gamma\{t, A(t)\} \tag{42}$$

It can be shown by dimensional arguments that the root-mean-square velocity gradients should be related to the rate of energy dissipation, ε, and to the length scale, L, over which the velocity gradient is measured. That is

$$\sqrt{\overline{\left(\frac{\partial v_i}{\partial x_j}\right)^2}} \sim \varepsilon^{1/3} L^{-2/3} \tag{43}$$

Equation (43) has been plotted in Figure 88 assuming that the constant of proportionality is of order unity and for $\varepsilon = 10^{-5}$ and 10^{-4} $cm^2 s^{-3}$, a range which seems reasonable.

The data from the March 1981 current meter array were available for confirmation of this relationship between rms velocity gradients and scale. Using the method of Okubo and Ebbesmeyer (1976) to calculate the velocity gradients and defining the scale, L, as the standard deviation of the x-coordinate of the current meter positions about the array's centroid, a line of slope -0.71 was obtained

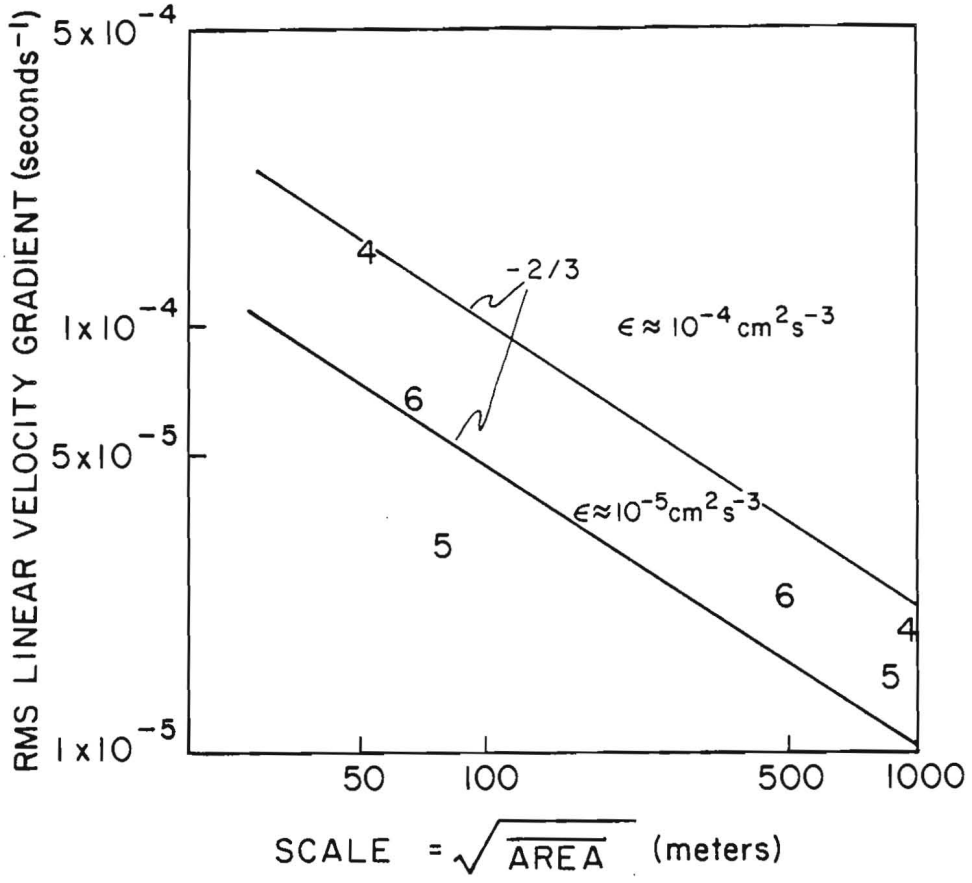

Figure 88. Root-mean-square velocity gradients as a function of the rate of energy dissipation, ε, and scale, $\sqrt{\text{Area}}$ from dimensional argument (Equation (43)). The numbers are calculated values of rms velocity gradients from drogue experiments #4, 5, and 6.

(not shown) confirming the dimensionally expected value of -0.67.

Three drifter experiments in which a small cluster of 8 drogues was surrounded by a larger cluster of 8 drogues was carried out during the July 1980 LEDS experiments (Experiments 4, 5, and 6). All drogues were set at 10 feet (3.05 m). The root mean square velocity gradients for each of these experiments is plotted in Figure 88 as a function of the length scale which is taken to be the square root of the cluster area, $A = 4\pi\sigma_x\sigma_y$. The fit to the -2/3 law is not unreasonable.

The above relation suggests that divergence is proportional to -1/3 power of the area of concern. If the area over which divergence is measured is written as A_m, then the divergence that could be expected over an area A(t) would be

$$\gamma(t,A(t)) = \gamma(t;A_m)(A(t)/A_m)^{-1/3} \tag{44}$$

Substitution of (44) into (42) gives

$$\frac{1}{A}\frac{dA}{dt} = \gamma(t;A_m)(A/A_m)^{-1/3} \tag{45}$$

Integration of (45) over time, given an initial area A_0, yields the following result.

$$A(t) = \{A_0^{1/3} + \frac{1}{3}A_m^{1/3}\int_0^t \gamma(t';A_m)dt'\}^3 \tag{46}$$

Equation (46) enables us to predict the area of a drogue cluster of initial area A_0, given the divergence measured as a function of time over an area A_m of a current meter array that is in the same vicinity as the drogue cluster.

Figure 89 shows the time behaviors of the observed cluster area ($A = 4\pi\sigma_X\sigma_Y$) and of the predicted cluster area according to (46). The area predicted from current meter measured divergence without any scale correction is also given in the figure. Clearly the scale correction improved the result and equation (46) provides a reasonable estimate of the cluster area. Thus the usefulness of a current meter array to predict horizontal dispersion of drogue clusters for short time intervals has been demonstrated.

For longer time intervals the drogue area cannot be predicted from divergence alone but will require the addition of a diffusion effect.

Velocity Gradient Estimates from Current Meters and Drogues

The results of auto spectrum and cross spectrum (coherency squared) calculations for instruments were used as a basis for estimating horizontal velocity gradients from the velocity time series provided by the moored instruments in the arrays. The spectrum and coherency estimates provided information on the frequency bands for which velocity fluctuations were spatially coherent within an array. Our objective was to compute horizontal velocity gradients for those velocity fluctuations which tended to be spatially coherent, and to avoid calculating gradients for those fluctuations which were spatially incoherent.

Consider, for example, two current velocity time series from adjacent instruments $w_1(t) = u_1(t) + iv_1(t)$

$$w_2(t) = u_2(t) + iv_2(t)$$

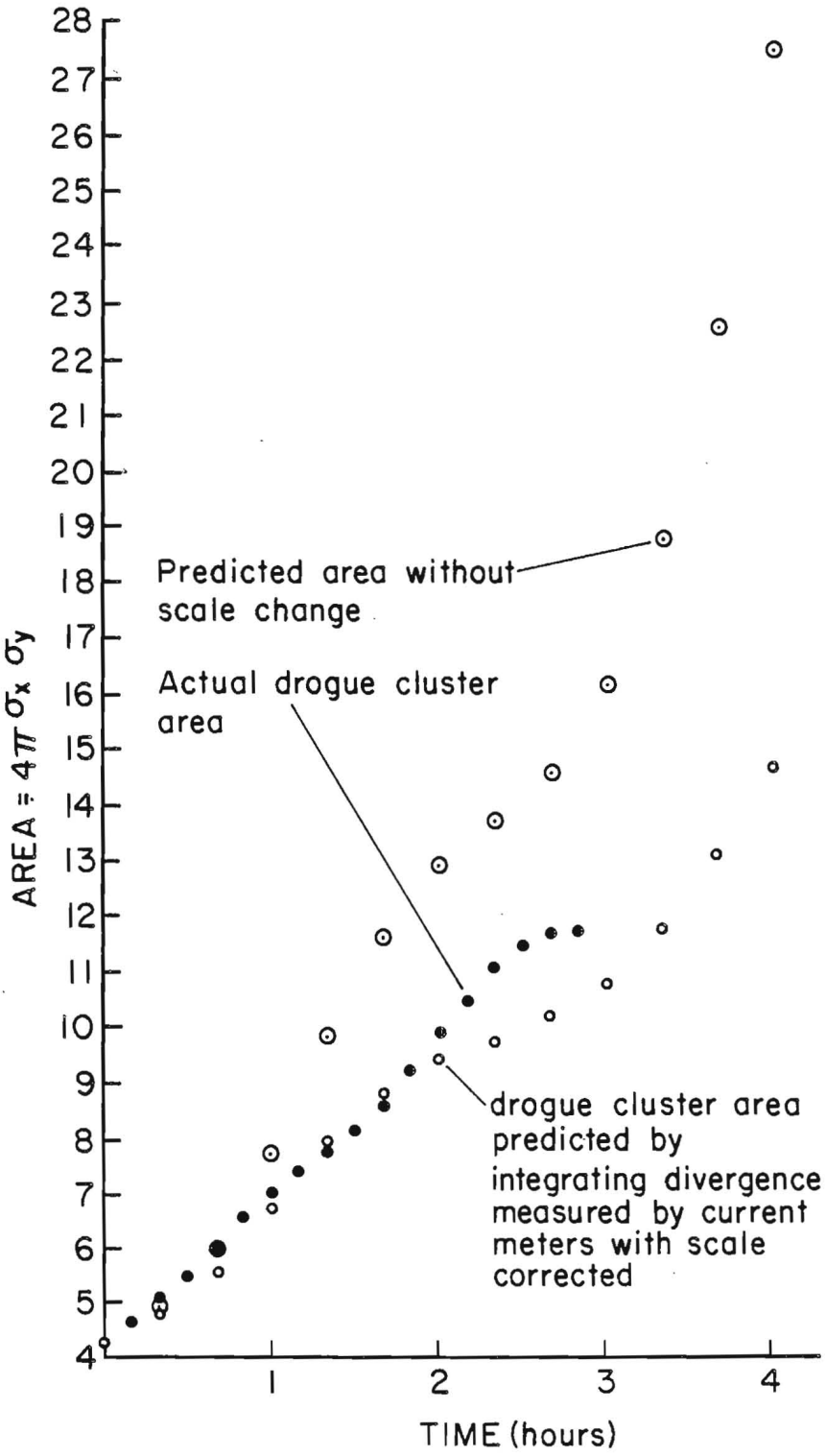

Figure 89. Comparison of time behavior of observed cluster area (●) and predicted area (o). Also shown is the predicted area without any correction for scale (⊙).

and the difference

$$w_3(t) = u_3+iv_3 = (u_1-u_2) + i(v_1-v_2).$$

The inner auto spectrum for the difference is

$$S_{w_3w_3} = (S_{u_3u_3} + S_{v_3v_3}) + i(S_{u_3v_3} - S_{v_3u_3})$$

$$= G_{u_1u_1} + G_{u_2u_2} - 2C_{u_1u_2} + G_{v_1v_1} + G_{v_2v_2} - 2C_{v_1v_2}$$

$$+ i[(C_{u_1v_1} - iQ_{u_1v_1}) - (C_{u_1v_2} - iQ_{u_1v_2}) - (C_{u_2v_1} - iQ_{u_2v_1})$$

$$+ (C_{u_2v_2} - iQ_{u_2v_2}) - (C_{v_1u_1} - iQ_{v_1u_1}) + (C_{v_1u_2} - iQ_{v_1u_2})$$

$$+ (C_{v_2u_1} - iQ_{v_2u_1}) - (C_{v_2u_2} - iQ_{v_2u_2})]$$

$$= (G_{u_1u_1} + G_{v_1v_1} + 2Q_{u_1v_1}) + (G_{u_2u_2} + G_{v_2v_2} + 2Q_{u_2v_2})$$

$$-2[(C_{u_1u_2} + C_{v_1v_2}) + (Q_{u_1v_2} + Q_{u_2v_1})]$$

$$= S_{w_1w_1} + S_{w_2w_2} - 4\mathrm{Re}(S_{w_1w_2}).$$

In the expressions above $S_{w_iw_j}$ is the inner auto cross spectrum between w_i and w_j, and $G_{u_iu_i}$, $C_{u_iv_j}$ and $Q_{u_iv_j}$ are, respectively, the regular one sided auto spectrum and the real and imaginary parts of the regular one sided cross spectrum. Remembering (Mooers (1973)) that the inner coherency squared and phase are defined by

$$\gamma^2 = \frac{|S_{w_1w_2}|^2}{S_{w_1w_1} S_{w_2w_2}}$$

$$\tan \phi = \frac{\mathrm{Im}(S_{w_1w_2})}{\mathrm{Re}(S_{w_1w_2})},$$

a more useful expression for the inner auto spectrum of the difference vector can be written as

$$S_{w_3w_3} = S_{w_1w_1} + S_{w_2w_2} - 4\gamma \cos\phi \, (S_{w_1w_1} S_{w_2w_2})^{\frac{1}{2}}.$$

This expression shows clearly the strong dependency of the inner auto spectrum for the difference vector on the coherency and phase between the two original vectors. When the coherency squared is below the significance level or the phase is $\pi/2$, the spectral density for the difference becomes very simply the sum of the density for the two original vectors. When the coherency squared is above the significance level the spectral density for the difference vector is affected by the degree of coherency and the phase.

All estimates for horizontal velocity gradients were based on groups of three current meters. For the July 1980 array (Figure 7) only three instruments were available at a given depth. For the March 1981 array (Figure 8) different groups of three instruments were used; each group provided velocity gradient information for a different horizontal scale.

For a given group of three instruments each of the four components of the horizontal velocity gradient tensor can be expressed in terms

of difference vectors calculated from the velocity vectors at the three instruments. If, for example, the three current velocity vectors are

$$w_1(t) = u_1(t) + iv_1(t)$$

$$w_2(t) = u_2(t) + iv_2(t)$$

$$w_3(t) = u_3(t) + iv_3(t),$$

the components of the velocity gradient tensor can be written as a linear combination of $w_1(t) - w_2(t)$ and $w_1(t) - w_3(t)$ or $w_2(t) - w_3(t)$. That is,

$$\frac{\partial u}{\partial x} + i\frac{\partial v}{\partial x} = a_1(w_1(t) - w_2(t)) + b_1(w_1(t) - w_3(t))$$

$$\frac{\partial u}{\partial y} + i\frac{\partial v}{\partial y} = a_2(w_1(t) - w_2(t)) + b_2(w_1(t) - w_3(t))$$

where a_1, a_2 and b_1, b_2 are constants. Extending the results presented above for the inner auto spectrum for the difference of two vectors, we have for the inner auto spectrum of $\frac{\partial u}{\partial x} + i\frac{\partial v}{\partial x}$ and $\frac{\partial u}{\partial y} + i\frac{\partial v}{\partial y}$, respectively,

$$a_1a_1(S_{w_1w_1} + S_{w_2w_2} - 2\gamma_{12}\cos\phi_{12}\,(S_{w_1w_1}S_{w_2w_2})^{\frac{1}{2}})$$

$$+ b_1b_1(S_{w_1w_1} + S_{w_3w_3} - 2\gamma_{13}\cos\phi_{13}(S_{w_1w_1}S_{w_3w_3})^{\frac{1}{2}})$$

$$+ 2a_1b_1\,\mathrm{Re}(S_{w_4w_5}), \text{ and}$$

$$a_2a_2(S_{w_1w_1} + S_{w_2w_2} - 2\gamma_{12}\cos\phi_{12}\,(S_{w_1w_1}S_{w_2w_2})^{\frac{1}{2}})$$

$$+ b_2b_2(S_{w_1w_1} + S_{w_3w_3} - 2\gamma_{13}\cos\phi_{13}\,(S_{w_1w_1}S_{w_3w_3})^{\frac{1}{2}})$$

$$+ 2a_2b_2\,\mathrm{Re}(S_{w_4w_5}).$$

In this expression the difference vectors w_4 and w_5 are defined by

$$w_4(t) = w_1(t) - w_2(t)$$

$$w_5(t) = w_1(t) - w_3(t)$$

and the real part of the inner cross spectrum can be expressed in terms of coherencies and phases γ_{13}, ϕ_{13}, γ_{12}, ϕ_{12}, γ_{23}, ϕ_{23}. In summary, the spectral characteristics of the vectors $\frac{\partial u}{\partial x} + i\frac{\partial v}{\partial x}$ and $\frac{\partial u}{\partial y} + i\frac{\partial v}{\partial y}$ can be shown to depend in the inner auto spectrum for each of the three current vectors *and* the inner coherency and phase between all possible pairs of instruments in the array.

For a given array of three instruments our objective was to calculate velocity gradients for velocity fluctuations which were *spatially coherent* over the array. Before computing velocity gradients, records were low pass filtered with the cut off frequency determined as the *lowest* frequency at which *any* of the inner coherency squared (estimates between pairs of instruments) falls and tends to remain below the significance level.

For the July 1980 experiment the inner coherency squared for instruments at 4.6 and 12.2 m shows a rather abrupt drop below the significance level for fluctuations with periods shorter than approximately 13 minutes. Coherency squared between instruments and moorings C and E tends to drop abruptly to the significance level at periods near 80 minutes; it then remains at or only slightly above the significance level up to periods of approximately 13 minutes. Velocity gradients were, therefore, computed for low pass

filtered records with filter cut off ranging from 13 to 80 minutes.

Time series of velocity gradients were plotted on stability diagrams (Okubo (1970)) in order to achieve as concise a graphical representation as possible. On this diagram the abscissa is the horizontal divergence and the ordinate is the quantity shearing deformation squared plus stretching deformation squared minus the square of the vertical component of vorticity. Diagrams for velocity gradients on successive days computed for the current records beginning on 14 July 1980 for 4.6 m depth are shown in Figures 90 through 93. Figure 93b represents a composite of the velocity gradients for the entire 13 day record. Corresponding diagrams for velocity gradients at 12.2 m depth are shown in Figures 94 through 97. The filter cut off for gradients in these figures was 80 minutes; gradients computed from records filtered at 20 and even 13 minutes show essentially the same characteristics but with relatively small amplitude short period fluctuations superposed.

Velocity gradients at 4.6 m and 12.2 m depth show significant temporal variability. The variability is characterized by apparently aperiodic events often lasting several hours. At 4.6 m depth the most common event is one characterized by divergence and strong stretching and shearing deformation. At 12.2 m depth convergent events are also common. In general, the sum of the squares of the stretching and shearing deformations exceeds the square of the vertical

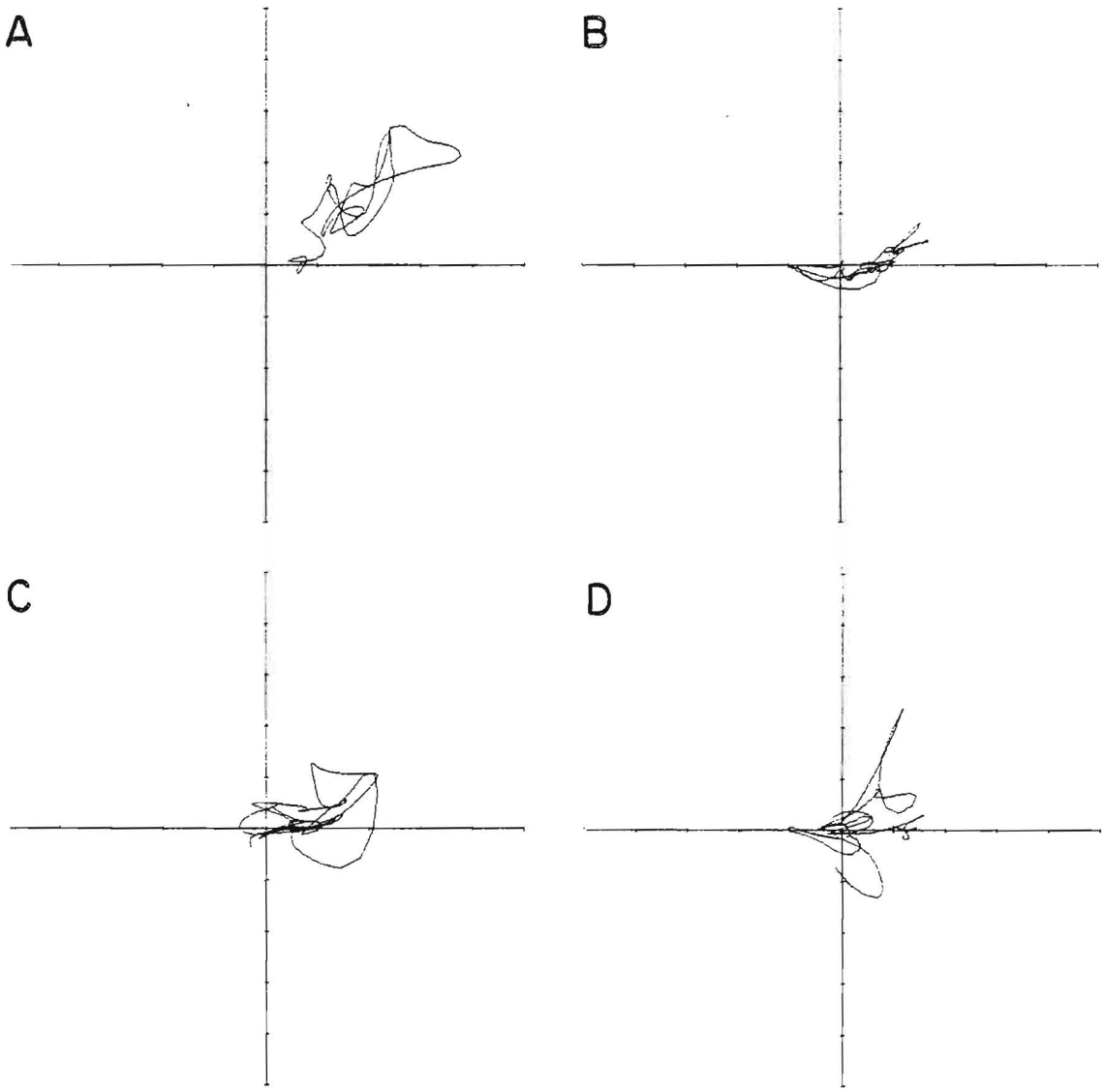

Figure 90. Stability diagrams for time series of horizontal velocity gradients estimated from current meters at 4.6 m depth on 14 July, 1980 (Figure A), 15 July, 1980 (Figure B), 16 July, 1980 (Figure C) and 17 July, 1980 (Figure D). Range of abscissa is $-1.34\times10^{-3}s^{-1}$ to $+1.34\times10^{-3}s^{-1}$; range of ordinate is $-1.39\times10^{-6}s^{-2}$ to $+1.39\times10^{-6}s^{-2}$ (see text).

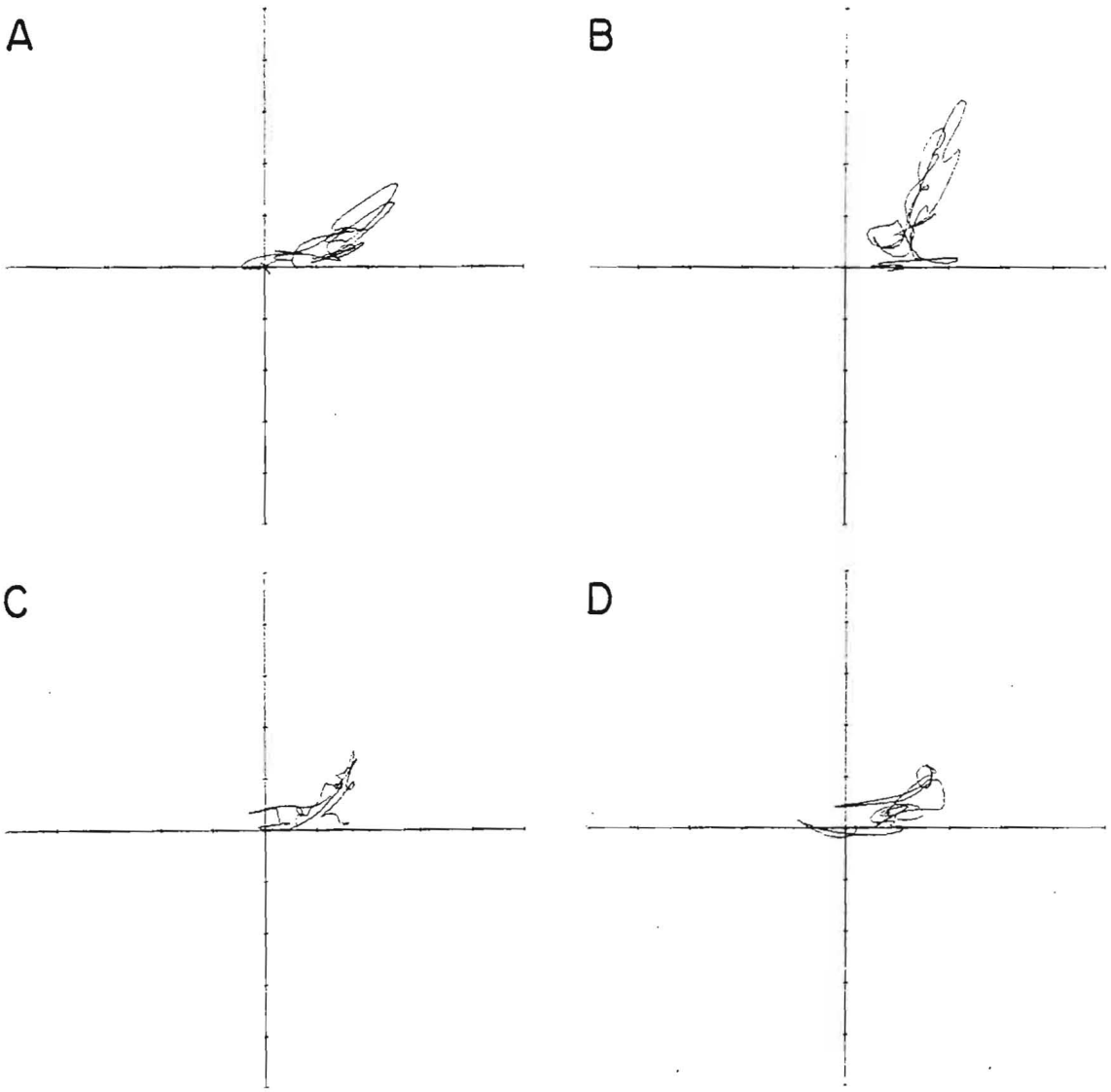

Figure 91. Stability diagrams for time series of horizontal velocity gradients estimated from current meters at 4.6 m depth on 18 July, 1980 (Figure A), 19 July, 1980 (Figure B), 20 July, 1980 (Figure C) and 21 July, 1980 (Figure D). Range of abscissa is $-1.34\times10^{-3}s^{-1}$ to $+1.34\times10^{-3}s^{-1}$; range of ordinate is $-1.39\times10^{-6}s^{-2}$ to $+1.39\times10^{-6}s^{-2}$ (see text).

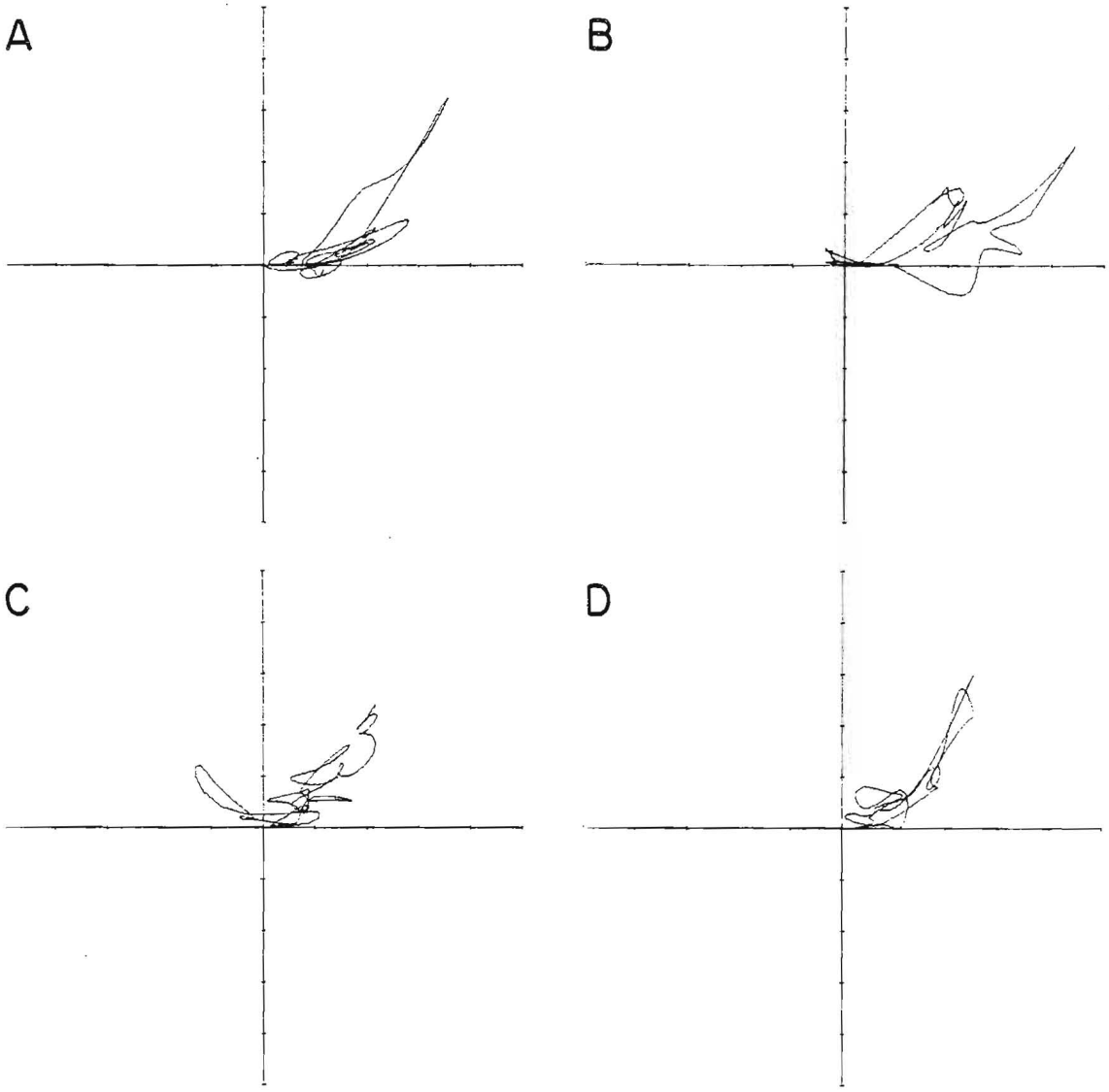

Figure 92. Stability diagrams for time series of horizontal velocity gradients estimated from current meters at 4.6 m depth on 22 July, 1980 (Figure A), 23 July, 1980 (Figure B), 24 July, 1980 (Figure C) and 25 July, 1980 (Figure D). Range of abscissa is $-1.34\times10^{-3}s^{-3}$ to $+1.34\times10^{-3}s^{-1}$; range of ordinate is $-1.39\times10^{-6}s^{-6}$ to $+1.39\times10^{-6}s^{-2}$ (see text).

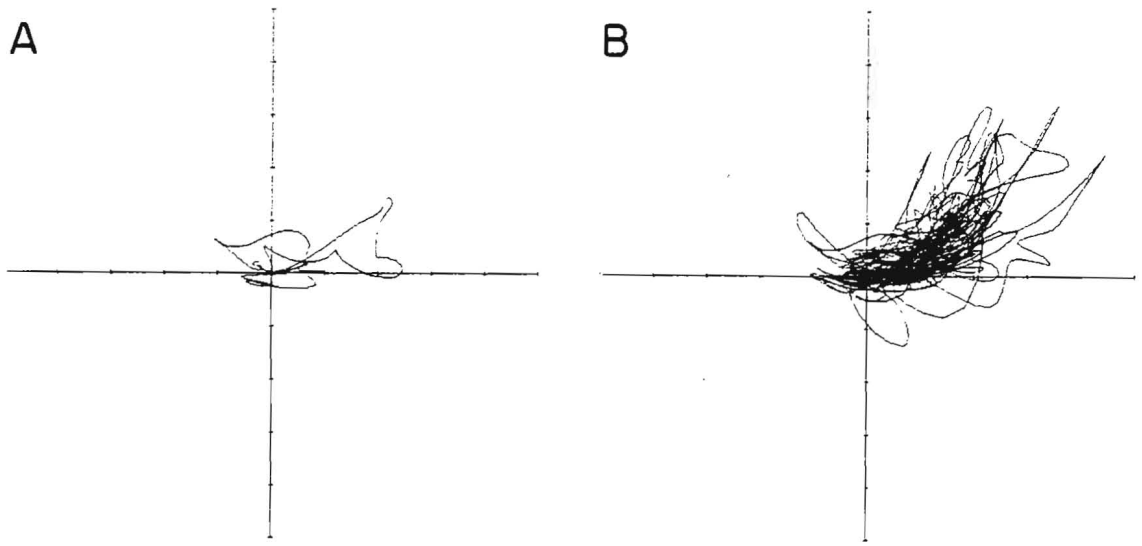

Figure 93. Stability diagrams for time series of horizontal velocity gradients estimated from current meters at 4.6 m depth on 26 July, 1980 (Figure A) and 14 July through 26 July, 1980 (Figure B). Range of abscissa is $-1.34\times10^{-3}s^{-1}$ to $+1.34\times10^{-3}s^{-1}$; range of ordinate is $-1.39\times10^{-6}s^{-2}$ to $+1.39\times10^{-6}s^{-2}$ (see text).

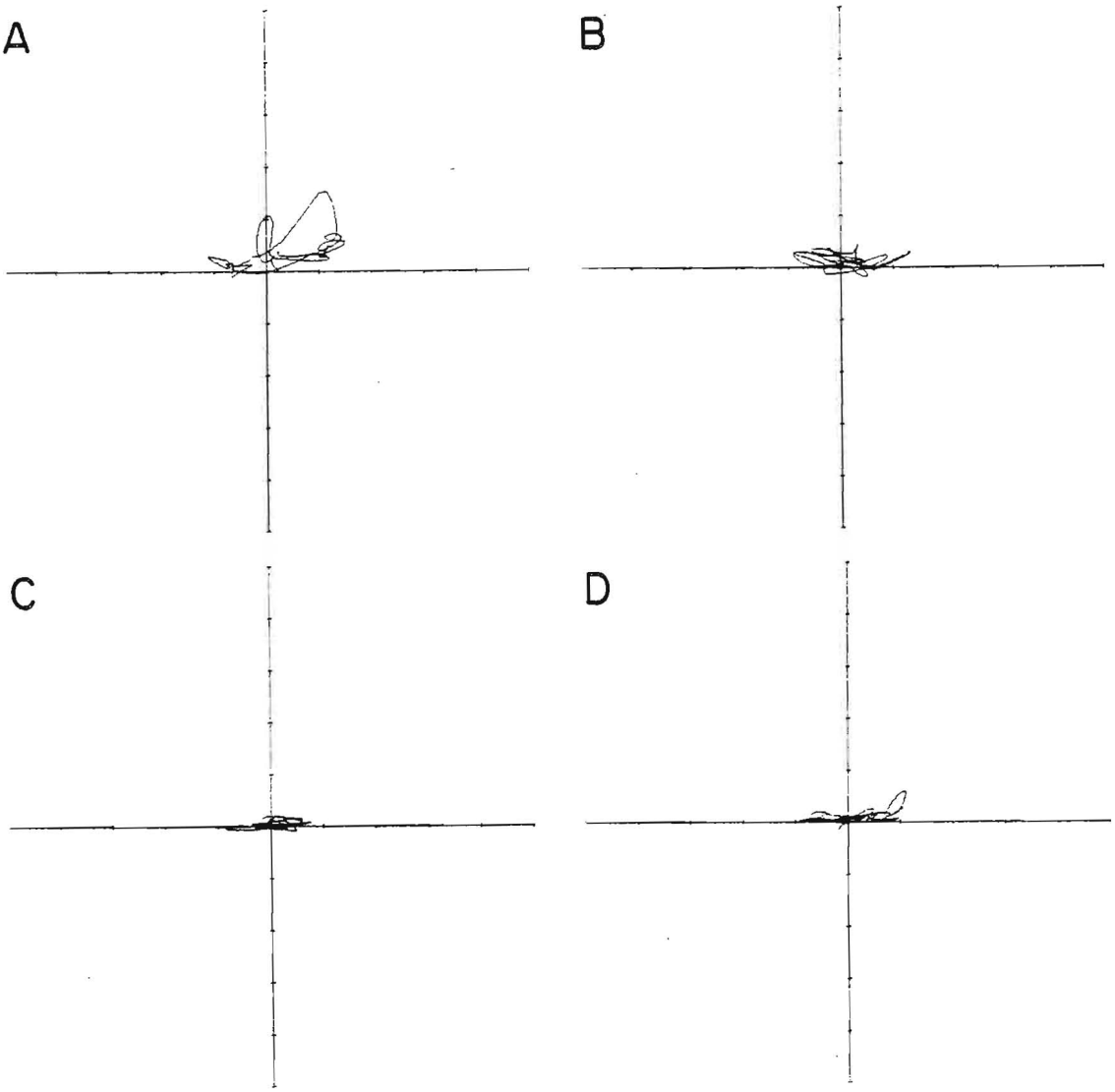

Figure 94. Stability diagrams for time series of horizontal velocity gradients estimated from current meters at 12.2 m depth on 14 July, 1980 (Figure A), 15 July, 1980 (Figure B), 16 July, 1980 (Figure C) and 17 July, 1980 (Figure D). Range of abscissa is $-1.34\times10^{-3}s^{-1}$ to $+1.34\times10^{-3}s^{-1}$; range of ordinate is $-1.39\times10^{-6}s^{-2}$ to $+1.39\times10^{-6}s^{-2}$ (see text).

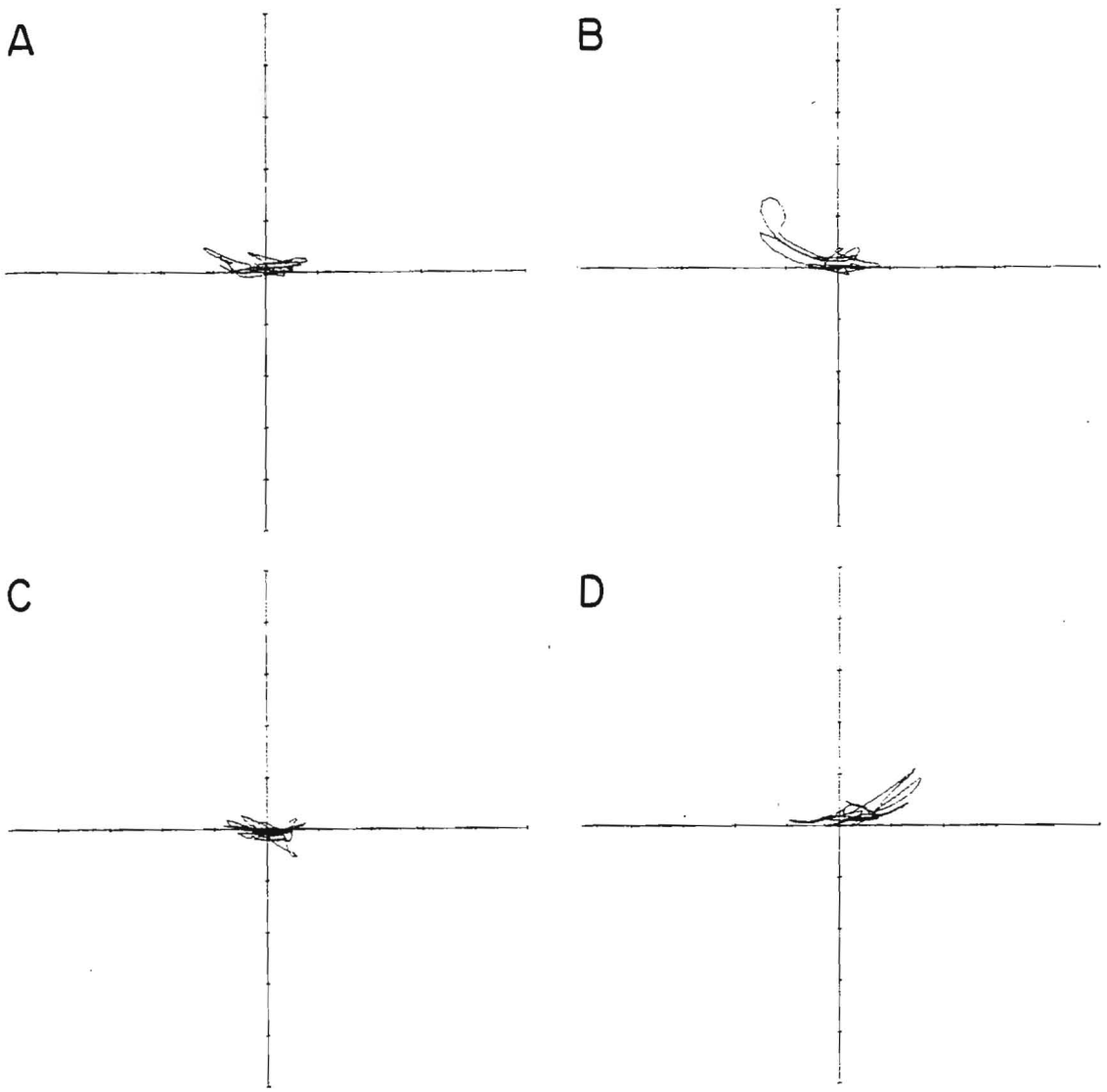

Figure 95. Stability diagrams for time series of horizontal velocity gradients estimated from current meters at 12.2 m depth on 18 July, 1980 (Figure A), 19 July, 1980 (Figure B), 20 July, 1980 (Figure C) and 21 July, 1980 (Figure D). Rate of abscissa is $-1.34\times10^{-3}s^{-1}$ to $+1.34\times10^{-3}s^{-1}$; rate of ordinate is $-1.34\times10^{-6}s^{-2}$ to $+1.39\times10^{-6}s^{-2}$ (see text).

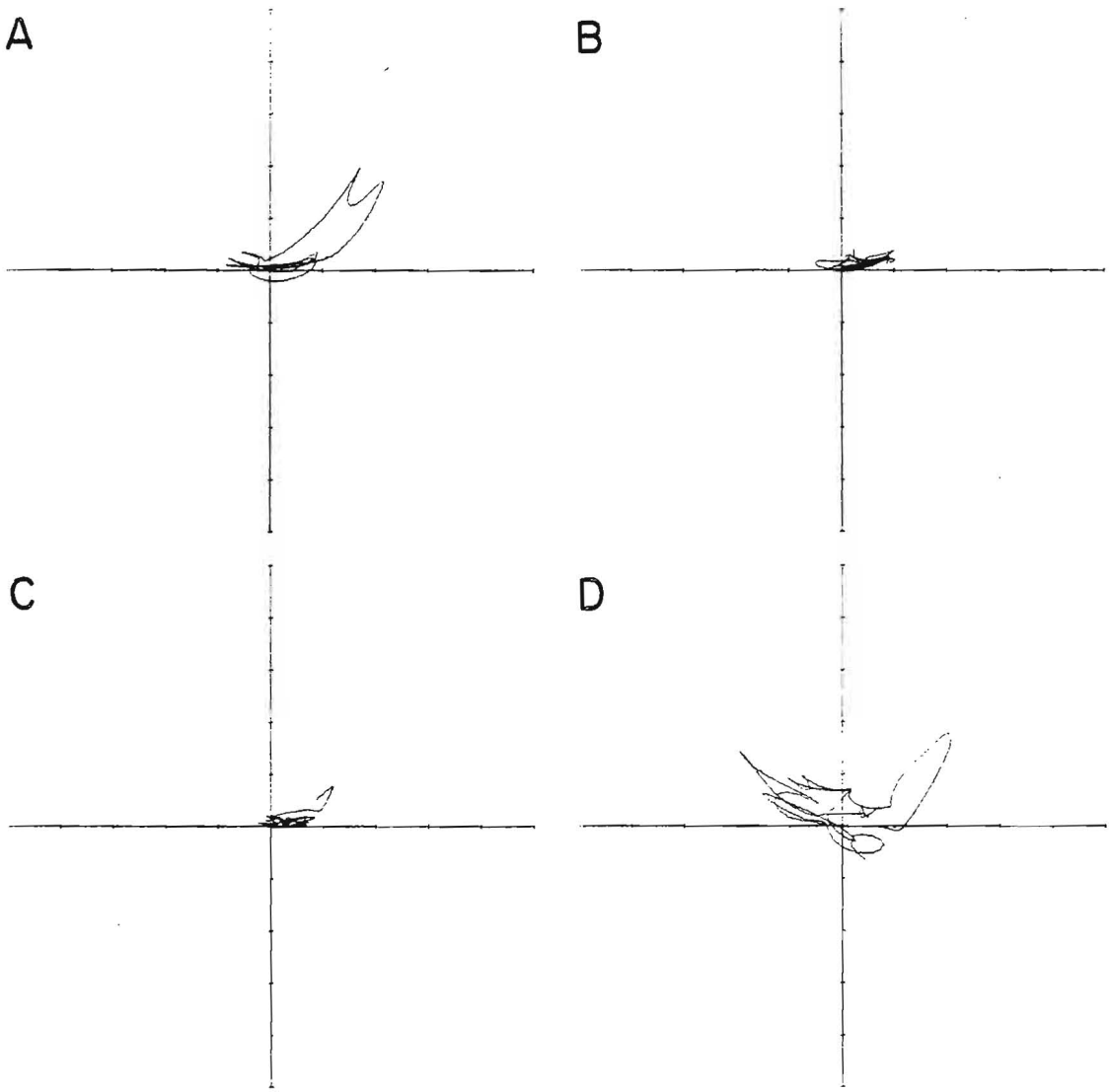

Figure 96. Stability diagrams for time series of horizontal velocity gradients estimated from current meters at 12.2 m depth on 22 July, 1980 (Figure A), 23 July, 1980 (Figure B), 24 July, 1980 (Figure C) and 25 July, 1980 (Figure D). Range of abscissa is $-1.34\times10^{-3}s^{-1}$ to $+1.34\times10^{-3}s^{-1}$; range of ordinate is $-1.39\times10^{-6}s^{-2}$ to $+1.39\times10^{-6}s^{-2}$ (see text).

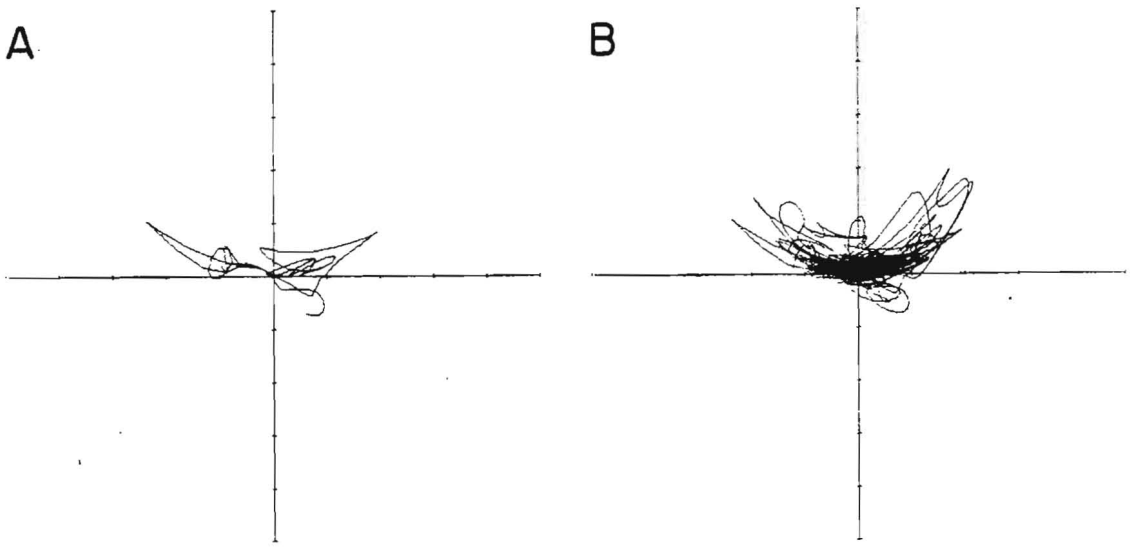

Figure 97. Stability diagrams for time series of horizontal velocity gradients estimated from current meters at 12.2 m depth on 26 July, 1980 (Figure A) and 14 July through 26 July, 1980 (Figure B). Range of abscissa is $-1.34\times10^{-3}s^{-1}$ to $+1.34\times10^{-3}s^{-1}$; range of ordinate is $-1.39\times10^{-6}s^{-2}$ to $+1.39\times10^{-6}s^{-2}$ (see text).

component of vorticity at both 4.6 m and 12.2 m. At 4.6 m depth, for example, the time history of a typical event is *usually* a monotonic increase in both the divergence and stretching and shearing deformation to maximum values of approximately $1 \times 10^{-3} s^{-1}$ and $1 \times 10^{-6} s^{-2}$, respectively, and then a monotonic decrease in divergence and stretching and shearing.

Before discussing the structure of features which might be responsible for producing these observed gradients, the implications of these gradients for dispersion, and the limited comparisons with Lagrangian velocity gradients, the characteristics of velocity gradients estimated from the March 1981 current meter deployment are described. The March 1981 deployment (Figure 8) afforded an opportunity to estimate velocity gradients at three different spatial scales: moorings B, E and D describe the largest scale, moorings C, D and E a somewhat smaller scale and moorings B, C and E a very much smaller scale. Coherency squared and phase estimates between pairs of instruments in both of the larger scale arrays (Figures 34 through 45) suggested that a filter cut off of 360 minutes was required to remove spatially incoherent fluctuations. Even for the small scale array a filter cut off of 120 minutes was required - considerably longer than the most conservative filter cut off of 80 minutes required for the July array which was nearly the same scale.

Velocity gradients for the two larger scale arrays (Figures 98 through 101 and Figures 102 through 105) show very similar features.

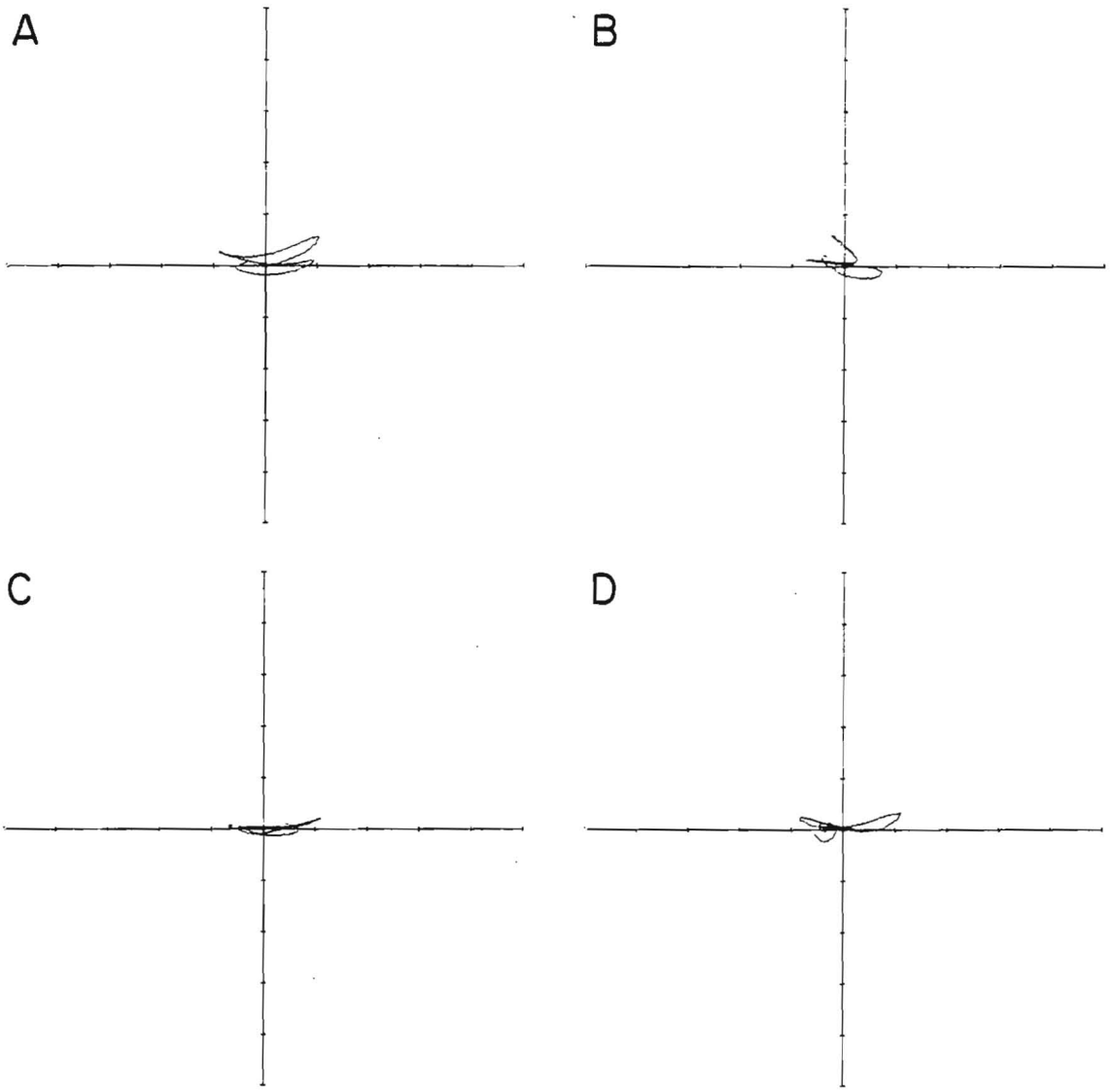

Figure 98. Stability diagrams for time series of horizontal velocity gradients estimated from current meters at 4.6 m depth at moorings B, D and E on 27 February, 1981 (Figure A), 28 February, 1981 (Figure B), 1 March, 1981 (Figure C) and 2 March, 1981 (Figure D). Range of abscissa is $-4.36\times10^{-4}s^{-1}$ to $+4.36\times10^{-4}s^{-1}$; range of ordinate is $-1.54\times10^{-7}s^{-2}$ to $+1.54\times10^{-7}s^{-2}$ (see text).

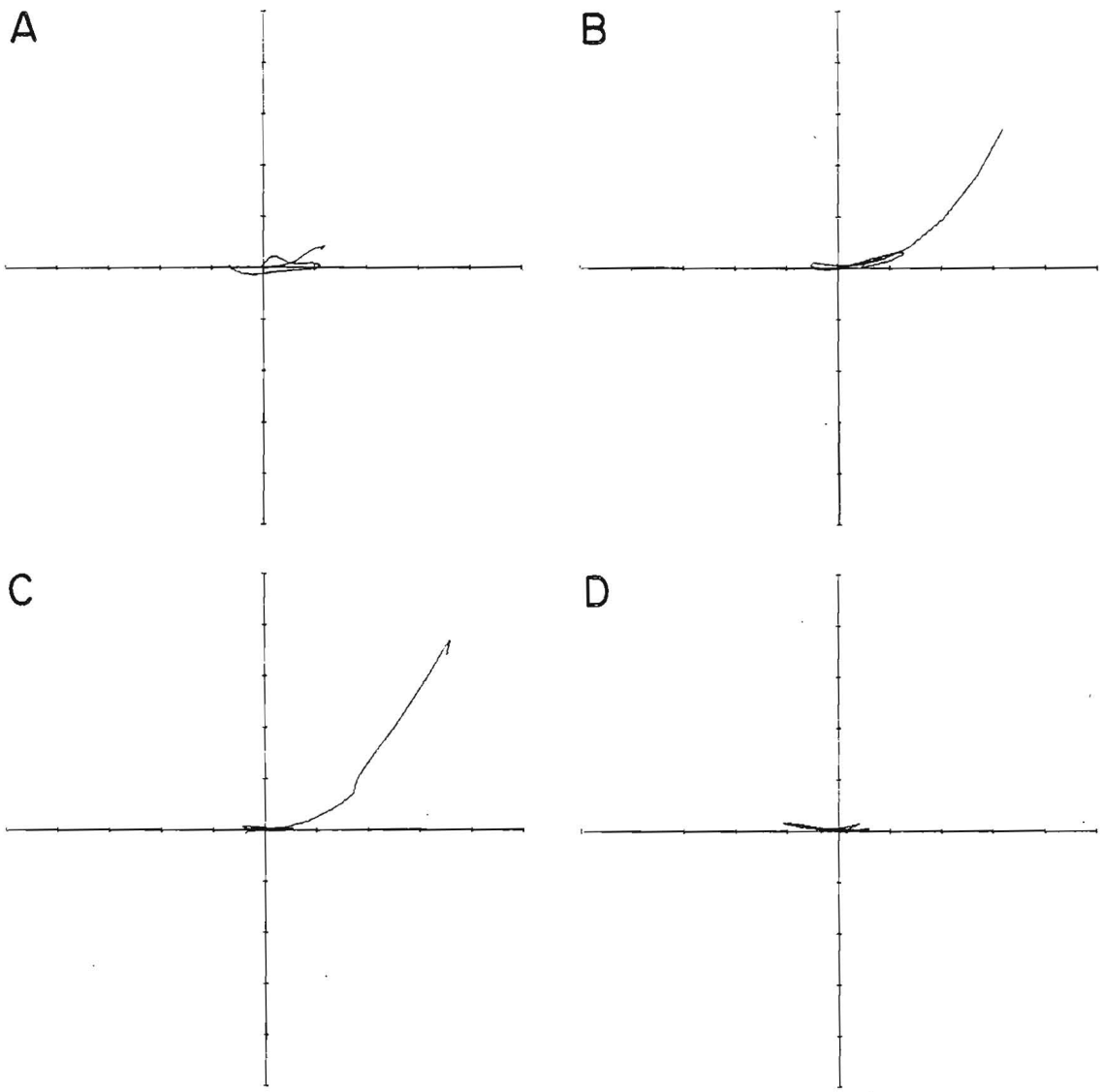

Figure 99. Stability diagrams for time series of horizontal velocity gradients estimated from current meters at 4.6 m depth at moorings B, D and E on 3 March, 1981 (Figure A), 4 March, 1981 (Figure B), 5 March, 1981 (Figure C) and 6 March, 1981 (Figure D). Range of abscissa is $-4.36\times10^{-4}s^{-1}$ to $+4.36\times10^{-4}s^{-1}$; range of ordinate is $-1.54\times10^{-7}s^{-2}$ to $+1.54\times10^{-7}s^{-2}$ (see text).

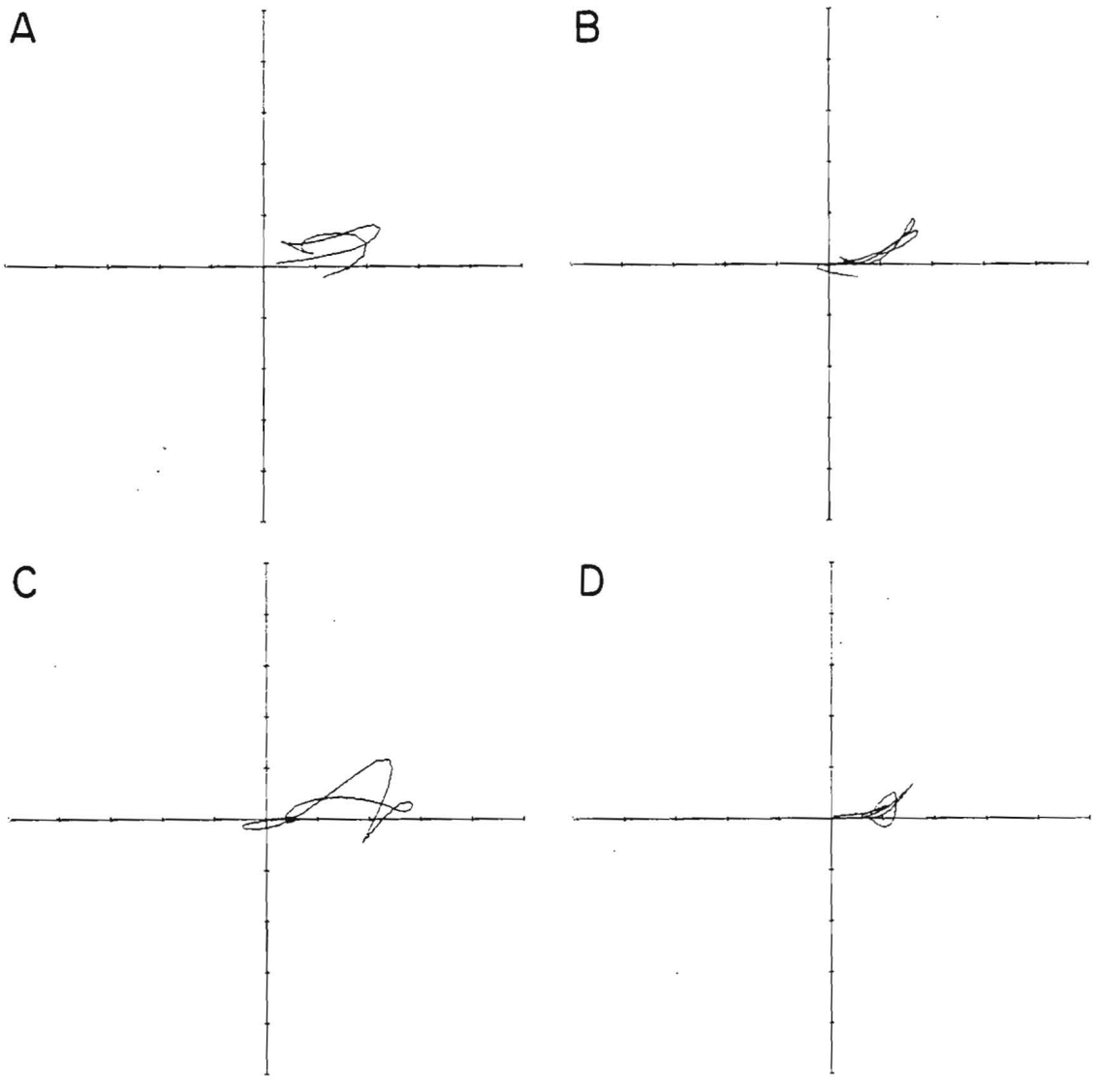

Figure 100. Stability diagrams for time series of horizontal velocity gradients estimated from current meters at 4.6 m depth at moorings B, D and E on 7 March, 1981 (Figure A), 8 March, 1981 (Figure B), 9 March, 1981 (Figure C) and 10 March, 1981 (Figure D). Range of abscissa is $-4.36\times10^{-4}s^{-1}$ to $+4.36\times10^{-4}s^{-1}$; range of ordinate is $-1.54\times10^{-7}s^{-2}$ to $+1.54\times10^{-7}s^{-2}$ (see text).

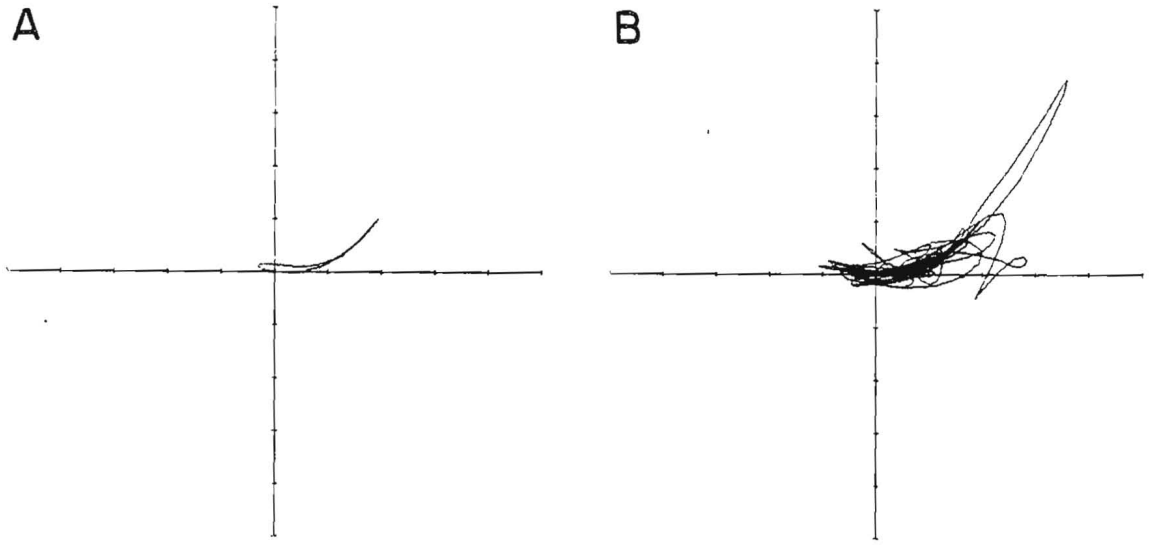

Figure 101. Stability diagrams for time series of horizontal velocity gradients estimated from current meters at 4.6 m depth at moorings B, D and E on 11 March, 1981 (Figure A) and 27 February through 11 March, 1981 (Figure B). Range of abscissa is $-4.36\times10^{-4}s^{-1}$ to $+4.36\times10^{-4}s^{-1}$; range of ordinate is $-1.54\times10^{-7}s^{-2}$ to $+1.54\times10^{-7}s^{-2}$ (see text).

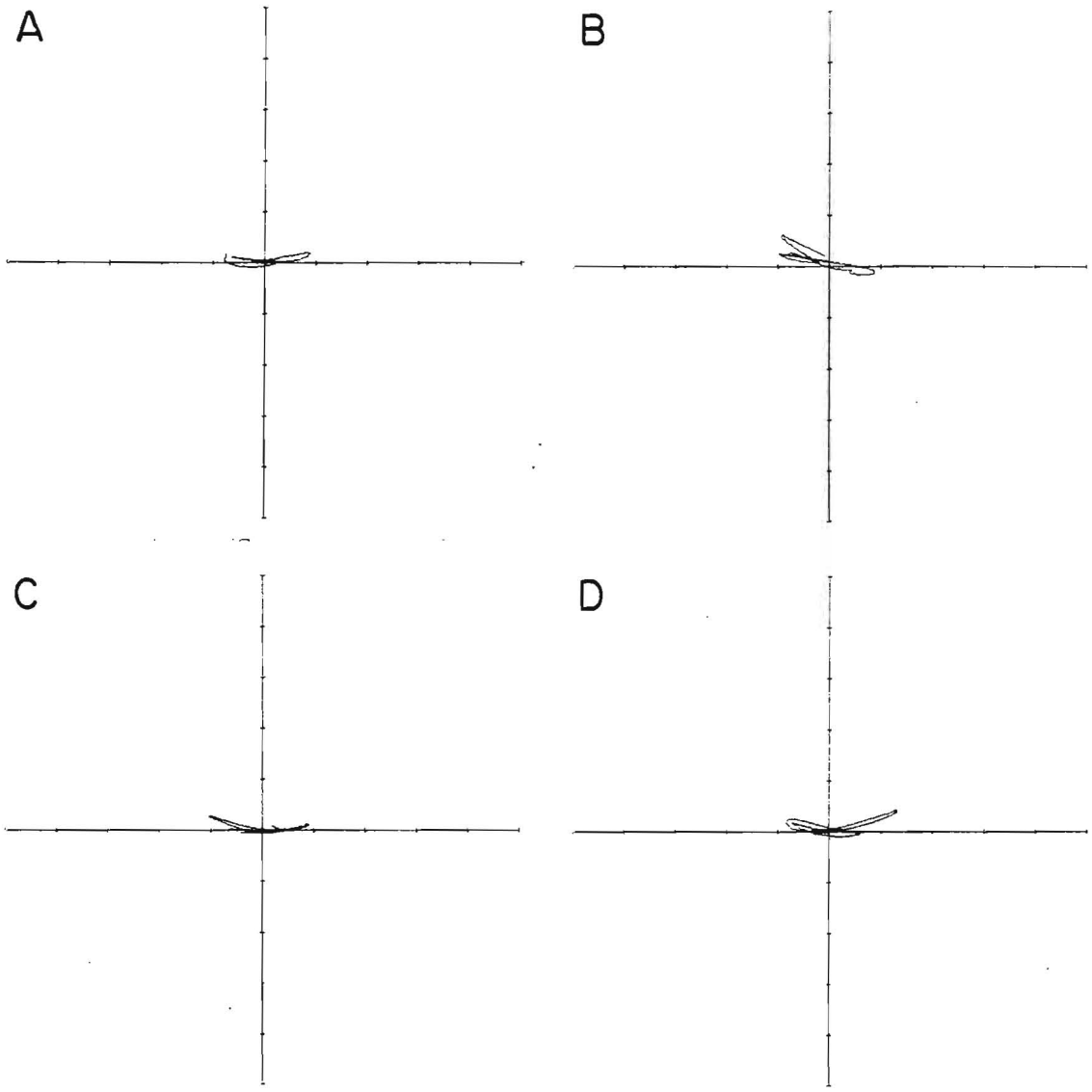

Figure 102. Stability diagrams for time series of horizontal velocity gradients estimated from current meters at 4.6 m depth at moorings C, D and E on 27 February, 1981 (Figure A), 28 February, 1981 (Figure B), 1 March, 1981 (Figure C) and 2 March, 1981 (Figure D). Range of abscissa is $-4.36\times10^{-4}s^{-1}$ to $+4.36\times10^{-4}s^{-1}$; range of ordinate is $-1.54\times10^{-7}s^{-2}$ to $+1.54\times10^{-7}s^{-2}$ (see text).

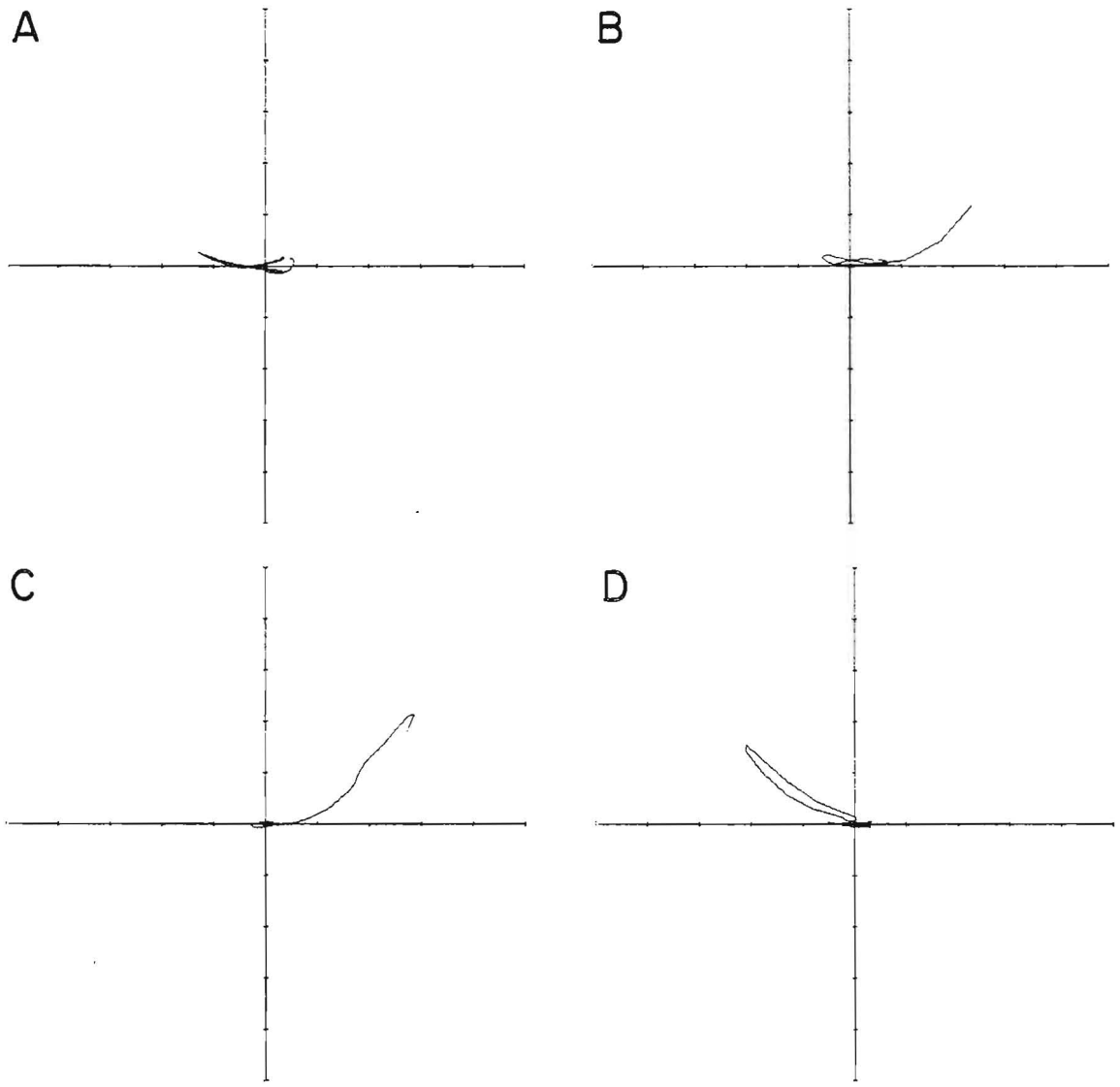

Figure 103. Stability diagrams for time series of horizontal velocity gradients estimated from current meters at 4.6 m depth at moorings C, D and E on 3 March, 1981 (Figures A), 4 March, 1981 (Figure B), 5 March, 1981 (Figures C) and 6 March, 1981 (Figure D). Range of absicssa is $-4.36\times10^{-4}s^{-1}$ to $+4.36\times10^{-4}s^{-1}$; range of ordinate is $-1.54\times10^{-7}s^{-2}$ to $+1.54\times10^{-7}s^{-2}$ (see text).

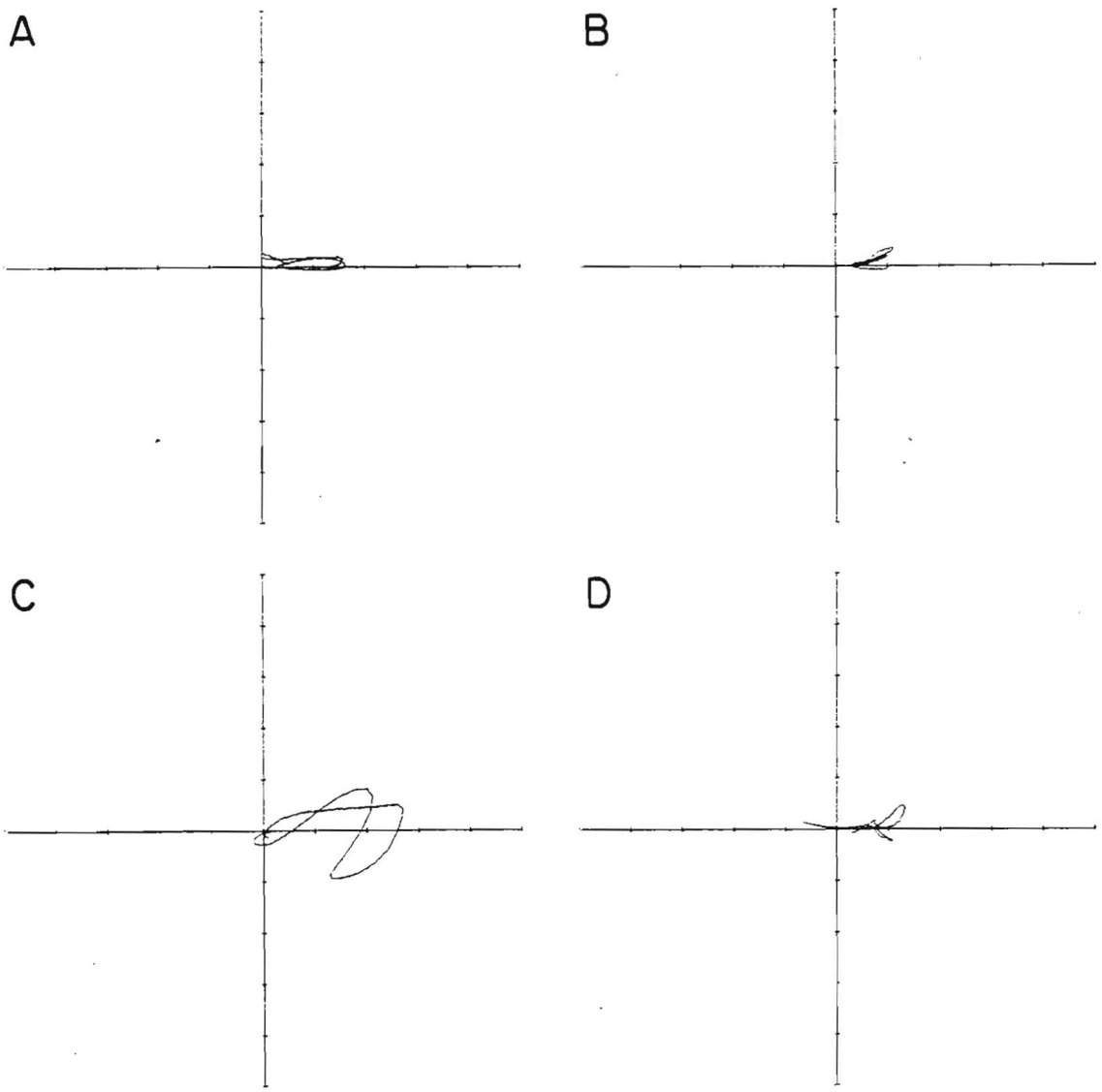

Figure 104. Stability diagrams for time series of horizontal velocity gradients estimated from current meters at 4.6 m depth at moorings C, D and E on 7 March, 1981 (Figure A), 8 March, 1981 (Figure B), 9 March, 1981 (Figure C) and 10 March, 1981 (Figure D). Range of abscissa is $-4.36\times10^{-4}s^{-1}$ to $+4.36\times10^{-4}s^{-1}$; range of ordinate is $-1.54\times10^{-7}s^{-2}$ to $+1.54\times10^{-7}s^{-2}$ (see text).

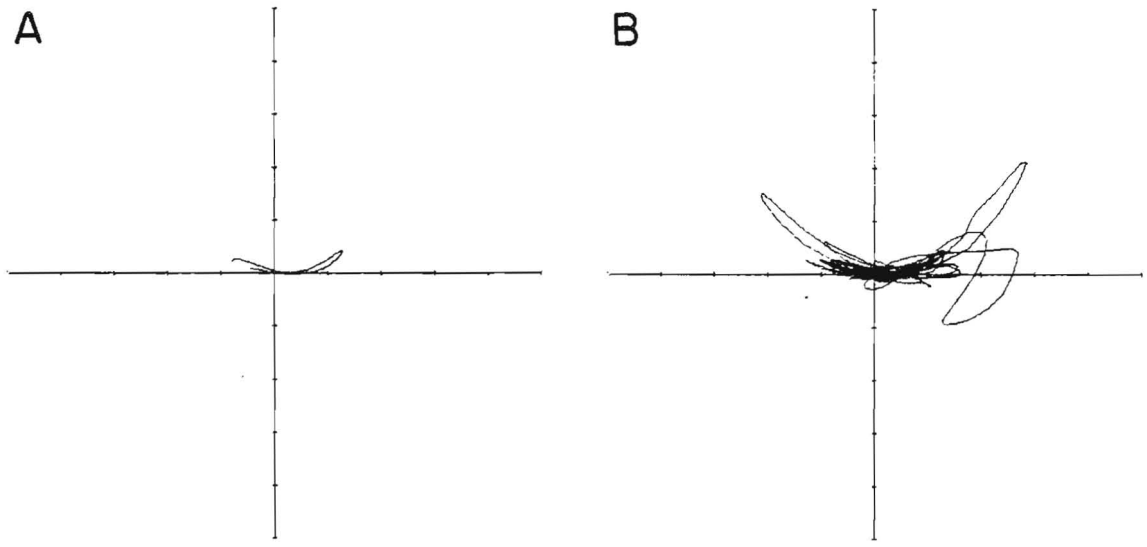

Figure 105. Stability diagrams for time series of horizontal velocity gradients estimated from current meters at 4.6 m depth at moorings C, D and E on 11 March, 1981 (Figure A) and 27 February through 11 March, 1981 (Figure B). Range of abscissa is $-4.36\times10^{-4}s^{-1}$ to $+4.36\times10^{-4}s^{-1}$; range of ordinate is $-1.54\times10^{-7}s^{-2}$ to $+1.54\times10^{-7}s^{-2}$ (see text).

The magnitude of these velocity gradients is considerably smaller than those estimated for the July deployment. This is certainly due at least in part to the difference in scale. They are highly variable and characterized by aperiodic events lasting several hours. On 4, 5 and 6 March (Figure 99), for example, there were a number of events characterized by strong divergence (or convergence) and strong stretching and shearing. Similar to the events in July, these events were characterized by a monotonic increase in the divergence and the stretching and shearing to a maximum value, and then a monotonic decrease.

Velocity gradients estimated for the small scale array (Figures 106 through 109) show an increase in magnitude from the gradients for the larger scale arrays although they remain considerably smaller than the July gradients (note the scale change on the diagrams). They also show features which are remarkably different from those for the larger scale arrays. They are highly variable and not characterized nearly as much by the occasional large event. They show also some increase in the relative magnitude of vorticity over stretching and shearing.

In summary, some of the most noteworthy features of the Eulerian velocity gradients are the temporal variability, the tendency for large disturbances to be both divergent (or convergent) and characterized by stretching (and shearing) rather than rotation, and the strong scale dependency of the magnitude of the gradients. Not only does the gradient magnitude change with array scale, but also

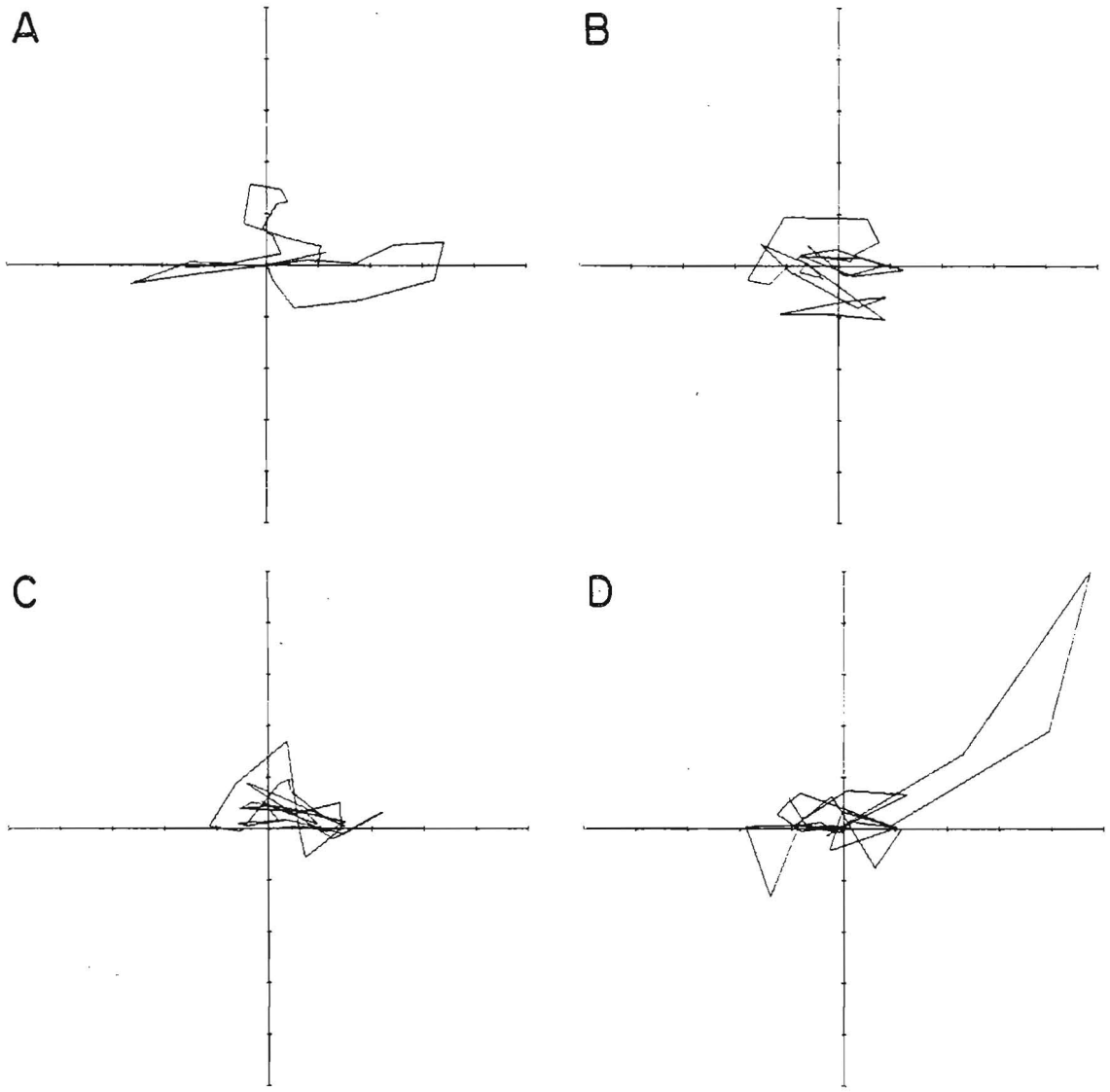

Figure 106. Stability diagrams for time series of horizontal velocity gradients estimated from current meters at 4.6 m depth at moorings B, C and E on 27 February, 1981 (Figure A), 28 February, 1981 (Figure B), 1 March, 1981 (Figure C) and 2 March, 1981 (Figure D). Range of abscissa is $-4.36\times10^{-4}s^{-1}$ to $+4.36\times10^{-4}s^{-1}$; range of ordinate is $-1.54\times10^{-7}s^{-2}$ to $+1.54\times10^{-7}s^{-2}$ (see text).

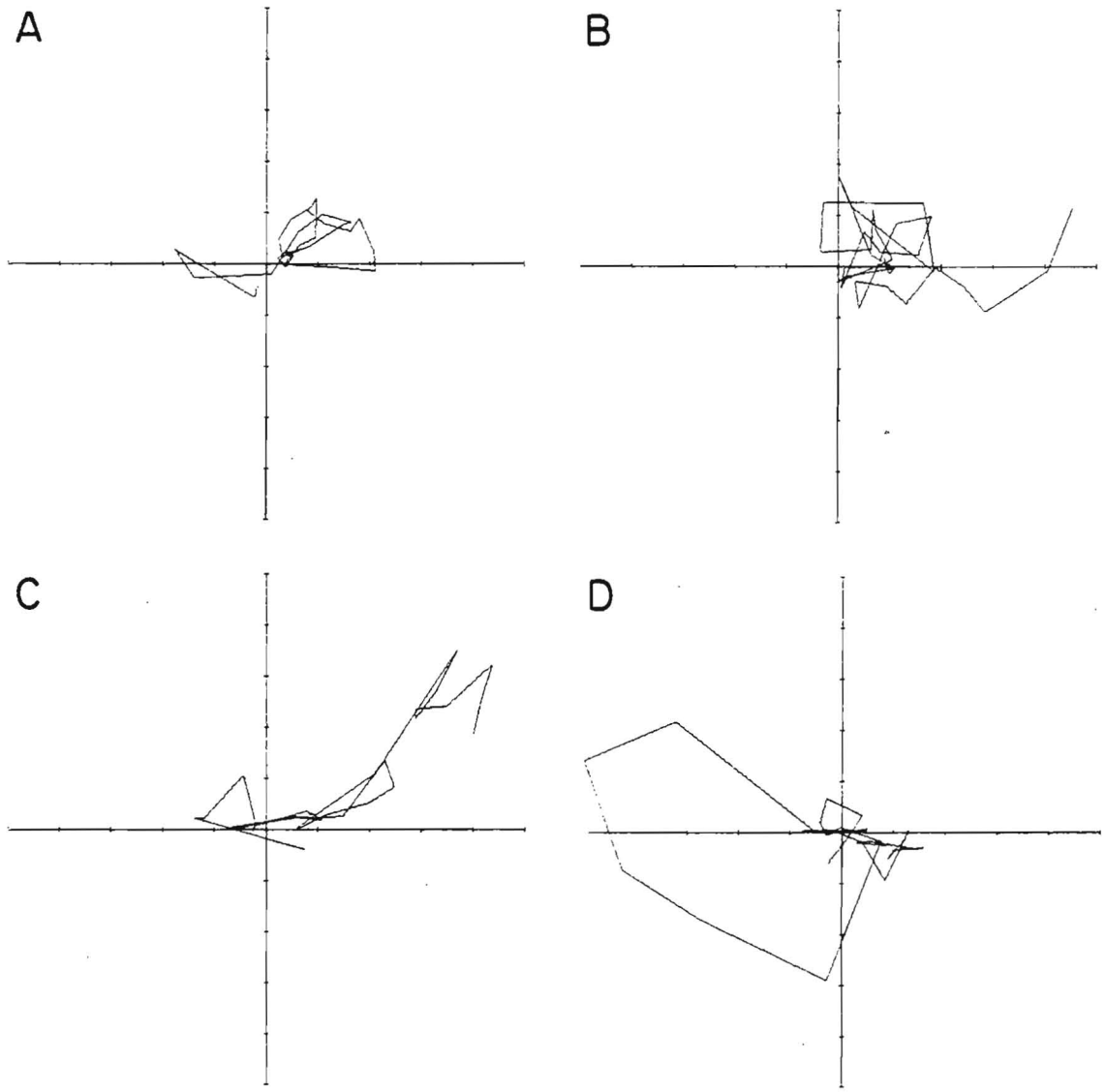

Figure 107. Stability diagrams for time series of horizontal velocity gradients estimated from current meters at 4.6 m depth at moorings B, C and E on 3 March, 1981 (Figure A), 4 March, 1981 (Figure B), 5 March, 1981 (Figure C) and 6 March, 1981 (Figure D). Range of abscissa is $-4.36\times10^{-4}s^{-1}$ to $+4.36\times10^{-4}s^{-1}$; range of ordinate is $-1.54\times10^{-7}s^{-2}$ to $+1.54\times10^{-7}s^{-2}$ (see text).

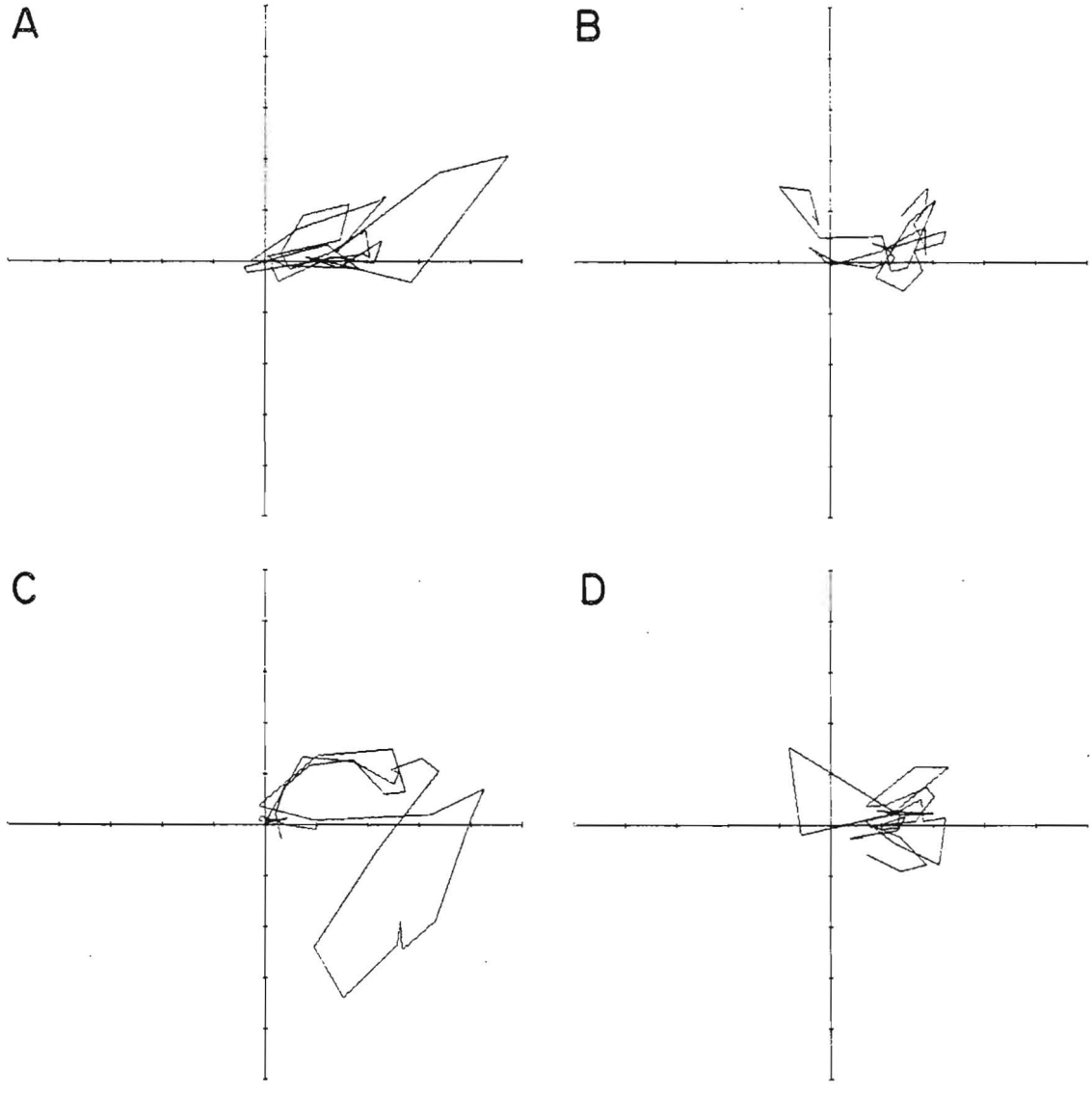

Figure 108. Stability diagrams for time series of horizontal velocity gradients estimated from current meters at 4.6 m depth at moorings B, C and E on 7 March, 1981 (Figure A), 8 March, 1981 (Figure B), 9 March, 1981 (Figure C) and 10 March, 1981 (Figure D). Range of abscissa is $-4.36\times10^{-4}s^{-1}$ to $+4.36\times10^{-4}s^{-1}$; range of ordinate is $-1.54\times10^{-7}s^{-2}$ to $+1.54\times10^{-7}s^{-2}$ (see text).

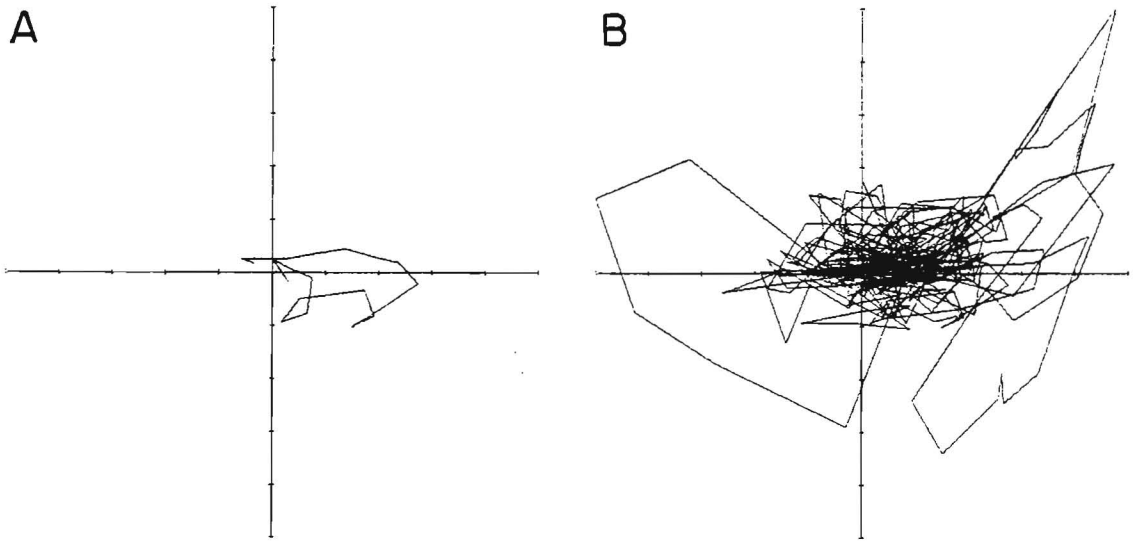

Figure 109. Stability diagrams for time series of horizontal velocity gradients estimated from current meters at 4.6 m depth at moorings B, C and E on 11 March, 1981 (Figure A) and 27 February through 11 March, 1981 (Figure B). Range of abscissa is $-4.36\times10^{-4}s^{-1}$ to $+4.36\times10^{-4}s^{-1}$; range of ordinate is $-1.54\times10^{-7}s^{-2}$ to $+1.54\times10^{-7}s^{-2}$ (see text).

apparently the structure may change significantly. Our observations also suggested that velocity gradients were considerably lower in winter than in summer at comparable scales.

A significant percentage of the measured velocity gradients fall within the first quadrant of the stability diagram, and these gradients should be most dispersive. The temporal variability and the dependence of both the magnitude and structure of velocity gradients on spatial scale would, however, complicate the application of simple formulas (Okubo *et al.*(1983)) to describe the areal change, elongation and orientation of a patch in terms of measured horizontal divergence and stretching and shearing deformation rates.

We should mention that both speed and direction calibration problems could certainly produce spurious velocity gradients. However, the rms value of our velocity gradients at 4.6 m depth during the July deployment is greater than $5\times10^{-4}s^{-1}$. For the spatial scales involved this represents a velocity difference of 10 cm s^{-1} which should be appreciably greater than any difference which might arise from uncertainties in speed and direction calibrations.

Limited comparisons can be made between the Eulerian and Lagrangian velocity gradients. Figures 110 through 112 show stability diagrams for Lagrangian velocity gradients estimated for drogue cluster experiments in July. These experiments are inventoried in Table 5. Summer drogue experiments with horizontal scales comparable to that of the Eulerian array are Experiment 1 (Figure 110a), Experiment 3

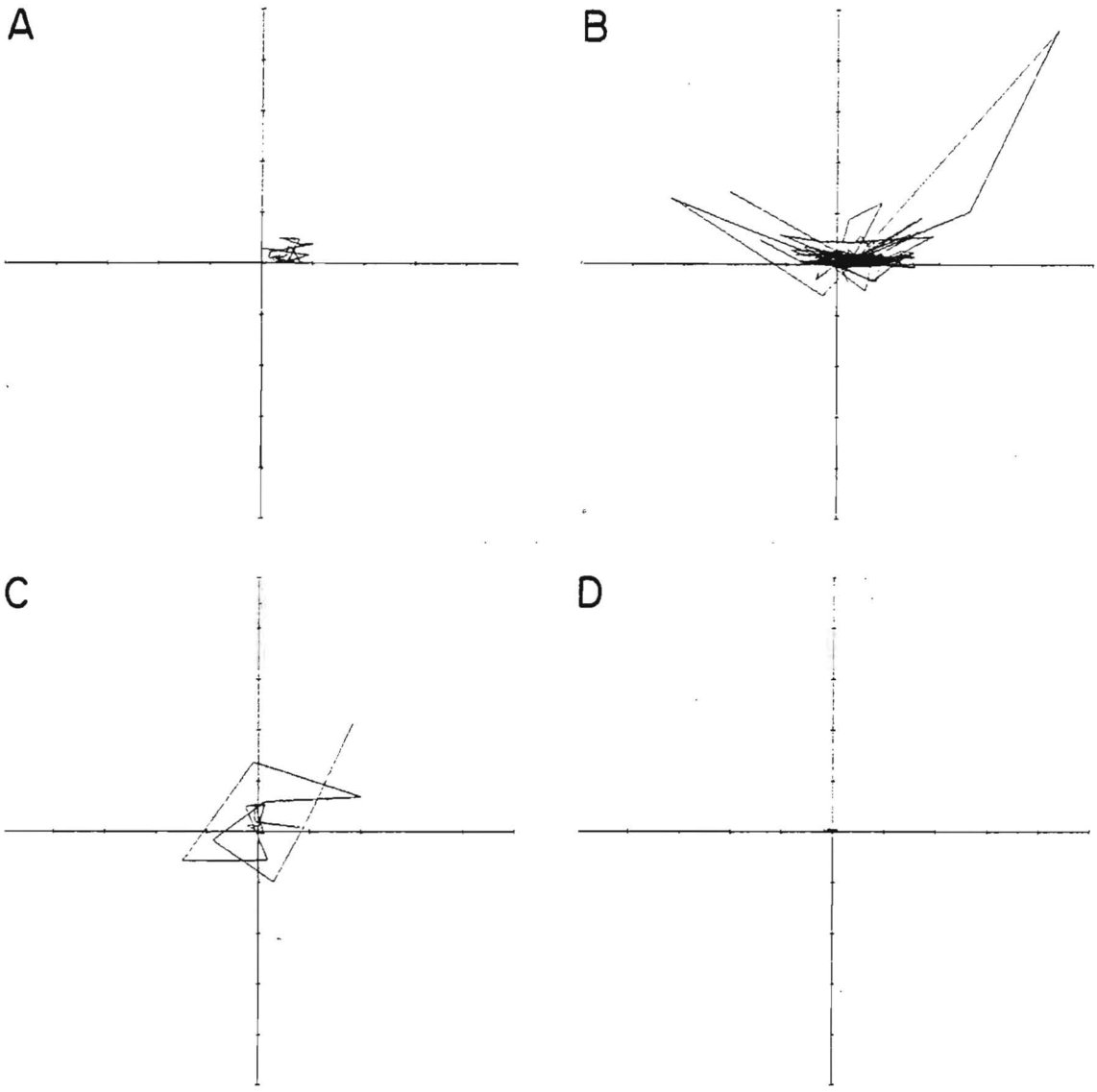

Figure 110. Stability diagrams for time series of horizontal velocity gradients estimated from drogue cluster for Experiment 1 on 21 July, 1980 (Figure A), Experiment 3 on 24 July, 1980 (Figure B), Experiment 4S on 25 July, 1980 (Figure C) and Experiment 4L on 25 July, 1980 (Figure D). Range of abscissa is $-1.34\times10^{-3}s^{-1}$ to $+1.34\times10^{-3}s^{-1}$; range of ordinate is $-1.39\times10^{-6}s^{-2}$ to $+1.39\times10^{-6}s^{-2}$ (see Table 5).

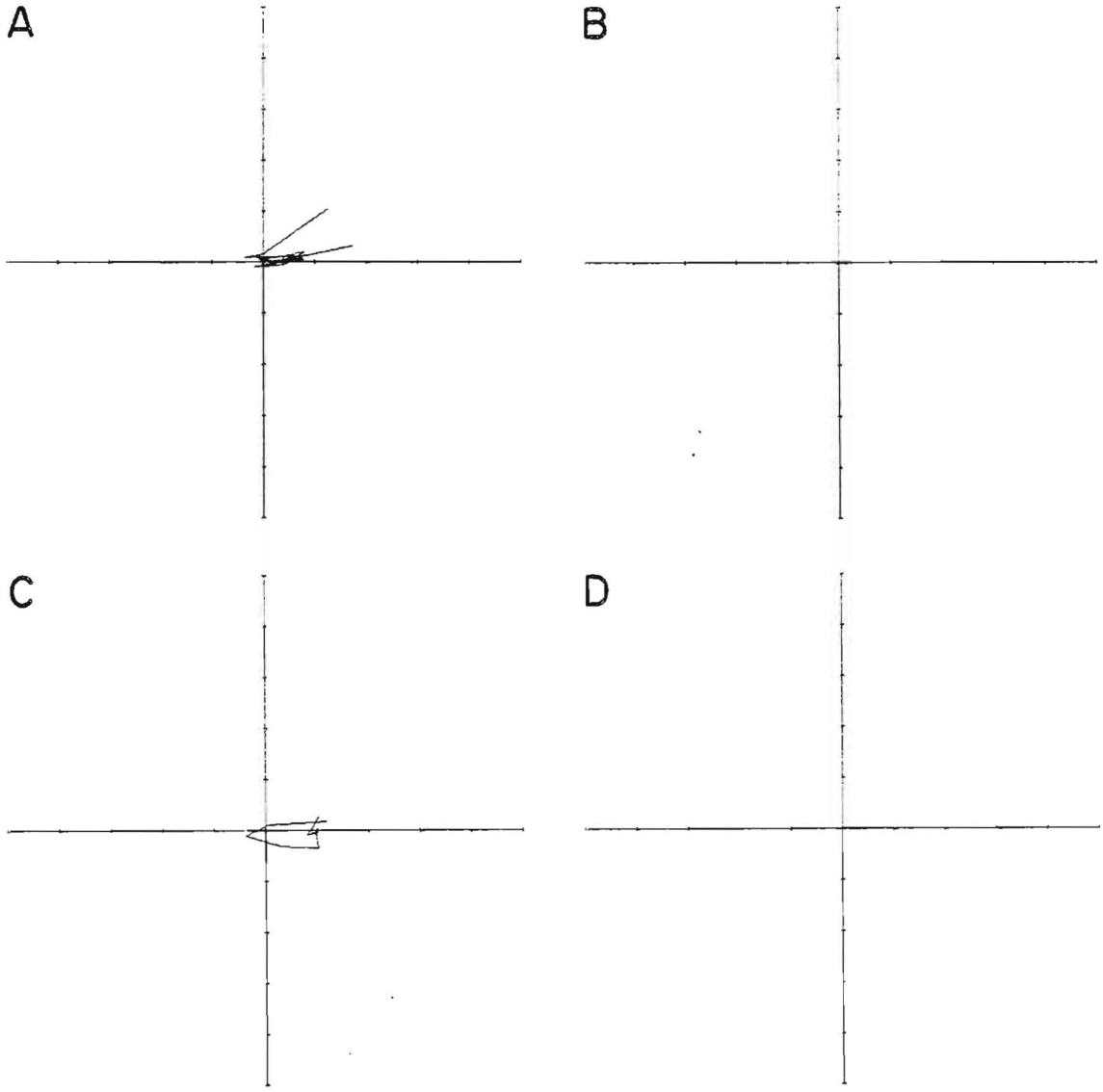

Figure 111. Stability diagrams for time series of horizontal velocity gradients estimated from drogue cluster for Experiment 5S on 25 July, 1980 (Figure A), Experiment 5L on 25 July, 1980 (Figure B), Experiment 6S on 25 July, 1980 (Figure C) and Experiment 6L on 25 July, 1980 (Figure D). Range of abscissa is $-1.34\times10^{-3}s^{-1}$ to $+1.34\times10^{-3}s^{-1}$; range of ordinate is $-1.39\times10^{-6}s^{-2}$ to $+1.39\times10^{-6}s^{-2}$ (see Table 5).

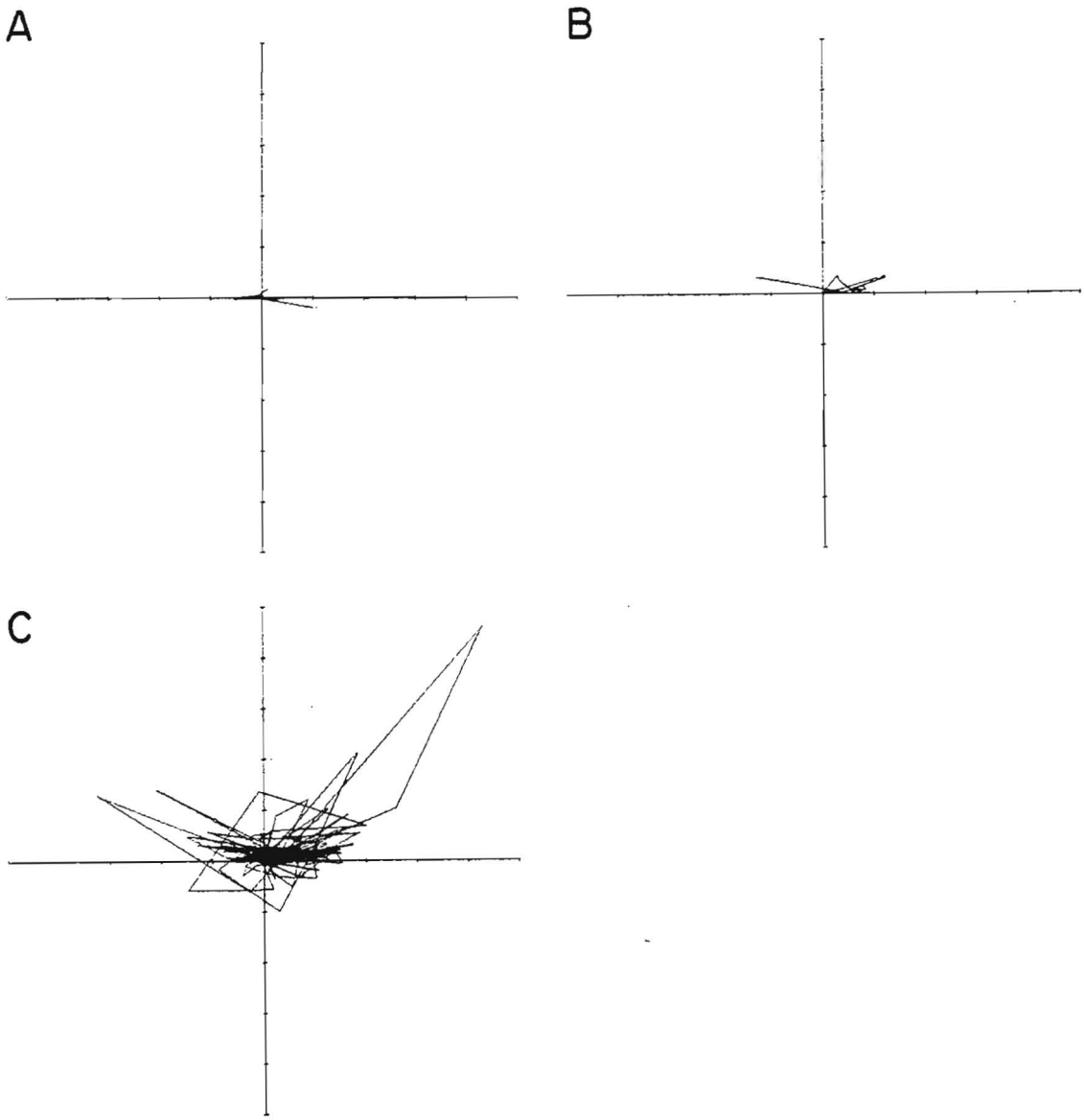

Figure 112. Stability diagrams for time series of horizontal velocity gradients estimated from drogue cluster for Experiment 8S on 26 July, 1980 (Figure A), Experiment 8D on 26 July, 1980 (Figure B) and Experiments 1 through 8D (Figure C). Range of abscissa is $-1.34\times10^{-3}s^{-1}$ to $+1.34\times10^{-3}s^{-1}$; range of ordinate is $-1.39\times10^{-6}s^{-2}$ to $+1.39\times10^{-6}s^{-2}$ (see Table 5).

(Figure 110b) and Experiments 8S and 8D (Figures 112a and 112b). Comparison of these Lagrangian gradients with Eulerian gradients for the same days in Figures 91d, 92c and 93a, respectively, show generally extremely good agreement for the magnitude of the gradients. Gradients for drogue Experiment 3 (Figure 110b) show large convergent and divergent events accompanied by shearing and stretching which was characteristic of many of the summer Eulerian gradients.

In general the velocity gradients for summer drogue experiments showed very large scale dependence. Experiments 4L and 5L, for example, both had horizontal scales of the order 10^3 m. Comparison of the velocity gradients for these experiments (Figures 110d and 111b) with those for Experiments 4S and 5S (Figures 110c and 111c) which had horizontal scales of the order 10^2 m shows the strong scale dependence.

Winter drogue experiments had horizontal scales comparable to that of the smallest winter Eulerian array. The velocity gradients for these drogue experiments (Figures 113a, 113b, 113c) show the same order of magnitude decrease in magnitude for a given scale from summer to winter as did the Eulerian gradients. Velocity gradients for the smallest winter Eulerian array (Figures 108c, 108d, 109a) show excellent agreement in both magnitude and general structure with the gradients for the drogues. In general, time series for individual Lagrangian and Eulerian gradients did not show good agreement. Such agreement should probably not have been expected because of the apparent small scale variability in the gradient field and because drogues were often not precisely within the Eulerian array.

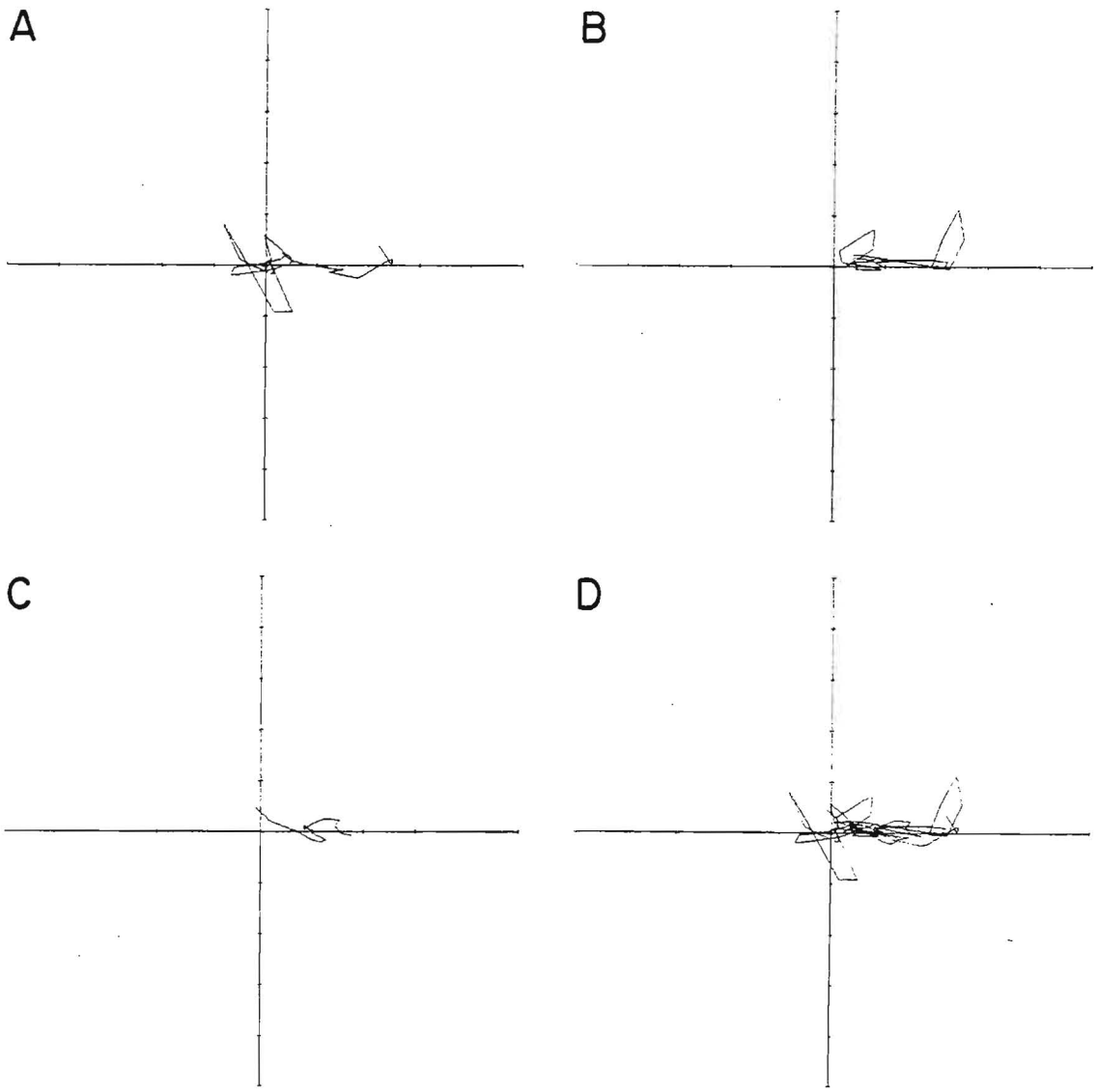

Figure 113. Stability diagrams for time series of horizontal velocity gradients estimated from drogue cluster for Experiment 10 on 9 March, 1981 (Figure A), Experiment 11 on 10 March, 1981 (Figure B), Experiment 12 on 11 March, 1981 (Figure C) and Experiments 10 through 12 (Figure D). Range of abscissa is $-4.36\times10^{-4}s^{-1}$ to $+4.36\times10^{-4}s^{-1}$; range of ordinate is $-1.54\times10^{-7}s^{-2}$ to $+1.54\times10^{-7}s^{-2}$ (see Table 5).

Estimation of Variance from Current Meter Records

Customarily Taylor's formula (Taylor (1921)) is used to estimate turbulent diffusion from current meter records. According to Taylor, the variance of particle displacements $\sigma^2(t)$ can be expressed as

$$\sigma^2(t) = \overline{2v'^2} \int_0^t dt' \int_0^{t'} d\tau \; R_L(\tau) \tag{47}$$

where $\overline{v'^2}$ is the mean squared turbulent velocity and $R_L(\tau)$ is the Lagrangian velocity autocorrelation coefficient, which is defined by

$$R_L(\tau) = \overline{v'(t)\; v'(t+\tau)}/\overline{v'^2} \tag{48}$$

In Taylor's formula the turbulent flow field is assumed to be stationary. (47) can be rewritten as

$$\sigma^2(t) = 2\,\overline{v'^2} \int_0^t (t-\tau) R_L(\tau) d\tau \tag{49}$$

Because of the assumption of stationary turbulence, Taylor's formula should be applied to absolute diffusion. For relative diffusion, the velocity field relative to the centroid of a cluster of particles cannot be assumed to be stationary, and Taylor's formula needs certain modifications. As mentioned in the preface to this section, diffusion from a continuous (fixed) source may be classified as either absolute or relative diffusion depending upon how we observe or sample the plume of substance.

Ogura (1957, 1959) presented a detailed analysis of the dependence of diffusion from a continuous source on the observation interval. Here we summarize Ogura's analysis.

Let v(t) be the random velocity of a particle. The sample mean value of v over the time interval, t_s, i.e., sampling or observation time, centered at a diffusion time* t is

$$\langle v(t)\rangle_{t_s} = \frac{1}{t_s}\int_{t-t_s/2}^{t+t_s/2} v(t')dt' \tag{50}$$

Then the turbulent component referred to this mean velocity is

$$v'_{t_s}(t) = v(t) - \langle v\rangle_{t_s} \tag{51}$$

and the Lagrangian autocorrelation coefficient, $R_{t_s}(\tau)$, for a finite sampling time, t_s, is given by

$$R_{t_s}(\tau) = \frac{1}{t_s}\int_{t-t_s/2}^{t+t_s/2} \overline{v'_{t_s}(t')\ v'_{t_s}(t'+\tau)}dt' \Big/ \frac{1}{t_s}\int_{t-t_s/2}^{t+t_s/2} \overline{v'^2_{t_s}}(t')dt' \tag{52}$$

where the overbar denotes the ensemble average of meandering plumes observed for an interval t_s.

Taylor's formula (49) can now be applied to diffusion from a continuous source for a finite sampling time, t_s, by using (52) in place of $R_L(\tau)$ and $\overline{v'^2_{t_s}}$ in place of $\overline{v'^2}$. It is expressed as

$$\sigma^2_{t_s}(t) = 2\ \overline{v'^2_{t_s}}\int_0^t (t-\tau)R_{t_s}(\tau)d\tau \tag{53}$$

Eq. (53) can be used to calculate the variances for various sampling intervals, t_s, on the basis of sufficiently long current meter data. There is a serious problem in the calculation, however. That is, $R_{t_s}(\tau)$ in (53) is the autocorrelation coefficient in a *Lagrangian*

---

*Identical to previously defined age, t_a.

sense whereas the current meter data provide only the *Eulerian* autocorrelation coefficient.

The Hay-Pasquill hypothesis (Hay and Pasquill (1959)) provides a relation between the Lagrangian (R_L) and Eulerian (R_E) autocorrelation coefficients as

$$R_L(\beta\tau) = R_E(\tau) \tag{54}$$

where β is a factor representing the ratio of the Lagrangian to the Eulerian time scales*. Substitution of (54) into (53) gives a basic expression for the variance in terms of the measured Eulerian autocorrelation coefficient

$$\sigma^2_{t_s}(t) = 2\beta\,\overline{v'^2_{t_s}} \int_0^{t/\beta} (t-\beta\tau) R_E(\tau)\, d\tau \tag{55}$$

A typical Eulerian autocorrelation coefficient calculated from one of the LEDS current meter records (unfiltered) is shown in Figure 114. Its principal feature is a pronounced periodicity due to the strong semidiurnal tidal oscillations in the velocity record superposed on a longer period oscillation (of which somewhat less than half a period is shown) arising from low frequency current fluctuations.

---

*T_L (Lagrangian integral time scale) $\equiv \int_0^\infty R_L(\xi)\, d\xi$

T_E (Eulerian integral time scale) $\equiv \int_0^\infty R_E(\tau)\, d\tau$

From (54) we obtain

$$T_L = \int_0^\infty R_L(\xi)\, d\xi = \int_0^\infty R_L(\beta\tau)\, d\beta\tau = \beta \int_0^\infty R_E(\tau)\, d\tau = \beta\, T_E$$

Therefore

$$\beta = T_L / T_E$$

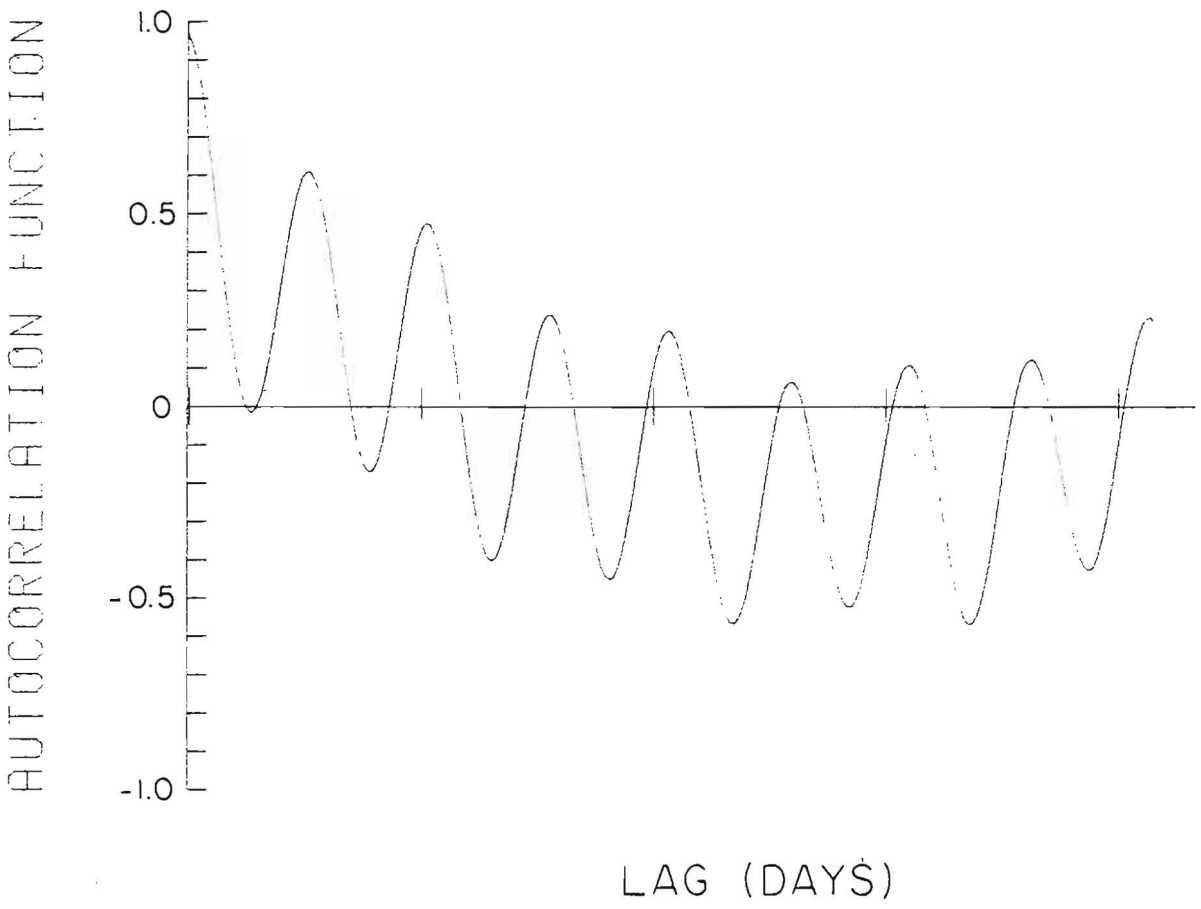

Figure 114. Typical Eulerian autocorrelation calculated from a LEDS current meter record #174107.

In previous attempts to compute dispersion from current meter records (Callaway (1974), Jackson *et al.* (1979)) this calculated autocorrelation coefficient was inserted in Taylor's formula (55) and the integral evaluated numerically. Several overlooked factors combine to render this apparently straightforward calculation unacceptable.

The measured frequency spectrum of oceanic velocity fluctuations has always been found to be "red", that is it contains oscillations longer than the record length and with progressively greater variance at lower frequencies. These comparatively energetic low frequencies dominate the autocorrelation with the result that wavy autocorrelations will always be obtained from oceanic current meter records.

The problems that the wavy autocorrelation function and the high energy at low frequencies cause can be appreciated if we consider modeling the autocorrelation as a decaying exponential,

$$R_E(\tau) = e^{-\tau/T_E} \tag{56}$$

where T_E is the Eulerian integral time scale of the turbulence defined as

$$T_E = \int_0^\infty R_E(\tau)\,d\tau \tag{57}$$

It is apparent from an examination of Figure 114 that the integral (57) does not converge over the period shown and T_E would in fact oscillate around zero as the integration limit is extended. Previous investigators have extended the integration only to the first zero

crossing of $R_E(\tau)$, a practice which leads to underestimates of the integral time scale. The use of the exponential function, however, allows Eq. (55) to be integrated, yielding an analytical form for the growth of variance with time.

$$\sigma^2_{t_s}(t) = 2\beta\ \overline{v'^2_{t_s}}\ T_E t - 2\beta^2\ \overline{v'^2_{t_s}}\ T_E^2\ \{1 - \exp(-t/\beta\ T_E)\} \tag{58}$$

Nuemann (1978) has pointed out that this form yields good results in atmospheric diffusion studies.

The practical application of this analytical form was done by making a least squares fit of the decaying exponential to the actual autocorrelation coefficient (Figure 115) which yielded an integral time scale. This parameter and the lateral velocity variance determined from current meter records was substituted into Eq. (58) yielding the uppermost curve in Figure 116. The essential elements of this theory of plume diffusion are exhibited in this figure. Two diffusion regimes exist connected by a transition zone whose position depends on the integral time scale for the particular flow. For times small compared to T_E the *lateral* variance, $\overline{y^2}$ or σ_y^2, increases at t^2 while at long times $\overline{y^2}$ grows as t. The center of the transition zone occurs at $t \sim 2T_E$. For diffusion times up to at least a day and probably longer depending on the distance to the nearest boundaries we do not expect to see $\overline{y^2} \sim t$ behavior since this can only occur when the distance from the source of diffusant is large compared to the integral space scale of the turbulence. Since we expect scales of motion up to the size of the ocean basin we expect then that plumes

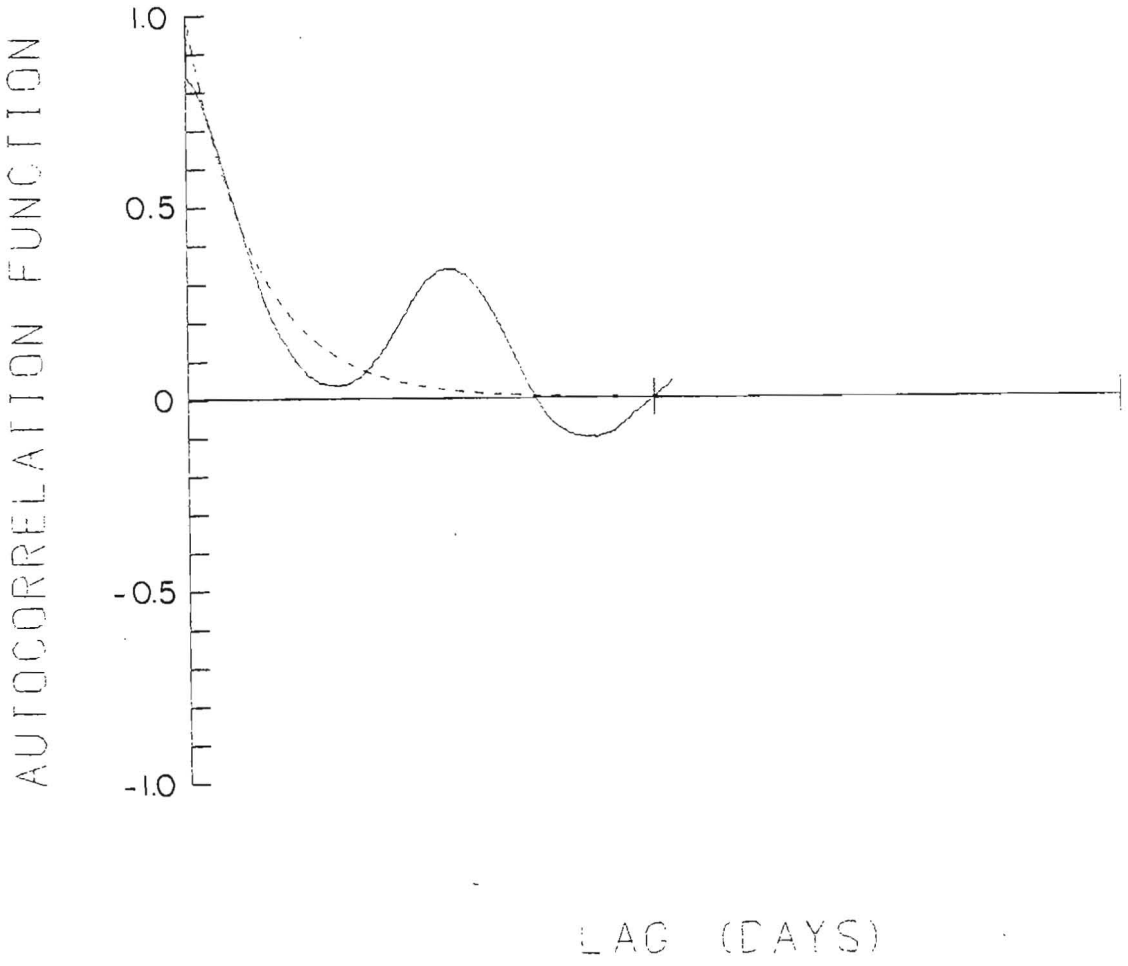

Figure 115. Least squares fit of Eq. (56) to autocorrelation of LEDS data (current meter #174107).

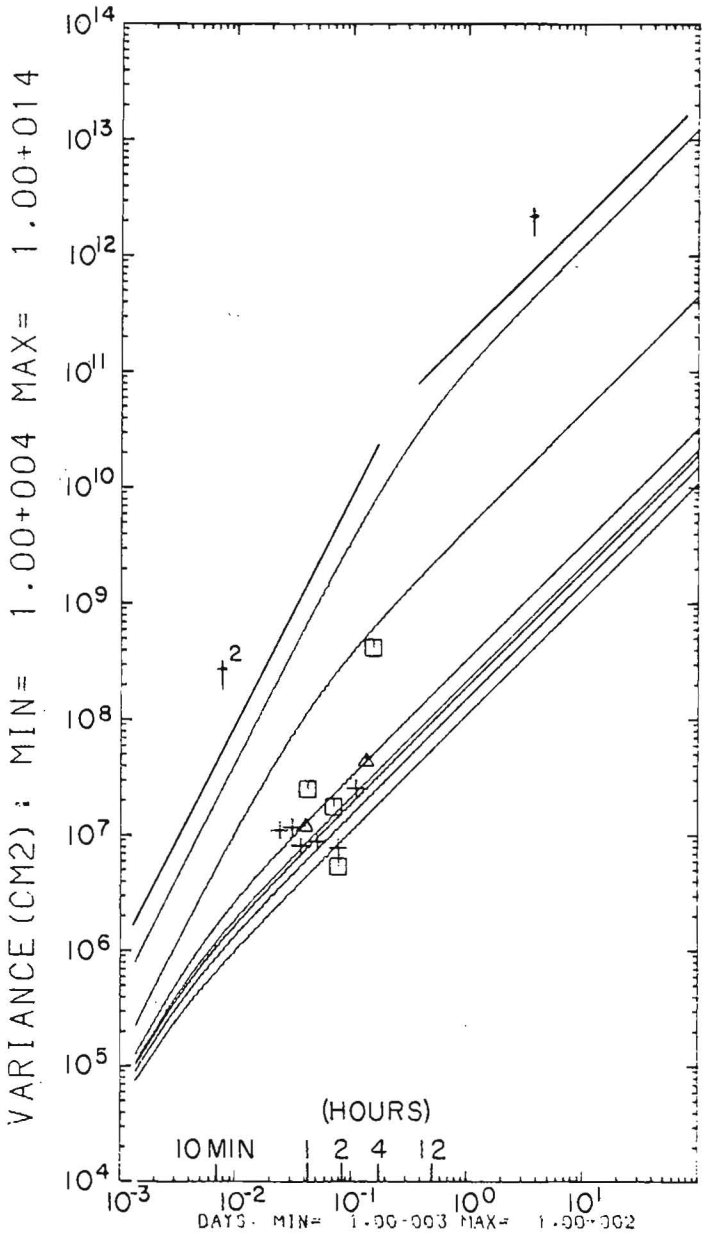

Figure 116. The growth of lateral variance with time, t (Eq. (58)) for LEDS data. The two straight line segments illustrate $\overline{y^2} \sim t^2$, $\overline{y^2} \sim t$. The top curve was calculated from an unfiltered record while those below it were calculated from high pass filtered records with 12, 6, 4, 3, 2, 1 hour filter cutoff periods respectively. The LEDS dye plume data (Δ, 07/24/80, +, 07/25/80, □, 07/26/80) are also shown for comparison.

in the ocean should remain in the initial period and diffuse as t^2. Support for this conclusion comes from aerial photographs of the LEDS plume diffusion experiments examples of which are shown in Figures 83-85. Diverging lines or envelopes (not shown) show the lateral extent of the plume growing linearly in time and thus the lateral variance grows at t^2 in accordance with the initial period prediction of the model.

The data* from the LEDS plume experiments is also shown in Figure 116. The prediction from the raw current meter record (uppermost curve) passes above the data. There are two reasons for this discrepancy. First, the lateral variance of the plume was measured for sampling periods approximately equal to the transit time, i.e., age from the source to the measuring position while the theory strictly requires that the sampling period be long compared to the transit time**. This means that the lateral plume variance is underestimated though probably not more than a factor of two. The second, and more influential reason is that the current meter records are two weeks long and thus contain low frequency as well as tidal fluctuations which are very energetic compared to the higher frequencies. For the short diffusion times in this experiment these

---

* Plotted are values of the lateral variance (absolute) from Table 12. for a depth of 0.9 m and various downstram distances between 0.52 km and 3.32 km on 7/24/80 (Δ), 7/25/80 (+), and 7/26/80 (□).

** When t_s is smaller than the transit time, we replace t_s by t_a in calculating the lateral variance.

energetic low frequencies act as mean flows and do not contribute to the diffusion of the plume. Thus the velocity records must be appropriately filtered to exclude the nondispersive low frequency fluctuations.

High-pass filtering the velocity records before calculating the lateral variance as a function of time has two effects which are shown in the family of curves in Figure 116. Shorter filter cut off periods reduce the predicted variance and the transition from initial (t^2) to final (t) period behavior shifts to shorter and shorter times. This shift exacerbates another discrepancy between the prediction and the data. As stated previously we expect the plumes to be in their initial period of diffusion whereas the final period of the predicted curves pass through the points. Thus the calculated integral time scales are too short. The same problem arises when using the actual autocorrelation functions directly in (55). Results are shown in Figure 117. Note the short times at which the predictions become spurious. These negative examples have been included because they illustrate the previously unappreciated problems involved in calculating the spread of material from current meter records and to emphasize the importance of our simultaneous Eulerian and Lagrangian measurements in detecting the discrepancies.

We have shown that high pass filtering cannot eliminate wavy autocorrelation functions and that the underestimate of the integral time scale (which results either from direct integration or fitting a decaying exponential to such functions) leads to erroneous predictions.

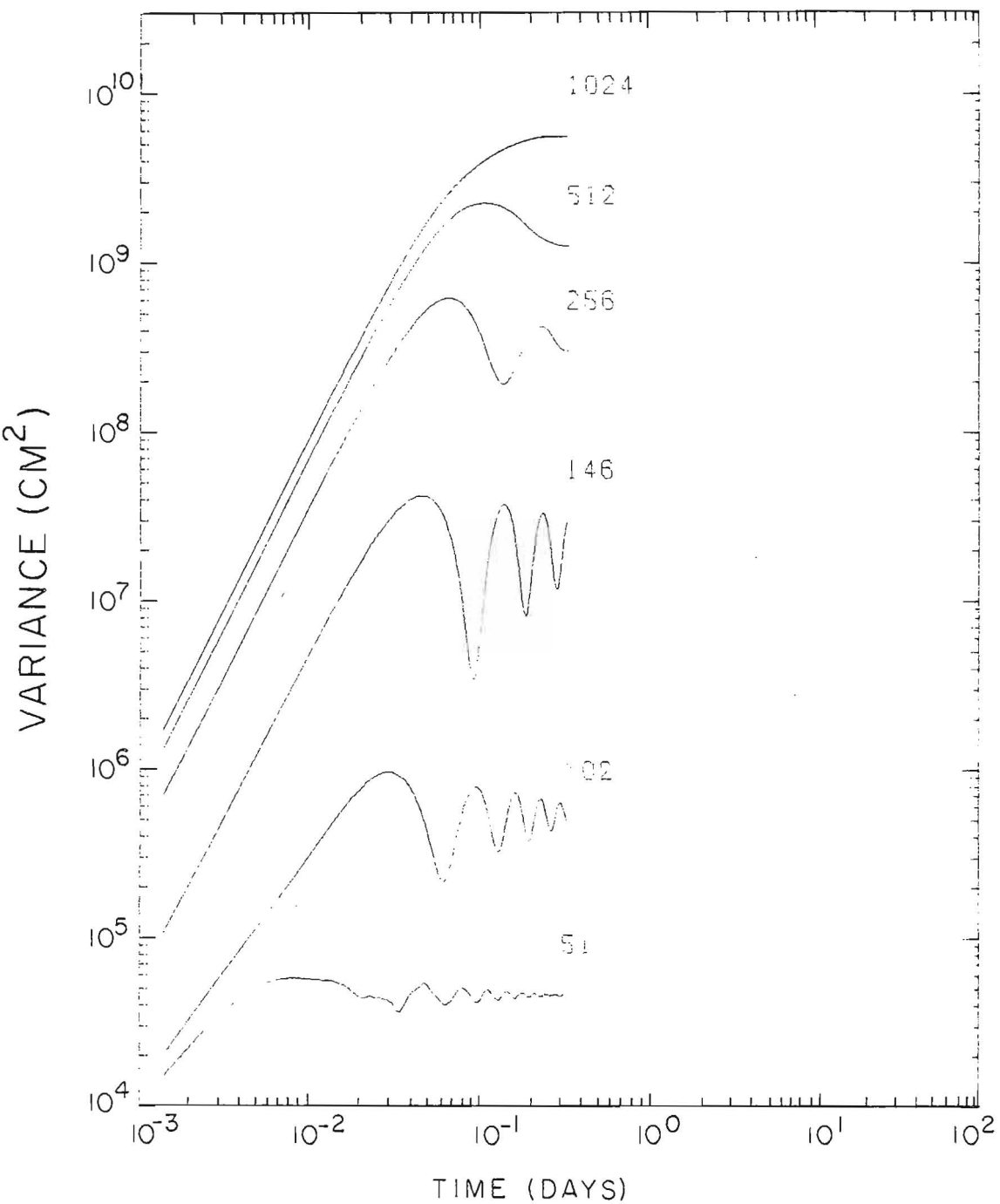

Figure 117. The growth of lateral variance with time, t, computed from Eq. (55) using Eulerian autocorrelation coefficients with the low frequency cutoff shown in minutes (e.g., for the bottom curve, the cutoff period is 51 minutes).

These problems can be eliminated, however, by fitting a decaying wavy form to the autocorrelation. The simplest possible form is given by

$$\tilde{R}_E(\tau) = e^{-a\tau}\cos m\tau \tag{59}$$

where $a \equiv 1/t_E$, an inverse of an Eulerian correlation time scale, t_E. If (59) is inserted into (55) the integration yields

$$\overline{y^2}(t) = 2\beta\overline{v'^2}\,t_s \left\{\frac{at}{a^2+m^2} + \frac{\beta(a^2-m^2)}{(a^2+m^2)^2}\left(e^{-a\,t/\beta}\cos m\,t/\beta - 1\right) - \frac{2\beta am\,e^{-a\,t/\beta}}{(a^2+m^2)^2}\sin m\,t/\beta\right\} \tag{60}$$

for the growth of lateral variance with time. Note the similarities to (58) which is recovered for $m = 0$. The integral time scale for (59) is $a/(a^2+m^2)$. It is apparent that waviness in the autocorrelation can reduce the calculated integral time scale substantially. The time scale for the decay of correlation is $1/a$ and might more properly be considered the integral time scale for the process in place of $a/(a^2+m^2)$. $t_E = 1/a$ will be called the *Eulerian correlation time scale*.

The practical implementation of this approach consists of least squares fitting (59) to autocorrelation coefficients calculated from filtered records for fixed m and then varying m to achieve the minimum square error. Table 21 shows the variation of correlation time scale and cosine period with filter cutoff frequency while Figure 118 shows (59) fitted to an autocorrelation coefficient computed from a band pass filtered current meter record (#174107).

Smoothing the highest frequencies in the velocity records was necessary due to the current meter data sampling scheme . This

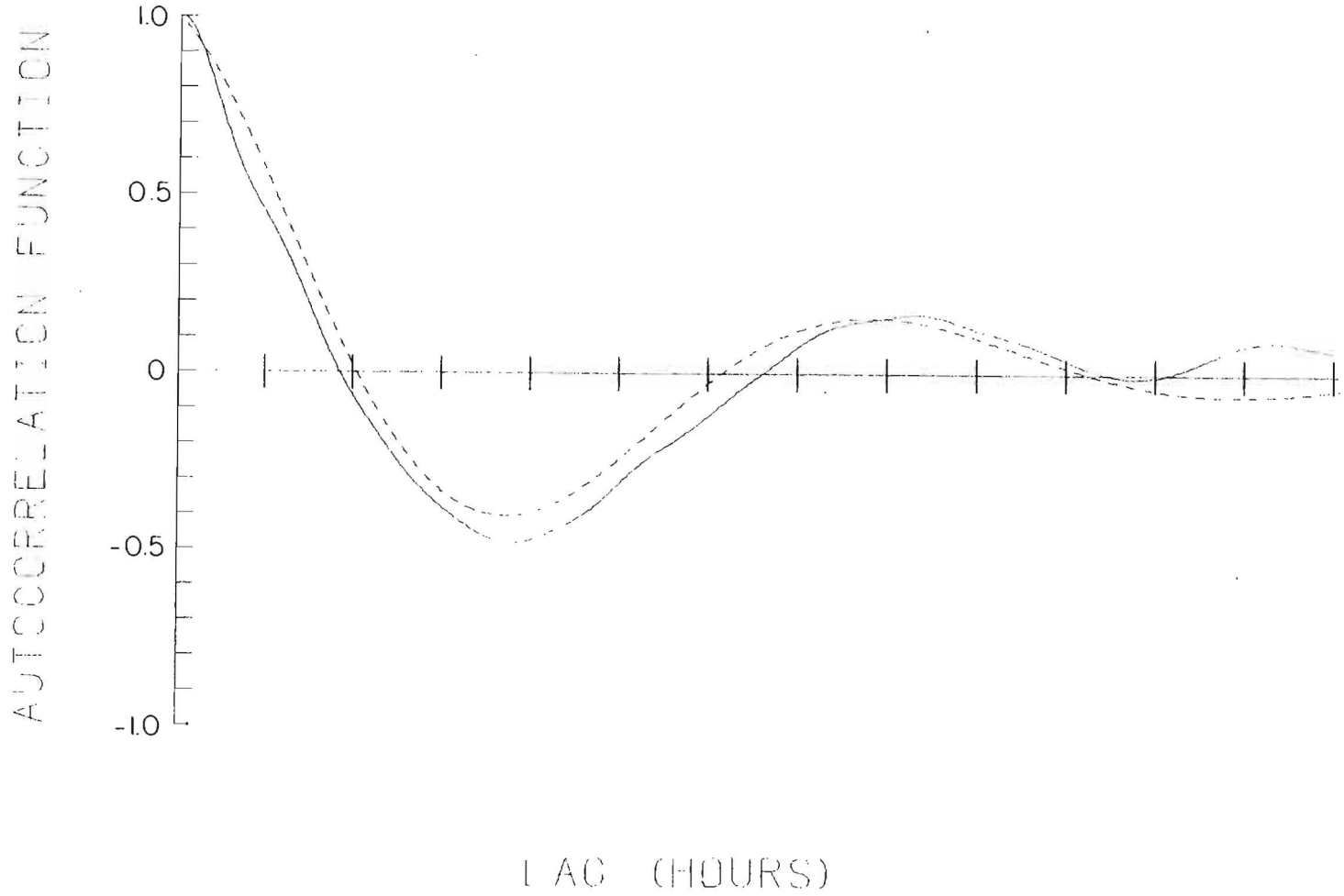

Figure 118. Autocorrelation coefficient calculated from LEDS current meter record (#174107) band pass filtered with pass band between 1 and 12 hours. The dotted curve is the fitted wavy autocorrelation coefficient (Eq. (59)).

Table 21

Variations of correlation time scale and cosine period with filter cutoff frequency.

Filter Cutoff (bandpass), hours	Correlation Time Scale t_e, hours	Period of cosine fit, hours
12 - 1	4.3	8.2
6 - 1	1.9	4.2
4 - 1	1.4	2.6
3 - 1	1.11	2.1
2 - 1	1.28	1.4

scheme, which is common to many types of current meters, entails averaging the speed over the sampling period but recording one instantaneous measurement of direction which is subsequently used to compute the velocity components. Sampling in this fashion aliases frequencies higher than one-half the sampling rate in the direction record and thus the velocity components. The effect of this aliased energy is to cause a very rapid fall-off in the autocorrelation function in the first few lags. This effect becomes progressively more severe as the low frequencies are removed to generate the filtered records. Satisfactory autocorrelation functions were obtained from records smoothed with a low pass filter with a half power point at 1 hour.

The growth of variance with time computed from (60) using band passed records is shown in Figures 119 and 120. Some important features should be noted. i) For a given β and t, the calculated variance increases with the period of the high pass filter cutoff. Obviously a larger cutoff period incorporates more turbulent energy

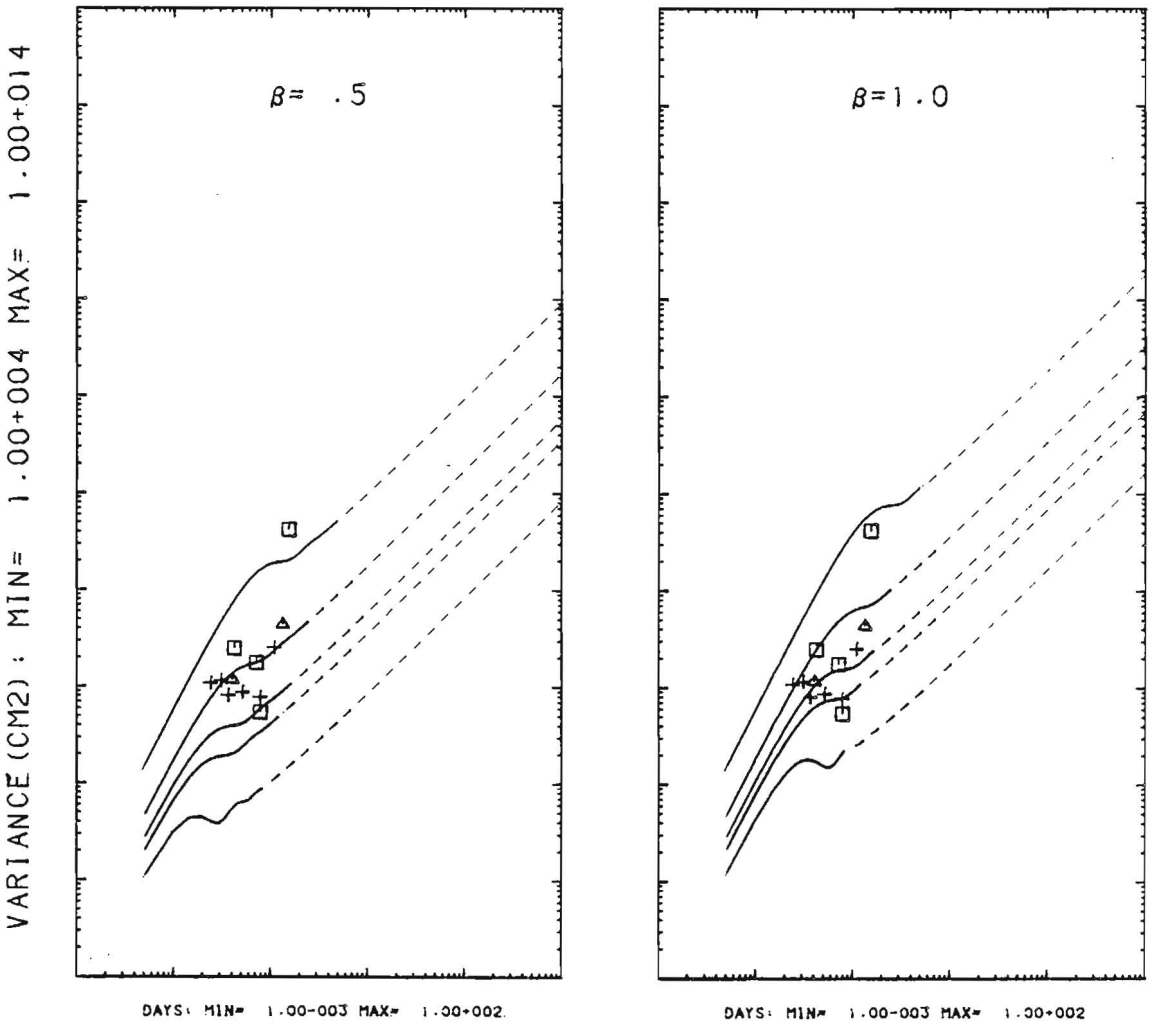

Figure 119. The growth of lateral variance with time, t, computed from Eq. (60) using autocorrelation coefficients (Eq. (59)) with band pass current meter records and various values of β (β = 0.5, 1). Low frequency cutoff periods are 12, 6, 4, 3, 2 hours respectively. The high frequency cutoff is 1 hour period. The LEDS dye plume data (see Figure 116 legend) are also shown for comparison.

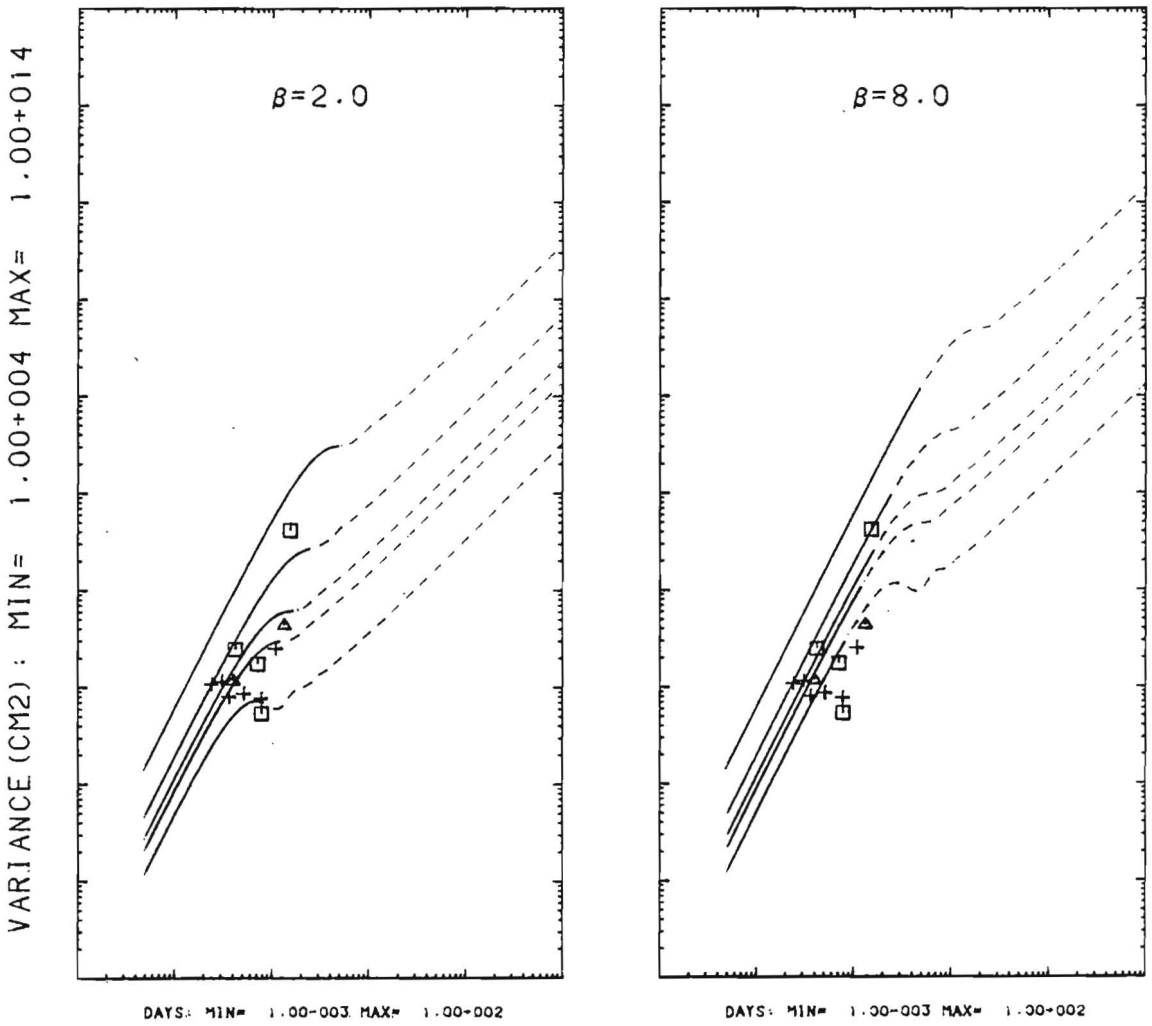

Figure 120. The growth of lateral variance with time, t, computed from Eq. (60) using autocorrelation coefficients (Eq. (59)) with band pass current meter records and various values of β (β = 2, 8). Low frequency cutoff periods are 12, 6, 4, 3, 2 hours respectively. The high frequency cutoff is 1 hour period. The LEDS dye plume data (see Figure 116 legend) are also shown for comparison.

in the calculation of variance. ii) For a given β, the t^2-regime of variance extends to larger values of t as the period of filter cutoff increases. Since the transition zone (from t^2- to t-regimes) occurs at a time of the order of T_E, this behavior is expected. iii) For a given filter cutoff period, the transition zone extends to larger values of t as β increases whereas the variance in t^2-regime is invariant with respect to β. In the t^2-regime the variance depends only on $\overline{v'^2_{t_s}}$ which in turn depends on the period of filter cutoff but not on β. Since β is a ratio of Lagrangian to Eulerian correlation time scales, an increase in β means that for a given Lagrangian correlation time scale we increase the Eulerian correlation time scale t_e by that factor and thus increase the time of the transition zone. iv) The wavy behavior of the variance is a reflection of the wavy behavior of the Eulerian autocorrelation coefficient. The waviness of variance does not occur in the early part of the t^2-regime. As seen in Table 21 the period of the cosine component is approximately equal to twice the correlation time scale which itself approximates the time of the transition zone.

Another remark is that the calculated variance should not be valid beyond a certain diffusion time, which is of the order of the high pass filter cutoff period, simply because a portion of the energy spectrum whose period is larger than the cutoff period has been arbitrarily removed from the filtered records. In Figures 119 and 120 the hatched curve indicates the invalid part of the calculated variance.

The wavy behavior of R_E is due to energetic low frequency fluctuations. Although they are energetic, these fluctuations in velocity act essentially as mean flows causing plume meandering and contribute little to dye diffusion relative to the plume centerline. Aerial photography shows some examples of the action of low frequency velocity fluctuations. The upper plume in Figure 83 shows a sudden local shift in the plume axis. Apparently this is caused by a localized action of low frequency fluctuations. Another example is seen in Figure 85, where the entire dye plume was translated from one direction to another within 4 hours. Again those low frequency motions have little effect on dye diffusion relative to the plume centerline.

For proper comparison of the calculations to dye plume data, therefore, we need to eliminate the effect of the low frequency fluctuations on the variance calculated from current meter records. Since the LEDS plume diffusion is in the t^2-regime and the wavy portion of the calculated variance occurs around and beyond the time of transition zone, we are permitted to remove the waviness by using only the exponential component of the autocorrelation (Eq. (59)), i.e., setting $m = 0$. Note that in so doing we have preserved the same correlation time scale as the original exponential-cosine correlation.

Figures 121 and 122 show the result of this calculation. The time behavior of the variance looks reasonable, and the comparison with plume data is improved.

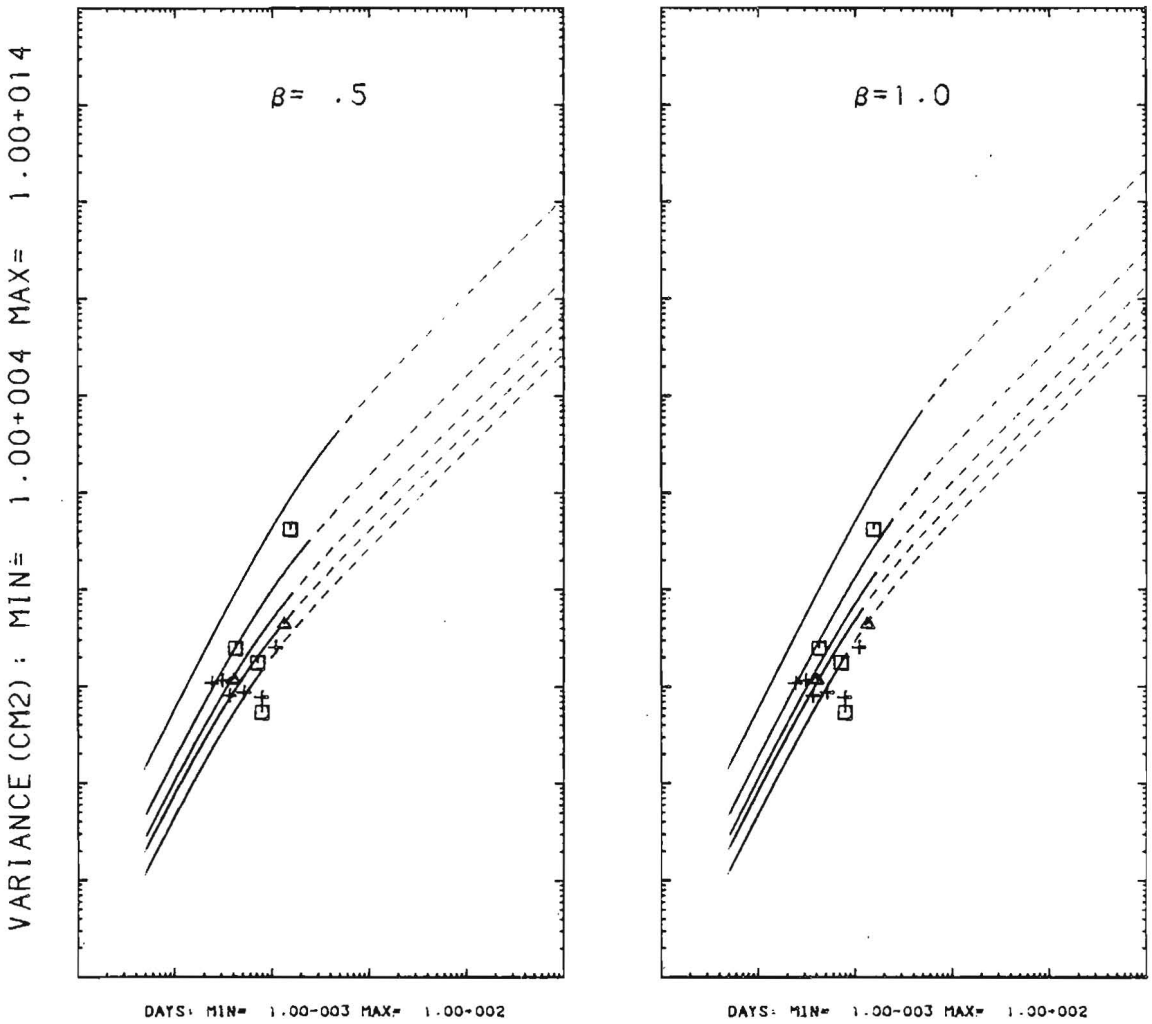

Figure 121. The growth of lateral variance with time, t, computed from Eq. (60) by setting $m \equiv 0$ and using the previous value of a, which was evaluated from (59) by fitting to autocorrelation coefficients with band pass filtered records. Values of β ($\beta = 0.5$, 1) are chosen in computation. Low frequency cutoff periods are 12, 6, 4, 3, 2 hours, respectively. The high frequency cutoff is 1 hour period. The LEDS dye plume data (see Figure 116 legend) are also shown for comparison.

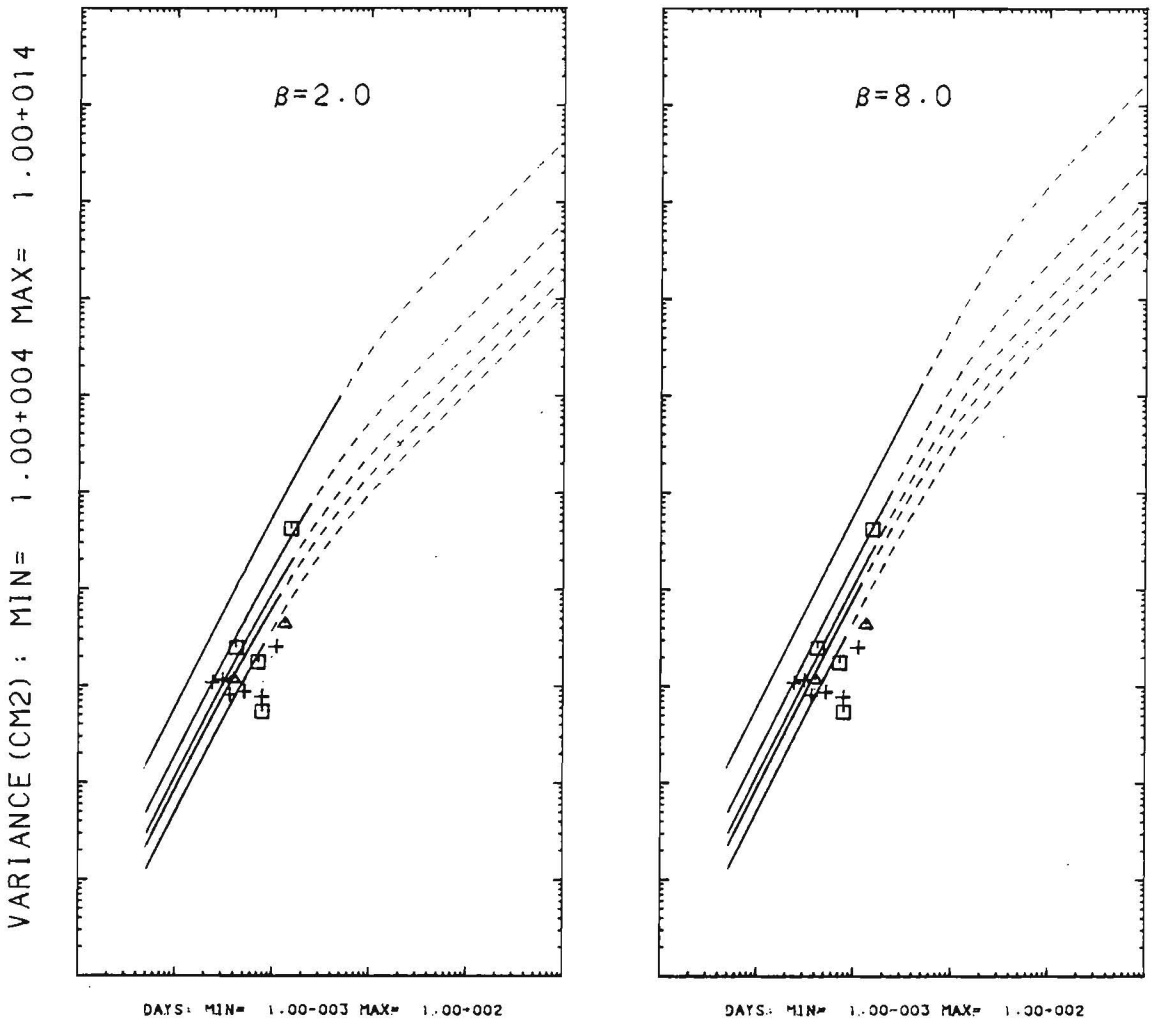

Figure 122. The growth of lateral variance with time, t, computed from Eq. (60) by setting $m \equiv 0$ and using the previous value of a, which was evaluated from (59) by fitting to autocorrelation coefficients with band pass filtered records. Values of β ($\beta = 2, 8$) are chosen in computation. Low frequency cutoff periods are 12, 6, 4, 3, 2 hours, respectively. The high frequency cutoff is 1 hour period. The LEDS dye plume data (see Figure 116 legend) are also shown for comparison.

Although Figures 121 and 122 are improvements of Figures 119 and 120, the method used is considered to be *ad hoc*. Nevertheless the method produces estimates of the correlation time scale and velocity variance which produce diffusion predictions in accord with the simultaneous dye diffusion measurements. Note that there is little to choose between the curves produced from the 2-6 hour cut-off high pass filtered records. This arises from the fact that the velocity spectrum at shorter than tidal periods is relatively flat resulting in only a four fold increase in predicted variance for the six hour cutoff record compared to the 2 hour cutoff record. Data presented in Okubo (1971) shows scatter of an order of magnitude in the variance at any given diffusion time. Thus a useful prediction of variance can be obtained from a current meter record which excludes fluctuations of tidal period and longer.

Figures 121 and 122 suggest that β is greater than two though how much greater cannot be determined given the relatively short diffusion times covered during the dye plume studies. This is in agreement with a value of approximately four obtained by Hay and Pasquill (1957) in the atmosphere. We attempted to determine β following Hay and Pasquill (1957) but found that the current meter sampling scheme, as described earlier, produced data unsuitable for the determination.

There are a number of areas in which future studies are required. These include the extension of this method to longer diffusion times, the direct measurement of β, and the elaboration of a method to

predict patch (relative) diffusion from current meter data.

Extending the predictions to longer times is problematical without concurrent measurements of diffusion extending over comparable times. The problem centers on determining the diffusive nature of tidal and longer period motions. These are very energetic but we do not know if they are as diffusive as the more random higher frequency motions. This question should be addressed with another LEDS type study with instrumentation and sampling procedures refined in light of the information acquired during this project. The direct measurement of β, the ratio of the Eulerian and Lagrangian integral time scales could be done in the context of the experiment suggested above. The major requirements are a vector measuring current meter and measurements of the lateral plume variance over a sufficiently long observation interval.

A scheme for the prediction of relative diffusion from current meter records does not currently exist. The fundamental problem arises because both plumes and moored current meters experience the entire spectrum of motions while the freely drifting particles in a patch are diffused relative to each other only by those scales of motion which are of a scale comparable to their separation. A number of approaches to this problem are possible. One is based on the Smith and Hay (1961) extension of the Hay and Pasquill (1957) model to patch diffusion which leads to a size dependent growth rate. A second considers the relative acceleration to be statistically steady as opposed to the relative velocity as in the plume model. This

yields functional forms for the variance which grow as t^3 and are thus in better accord with patch diffusion data as presented in Okubo (1971).

A third entirely hueristic approach is to evalute the non-stationarity of the velocity variance directly from current meter records as a function of increasing averaging time which is equivalent to increasing diffusion time. This can be combined with our evaluation of the variation of integral time scale with filter cutoff period to yield an empirical extension of Eq. (58)

$$\sigma_y^2(t) = 2\beta v'^2_{t_s}(t) T_E(t) t + 2\beta v'^2_{t_s}(t) T_E^2(t) (1 - e^{t/\beta T_E(t)}) \tag{61}$$

in which all the terms are obtainable from single current meter records.

The crucial element in evaluating these approaches is the availability of high quality current meter and dye diffusion data taken for sufficiently long times. A data set meeting all these criteria does not currently exist.

REFERENCES

Ahn, C.S. 1974. Pollutant dispersion in shallow coastal water. Ocean '74 IEEE International Conference on Engineering in the Ocean Environment. Vol. 1, p. 411-417. Inst. Electrical & Electronic Engineers, New York.

Batchelor, G.K. and A.A. Townsend. 1956. Turbulent Diffusion. Surveys in Mechanics (The G.I. Taylor 70th Anniv. Volume), edited by G.K. Batchelor & R.M. Davies, Cambridge Univ. Press, 475 pp.

Bendiner, W.P. and T.E. Ewart. 1972. Techniques for estuarine and open ocean dye dispersal measurement. A paper presented in Symposium on the Physical Processes responsible for the Dispersal of Pollutants in the Sea with special reference to the nearshore zone. Aarhus University, Denmark, 4-7 July, 1972.

Bowden, K.F. 1965. Horizontal mixing in the sea due to a shearing current. J. Fluid Mech., 21:83-95.

Callaway, R.J. 1974. Subsurface horizontal dispersion of pollutants in open coastal waters. Int. Symposium on Discharge of Sewage from Sea Outfalls, London, 27 August-2 September, 1974.

Carpenter, J.H. 1960. Tracer for circulation and mixing in natural waters. Public Works, 91:110-112.

Carter, H.H. 1974. Prediction of far-field exclusion areas and effects. Int. Symposium on Discharge of Sewage from Sea Outfalls, London, 27 August-2 September, 1974.

Carter, H.H. and A. Okubo. 1965. A study of the physical processes of movement and dispersion in the Cape Kennedy area. Final Report under the U.S. Atomic Energy Commission, Report No. NYO-2973-1, Chesapeake Bay Institute, The Johns Hopkins Univ., 164 pp.

Carter, H.H. and A. Okubo. 1966. Comments on paper by G.T. Csanady, "Acceleration Diffusion in the Skewed Shear Flow of Lake Currents", Journal of Geophysical Research, 71:5012-5014.

Carter, H.H. and A. Okubo. 1978. A study of turbulent diffusion by dye tracers, p. 95-111. *In:* B. Kjerfve (ed.), Estuarine Transport Processes. Univ. of South Carolina Press.

Carter, H.H., A. Okubo, R.E. Wilson, B. Sanderson and D.W. Pritchard. 1980. A Lagrangian and Eulerian diffusion study in the coastal surface layers. Progress Report for the U.S. Dept. of Energy.

Cederwall, K. 1971. A float diffusion study. Water Research, 5:889-907.

Chew, F. and G.A. Berberian. 1970. Some measurements of current by shallow drogues in the Florida Current. Limnol. Oceanogr., 15:88-99.

Chew, F. and G.A. Berberian. 1971. A determination of horizontal divergence in the Gulf Stream off Cape Lookout. J. Phys. Oceanogr., 1:39-44.

Chew, F. and G.A. Berberian. 1972. Neighbor diffusivity as related to lateral shear in the Florida Current. Deep-Sea Res., 19:493-506.

Corrsin, S. 1962. Theories of turbulent dispersion. Mecanique de la Turbulence. No. 108, Centre National de la Recherche Scientifique, Paris, p. 27-52.

Csanady, G.T. 1963. Turbulent diffusion in Lake Huron. J. Fluid Mech., 17:360-384.

Csanady, G.T. 1964. Turbulence and diffusion in the Great Lakes. Pub. No. 11, Great Lakes Div., Univ. Michigan, pp. 326-339.

Csanady, G.T. 1966. Accelerated diffusion in the skewed shear flow of Lake currents. J. Geophys. Res., 71:411-420.

Csanady, G.T. 1970. Dispersal of effluents in the Great Lakes. Water Research, 4:79-114.

Csanady, G.T. 1973. Turbulent Diffusion in the Environment, Geophys. and Astrophys. Monogr. Dordrecht, Holland/Boston, U.S.A.: Riedel Publ. Co., 248 pp.

Davis, Russ E. 1982. On relating Eulerian and Lagrangian velocity statistics: single particles in homogeneous flows. J. Fluid Mech., 114:1-26.

Denner. W.W., T. Green and W.H. Snyder. 1968. Large scale oceanic drogue diffusion. Nature, 219:361-362.

El-Shaarawi, A. and C.R. Murthy. 1976. Probability distribution of concentrations measured in the wake of a continuous point source in coastal currents. J. Phys. Oceanogr., 6:735-740.

Ewart, T.E. and W.P. Bendiner. 1981. An observation of the horizontal and vertical diffusion of a passive tracer in the deep ocean. J. Geophys. Res., 86:10974-10982.

Foxworthy, J.E., R.B. Tibby and G.M. Barsom. 1966. Dispersion of a surface waste field in the sea. J. Water Pollution Control Federation, Washington, D.C., 1170-1193. See also Allan Hancock Foundation, "An investigation of the fate of organic and inorganic wastes discharged into the marine environment and their effects on biological productivity". State Water Quality Control Board, Pub. No. 29, Sacramento, California, 1965, 117 pp.

Franz, H., U. Gehlhaar, K.P. Gunther, A. Klein, J. Luther, R. Reuter and H. Weidemann. 1982. Airborne fluorescence LIDAR monitoring of tracer dye patches - a comparison with shipboard measurements. Deep-Sea Research, 29:893-901.

Frenkiel, F.N. 1953. Turbulent diffusion. Advances in Applied Mechanics, 3:61-107, Academic Press, New York.

Gifford, F. 1959. Statistical properties of a fluctuating plume dispersal model, Atmospheric Diffusion and Air Pollution, edited by F.N. Frenkiel and P.A. Sheppard, Advances in Geophysics, 6, 117, Academic Press, New York.

Hay, J.S. and F. Pasquill. 1959. Diffusion from a continuous source in relation to the spectrum and scale of turbulence. Adv. in Geophys., 6:345-365.

Huang, J.C.K. 1971. Eddy diffusivity in Lake Michigan. J. Geophys. Res., 76:8147-9152.

Ichiye, T. 1967. Upper ocean boundary-layer flow determined by dye diffusion. Phys. Fluids, Suppl. 1967: S270-S277.

Ichiye, T. and N.B. Plutchak. 1966. Photodensitometric measurement of dye concentration in the ocean. Limnol. Oceanogr., 11:364-370.

Ichiye, T. and M. Carnes. 1980/81. Application of aerial photography to the study of small scale upper ocean phenomena. Pageoph, 119:294-308.

Ichiye, T. M. Inoue and M. Carnes. 1981. Horizontal diffusion in ocean dumping experiments. *In:* Ocean Dumping of Industrial Wastes, B.H. Ketchum, D.R. Kester, and P.K. Park (eds.), Plenum Press, New York.

Jackson, G.A., R.C.Y. Koh, N.H. Brooks, and J.J. Morgan. 1979. Assessment of alternative strategies for sludge disposal into deep ocean basins off southern California. Envir. Qual. Lab. Rep. 14, Calif. Inst. Tech.

Joseph, J. and H. Sendner. 1958. Über die horizontale Diffusion im Meere, Dt. Hydrogr. Z. 11, 49.

Joseph, J., H. Sendner and H. Weidemann. 1964. Untersuchungen über die horizontale Diffusion in der Nordsee. Dt. Hydrogr. Z., 17:57-75.

Katz, B., R. Gerard and M. Costin. 1965. Response of dye tracers to sea surface conditions. J. Geophys. Res., 70:5505-5513.

Kenny, B.C. 1967. Dye plume meandering. Proc. 10th Conf. Great Lakes Res., Int. Assoc. Great Lakes Res., Univ. Michigan, 277-288.

Kodak Data for Aerial Photography (Code No. M-29); 4th Edition, 1976 Eastman Kodak Co., Rochester, NY.

Kullenberg, G. 1969. Measurements of horizontal and vertical diffusion in coastal waters. Kungl. Vetenskaps-och Vitterhets-Samhället, Göteborg, Series Geophysica, 2:51 pp.

Kullenberg, G. 1971. Vertical diffusion in shallow waters. Tellus: 23:129-135.

Kullenberg, G. 1972. Apparent horizontal diffusion in stratified vertical shear flow. Tellus: 24:17-28.

Linfield, R.W. 1965. Time and tide wait for Johns Hopkins. Photo Methods for Industry, 8:40-41 & 76.

Ling, Beibei. 1981. A study of the laws of small-scale horizontal turbulent diffusion and the predictions of pollution near the Chinese coastal areas. Acta Oceanologica Sinica, 3:165-183.

Lumley, J.L. 1962. An approach to the Eulerian-Lagrangian problem. J. Math. Phys., 3:309-312.

Molinari, R. and A.D. Kirwan, Jr. 1975. Calculations of differential kinematic properties from Lagrangian observations in the western Caribbean Sea. J. Phys. Oceanogr., 5:483-491.

Mooers, C.N.K. 1973. A technique for the cross spectrum analysis of pairs of complex-valued time series, with emphasis on properties of polarized components and rotational invariants. Deep-Sea Research, 20:1129-1141.

Murthy, C.R. 1972. Complex diffusion processes in coastal currents of a lake. J. Phys. Oceanogr. 2:80-90.

Murthy, C.R. and G.T. Csanady. 1971. Experimental studies of relative diffusion in Lake Huron. J. Phys. Oceanogr., 1:17-24.

Neumann, J. 1978. Some observations on the simple exponential function as a Lagrangian velocity correlation function in turbulent diffusion. Atmospheric Environment, 12:1965-1968.

Ogura, Y. 1952. The theory of turbulent diffusion in the atmosphere (1). J. Meteorol. Soc. Japan, 30:23-28.

Ogura, Y. 1957. The influence of finite observation intervals on the measurement of turbulent diffusion parameters. J. Met. 14:176-181.

Ogura, Y. 1959. Diffusion from a continuous source in relation to a finite observation interval. Adv. in Geophys., 6:149-159.

Okubo, A. 1966. A note on horizontal diffusion from an instantaneous source in a nonuniform flow. J. Oceanogr. Soc., Japan, 22:35-40.

Okubo, A. 1970. Horizontal dispersion of floatable particles in the vicinity of velocity singularities such as convergences. Deep-Sea Res., 17:445-454.

Okubo, A. 1971. Ocean diffusion diagrams. Deep-Sea Res., 18:789-802.

Okubo, A. 1974. Some speculations on oceanic diffusion diagrams. Symposium on physical processes responsible for the dispersal of pollutants in the sea with special reference to the nearshore zone. Aarhus, Denmark, July 4-8, 1972. AEC Document No. C00-3062-4.

Okubo, A. and C.C. Ebbesmeyer. 1976. Determination of vorticity, divergence, and deformation rates from analysis of drogue observations. Deep-Sea Research, 23:349-352.

Okubo, A., C.C. Ebbesmeyer, and J.M. Helseth. 1976a. Determination of Lagrangian deformation from analysis of current followers. J. Phys. Oceanogr., 6:524-527.

Okubo, A., C.C. Ebbesmeyer, J.M. Helseth and A.S. Robbins. 1976b. Reanalysis of the Great Lakes drogue studies data. SUNY, Marine Sciences Research Center, Spec. Report 2, Ref. 76-2, 84 pp.

Okubo, A. and J.S. Farlow. 1967. Analysis of some Great Lakes drogue studies. Proc. 10th Conf. Great Lakes Res., Int. Assoc. for Great Lakes Res., p. 299-308.

Okubo, A., C.C. Ebbesmeyer and B.G. Sanderson. 1983. Lagrangian diffusion equation and its application to oceanic dispersion. (In preparation).

Okubo, A. and D.W. Pritchard. 1960. Unpublished note. (See Pritchard, D.W. The application of existing oceanographic knowledge to the problem of radioactive waste disposal into the sea. In: Disposal of radioactive wastes, Vol. 2, International Atomic Energy Agency, Vienna, 1960, pp. 229-253).

Palmer, M.D. and J.B. Izatt. 1970. Dispersion prediction from current meters. J. Hydraul. Div., Proc. A.S.C.E., 96 (HY8): 1667-1680.

Pritchard, D.W. and J.H. Carpenter. 1960. Measurements of turbulent diffusion in estuarine and inshore waters. Bull. Int. Assoc. Sci. Hydrol. No. 20, 37-50, December 1960.

Pritchard, D.W., A. Okubo and H.H. Carter. 1966. Observations and theory of eddy movement and diffusion of an introduced tracer material in the surface layers of the sea. In: Disposal of Radioactive Wastes into Seas, Oceans, and Surface Waters, Int. Atomic Energy Agency, Vienna, pp. 397-424.

Pritchard, D.W. and J.A. Zertuche-Gonzalez. 1982. Mitigation of natural background interference with fluorometric dye measurements in natural waters. Draft report to Dept. of Nat. Res., State of MD.

Reed, R.K. 1971. An observation of divergence in the Alaskan Stream. J. Phys. Oceanogr., 1:282-283.

Sanderson, B.G. 1982. A Lagrangian description of drifter dispersion. Ph.D. Dissertation, SUNY, Marine Sciences Research Center, Stony Brook, NY.

Sanderson, B.G., C.C. Ebbesmeyer, R.E. Wilson and A. Okubo. 1983. Predicting dispersion using velocity gradients calculated from a current meter array. (In preparation).

Schott, F. and D. Quadfasel. 1979. Lagrangian and Eulerian measurements of horizontal mixing in the Baltic. Tellus, 31:138-144.

Schuert, E.A. 1970. Turbulent diffusion in the intermediate waters of the North Pacific Ocean. J. Geophys. Res., 75:673-682.

Schlein, D.J. and S. Corrsin. 1974. A measurement of Lagrangian velocity autocorrelation in approximately isotropic turbulence. J. Fluid Mech., 62:255-271.

Smith, F.B. and J.S. Hay. 1961. The expansion of clusters of particles in the atmosphere. Quart. J. R. Met. Soc., 87:549.

Stevenson, M.R., R.W. Garvine and B. Wyatt. 1974. Lagrangian measurements in a coastal upwelling zone off Oregon. J. Phys. Oceanogr., 4:321-336.

Stommel, H. 1949. Horizontal diffusion due to oceanic turbulence. J. Mar. Res., 8:199-225.

Taylor, G.I. 1921. Diffusion by continuous movements. Proc. London Math. Soc. A20:196-211.

Venkatram, A. 1979. The expected deviation of observed concentrations from predicted ensemble means. Atmospheric Environment, 13:1547-1549.

Yanaki, T., K. Murashita and H. Higuchi. 1982. Horizontal turbulent diffusivity in the sea. Deep-Sea Research, 29:217-226.